ABSTRACT

DESIGN OF SINGLE-CARRIER FREQUENCY DOMAIN EQUALIZATION (SC-FDE) WITH TRANSMIT DIVERSITY FOR WIRELESS AND OPTICAL COMMUNICATIONS

by
Kodzovi Acolatse

As the demand of wireless service is rising, there is a need to transmit high-speed packets over the wireless communication channel. Broadband data transmission over wireless channels commonly faces the challenges of multipath fading channels, which are both time and frequency selective. There is then a need to design transmission techniques that can combat the adverse effects of the channel, and enable reliable high data rate wireless services. Orthogonal frequency division multiplexing (OFDM) has become widely accepted primarily because of its robustness against frequency selective fading channels, but it suffers a number of drawbacks such as high peak-to-average power ratio (PAPR), a need for an adaptive or coded scheme to overcome spectral nulls in the channel, and high sensitivity to frequency offset and phase noise. Single carrier with frequency domain equalization (SC-FDE) transmission utilizes single carrier modulation at the transmitter, and it performs frequency domain equalization at the receiver. SC-FDE is a technique in which, similar to OFDM, equalization is performed in the frequency domain, but has the advantage of having lower PAPR. This is important especially in the uplink communications, where lower PAPR greatly benefits the mobile terminal in terms of transmit power efficiency and manufacturing cost. Transmit diversity systems, such space-time block coding (STBC) and space-frequency block coding (SFBC) have be proven to increase the performance of wireless system by exploiting the spatial diversity of the channel.

In this dissertation, the authors focus on a transceiver (transmitter and receiver) design for effective and efficient transmission and reception of single carrier

transmission through radio-frequency (RF) and optical wireless (OW) communication dispersive channels. This dissertation is divided into five main sections.

In the first part, a physical layer hybrid automatic repeat request (HARQ) system that combines the advantages of the SC-FDE and transmit diversity on the uplink of wireless communication is presented. The proposed technique can achieve high throughput and high spectral efficiency in both time and frequency selective multipath channel. An analytical and numerical analysis of the proposed transmit diversity SC-FDE/HARQ in a single user system is provided. In general, redundant symbols are de facto transmitted in a space-time block coding system. It is shown that the system throughput can be optimized by sending the redundant symbol of a STBC block only if necessary. The performance of the proposed technique is analyzed in both slow and fast fading channel.

In the second part, the authors extend the proposed SC-FDE/HARQ to a multiuser system. This dissertation offers a new approach to designing a low complexity transmission scheme based on space-time block spreading technique that achieves a multiuser interference (MUI)-free detection at the receiver in a slow and fast fading dispersive channel. Two approaches respectively relying on chip-interleaving and chip-superimposition have been proposed to achieve the MUI-free detection.

In the third part the performance of multiuser space-time spreading system in a time varying channel is presented and a closed form expression for the average bit error rate as a function of the channel correlation coefficient is derived.

In the fourth part of this dissertation, a transmission technique for optical wireless transmission using SC-FDE is proposed. While in RF systems, the power amplifier (PA) in the transmitter is the main component that cause non-linearity distortion due to large PAPR signals, in optical wireless systems, the main source of non-linearity is the light emitting diode (LED) that is used to convert the electrical signal into optical power to be transmitted using intensity modulated direct detection (IM/DD).

Since in IM/DD, a real positive signal must be used to modulate the instantaneous power of the optical carrier, and since the LED is a non linear device, a new technique to generate low PAPR signal over a frequency selective optical channel is proposed.

Finally in the last part of this dissertation, a new technique to generation MIMO correlated fading channel impulse responses is proposed. The applicability of the proposed techniques is demonstrated by examples involving the accurate simulation of nonisotropic fading channel models.

DESIGN OF SINGLE-CARRIER FREQUENCY DOMAIN EQUALIZATION (SC-FDE) WITH TRANSMIT DIVERSITY FOR WIRELESS AND OPTICAL COMMUNICATIONS

by
Kodzovi Acolatse

A Dissertation
Submitted to the Faculty of
New Jersey Institute of Technology
in Partial Fulfillment of the Requirements for the Degree of
Doctor of Philosophy in Electrical Engineering

Department of Electrical and Computer Engineering, NJIT

January 2011

APPROVAL PAGE

DESIGN OF SINGLE-CARRIER FREQUENCY DOMAIN EQUALIZATION (SC-FDE) WITH TRANSMIT DIVERSITY FOR WIRELESS AND OPTICAL COMMUNICATIONS

Kodzovi Acolatse

Dr. Yeheskel Bar-Ness, Dissertation Advisor — Date
Distinguished Professor Professor, Department of Electrical and Computer Engineering, NJIT

Dr. Alexander M. Haimovich, Committee Member — Date
Professor of Electrical and Computer Engineering, NJIT

Dr. Ali Abdi, Committee Member — Date
Assistant Professor of Electrical and Computer Engineering, NJIT

Dr. Osvaldo Simeone, Committee Member — Date
Assistant Professor of Electrical and Computer Engineering, NJIT

Dr. Narayan Mandayam, Committee Member — Date
Associate Director, WINLAB, Rutgers University

BIOGRAPHICAL SKETCH

Author: Kodzovi Acolatse

Degree: Doctor of Philosophy

Date: January 2011

Undergraduate and Graduate Education:

- Doctor of Philosophy in Electrical Engineering,
  New Jersey Institute of Technology, Newark, NJ, 2011
- Master of Science in Electrical Engineering,
  New Jersey Institute of Technology, Newark, NJ, 2003
- Bachelor of Science in Electrical Engineering,
  School of Engineering, Lome, Togo, 1994

Major: Electrical Engineering

Presentations and Publications:

K. Acolatse, Y. Bar-Ness, and Sarah Kate Wilson, "Novel Techniques Single Carrier Frequency Domain Equalization for Optical Wireless Communications," *EURASIP Journal on Advances in Signal Processing,* 2011.

K. Acolatse and Y. Bar-Ness, "Performance Analysis of Space-Time Spreading DS-CDMA Systems over Fast-Fading Time-Correlated Channels," *IEEE communication Letters,* vol. 99, pp. 1-3, Oct. 2010.

K. Acolatse and Y. Bar-Ness, "Single Carrier Frequency Domain Equalization (SCFDE) Space-Time Block-Spread CDMA (STBS-CDMA)with Multiuser Interference(MUI)-Free Detection," *Wireless Personal Communications,* 5G Networks, Services and Applications, July 2010.

K. Acolatse and Y. Bar-Ness, "SCFDE with Space-Time Coding for IM/DD Optical Wireless Communication," *Accepted for publication in IEEE WCNC,* 2011.

K. Acolatse and Y. Bar-Ness,, "A New SCFDE STS Scheme with Joint Channel Estimation and Multiuser Detection," *IEEE Ninth International Symposium on Spread Spectrum Techniques and Applications(ISSSTA'08),* Aug. 2008, pp. 267-271.

K. Acolatse and Y. Bar-Ness, "Space Time Block Coding HARQ scheme for Highly Frequency Selective Channels," *IEEE International Conference on Communications(ICC),* June 24-28, 2007, pp. 4416-4420.

K. Acolatse and Y. Bar-Ness, Dongho Kim, "A Novel MIMO SC-DS-CDMA HARQ scheme for Frequency Selective and Time Varying Channels," *IEEE Ninth International Symposium on Spread Spectrum Techniques and Applications(ISSSTA'06,* Manaus, Brazil, Aug 2006, pp. 297-301.

K. Acolatse and Y. Bar-Ness, "An Alamouti-based Hybrid-ARQ Scheme for MIMO Systems," *International Symposium on Telecommunications (IST'05),* June 2005.

K. Acolatse and A. Abdi, "Efficient simulation of space-time correlated MIMO mobile fading channels," *IEEE 58th Vehicular Technology Conference,* vol. 1, pp. 652-656, Oct. 2003.

I dedicate this dissertation...

To my understanding, patient and beloved wife, Katsumi, who has put up with these many years of research

To our precious children Sarah, Michael, Anna, Rebecca and Ayoung, who are the joy of our lives.

To my parents, Agouvi and Leontine Acolatse, for giving me life and for instilling in me the importance of hard work and higher education.

To my brothers and sisters, my aunts and uncles, especially uncle Antoine Fumey, for their continuous support and encouragement.

Finally to Rev. and Mrs Sun Myung Moon, the True Parents of humankind and the Messiah of this age, for being the spiritual and moral guide for my life.

ACKNOWLEDGMENT

I would like to express my sincere gratitude to those who have inspired me to learn and create including the colleagues and faculty members in the Center for Wireless Communication and Signal Processing Research.

Special thanks to Dr. Ali Abdi who inspired me at the beginning of my PhD journey and to Dr. Osvaldo Simeone who kindly accepted to present my paper at IEEE International Conference on Communications in 2008.

To Dr. Alex Haimovich and Dr. Narayan Mandayam, I would like to thank for serving as members of my dissertation committee.

Most of all, I owe my heartfelt thanks to Dr. Yeheskel Bar-Ness, my advisor, who provided constant supervision, many suggestions and encouraged me throughout the course of my PhD. It was a great privilege to work with you these past years. Your continuous support has been valuable to my study and research.

I also would like to express deep gratitude to Marlene Toeroek who has supported me in every respect.

TABLE OF CONTENTS

Chapter **Page**

TABLE OF CONTENTS
(Continued)

Chapter **Page**

TABLE OF CONTENTS
(Continued)

Chapter **Page**

LIST OF TABLES

Table **Page**

LIST OF FIGURES

Figure **Page**

LIST OF FIGURES
(Continued)

Figure **Page**

LIST OF FIGURES
(Continued)

Figure **Page**

LIST OF FIGURES
(Continued)

Figure **Page**

LIST OF FIGURES
(Continued)

Figure **Page**

LIST OF FIGURES
(Continued)

CHAPTER 1

INTRODUCTION

1.1 Background and Motivation

Future generation wireless systems are required to support a high quality of service at high data rates. For such high data rates, we can have severe time-dispersion effects with a very long intersymbol interference (ISI) span in which case the conventional time-domain equalization schemes are not practical. Cyclic prefix (CP)-assisted block transmission techniques employing frequency-domain equalization (FDE) schemes are known to be excellent candidates for severe time-dispersive channels, allowing good performance and implementation complexity that is much lower than those of traditional time-domain equalization techniques. Orthogonal frequency-division multiplexing (OFDM) [1] is the most popular frequency-domain technique. Single-carrier modulation using frequency domain equalization (SC-FDE) technique is another valuable candidate for highly dispersive channels in broadband wireless communications [2], [3]. In both cases, a CP is appended to each block, eliminating the inter-block interference and converting the linear convolution that is associated with the channel into a circular convolution with respect to the useful part of the transmitted block. This allows low complexity fast Fourier transform (FFT)-based receiver implementations.

In recent years OFDM has been proposed as an efficient high data rate solution for wireless applications. Particular examples include the physical layer of high-performance wireless local area networks (WLANs), such as the 802.11$a/g/n$, DVB-T/H, and 802.16 WiMAX standards. This trend has occurred since OFDM offers excellent performance in highly dispersive channels with low terminal complexity. Although OFDM has become the physical layer of choice for broadband communications standards as it simplifies the equalization at the receiver, it suffers from several

drawbacks including a large peak-to-average power ratio (PAPR), intolerance to amplifier non-linearities, and high sensitivity to carrier frequency offsets (CFO) and phase noise [4], [5]. In [6] the statistical PAPR characteristics are investigated for OFDM signals. Different techniques for PAPR reduction in OFDM are summarized in [6]. As demonstrated by these articles, PAPR reduction is motivated by a desire to increase the mean transmit power, improve the power amplifier efficiency, increase the data rate, and reduce the bit error rate (BER). This comes at the expense of cost, complexity, and efficiency.

Single carrier modulation is another potential solution. Traditionally, it has been combined with time domain equalizer (TDE) to deal with the detrimental effects of multipath fading delay spread. Typically, a conventional TDE consists of one or more transversal filters for which the number of adaptive tap coefficients is of the order of the number of data symbols spanned by the multipath channel. As a result, SC-TDE may be impractical for broadband wireless services with very high data rates, as it is clear that the complexity and the required digital processing speed of TDE will become exorbitant [3], [2]. An alternative promising approach to ISI mitigation is the use of single-carrier (SC) modulation combined with frequency domain equalization (FDE). In recent years, SC-FDE has become a powerful and an attractive link access method for the next-generation broadband wireless networks [7], [8], [9] , [2]. SC-FDE does not have some of the inherent problems of OFDM such as high PAPR and the sensitivity to CFO because of its single carrier transmission [10], [2]. As a result, SC-FDE has recently been receiving remarkable attention. It is now one of the air interface standards adopted by the IEEE 802.16 air interface for fixed broadband wireless access. It is also under active consideration in the IEEE 802.20 Working group on mobile broadband wireless access (MBWA). In recent years, SC-FDE has also been considered as a single carrier frequency division multiple access (SC-FDMA) [11] for

the uplink multiple access scheme in Third Generation Partnership Project (3GPP) Long Term Evolution (LTE) [12].

This dissertation investigates the design of low-complexity and power efficient transmit diversity hybrid-ARQ (HARQ) for SC-FDE in a slow and time varying frequency selective fading channel for the uplink of wireless cellular communication. The author endeavors to investigate the use of SC-FDE using block transmission and transmit diversity for ubiquitous broadband wireless communications in both slow and rapidly varying fading channels. Specifically, a design of efficient transceiver using SC-FDE by employing advanced signal processing techniques, such as space-time, space-frequency block coding systems and in multiuser system, space-time block spreading coding is investigated for RF and optical wireless communications. Furthermore, the author considers the joint transmit-receiver signal processing design in SC-FDE/HARQ systems in order to achieve high data rate and diversity even in rapidly varying fading channel. In multiuser system,a design SC-FDE system using block spreading with code division multiple access and transmit diversity that achieve multiuser interference (MUI)-free detection is proposed using chip-interleaving and chip-superimpositions approaches.

1.2 System Model Overview

In this dissertation, a wireless system with a single base station equipped with multiple antenna and a number of mobile active users each equipped with two antennas is considered. The author focuses on the performance of the uplink transmission where the users simultaneously send their blocks of data to the base station oven a common wireless channel. The wireless channel is assumed dispersive both in time and frequency. this dissertation aims in designing transceivers using SC-FDE that can achieve high throughput while exploiting all the available diversity in the system. This dissertation will especially focus on the design of the single and multiuser

encoder that provide maximum throughput and diversity by using hybrid automatic repeat request (HARQ) system in order to control the transmission errors caused by the channel noise so that error free data can be delivered. The overall performance of the SC-FDE/HARQ will depend on the followings:

- *Error Detection and HARQ*:

  When data is transmitted in packets, an Automatic Repeat reQuest (ARQ) scheme [13] can be used. Whenever a packet arrives and an error is detected, the receiver requests a retransmission through a feedback channel. To determine whether or not a retransmission should be requested the receiver checks the quality or the reliability of the received packet. Usually this is done by means of an error detecting code, like a cyclic redundancy check code (CRC) [14]. A hybrid ARQ (HARQ) scheme, first suggested in [15], uses an error control code in conjunction with the retransmission scheme. Consequently, it tries to decode the received code word first and only requests a retransmission if the uncertainty of the decoding decision is considered too high, i.e. if the detection is below a certain reliability threshold. There are two main types of hybrid ARQ schemes, denoted type-I, [13], and type-II, [16], [17]. A HARQ system of type-I implies that the same message, i.e. the same packet content, is sent each time that the receiver asks for a retransmission. In a type-II scheme the first transmission usually includes information bits and a limited amount of redundant bits. These are only intended for determining the reliability of the transmission, as if it was a pure ARQ scheme. If a retransmission is needed, additional redundant bits are sent which are combined with the previously received redundant bits. This way a stronger code with a lower code rate is obtained and the received packet can be decoded accordingly, making it a hybrid scheme. There are different methods of determining whether a decoding decision is sufficiently reliable and hence different criteria for requesting a retransmission.

In this dissertation, the author propose the design of a *symbol-level* HARQ type-II scheme that uses Alamouti space-time coding [18]. In the conventional Alamouti coding, the space-time codes are transmitted successively in two consecutive symbol periods. In the proposed HARQ, the second time period code-symbol is transmitted only if the first time period symbol is not decoded successfully. We will present an analytic study of the throughput as well as the bit error rate (BER) of the proposed symbol-level HARQ using SC-FDE in both flat and frequency selective fading channels and slow and fast fading. We note that the proposed HARQ scheme is applied to the transmitted symbols instead of the transmitted bits as conventional done.

- *Forward Error Coding*:

  Forward error correction (FEC) is a system of error control for data transmission, whereby the sender adds redundant data to its messages, also known as an error-correction code. This allows the receiver to detect and correct errors (within some bound) without the need to ask the sender for additional data. The advantage of forward error correction is that a feedback channel is not required, or that retransmission of data can often be avoided, at the cost of higher bandwidth requirements on average. FEC is therefore applied in situations where retransmissions are relatively costly or impossible. There are a variety of FEC codes such as Turbo Coding, Convolutional coding, Concatenated Convolutional coding, Low-density parity-check (LDPC) coding and more. Since the focus of this dissertation is not the FEC, we will employ convolutional coding as FEC.

- *Multiuser Encoder*:

  This dissertation also studies the design of the multiuser encoder based on block spreading [19] such that high throughput and maximum diversity gain can be achieved using SC-FDE/HARQ. The users in the uplink can be sepa-

rated either in time (time division multiple access (TDMA)) or in frequency (frequency division multiple access (FDMA)) or in code (code division multiple access(CDMA)) or in space (space division multiple access(SDMA)). In this dissertation a transceiver design for multiple access scheme that combines FDMA, CDMA and that enable MUI-free detection is proposed.

The proposed transceiver design for SC-FDE multiple access scheme uses block spreading and transmit diversity where each user (each equipped with two transmit antennas) is assigned a set of orthogonal spreading codes such that they can be detected at the base station with no multiple access interference (MAI) and with maximum diversity. We present an analytical study of the BER of the proposed system in slow and fast frequency selective fading channel. We derive a closed form expression of the BER as a function of the time correlation of the channel when space-time spreading is employed.

- *Frequency Domain Equalization and Combiner* : Frequency domain equalization was first investigated by Walzman and Schwartz [20] in 1973; they showed that adaptive channel equalization in the frequency domain leads to a lower computational complexity and offers better convergence properties compared to its time domain counterpart. It was not until the publication of a paper by Sari et al. [3] in 1995 that the communications research community realized the considerable potential of FDE. In fact, in [3], the striking similarities between the implementation of an OFDM system and that of an SC-FDE was pointed out and FDE was proposed as a low-complexity solution to digital terrestrial broadcasting which is characterized by a highly time dispersive channel. This has renewed interest in SC-FDE as a strong competitor to OFDM and demonstrated the potential of FDE in high-speed broadband wireless access [2]. FDE is currently enjoying a growing popularity as evidenced by the large number of

publications in the last few years (e.g., see [2] and [21], [22], [4], [23]). Specific topics in recent research on FDE concern the joint exploitation of the spatial and frequency diversities. In particular, interest in the first topic is mainly due to the recent success of multiple-input, multiple-output (MIMO) communication techniques. The integration of FDE into various MIMO systems has been investigated by several authors [21], [4], [23], [24].

In this dissertation, the author proposes the design of a system to perform FDE by combining the signal from the different users in such a way that MUI-free detection is possible and to achieve maximum diversity. The transmitter and receiver design constitute an important part of this dissertation.

1.3 Dissertation Overview

This dissertation can be roughly divided into five parts as follow:

1. An overview of the wireless channel characteristic and a presentation of SC-FDE system is presented in Chapter 1

2. In Chapter 2, the author presents the HARQ design using SC-FDE on the uplink in both frequency flat and frequency selective channel and both slow and fast fading channel.

3. The design of SC-FDE multiuser transmitter/receiver based on space-time block spreading in slow and fast fading channel is proposed in Chapter 3.

4. in Chapter 4, a performance analysis of space-time spreading in time varying channel is presented and a closed form expression of the BER is derived.

5. A new application of SC-FDE for optical wireless (OW) communication and the design of a transmit diversity technique suited for OW system are presented in Chapter 5 and 6 respectively.

6. New techniques to generating MIMO correlated fading channels are proposed and presented in Chapter 7.

CHAPTER 2

WIRELESS CHANNEL AND SCFDE SYSTEM OVERVIEW

In this chapter, the authors first characterize the wireless mobile communications channel. An overview of SC-FDE and OFDM is presented. It is then shown that SCFDE is an alternative modulation to OFDM in frequency selective channel. Without channel coding, SC-FDE combined with MMSE outperforms OFDM.

2.1 Characteristics of the Wireless Channel

One of the main challenging problem in wireless communications system is to develop advanced techniques that can mitigate the detrimental effects of the multipath wireless fading channel, which originates from the complicated and time-varying wireless environments. Indeed, in a wireless mobile communication system, a transmitted signal propagating through the wireless channel often encounters multiple reflective paths until it reaches the receiver [25]. The received signal consists of a large number of plane waves having randomly distributed amplitudes, phases, and angles of arrival. The vectorial combination of these multipath components causes dramatic fluctuations in the signal strength when the receiver moves even in a small distance as shown in Figure 2.1. This fluctuation is called multipath fading and it can occur either in large scale or in small scale. Large-scale fading represents the average signal power attenuation or path loss due to motion over large areas. Small-scale fading occurs due to small changes in position which is called Rayleigh fading since the fading is often statistically characterized with Rayleigh probability density function (pdf). Besides that, the motion of surrounding objects will make the channel time varying which degrades the performance of the system.

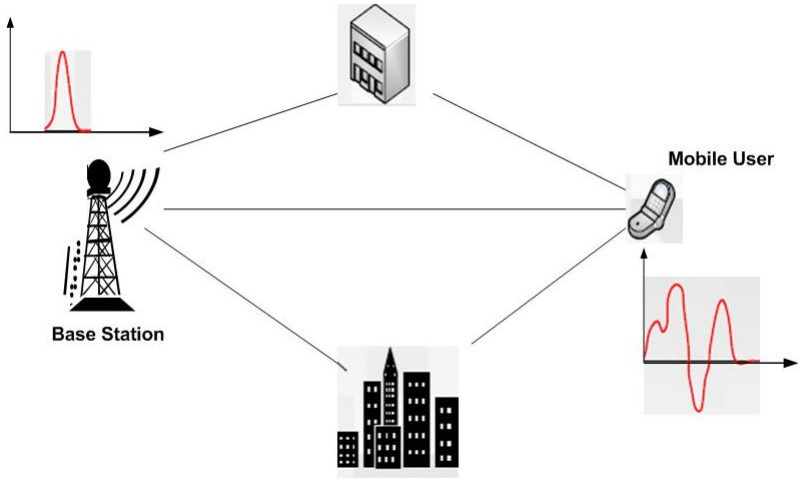

Figure 2.1 Multipath Propagation.

The Rayleigh fading channel can be categorized into either *flat fading* channel or *frequency-selective* fading channel. Flat fading occurs when the coherence bandwidth, which is inversely proportional to channel delay spread, is much larger than the transmission bandwidth whereas frequency-selective fading happens when the coherence bandwidth is much smaller than the transmission bandwidth. Figure 2.2 shows an example of the impulse response and frequency response of a frequency-selective fading channel.

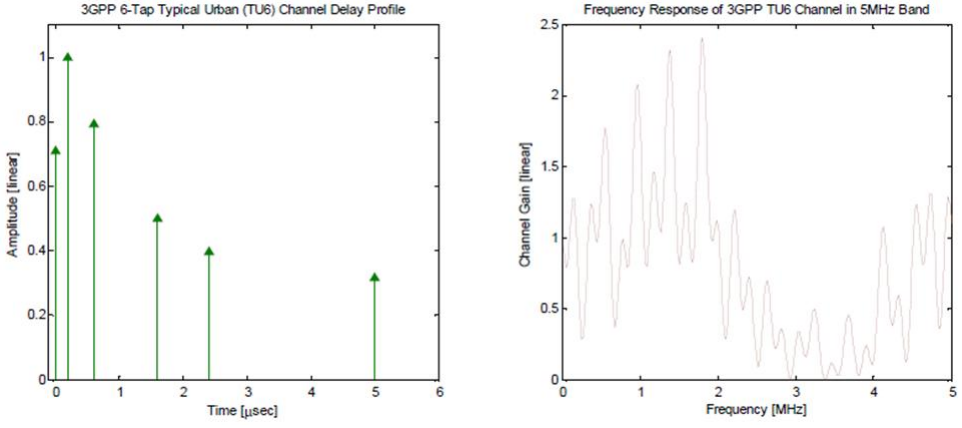

Figure 2.2 Frequency Selective Fading Channel.

The multipath fading channel can also be characterized in terms of the degree of time variation of the channel as *slow fading* and *fast fading*. The time-varying nature of the channel is directly related to the movement of the user and the user's surrounding, and the degree of the time variation is associated with the Doppler frequency f_d which is given by [26]

$$f_d = \frac{\nu}{\lambda} \tag{2.1}$$

where where ν is the relative speed of the user and λ is the wavelength of the carrier. For a given Doppler frequency f_d, the time correlation function ρ_t specifies the extent to which there is correlation between the channel's response in dt time interval and it is given by

$$\rho_t = J_0(2\pi f_d dt). \tag{2.2}$$

where $J_0(\cdot)$ is the zero-order Bessel function of the first kind. As the Doppler frequency increases, the correlation decreases at a given time interval.

Future wireless communication services featuring high-data-rate with wider transmission bandwidth (see Table 2.1) and high-mobility can aggravate the multipath and Doppler effect. In digital communication systems, for most of the channels, the discrete information bearing symbols are modulated with a continuous pulse shape and transmitted across the channel. In most cases, the pulse shapes are localized in time and frequency so that transmission of each symbol consumes a small tile in the time-frequency plane. For high data rate transmission, the duration of the pulse becomes small and comparable to the multipath delay, thus creating inter-symbol-interference (ISI) in the time domain which is a major impairment in wireless communications and can significantly degrade the link performance. In high-mobility scenarios, the channel response varies significantly in the signaling duration due to Doppler effect, thus the channel distortion becomes time-selective within

Table 2.1 Transmission Bandwidths of Current and Future Cellular Wireless Standards

Generation	Standard	Transmission Bandwidth
2G	GSM	200 KHz
	IS-95 (CDMA)	1.25 MHz
3G	WCDMA	5 MHz
	cdma2000	5 MHz
3.5 to 4G	3GPP LTE	Up to 20 MHz
	WiMAX (IEEE 802.16)	Up to 20 MHz

a single processing block. Channels whose response are both time and frequency selective are commonly referred as doubly-selective channels.

With a wider transmission bandwidth, frequency selectivity of the channel becomes more severe and thus the problem of ISI becomes more serious. In a conventional single carrier communication system, time domain equalization in the form of tap delay line filtering is performed to eliminate ISI. However, in case of a wide band channel, the length of the time domain filter to perform equalization becomes prohibitively large since it linearly increases with the channel response length. Frequency domain equalization (FDE) which is one of the main subject of this dissertation is more practical for such channels.

In this dissertation, the authors consider a wireless channel connection scheme between a base station (BS) and a user as depicted in Figure 2.3. The BS, which is not surrounded by many local scatterers, receives the signal primarily from a particular direction through a narrow beamwidth. On the other hand, the local scatterers around the user may give rise to different modes of signal propagation toward the user.It is assumed that scattering around the mobile user is either isotropic or non-isotropic as depicted in Figure 2.4 taken from [27]. In the isotropic scattering case the user

receives signals from all directions with equal probabilities. The isotropic scattering model, also known as the Clarke's model, corresponds to the uniform distribution for the angle of arrival (AOA). In the case of non-isotropic scattering, which corresponds to directional signal reception, the user receives the signal only from particular directions. Using the one-ring channel correlation model of [27], the correlation of the fading coefficients between the user's transmit antennas 1 and 2 and the base station receive antenna m can be expressed in terms of the array configurations and Doppler spread as

$$\rho_{m1,m2}(\tau) = E[h_{m1,t} h^*_{m2,t+\tau}] = J_0(\sqrt{a^2 + b^2 - 2ab\cos(\beta - \gamma)}), \tag{2.3}$$

and the correlation between the BS antennas m and p and the user antenna i is given by

$$\rho_{mi,pi}(\tau) = E[h_{mi,t} h^*_{pi,t+\tau}] = J_0(\sqrt{a^2 + c^2\Delta^2 - 2ac\Delta\sin\alpha\sin\gamma}), \tag{2.4}$$

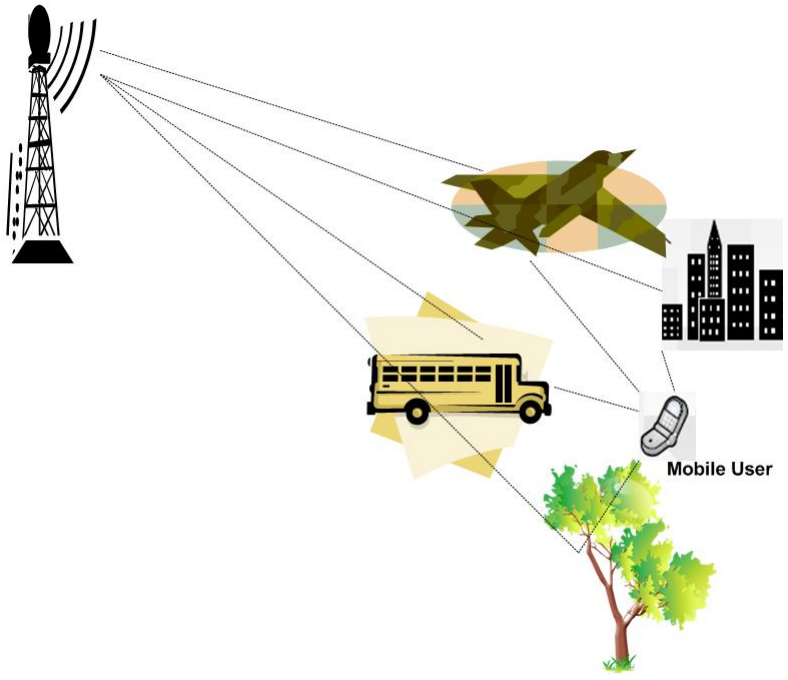

Figure 2.3 Wireless channel model between the base station and mobile user.

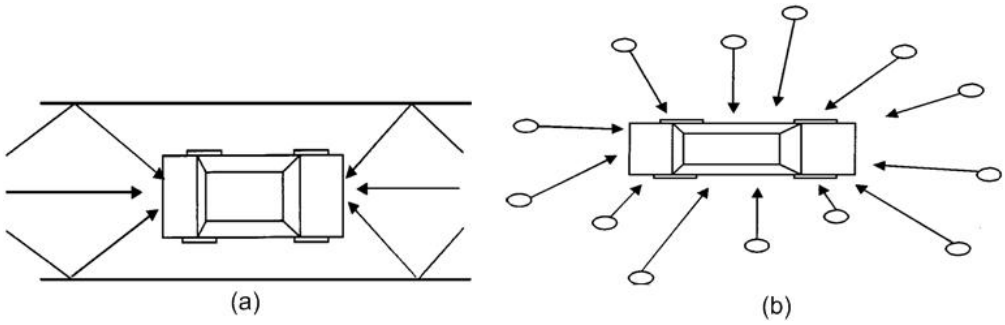

Figure 2.4 (a)- Non-isotropic scattering in a narrow street; (b) Isotropic scattering in an open area.

where $a = 2\pi f_d \tau$, $b = 2\pi d/\lambda$, $c = 2\pi\delta/\lambda$, d denotes the distance between the user antennas, δ denotes the separation between base station antennas, Δ specifies the beamwidth at the base, and α,β, and γ are angles which specify the orientations of the base station and mobile arrays and the direction of user motion, respectively (see [27] for geometrical details). It is assumed throughout this thesis that the antenna elements are linear and parallel ($\alpha = \beta = 90°$) and $\gamma = 0$. The BS antenna can be designed such that the channel seen by them are uncorrelated. In general Δ is very small [27], [28] since the BS is usually far away from the MS. It is also assumed that $\Delta = 4°$ and $\delta = 15\lambda$ which correspond to a BS antennas spatial correlation of 0.03 (uncorrelated elements, a spatial correlation of less that 0.5 is usually considered as no correlation [28]) using (2.4). The MS however has some design constraint due to its size limitation. Hence, throughout this thesis both scenario where the MS antennas are correlated and uncorrelated will be considered. It is assumed that $d = \lambda/2$ and $d = \lambda/10$ which correspond to respectively an absolute spatial correlation of 0.3 and 0.9 respectively using (2.3). Hence, the effect of the spatial channel correlation of the MS antennas on the performances of the proposed schemes will be studied in this dissertation.

The power delay profiles specified by ITU Pedestrian A and ITU Vehicular A channels [29] with additive white Gaussian noise (AWGN) is considered. The

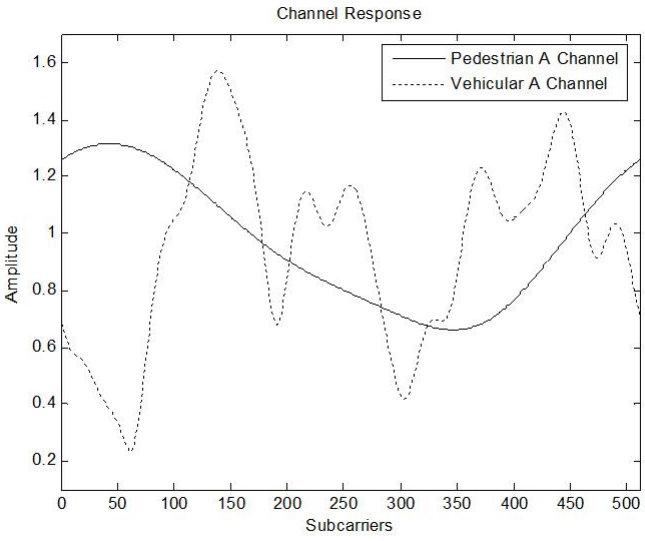

Figure 2.5 Frequency Domain Channel Response of ITU Pedestrian A and Vehicular A Channels.

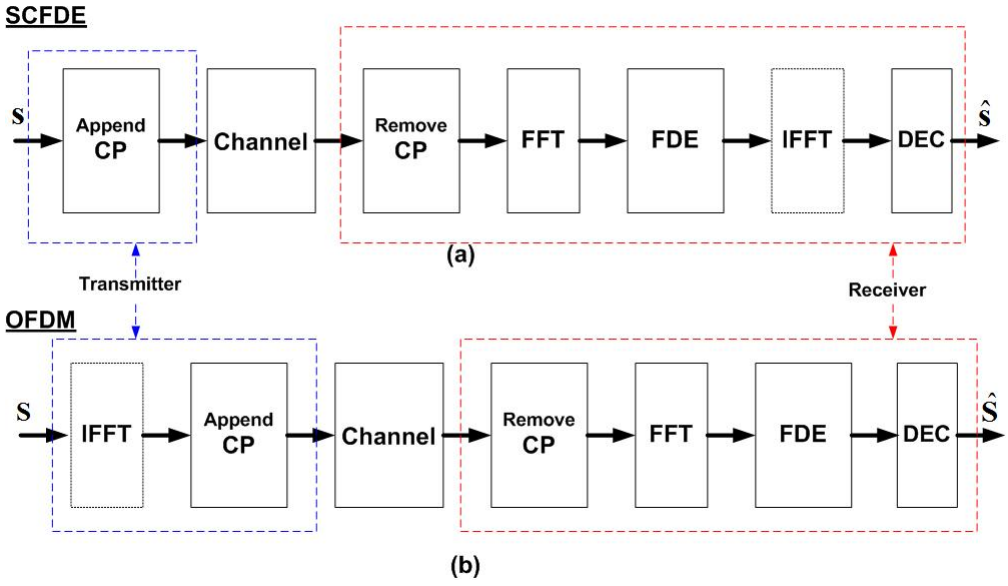

Figure 2.6 Block Diagrams of SCFDE (a) and OFDM (b) Systems; DEC stands for Decision.

Pedestrian A channel has relatively short channel delay whereas the Vehicular A channel has much longer delay. Hence, the Vehicular A channel has much more severe frequency selectivity in the frequency domain which is illustrated in Figure 2.5.

2.2 Single Carrier Frequency Domain Equalization (SC-FDE)

The block diagram of an SCFDE wireless communication system is depicted in Figure 2.6. Each group of consecutive $log_2 M$ information bits is mapped into a complex symbol belonging to a M-ary complex constellation. Data blocks consisting of N symbols are fed to the SCFDE transmit encoder. Then, each block is cyclically extended, inserting at its beginning a repetition of its last N_{cp} symbols, i.e., a cyclic prefix (CP), transmitted during the so-called guard interval. This introduces the elegant mathematical property of periodicity over a limited observation interval in the transmitted signal, at the price of a bandwidth/energy loss due to the presence of data redundancy. The CP prevents inter-block interference (IBI) and also makes linear convolution of the channel impulse response look like a circular convolution [30]. It should be noted that circular convolution in the time domain (TD) is equivalent to multiplication in the frequency domain (FD). The sequence of cyclically extended blocks undergoes parallel-to-serial (P/S) conversion, so that one complex symbol is available every T_s seconds, with T_s being the symbol period for digital transmission. This requires the usual operations of digital-to-analog (D/A) conversion, frequency up-conversion, and filtering implemented in any single carrier modulator. The resulting radio frequency signal is transmitted over a wireless channel, characterized by a time dispersion not exceeding L channel symbol intervals (this includes the contributions of transmit and receive filtering also). The signal at the output of the wireless channel undergoes frequency down-conversion, filtering, and analog-to-digital (A/D) conversion, producing a sequence of noisy samples that are grouped into equal-length blocks, each associated with a transmitted data block. For each noisy data block, the CP samples are discarded and the resulting block is sent to an FFT block converting it to the frequency domain. This is followed by an frequency domain equalization (FDE) compensating for channel distortion. Most of the well-known time domain equalization techniques, such as Zero-forcing (ZF), minimum

mean-square error (MMSE) equalization and decision feedback equalization (DFE) can be applied. The equalized symbols are then sent to an IFFT block bringing the noisy signal vector back to the time domain. Finally, data decisions are made on a block-by-block basis and sent to the data link layer after S/P conversion.

Note that SCFDE is very similar to the well-known OFDM system also shown in Figure 2.6. OFDM is another way to mitigate the frequency-selective fading seen in a wide band channel. It uses a multicarrier technique which subdivides the entire channel into smaller sub-bands, or subcarriers. In OFDM, after symbol mapping and P/S conversion, the blocks of N complex information symbols belonging are first processed by an inverse Fast Fourier Transform (IFFT) block. Each block at the IFFT output, after P/S conversion, is cyclically extended by adding a CP. The resulting sequence undergoes A/D conversion, frequency conversion, and filtering like in the SCFDE system. It can be shown that [30], in this case, the transmitted signal associated with each data block consists of a superposition of oscillations over a limited time interval, each associated with a distinct information symbol and a specific subcarrier frequency. Moreover, over that interval, the family of complex oscillations forms a set of orthogonal signals and this property plays a fundamental role, since it greatly simplifies the task of separating their contributions in the detection process. Note that the generation of multiple waveforms is not accomplished via a bank of oscillators but by exploiting IFFT processing in the baseband section of the OFDM modulator. In the frequency domain, since the bandwidth of a subcarrier is designed to be smaller than the coherence bandwidth, each subchannel is seen as a flat fading channel which simplifies the channel equalization process. In the time domain, by splitting a high-rate data stream into a number of lower-rate data stream that are transmitted in parallel, OFDM resolves the problem of ISI in wide band communications. More technical details on OFDM can be found in [1] , [31] and references therein.

From Figure 2.6, one can note the similarities and differences between the SCFDE and OFDM as follow:

- In both cases, one FFT and one IFFT block are employed in the system, even though in different places and for different reasons
- Both systems usually employ a CP to eliminate IBI so that each data block can be processed independently and the linear convolution associated with channel filtering is turned to a circular convolution, provided that the duration of the prefix is longer than that of the channel delay spread.
- Both systems have overall the same complexity.
- Despite the above-mentioned similarities, the different use of FFT processing leads to very different detection processes. In fact, in OFDM systems, the optimal detection is performed in the FD after the FFT operation, whereas for SCFDE systems after the FDE, the signal is transformed into the TD before detection.
- Unlike SCFDE systems, OFDM systems suffer from larger PAPR which are impairments related to the large dynamic range of the transmitted signal.

The BER performance of SCFDE and OFDM using MMSE and ZF equalization is depicted in Figure 2.8 and Figure 2.9 for both ITU Pedestrian A and Vehicular A channels. One can see that in Pedestrian channel when the delay spread is short, ZF and MMSE performance are the same for both SCFDE and OFDM but SCFDE outperforms OFDM. However in Vehicular channel where the delay spread is much longer, MMSE performance is better than ZF as expected. Using MMSE, SCFDE outperforms OFDM for all receive signal-to-noise ration (SNR). However, when ZF is used, one can se that for SNR greater than 10dB, OFDM performance is better. Figure 2.10 and Figure 2.11 shows the BER comparison of SCFDE and OFDM in both

Pedestrian A and Vehicular A channels with MMSE and ZF equalization respectively. One can see that SCFDE outperforms OFDM because of the inherent frequency diversity. This is more evident in the Vehicular A channel where the frequency selectivity is severe; OFDM system needs a good channel coding or adaptive modulation scheme to overcome this limitation. In AWGN, SCFDE and OFDM essentially have the same performance.

The BER performance results depicted in the figures above show that without channel coding MMSE-SCFDE outperforms MMSE-OFDM for all channels and ZF-SCFDE outperforms ZF-OFDM when the received SNR is above a threshold SNR_0. This is proved mathematically below.

Assuming that the frequency selective channel impulse response (CIR) is given by $\mathbf{h} = [h_0, h_1, \cdots, h_{L-1}]$ whose N-point DFT is given by $\mathbf{H} = [H_0, H_1, \cdots, H_{N-1}]$. The bit error rate (BER) of SCFDE and OFDM can be shown to be given by [32]

$$\begin{aligned} BER_{SCFDE} &= Q\left(\sqrt{\frac{1}{\frac{1}{N}\sum_{i=0}^{N-1}\frac{1}{\theta+\gamma_o|H_i|^2}}}\right) \\ BER_{OFDM} &= \frac{1}{N}\sum_{i=0}^{N-1} Q\left(\sqrt{\theta+\gamma_o|H_i|^2}\right) \end{aligned} \tag{2.5}$$

where $\gamma_o = E_S/N_0$ and $\theta = 1$ for MMSE and $\theta = 0$ for ZF. E_S and N_0 represent the energy per input symbol and the AWGN spectral density respectively. $Q(\cdot)$ is the Q-function defined as

$$Q(x) = \frac{1}{\sqrt{2\pi}}\int_x^\infty e^{-t^2/2}dt; x \geq 0. \tag{2.6}$$

It is shown in [32] that $BER_{SCFDE} \leq BER_{OFDM}$ if $1/(\theta+\gamma_o|H_i|^2) < 1/3, \forall H_i$, i.e. $\gamma_o > (3-\theta)/|H_i|^2, \forall H_i$.

The proof is provided here for the reader convenience. Let

$$f(x) = Q(\sqrt{1/x}), x > 0. \tag{2.7}$$

The second derivative of f is given by

$$\frac{d^2}{dx^2}f(x) = \frac{e^{-1/2x}(1-3x)}{16\pi x^3\sqrt{s}}. \tag{2.8}$$

One can see that $\frac{d^2}{dx^2}f(x) > 0$ if $x < 1/3$. Hence, the function f is convex if $x < 1/3$ and concave if $x > 1/3$. The function f is plotted in Figure 2.7 when it can be seen that at the point $x = 1/3$ the function changes from being convex to being concave.

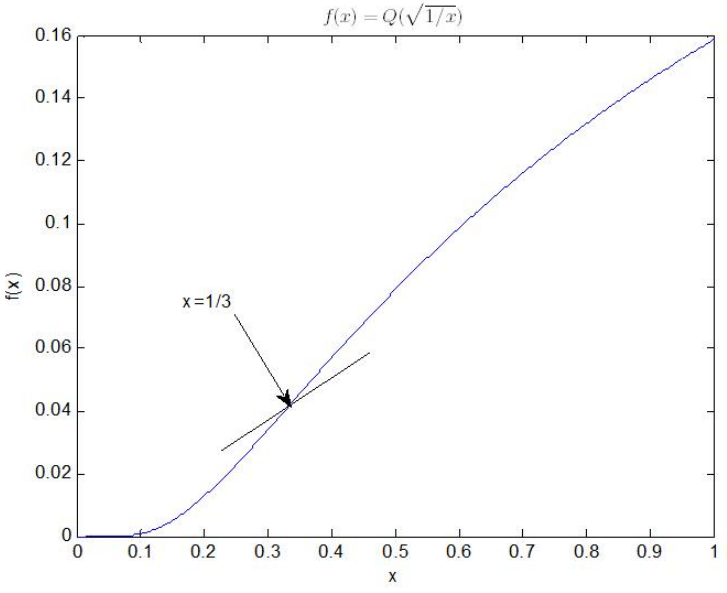

Figure 2.7 Function $f(x) = Q(\sqrt{1/x})$.

Using Jensen inequality, which states that, for a convex (concave) function f and for N numbers $x_i, i = 0, 1, \cdots, N-1$ in its domain, it follows

$$f\left(\frac{1}{N}\sum_{i=0}^{N-1} x_i\right) \leq \frac{1}{N}\sum_{i=0}^{N-1} f(x_i). \tag{2.9}$$

Let $x_i = 1/(\theta + \gamma_o|H_i|^2)$, it then follows

$$\begin{aligned} BER_{SCFDE} &= f\left(\frac{1}{N}\sum_{i=0}^{N-1} x_i\right) \\ BER_{OFDM} &= \frac{1}{N}\sum_{i=0}^{N-1} f(x_i) \end{aligned} \tag{2.10}$$

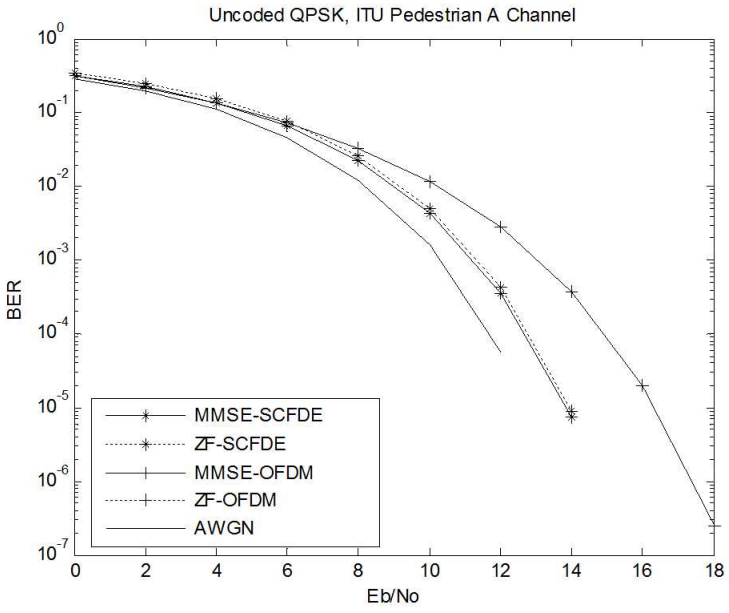

Figure 2.8 BER performance of SCFDE and OFDM in ITU Pedestrian A Channel with ZF and MMSE equalization; N=512.

Hence, using the Jensen inequality state above, $BER_{SCFDE} \leq BER_{OFDM}$ if $1/(\theta + \gamma_o|H_i|^2) < 1/3, \forall H_i$, i.e. $\gamma_o > (3-\theta)/|H_i|^2, \forall H_i$.

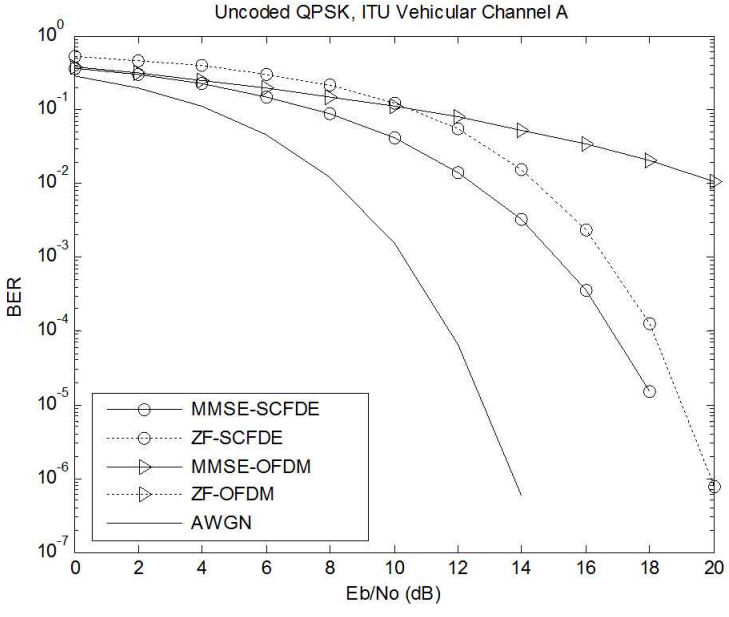

Figure 2.9 BER performance of SCFDE and OFDM in ITU Vehicular A Channel with ZF and MMSE equalization; N=512.

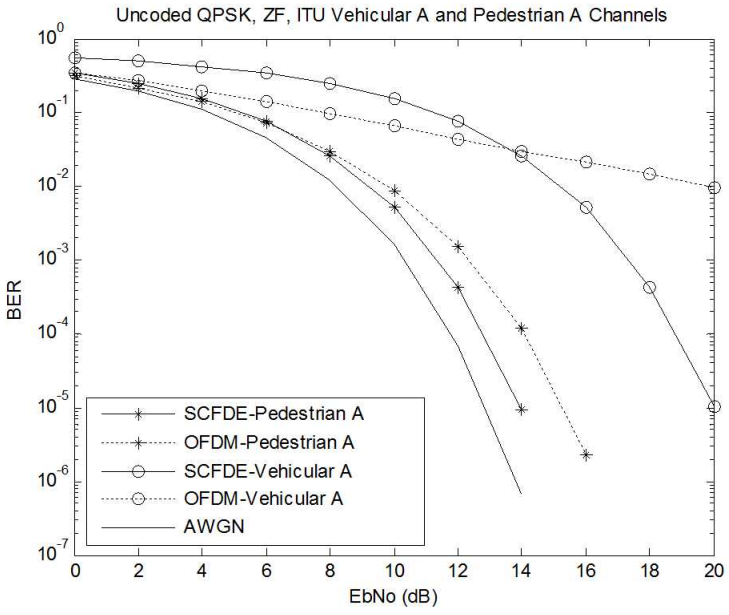

Figure 2.10 BER performance of SCFDE and OFDM in ITU Pedestrian A (Left) and Vehicular A (Right) Channel with ZF and MMSE equalization; N=512.

It is learned in this chapter that ISI can arise in a frequency selective fading channel and OFDM and SCFDE are two modulation that can effectively combat the

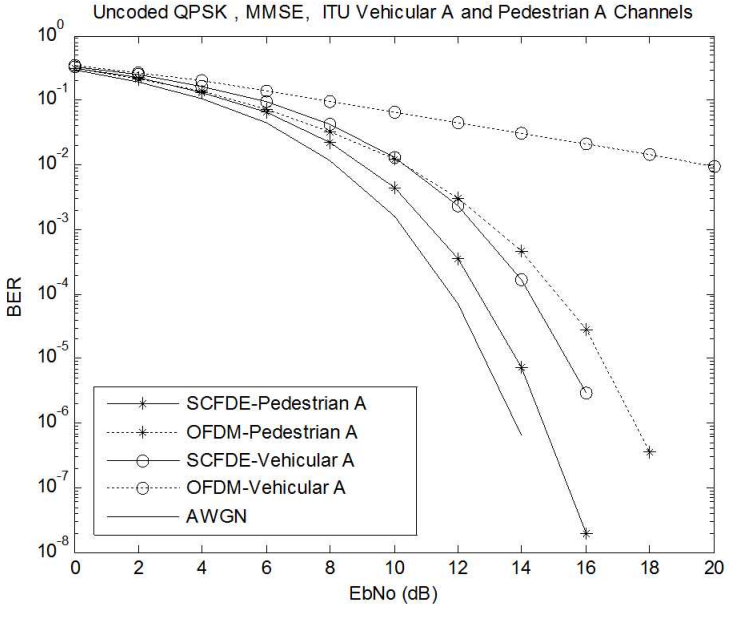

Figure 2.11 BER performance comparison of SCFDE and OFDM in ITU Pedestrian A and Vehicular A Channel with MMSE ; N=512.

ISI. OFDM and SCFDE have the overall same complexity, but OFDM due to the use of multicarrier suffers from high peak-to-average power ratio (PAPR) which can affect the performance of the system due to the non-linearity presented in the RF amplifier that are needed in the transmitter. SCFDE, because it does not use multicarrier,has low PAPR and represent an interesting alternative to OFDM in combatting the ISI in frequency selective channel. Without channel coding, when combined with MMSE, SCFDE always outperforms OFDM in all channel conditions. Hence, throughout this thesis SCFDE will be combined with MMSE and the different transceiver design.

CHAPTER 3

SINGLE USER SC-FDE WITH FEC/HARQ ON THE UPLINK OF WIRELESS COMMUNICATIONS

3.1 System Model

In this chapter a new Hybrid Automatic Repeat reQuest (HARQ) transmission scheme for a Multiple Input Multiple Output MIMO system consisting of two transmit antennas at each mobile station (MS) and M_r receive antennas at the based station (BS) in a Raleigh fading channel using SCFDE as shown in Figure 3.1 is considered. The new scheme exploits the coding gain of Alamouti Space-Time Block Coding (STBC) [18] in the packet retransmission. HARQ is employed at the symbol level instead of the bit level as it is done conventionally. The proposed HARQ scheme in slow and fast fading Rayleigh channel are presented. In slow fading it is assumed that the channel remains invariant for the duration of R transmissions while in fast fading channel, it is assumed that the channel varies from one transmission to another with a certain time correlation ρ.

In this scheme a packet is retransmitted only if the previous transmission is not successfully decoded; Alamouti space-time block coding is used in the retransmission of packets and all the received packets are combined at the symbol level using maximal ratio combining (MRC). As described in the previous section, a wireless system with U users ($U = 1$ in this chapter) each equipped with two transmit antennas transmitting to a base station equipped with M_r antennas is considered. Information bits are first encoded with a high rate code $\mathcal{C}_0$ for error detection and then with a channel code $\mathcal{C}_1$ for error correction. The coded packet denoted by $\mathbf{p}_s$ is then modulated using

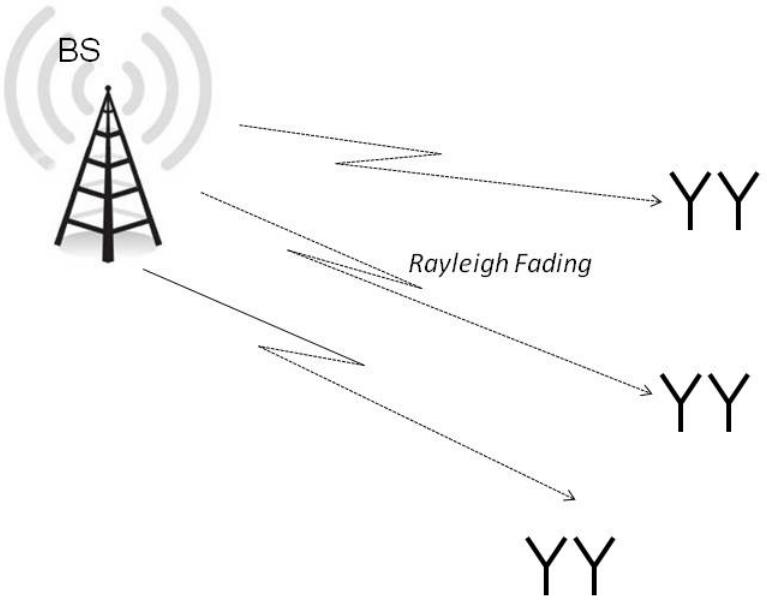

Figure 3.1 Schematic System Model.

symbols from a M-ary constellation into blocks of N [1] symbols denoted by

$$\mathbf{s} = [s_i(0), s_i(0), \cdots, s_i(N-1)]^{\mathcal{T}} \tag{3.1}$$

which is then de-multiplexed into two separate data blocks of length $N/2$ denoted by

$$\mathbf{s}_i = [s_i(0), s_i(0), \cdots, s_i(N/2-1)]^{\mathcal{T}} = \mathbf{D}_i\mathbf{s}, \quad i = 1, 2 \tag{3.2}$$

which represents the data block transmitted by the single user i^{th} antenna. $\mathbf{D}_i$ is the $N/2 \times N$ de-multiplexing matrix, i.e. pre-multiplying by $\mathbf{D}_1$ and $\mathbf{D}_2$ returns the vector of the even $(0, 2, 4, \cdots, N)$ and odd $(1, 3, 5, \cdots, N-1)$ elements of $\mathbf{s}$ respectively. The symbol period and energy are denoted by T_s and E_s respectively and the symbols of

[1] Throughout this dissertation, it is assumed than N is even and chosen to be a power of 2 to facilitate the FFT operations

$\mathbf{s}_i$ are white with covariance matrix $\mathbf{R}_s = \mathbb{E}[\mathbf{s}_i \mathbf{s}_i^{\mathcal{H}}] = E_s \mathbf{I}_{N/2}$ where $\mathbb{E}[\cdot]$ represents the expectation operation.

A cyclic prefix (CP) is added to each of the blocks $\mathbf{s}_i$ to eliminate the inter-block interference (IBI) and to make the channel matrix circulant. At the receiver, after the removal of the CP, an $N/2$-Point FFT is applied to each of the received block to transform the signals into the frequency domain (FD). The block diagram of a SCFDE is shown in Figure 2.6.

The frequency selective fading channel between the base station (BS) antenna m and the mobile station (MS) transmit antenna i during the n^{th} block transmission is denoted by L-length equivalent discrete-time channel impulse response (that includes transmit and receive filters as well as multipath effects) vector with symbol rate sampling

$$\mathbf{h}_{mi,n} = [h_{mi,n}(0), h_{mi,n}(1), \cdots, h_{mi,n}(L-1)]^{\mathcal{T}} \tag{3.3}$$

with $h_{mi,n}(l) = 0$, for $L \leq l \leq N/2 - 1$. With the CP length at least as long as the channel delay spread LT_s, the inter-block interference (IBI) can be avoided at the receiver by discarding the received samples corresponding to the CP [30].

3.2 SCFDE-HARQ in Slow Fading Channel

In the slow fading case, it is assumed that the channel does not change for the duration of R transmissions, i.e. $\mathbf{h}_{mi,n_1}$=$\mathbf{h}_{mi,n_2}, \forall n_1 \neq n_2, n_1, n_2 \leq R$. Denote by $\mathbf{s}_{i,n}$ the transmitted block by the user transmit antenna i during the n^{th} transmission. In the following, two different schemes for SCFDE/HARQ using STBC are presented and compared.

3.2.1 First Scheme of Space-Time SCFDE/HARQ

The proposed SCFDE/HARQ scheme, denoted as SCHEME I, works as follow:

During the odd n^{th}, i.e. $n = 1, 3, 5, \ldots$ transmission, the transmitted blocks by the user antenna 1 and 2 are respectively given by

$$\begin{aligned} \mathbf{s}_{1,n} &= \mathbf{s}_1 \\ \mathbf{s}_{2,n} &= \mathbf{s}_2 \end{aligned} \tag{3.4}$$

and during the next transmission i.e. $(n+1)^{th}$ which corresponds to even transmission number, the transmitted blocks by antenna 1 and 2 are respectively given by

$$\begin{aligned} \mathbf{s}_{1,(n+1)} &= -\mathbf{P}^{(1)}_{N/2}\ \mathbf{s}_2^* \\ \mathbf{s}_{2,(n+1)} &= \ \ \mathbf{P}^{(1)}_{N/2}\ \mathbf{s}_1^* \end{aligned} \tag{3.5}$$

where $\mathbf{P}^{(1)}_{N/2}$ is a $N/2 \times N/2$ permutation matrix that performs a reverse cyclic shift defined in [33], i.e.

$$\mathbf{P}^{(1)}_{N/2}\mathbf{s}_i = [s_i(0), s_i(N/2-1), s_i(N/2-2), \cdots, s_i(1)]^{\mathcal{T}}. \tag{3.6}$$

Using the DFT property, it can be easily shown that the $N/2$-point FFT of $\mathbf{s}_{i,(n+1)}$ is given by [21]

$$\begin{aligned} \mathbf{S}_{1,n+1} &= -\mathbf{S}_2^* \\ \mathbf{S}_{2,n+1} &= \ \ \mathbf{S}_1^* \end{aligned} \tag{3.7}$$

where $\mathbf{S}_i = [S_i(0), S_i(1), \cdots, S_i(N/2-1)]^T$ are the $N/2$-point FFT of $\mathbf{s}_i$.

At the BS antenna m, the received received block after the removal of the CP during the odd transmission is given by

$$\mathbf{y}_{m,n} = \mathbf{h}_{m1,n}\mathbf{s}_1 + \mathbf{h}_{m2,n}\mathbf{s}_2 + \mathbf{w}_{m,n} \tag{3.8}$$

where $\mathbf{h}_{mi,n}$ is the channel matrix which is circulant (due to the use of CP [30]) with entries $[\mathbf{h}_{mi,n}]_{p,q} = h_{mi,n}((p-q) \mod (N/2))$ and $\mathbf{w}_{m,n}$ is the additive Gaussian noise at the BS antenna m receiver front end which is assumed to be white with each entry

having a variance of $\sigma_w^2 = N_0$. The receiver then take an $N/2$-point FFT of $\mathbf{y}_{m,n}$ to yield

$$\begin{aligned} \mathbf{Y}_{m,n} &= \mathbf{\Lambda}_{m1,n}\ \mathbf{S}_1 + \mathbf{\Lambda}_{m2,n}\ \mathbf{S}_2 + \mathbf{W}_{m,n} \\ &\triangleq \mathbf{\Lambda}_{m,n}\ \mathbf{S} + \mathbf{W}_{m,n} \end{aligned} \tag{3.9}$$

where $\mathbf{W}_{m,n} = [W_{m,n}(0), W_{m,n}(1), \cdots, W_{m,n}(N/2-1)]^T$ is the $N/2$-point FFT of $\mathbf{w}_{m,n}$ and

$$\mathbf{\Lambda}_{mi,n} = \begin{bmatrix} \mathbf{H}_{mi,n}(0) & 0 & \cdots & 0 \\ 0 & \mathbf{H}_{mi,n}(1) & \cdots & 0 \\ \vdots & \cdots & \ddots & \vdots \\ 0 & \cdots & 0 & \mathbf{H}_{mi,n}(N/2-1) \end{bmatrix} \tag{3.10}$$

is a $N/2 \times N/2$ diagonal matrix with the $N/2$-point FFT of $\mathbf{h}_{mi,n}$ given by $\mathbf{H}_{m,n} = [W_{mi,n}(0), H_{mi,n}(1), \cdots, H_{mi,n}(N/2-1)]$ on the diagonal. Note that $\mathbf{\Lambda}_{mi,n}$ is diagonal because circulant matrices are diagonalized by FFT operations [34] i.e. $\mathbf{\Lambda}_{mi,n} = \mathbf{F}_{N/2}\mathbf{H}_{mi,n}\mathbf{F}_{N/2}^H$, where $\mathbf{F}_{N/2}$ represents the $N/2 \times N/2$ FFT matrix. In (3.9), the authors have defined the $N/2 \times N$ matrix $\mathbf{\Lambda}_{m,n}$ and the $N \times 1$ vector $\mathbf{S}$ as follow

$$\begin{aligned} \mathbf{\Lambda}_{m,n} &= [\mathbf{\Lambda}_{m1,n},\ \mathbf{\Lambda}_{m2,n}] \\ \mathbf{S} &= [\mathbf{S}_1^{\mathcal{T}},\ \mathbf{S}_2^{\mathcal{T}}]^{\mathcal{T}}. \end{aligned} \tag{3.11}$$

Collecting the received signal from the M_r BS antennas into a $MN/2 \times 1$ vector $\mathbf{Y}_n = [\mathbf{Y}_{1,n}^{\mathcal{T}}, \mathbf{Y}_{2,n}^{\mathcal{T}}, \cdots, \mathbf{Y}_{M_r,n}^{\mathcal{T}}]^{\mathcal{T}}$, it yields

$$\mathbf{Y}_n = \mathbf{\Lambda}_n\ \mathbf{S} + \mathbf{W}_n \tag{3.12}$$

where $\mathbf{\Lambda}_n = [\mathbf{\Lambda}_{1,n}^{\mathcal{T}}, \mathbf{\Lambda}_{2,n}^{\mathcal{T}}, \cdots, \mathbf{\Lambda}_{M_r,n}^{\mathcal{T}}]^{\mathcal{T}}$ and $\mathbf{W}_n = [\mathbf{W}_{1,n}^{\mathcal{T}}, \mathbf{W}_{2,n}^{\mathcal{T}}, \cdots, \mathbf{W}_{M_r,n}^{\mathcal{T}}]^{\mathcal{T}}$.

It is apparent from (3.12) that the symbols of $\mathbf{S}_1$ and $\mathbf{S}_2$ interfere with one another. In this case, an interference resistant receiver can be used to provide reliable soft symbol decisions for $\mathbf{S}$. Examples of interference-resistant receiver include

linear zero-forcing (ZF) and minimum mean-square error (MMSE). When additional complexity is feasible, decision feedback (iterative) receivers based on ZF and MMSE criteria can be used. Throughout this dissertation the low complexity equalizers ZF and MMSE are considered. The MMSE and ZF detection of $\mathbf{S}$ are respectively given by

$$\begin{aligned} \widehat{\mathbf{S}}_{mmse} &= [\mathbf{\Lambda}_n^{(H)}\mathbf{\Lambda}_n + (E_s/N_0)\mathbf{I}_N]^{-1}\mathbf{\Lambda}_n^{(H)}\mathbf{Y}_n \\ \widehat{\mathbf{S}}_{zf} &= [\mathbf{\Lambda}_n^{(H)}\mathbf{\Lambda}_n]^{-1}\mathbf{\Lambda}_n^{(H)}\mathbf{Y}_n \end{aligned} \tag{3.13}$$

Hence the i^{th} block $\mathbf{S}_i$ can be obtained as follow

$$\begin{aligned} \widehat{\mathbf{S}}_{1,mmse} = [\widehat{\mathbf{S}}_{mmse}(k)]_{k=0}^{N/2-1} \quad ; \quad \widehat{\mathbf{S}}_{2,mmse} = [\widehat{\mathbf{S}}_{mmse}(k)]_{k=N/2}^{N-1} \\ \widehat{\mathbf{S}}_{1,zf} = [\widehat{\mathbf{S}}_{zf}(k)]_{k=0}^{N/2-1} \quad ; \quad \widehat{\mathbf{S}}_{2,zf} = [\widehat{\mathbf{S}}_{zf}(k)]_{k=N/2}^{N-1} \end{aligned} \tag{3.14}$$

The MMSE (ZF) output $\widehat{\mathbf{S}}_{i,mmse}$ ($\widehat{\mathbf{S}}_{i,zf}$) are then transformed back to the TD where decisions are made as follow

$$\begin{aligned} \widehat{\mathbf{s}}_{i,mmse} &= \mathbf{F}_{N/2}^{\mathcal{H}}\widehat{\mathbf{S}}_{i,mmse} \\ \widehat{\mathbf{s}}_{i,zf} &= \mathbf{F}_{N/2}^{\mathcal{H}}\widehat{\mathbf{S}}_{i,zf} \end{aligned} \tag{3.15}$$

where $\mathbf{F}_{N/2}^{\mathcal{H}}$ is the $N/2\times N/2$ IFFT matrix. The detected blocks $\widehat{\mathbf{s}}_{i,mmse}$ ($\widehat{\mathbf{s}}_{i,zf}$) are then multiplexed to form the vectors $\widehat{\mathbf{s}}_{mmse}$ ($\widehat{\mathbf{s}}_{zf}$) which are fed to the channel decoder and then to the CRC decoder for errors detection. If there is no error the packet is accepted by the base station (BS) receiver and a positive Acknowledgement (ACK) is sent to the mobile user transmitter otherwise the BS receiver sends a negative Acknowledgement (NACK) to the mobile user. The mobile transmitter then retransmits the packet using Alamouti Space Time Block Coding by sending in the next transmission the blocks $\mathbf{s}_{i,n+1}$ as defined in (3.5). After removing the CP and taking the $N/2$-point FFT as in the previous transmission case, it follows

$$\mathbf{Y}_{m,n+1} = -\mathbf{\Lambda}_{m1,n+1}\ \mathbf{S}_2^* + \mathbf{\Lambda}_{m2,n+1}\ \mathbf{S}_1^* + \mathbf{W}_{m,n+1}. \tag{3.16}$$

By taking the conjugate of $\mathbf{Y}_{m,n+1}$, one can write (3.16) as

$$\begin{aligned}\mathbf{Y}^*_{m,n+1} &= -\mathbf{\Lambda}^*_{m1,n+1}\ \mathbf{S}_2 + \mathbf{\Lambda}^*_{m2,n+1}\ \mathbf{S}_1 + \mathbf{W}^*_{m,n+1} \\ &\triangleq \widetilde{\mathbf{\Lambda}}_{m,n+1}\ \mathbf{S} + \mathbf{W}^*_{m,n+1}\end{aligned} \tag{3.17}$$

where $\widetilde{\mathbf{\Lambda}}_{m,n+1} = [\mathbf{\Lambda}^*_{m2,n+1}, -\mathbf{\Lambda}^*_{m1,n+1}]$. Collecting the received signal from the M_r base station antennas into a $M_rN/2 \times 1$ vector $\mathbf{Y}_{n+1} = [\mathbf{Y}^{\mathcal{T}}_{1,n+1}, \mathbf{Y}^{\mathcal{T}}_{2,n+1}, \cdots, \mathbf{Y}^{\mathcal{T}}_{M_r,n+1}]^{\mathcal{T}}$, one gets

$$\mathbf{Y}^*_{n+1} = \widetilde{\mathbf{\Lambda}}_{n+1}\ \mathbf{S} + \mathbf{W}^*_{n+1}, \tag{3.18}$$

where $\widetilde{\mathbf{\Lambda}}_{n+1} = [\widetilde{\mathbf{\Lambda}}^{\mathcal{T}}_{1,n+1}, \widetilde{\mathbf{\Lambda}}^{\mathcal{T}}_{2,n+1}, \cdots, \widetilde{\mathbf{\Lambda}}^{\mathcal{T}}_{M,n+1}]^{\mathcal{T}}$.

The BS receiver then combines the frequency domain (FD) signal vector received at the $(n+1)^{th}$ transmission $\mathbf{Y}_{n+1}$ with that of the n^{th} transmission $\mathbf{Y}_n$ as follow

$$\begin{aligned}\mathbf{Z}_{n+1} &= \widetilde{\mathbf{\Lambda}}^{\mathcal{H}}_{n+1}\mathbf{Y}^*_{n+1} + \mathbf{\Lambda}^{\mathcal{H}}_n\mathbf{Y}_n \\ &\triangleq \mathbf{\Delta}_{n+1}\ \mathbf{S} + \mathbf{\Psi}_{n+1},\end{aligned} \tag{3.19}$$

where

$$\begin{aligned}\mathbf{\Delta}_{n+1} &= \widetilde{\mathbf{\Lambda}}^{\mathcal{H}}_{n+1}\widetilde{\mathbf{\Lambda}}_{n+1} + \mathbf{\Lambda}^{\mathcal{H}}_n\mathbf{\Lambda}_n \\ \mathbf{\Psi}_{n+1} &= \widetilde{\mathbf{\Lambda}}^{\mathcal{H}}_{n+1}\mathbf{W}^*_{n+1} + \mathbf{\Lambda}^{\mathcal{H}}_n\mathbf{W}_n.\end{aligned} \tag{3.20}$$

The MMSE and ZF detection of $\mathbf{S}$ are respectively given in this case by

$$\begin{aligned}\widehat{\mathbf{S}}_{mmse} &= [\mathbf{\Delta}^{\mathcal{H}}_{n+1}\mathbf{\Delta}_{n+1} + (E_s/N_0)\mathbf{I}_N]^{-1}\mathbf{\Delta}^{\mathcal{H}}_{n+1}\mathbf{Z}_{n+1} \\ \widehat{\mathbf{S}}_{zf} &= [\mathbf{\Delta}^{\mathcal{H}}_{n+1}\mathbf{\Delta}_{n+1}]\mathbf{\Delta}^{\mathcal{H}}_{n+1}\mathbf{Z}_{n+1}.\end{aligned} \tag{3.21}$$

As in the previous transmission, the output in (3.21) are then transformed back to time domain where decisions are made. If there is no error the packet is accepted and the BS sends a positive ACK to the mobile user otherwise the BS sends another

NACK and the mobile transmitter re-sends the packet as during the first transmission, i.e. as in Equation (3.4). The BS will then combine the three received signal vectors and proceed to detection as described above. This procedure depicted in Figure. 3.2 continues until the packet is successfully decoded or a maximum number of transmissions denoted by R is reached in which case the receiver drops all received packets and the transmitter start over by sending the same packet. In this slow fading case, it is assumed that the channel remains unchanging for the duration of the R transmissions.

Let's assume that the number of transmission until successful decoding is R_s with $R_s \leq R$.

If R_s is even, one can write (3.19) for $R_s \geq 2$ transmissions as

$$\begin{aligned} \mathbf{Z}_e &= \sum_{n=1}^{R_s/2} \widetilde{\mathbf{\Lambda}}_{2n}^{\mathcal{H}} \mathbf{Y}_{2n}^{*} + \mathbf{\Lambda}_{2n-1}^{\mathcal{H}} \mathbf{Y}_{2n-1} \\ &\triangleq \mathbf{\Delta}_e \, \mathbf{S} + \mathbf{\Psi}_e, \end{aligned} \tag{3.22}$$

where

$$\begin{aligned} \mathbf{\Delta}_e &= \sum_{n=1}^{R_s/2} \widetilde{\mathbf{\Lambda}}_{2n}^{\mathcal{H}} \widetilde{\mathbf{\Lambda}}_{2n} + \mathbf{\Lambda}_{2n-1}^{\mathcal{H}} \mathbf{\Lambda}_{2n-1} \\ \mathbf{\Psi}_e &= \sum_{n=1}^{R_s/2} \widetilde{\mathbf{\Lambda}}_{2n}^{\mathcal{H}} \mathbf{W}_{2n}^{*} + \mathbf{\Lambda}_{2n-1}^{\mathcal{H}} \mathbf{W}_{2n-1}. \end{aligned} \tag{3.23}$$

Since in the slow fading case, the channel remains the same for the duration of the R_s transmissions, one obtains $\mathbf{\Lambda}_{mi,n+1} = \mathbf{\Lambda}_{mi,n} = \mathbf{\Lambda}_{mi}$. Hence, $\mathbf{\Delta}_e$ is given by

$$\begin{aligned} \mathbf{\Delta}_e &= \sum_{n=1}^{R_s/2} \widetilde{\mathbf{\Lambda}}^{(H)} \widetilde{\mathbf{\Lambda}} + \mathbf{\Lambda}^{(H)} \mathbf{\Lambda} \\ &= \begin{bmatrix} \frac{R_s}{2} \sum_{m=1}^{M_R} |\mathbf{\Lambda}_{m1}|^2 + |\mathbf{\Lambda}_{m2}|^2 & \mathbf{0} \\ \mathbf{0} & \frac{R_s}{2} \sum_{m=1}^{M_R} |\mathbf{\Lambda}_{m1}|^2 + |\mathbf{\Lambda}_{m2}|^2 \end{bmatrix}; \end{aligned} \tag{3.24}$$

The $N \times N$ matrix $\mathbf{\Delta}_e$ is diagonal with diagonal element

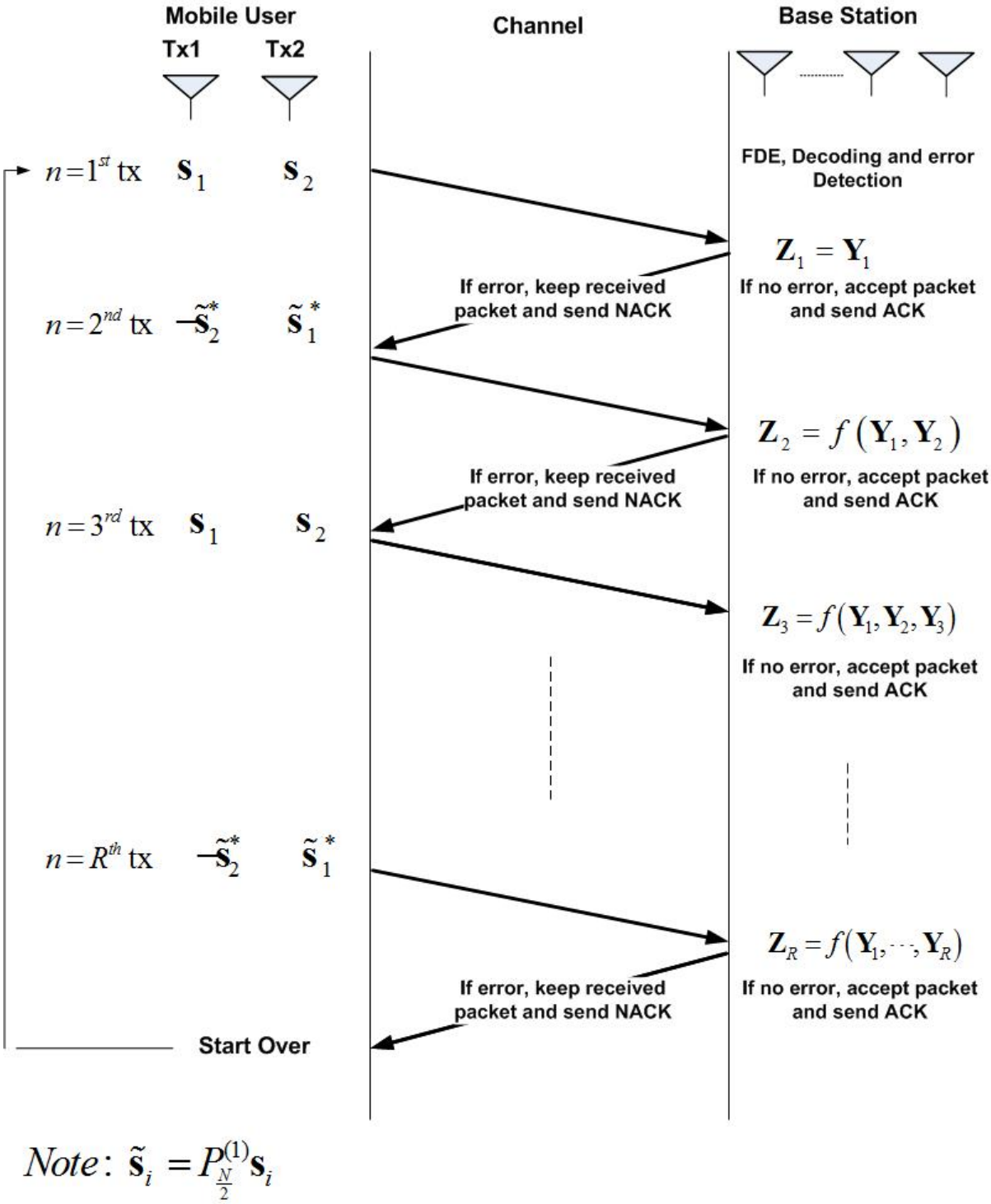

Figure 3.2 Operation of the proposed SCFDE-HARQ operation using STBC in the retransmission process; the function f represents the MRC combining of (3.19).

$\mathbf{\Delta}_e(k,k) = \frac{R_s}{2}\sum_{m=1}^{M_r} |\mathbf{H}_{m1}(k)|^2 + |\mathbf{H}_{m2}(k)|^2$. The covariance matrix of the noise component $\mathbf{\Psi}_e$ is given by

$$\begin{aligned}\mathbf{R}_{\Psi_e} &= \mathcal{E}[\mathbf{\Psi}_e \mathbf{\Psi}_e^{\mathbf{H}}] \\ &= N_0 \begin{bmatrix} \frac{R_s}{2}\sum_{m=1}^{M_r} |\mathbf{\Lambda}_{m1}|^2 + |\mathbf{\Lambda}_{m2}|^2 & \mathbf{0} \\ \mathbf{0} & \frac{R_s}{2}\sum_{m=1}^{M_r} |\mathbf{\Lambda}_{m1}|^2 + |\mathbf{\Lambda}_{m2}|^2 \end{bmatrix} \\ &= N_0 \mathbf{\Delta}_e.\end{aligned} \tag{3.25}$$

$\mathbf{R}_{\Psi_e}$ is also a diagonal matrix. When the number of transmission is even, the two transmitted symbols block from the two transmit antennas are completely decoupled and a FD $2M_r$ diversity gain can be achieved.

The MMSE and ZF detection of $\mathbf{S}$ are respectively given in this case by

$$\begin{aligned}\widehat{\mathbf{S}}_{mmse,e} &= [\mathbf{\Delta}_e^{\mathcal{H}}\mathbf{\Delta}_e + (\sigma_s^2/N_0)\mathbf{I}_N]^{-1}\mathbf{\Delta}_e^{\mathcal{H}}\mathbf{Z}_e \\ \widehat{\mathbf{S}}_{zf,e} &= [\mathbf{\Delta}_e^{\mathcal{H}}\mathbf{\Delta}_e]\mathbf{\Delta}_e^{\mathcal{H}}\mathbf{Z}_e.\end{aligned} \tag{3.26}$$

From (3.22) and (3.25), it is seen that the instantaneous signal-to-noise ratio (SNR) per subcarrier $k, k = 0, 1, \cdots, N/2$ is given by

$$\Gamma_e(k) = \gamma_o(R_s/2)\sum_{m=1}^{M_r} |\mathbf{H}_{m1}(k)|^2 + |\mathbf{H}_{m2}(k)|^2 \tag{3.27}$$

where $\gamma_o = \sigma_s^2/N_0$.

The FD estimated are then converted back into TD when detection is done. It follows

$$\begin{aligned}\widehat{\mathbf{s}}_{i,mmse,e} &= F_{N/2}\ \widehat{\mathbf{S}}_{i,mmse,e} \\ \widehat{\mathbf{s}}_{i,zf,e} &= F_{N/2}\ \widehat{\mathbf{S}}_{i,zf,e}.\end{aligned} \tag{3.28}$$

The output SNR can be found as

$$\begin{aligned}\gamma_{zf,e} &= \frac{1}{\frac{1}{N}\sum_{k=0}^{N/2-1}\frac{1}{\Gamma_e(k)}} \\ \gamma_{mmse,e} &= \frac{1}{\frac{1}{N}\sum_{k=0}^{N/2-1}\frac{1}{(1+\Gamma_e(k))}}\end{aligned} \tag{3.29}$$

In brief, when the number of transmissions is even in a slowly varying channel when the channel remains constant for the duration of all transmissions, the proposed HARQ system provide a FD $2M_r$ diversity gain.

If R_s is odd, one can write (3.19) for $R_s > 1$ transmissions as

$$\begin{aligned}\mathbf{Z}_o &= \mathbf{\Lambda}_{R_s}^{\mathcal{H}}\mathbf{Y}_{R_s} + \sum_{n=1}^{(R_s-1)/2}\widetilde{\mathbf{\Lambda}}_{2n}^{\mathcal{H}}\mathbf{Y}_{2n}^{*} + \mathbf{\Lambda}_{2n-1}^{\mathcal{H}}\mathbf{Y}_{2n-1} \\ &\triangleq \mathbf{\Delta}_o\,\mathbf{S} + \mathbf{\Psi}_o,\end{aligned} \tag{3.30}$$

where

$$\begin{aligned}\mathbf{\Delta}_o &= \mathbf{\Lambda}_{R_s}^{\mathcal{H}}\mathbf{\Lambda}_{R_s} + \sum_{n=1}^{(R_s-1)/2}\widetilde{\mathbf{\Lambda}}_{2n}^{\mathcal{H}}\widetilde{\mathbf{\Lambda}}_{2n} + \mathbf{\Lambda}_{2n-1}^{\mathcal{H}}\mathbf{\Lambda}_{2n-1} \\ \mathbf{\Psi}_o &= \mathbf{\Lambda}_{R_s}^{\mathcal{H}}\mathbf{W}_{R_s} + \sum_{n=1}^{(R_s-1)/2}\widetilde{\mathbf{\Lambda}}_{2n}^{\mathcal{H}}\mathbf{W}_{2n}^{*} + \mathbf{\Lambda}_{2n-1}^{\mathcal{H}}\mathbf{W}_{2n-1}.\end{aligned} \tag{3.31}$$

Since in the slow fading case, the channel remains the same for the duration of the $R_s > 1$ transmissions, one gets $\mathbf{\Lambda}_{mi,n+1} = \mathbf{\Lambda}_{mi,n} = \mathbf{\Lambda}_{mi}$. it follows that $\mathbf{\Delta}_o$ is given by

$$
\begin{aligned}
\boldsymbol{\Delta}_o &= \boldsymbol{\Lambda}^{(H)}\boldsymbol{\Lambda} + \sum_{n=1}^{(R_s-1)/2} \widetilde{\boldsymbol{\Lambda}}^{(H)}\widetilde{\boldsymbol{\Lambda}} + \boldsymbol{\Lambda}^{(H)}\boldsymbol{\Lambda} \\
&= \begin{bmatrix} \boldsymbol{\Lambda}_{11}^* & \boldsymbol{\Lambda}_{21}^* & \cdots & \boldsymbol{\Lambda}_{M1}^* \\ \boldsymbol{\Lambda}_{12}^* & \boldsymbol{\Lambda}_{22}^* & \cdots & \boldsymbol{\Lambda}_{M2}^* \end{bmatrix} \begin{bmatrix} \boldsymbol{\Lambda}_{11} & \boldsymbol{\Lambda}_{12} \\ \boldsymbol{\Lambda}_{21} & \boldsymbol{\Lambda}_{22} \\ \vdots & \vdots \\ \boldsymbol{\Lambda}_{M1} & \boldsymbol{\Lambda}_{M2} \end{bmatrix} \\
&\quad + \sum_{n=1}^{(R_s-1)/2} \begin{bmatrix} \boldsymbol{\Lambda}_{12} & \boldsymbol{\Lambda}_{22} & \cdots & \boldsymbol{\Lambda}_{M2} \\ -\boldsymbol{\Lambda}_{11} & -\boldsymbol{\Lambda}_{21} & \cdots & -\boldsymbol{\Lambda}_{M1} \end{bmatrix} \begin{bmatrix} \boldsymbol{\Lambda}_{12}^* & -\boldsymbol{\Lambda}_{11}^* \\ \boldsymbol{\Lambda}_{22}^* & -\boldsymbol{\Lambda}_{21}^* \\ \vdots & \vdots \\ \boldsymbol{\Lambda}_{M2}^* & -\boldsymbol{\Lambda}_{M1}^* \end{bmatrix} \\
&\quad + \begin{bmatrix} \boldsymbol{\Lambda}_{11}^* & \boldsymbol{\Lambda}_{21}^* & \cdots & \boldsymbol{\Lambda}_{M1}^* \\ \boldsymbol{\Lambda}_{12}^* & \boldsymbol{\Lambda}_{22}^* & \cdots & \boldsymbol{\Lambda}_{M2}^* \end{bmatrix} \begin{bmatrix} \boldsymbol{\Lambda}_{11} & \boldsymbol{\Lambda}_{12} \\ \boldsymbol{\Lambda}_{21} & \boldsymbol{\Lambda}_{22} \\ \vdots & \vdots \\ \boldsymbol{\Lambda}_{M1} & \boldsymbol{\Lambda}_{M2} \end{bmatrix} \\
&= \begin{bmatrix} \frac{R_s+1}{2}\sum_{m=1}^{M_R} |\boldsymbol{\Lambda}_{m1}|^2 + \frac{R_s-1}{2}\sum_{m=1}^{M_R} |\boldsymbol{\Lambda}_{m2}|^2 & \sum_{m=1}^{M_R} \boldsymbol{\Lambda}_{m1}\boldsymbol{\Lambda}_{m2}^* \\ \sum_{m=1}^{M_R} \boldsymbol{\Lambda}_{m1}^*\boldsymbol{\Lambda}_{m2} & \frac{R_s-1}{2}\sum_{m=1}^{M_R} |\boldsymbol{\Lambda}_{m1}|^2 + \frac{R_s+1}{2}\sum_{m=1}^{M_R} |\boldsymbol{\Lambda}_{m2}|^2 \end{bmatrix}
\end{aligned}
\tag{3.32}
$$

The covariance matrix of the noise component $\boldsymbol{\Psi}_o$ is given by

$$
\begin{aligned}
\mathbf{R}_{\Psi_o} &= \mathcal{E}[\boldsymbol{\Psi}_o \boldsymbol{\Psi}_o^{\mathbf{H}}] \\
&= N_0 \begin{bmatrix} \frac{R_s+1}{2}\sum_{m=1}^{M_r} |\boldsymbol{\Lambda}_{m1}|^2 + \frac{R_s-1}{2}\sum_{m=1}^{M_r} |\boldsymbol{\Lambda}_{m2}|^2 & \sum_{m=1}^{M_r} \boldsymbol{\Lambda}_{m1}\boldsymbol{\Lambda}_{m2}^* \\ \sum_{m=1}^{M_r} \boldsymbol{\Lambda}_{m1}^*\boldsymbol{\Lambda}_{m2} & \frac{R_s-1}{2}\sum_{m=1}^{M_r} |\boldsymbol{\Lambda}_{m1}|^2 + \frac{R_s+1}{2}\sum_{m=1}^{M_r} |\boldsymbol{\Lambda}_{m2}|^2 \end{bmatrix} \\
&= N_0 \boldsymbol{\Delta}_o.
\end{aligned}
\tag{3.33}
$$

When the number of transmission is odd, the transmitted symbols block from the two transmit antennas interfere with one another. The ZF equalizer will completely remove the interference while the MMSE equalizer will minimize the noise variance and leave some residual interference. The MMSE and ZF detection of $\mathbf{S}$ are respectively given in this case by

$$\begin{aligned}\widehat{\mathbf{S}}_{mmse,o} &= [\mathbf{\Delta}_o^{\mathcal{H}}\mathbf{\Delta}_o + (\sigma_s^2/N_0)\mathbf{I}_N]^{-1}\mathbf{\Delta}_o^{\mathcal{H}}\mathbf{Z}_o \\ \widehat{\mathbf{S}}_{zf,o} &= [\mathbf{\Delta}_o^{\mathcal{H}}\mathbf{\Delta}_o]\mathbf{\Delta}_o^{\mathcal{H}}\mathbf{Z}_o.\end{aligned} \tag{3.34}$$

The instantaneous signal-to-interference-noise ratio (SINR) per subcarrier $k, k = 0, 1, \cdots, N/2$ is given in this case by

$$\Gamma_o(k) = \frac{\gamma_o\left[\frac{R_s+1}{2}\sum_{m=1}^{M_r}|\mathbf{H}_{m1}(k)|^2 + \frac{R_s-1}{2}\sum_{m=1}^{M_r}|\mathbf{H}_{m2}(k)|^2\right]^2}{\frac{R_s+1}{2}\sum_{m=1}^{M_r}|\mathbf{H}_{m1}(k)|^2 + \frac{R_s-1}{2}\sum_{m=1}^{M_r}|\mathbf{H}_{m2}(k)|^2 + \gamma_o\left[\sum_{m=1}^{M_r}\mathbf{H}_{m1}(k)\mathbf{H}_{m2}^*(k)\right]^2} \tag{3.35}$$

where $\gamma_o = \sigma_s^2/N_0$ and the output SINR is given by the output SNR can be found as

$$\begin{aligned}\gamma_{zf,o} &= \frac{1}{\frac{1}{N}\sum_{k=0}^{N/2-1} 1/\left(\Gamma_o(k)\right)} \\ \gamma_{mmse,o} &= \frac{1}{\frac{1}{N}\sum_{k=0}^{N/2-1} 1/\left(1+\Gamma_o(k)\right)}.\end{aligned} \tag{3.36}$$

The FD estimated are then converted back into time domain when detection is done. The BER and throughput performance of Scheme I are depicted in Figure 3.3.

3.2.2 Throughput Analysis

The throughput depicted in Figure 3.3 is now defined in this section. Define the throughput (in bit per second (bps)) as the number of information bits which are correctly received divided by the total time (in seconds) it took the transmit them. Since each packet is composed of N information symbols, for a M-ary constellation, the number of information bits is given by $Nlog_2(M)$. If it takes R_s transmissions to successfully decode a packet, hence, the total time it takes is given by $R_s(N/2 +$

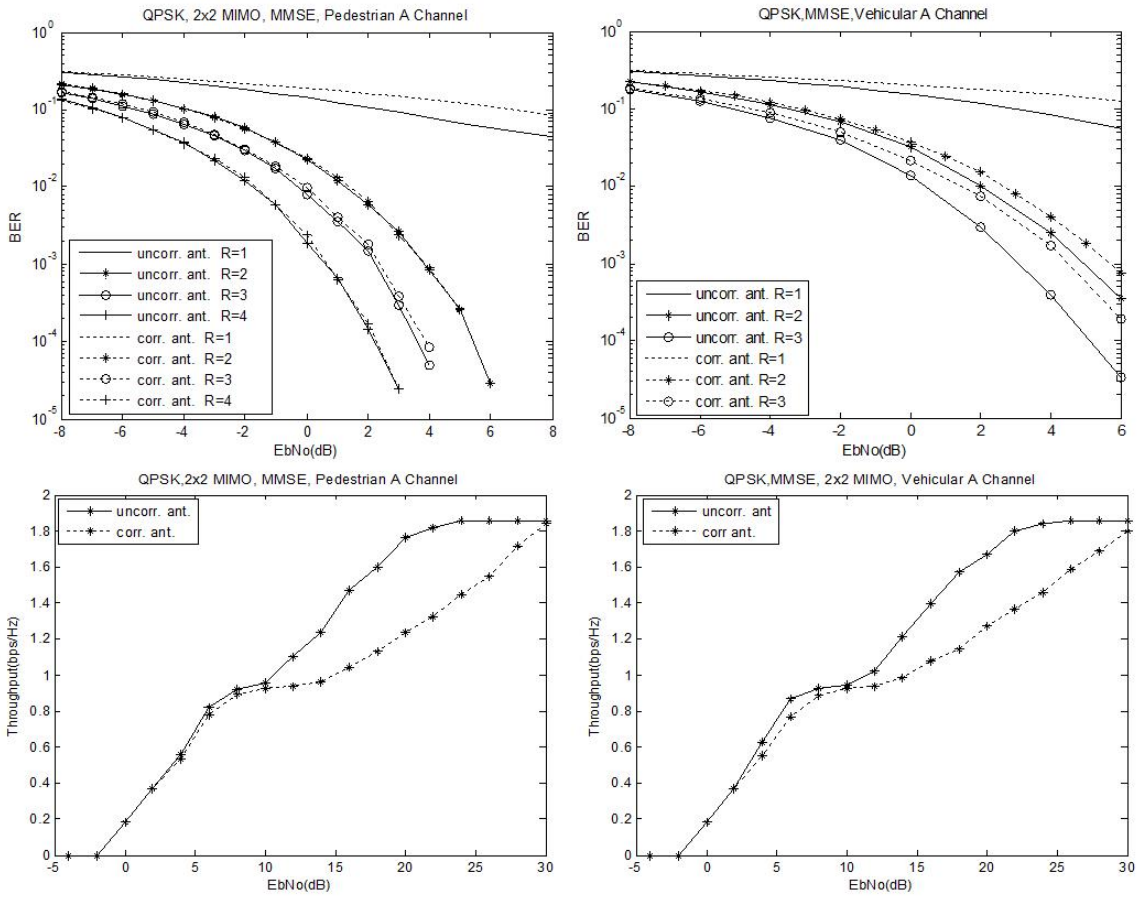

Figure 3.3 Performance of the proposed SCFDE/HARQ denoted SCHEME I in a time invariant fading channel; Top: BER performance, bottom: throughput performance.

$N_{cp})T_s$ where N_{cp} and T_s are the number of symbol in the CP and the symbol period respectively. Applying the BER obtained above for different modulation schemes, one can derive the system throughput for a M-ary constellation as

$$\eta = \frac{Nlog_2(M)}{\left(\sum_{n=1}^{R} nP_s^{(n)}\right)(N/2 + N_{cp})T_s} \tag{3.37}$$

where $P_s^{(n)}$ is the probability of packet success at the n^{th} trial given by

$$P_s^{(n)} = (1 - P_f^{(n)})\Pi_{j=1}^{n-1} P_f^{(j)} \tag{3.38}$$

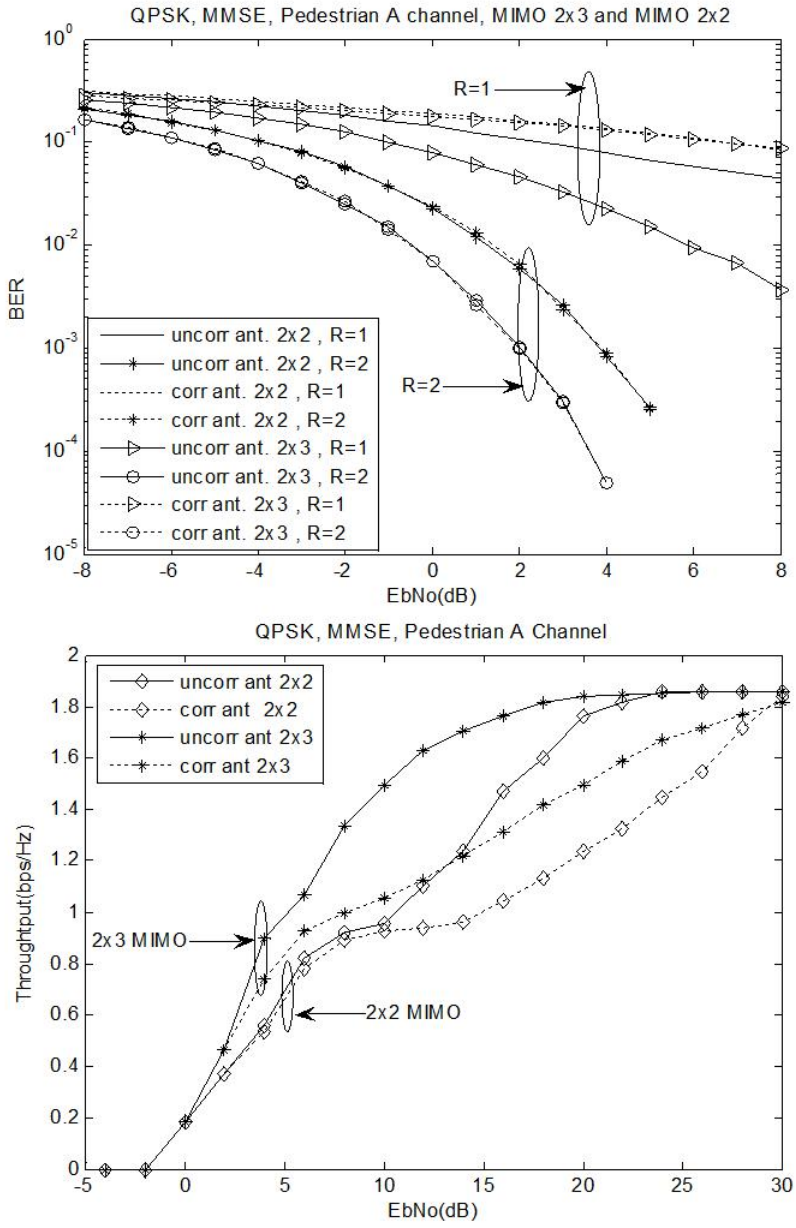

Figure 3.4 Performance of the proposed SCFDE/HARQ denoted SCHEME I in a time invariant fading channel for 2×2 and 2×3 MIMO system; Top: BER performance, bottom: throughput performance.

where $nP_s^{(n)}$ is the probability of packet failure at the n^{th} trial. For an uncoded system, the probability of packet failure is given by $P_f^{(n)} = [1 - P_e(\gamma)]^N$ where $P_e(\gamma)$ is the BER for a given SNR γ.

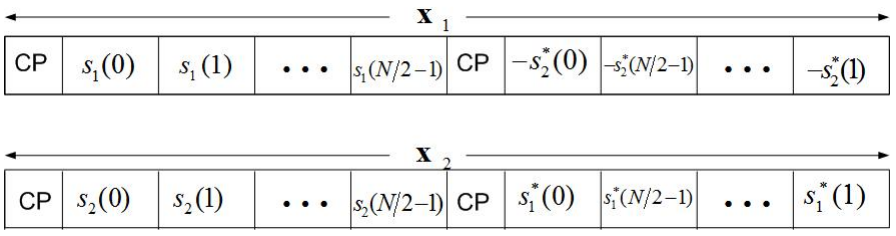

Figure 3.5 The block structure of the STBC SCFDE-HARQ second scheme.

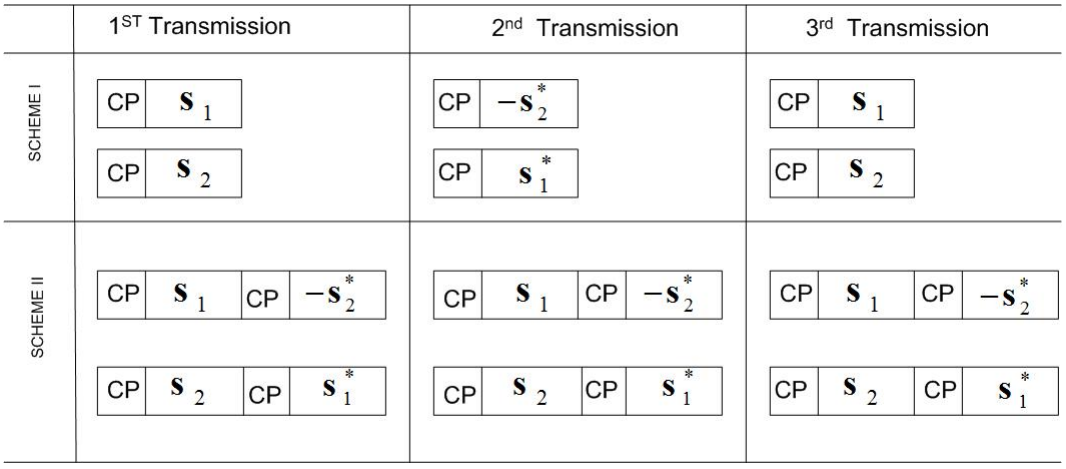

Figure 3.6 The block Diagrams of the proposed SCFDE/HARQ denoted Scheme I and Scheme II.

3.2.3 Second Scheme of Space-Time SCFDE/HARQ

The second scheme, called as SCHEME II, applies HARQ to the conventional STBC where the space-time block consisting of redundant symbols is sent in the first transmission as follow. The MS transmitter first forms the STBC blocks

$$\begin{aligned} \mathbf{x}_1 &= [\mathbf{T}_{cp}\mathbf{s}_1, -\mathbf{T}_{cp}\mathbf{P}_{N/2}\mathbf{s}_2^*]^{\mathcal{T}} \\ \mathbf{x}_2 &= [\mathbf{T}_{cp}\mathbf{s}_2,\ \mathbf{T}_{cp}\mathbf{P}_{N/2}\mathbf{s}_1^*]^{\mathcal{T}}, \end{aligned} \tag{3.39}$$

where $\mathbf{T}_{cp}$ is the CP insertion matrix. Note that the duration of a transmitted block in the second scheme is double of that of the first scheme as shown in Figure 3.5 and the HARQ operation of both scheme is depicted in Figure 3.6.

In comparing both schemes, the authors choose in the simulation of SCHEME II, a block size that is half of that of the first scheme in order to have the same data rate.

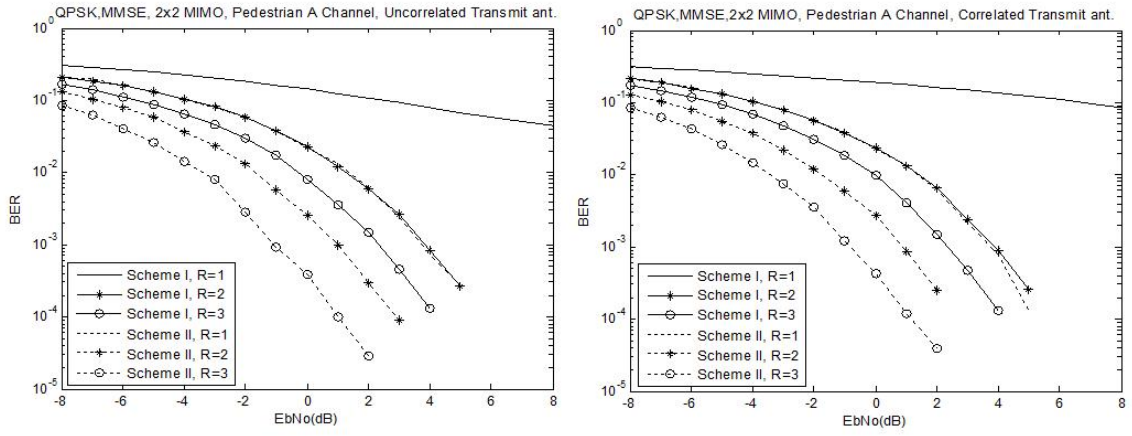

Figure 3.7 Performance comparison of Scheme I and Scheme II in a Pedestrian slow fading channel.

The MS transmitter will transmit the block $\mathbf{x}_i$ in 3.39 for the i^{th} transmitted antenna in every transmission. In the second scheme, the whole STBC block is transmitted in a single transmission. At the receiver, after removing the CP's the received blocks are transformed into the FD to yield (see (3.12))

$$\begin{aligned} \mathbf{Y}_{1,n} &= \mathbf{\Lambda}_{1,n}\mathbf{S}_1 + \mathbf{\Lambda}_{2,n}\mathbf{S}_2 + \mathbf{W}_{1,n} \\ \mathbf{Y}_{2,n} &= -\mathbf{\Lambda}_{1,n}\mathbf{S}_2^* + \mathbf{\Lambda}_{2,n}\mathbf{S}_1^* + \mathbf{W}_{2,n} \end{aligned} \tag{3.40}$$

where $\mathbf{Y}_{1,n}$ and $\mathbf{Y}_{2,n}$ correspond to the first and second half of the transmitted blocks $\mathbf{x}_i$ respectively and $\mathbf{W}_{i,n}$ is the FD AWGN. By letting $\mathbf{Z}_n = [\mathbf{Y}_{1,n}^{\mathcal{T}}, \mathbf{Y}_{2,n}^{\mathcal{H}}]^{\mathcal{T}}$, one can write (3.40) as

$$\mathbf{Z}_n = \mathbf{\Delta}_n\mathbf{S} + \mathbf{W}_n \tag{3.41}$$

where

$$\mathbf{\Delta}_n = \begin{bmatrix} \mathbf{\Lambda}_{1,n} & \mathbf{\Lambda}_{2,n} \\ \mathbf{\Lambda}_{2,n}^* & -\mathbf{\Lambda}_{1,n}^* \end{bmatrix}. \tag{3.42}$$

The matrix is easily shown to be orthogonal. The MMSE and ZF receivers yield

$$\begin{aligned} \widehat{\mathbf{S}}_{mmse} &= [\boldsymbol{\Delta}^{\mathcal{H}}\boldsymbol{\Delta} + (\sigma_s^2/N_0)\mathbf{I}_N]^{-1}\boldsymbol{\Delta}^{\mathcal{H}}\mathbf{Z} \\ \widehat{\mathbf{S}}_{zf} &= [\boldsymbol{\Delta}^{\mathcal{H}}\boldsymbol{\Delta}]\boldsymbol{\Delta}^{\mathcal{H}}\mathbf{Z}. \end{aligned} \tag{3.43}$$

which are then transformed back into the TD for detection. If error is detected, the BS send a NACK to the MS which then retransmitted the blocks exactly as in the first transmission. MRC is used at the BS to combine all the received block as in the previous scheme. One can easily see that the BER performance of this scheme is the same as that of the previous scheme with even number of transmission. The performances of SCHEME II are shown in Figure 3.8 and the throughput comparison of both schemes is depicted in Figure 3.9.

It can be seen that in low SNR regions, the throughput of both schemes are the same , however in high SNR regions, the throughput of Scheme I is much better. This is because in high SNR, only a single transmission is needed to decode the packet successfully hence, sending the STBC block is not necessary and in consequence one looses in throughput. We can conclude that it's always better to use SCHEME I in slow fading channels.

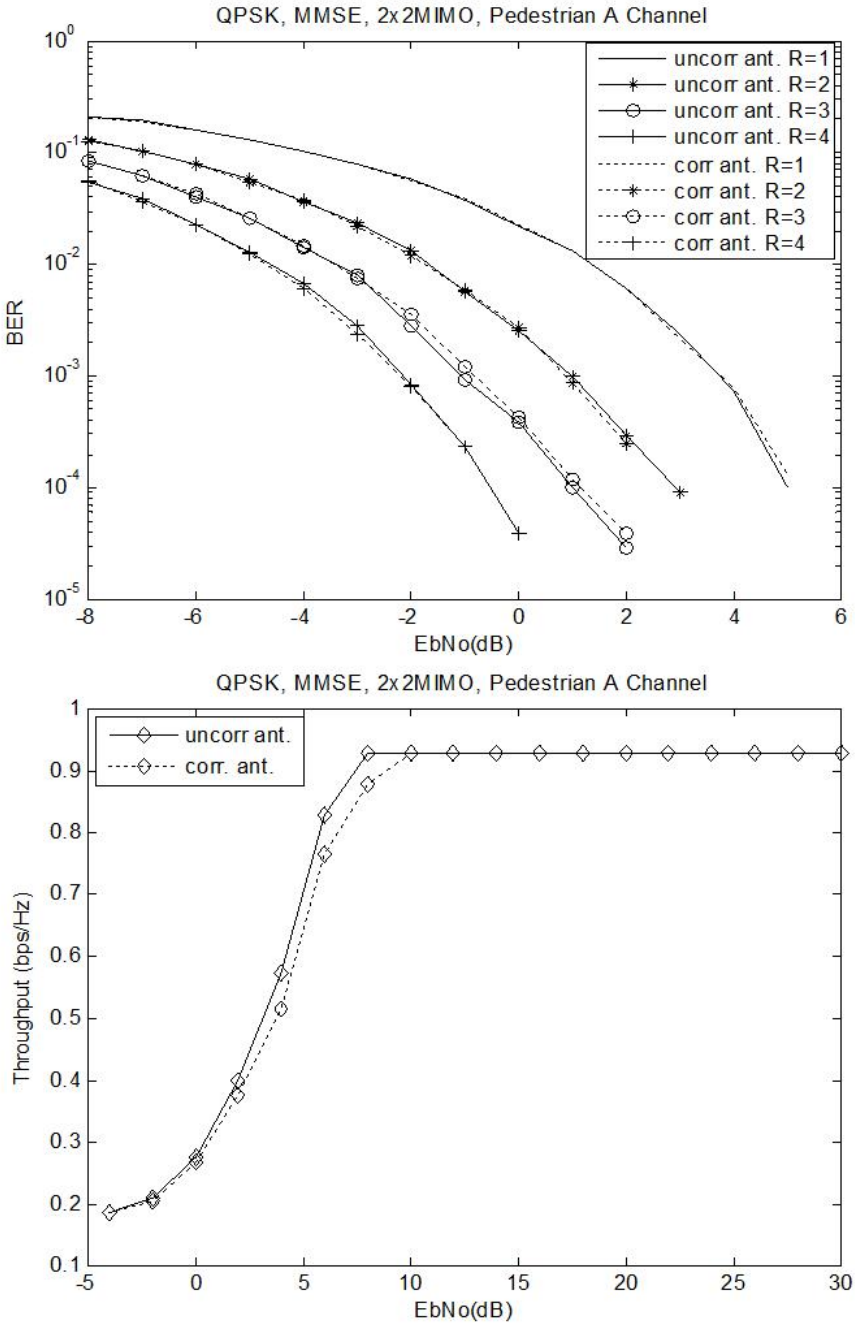

Figure 3.8 Performance of the proposed SCFDE/HARQ denoted SCHEME II in a time invariant fading channel; Top: BER performance, bottom: Throughput performance.

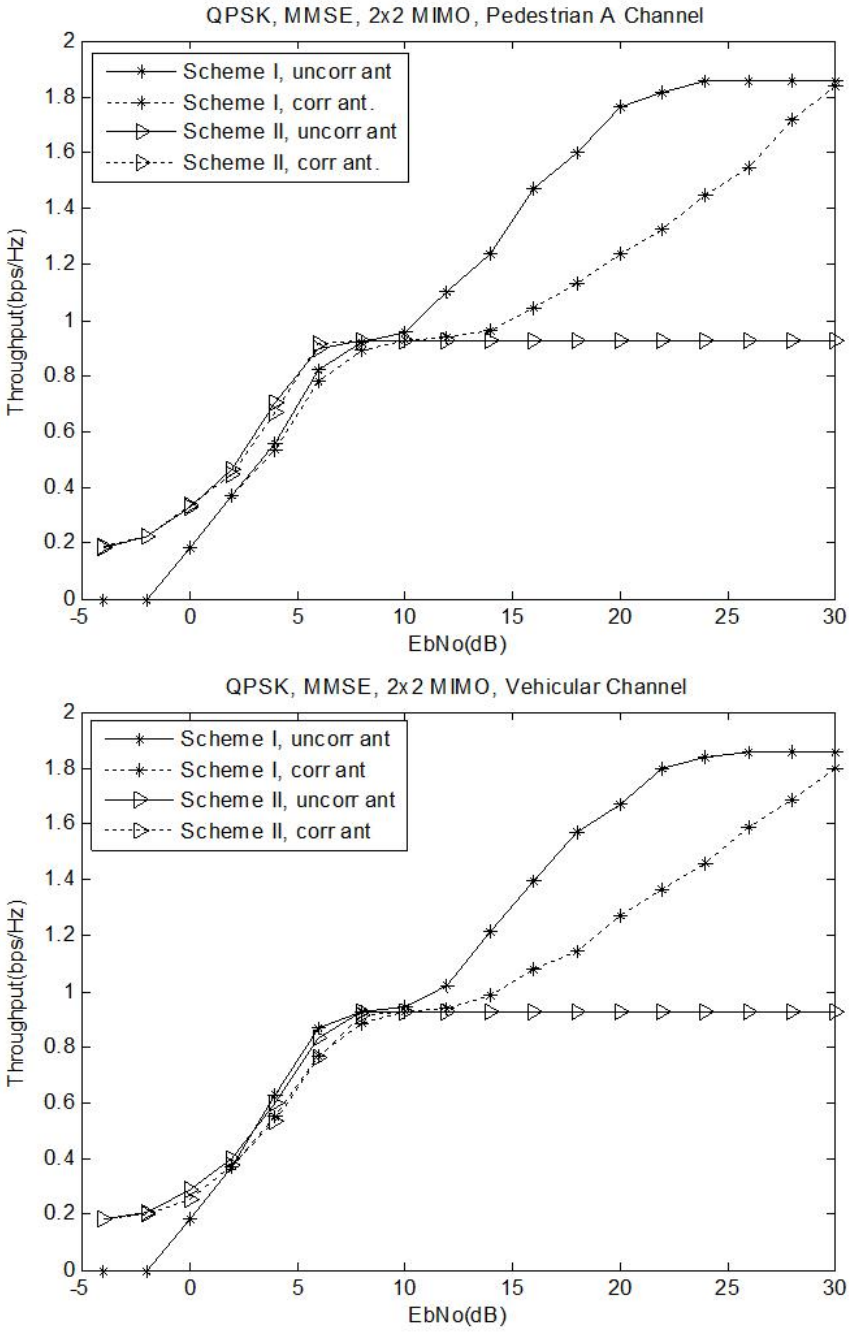

Figure 3.9 Throughput comparison of Scheme I and Scheme II in a Pedestrian A slow fading channel.

3.3 SCFDE-HARQ in Fast Fading Channel

In the fast fading channel case, it is assumed that the channel changes from one transmission to another for the duration of R transmissions. Consider a Rayleigh fading and the channel correlation ρ between two consecutive transmissions is modeled by the zeroth-order Bessel function of the first kind, i.e. $\rho = J(2\pi f_d T)$, which is derived from Jake's model [26], with f_d being the maximum Doppler frequency and T the time duration between two consecutive transmission. With the above assumption, it follows

$$E[h_{mi,n}(l)h^*_{mi,n+k}(l)] = \rho^k. \tag{3.44}$$

3.3.1 Space-Time SCFDE/HARQ Scheme I

In Scheme I, after R_s transmissions, one can rewrite (3.19) as

$$\begin{aligned}\mathbf{Z}_{R_s} &= \sum_{n=1}^{R_s} \alpha_n \widetilde{\mathbf{\Lambda}}^{\mathcal{H}}_{n+1} \mathbf{Y}^*_{n+1} + \beta_n \mathbf{\Lambda}^{\mathcal{H}}_n \mathbf{Y}_n \\ &\triangleq \mathbf{\Delta}_v\, \mathbf{S} + \mathbf{\Psi}_v,\end{aligned} \tag{3.45}$$

where

$$\begin{aligned}\mathbf{\Delta}_v &= \sum_{n=1}^{R_s} \alpha_n \widetilde{\mathbf{\Lambda}}^{\mathcal{H}}_{n+1} \widetilde{\mathbf{\Lambda}}_{n+1} + \beta_n \mathbf{\Lambda}^{\mathcal{H}}_n \mathbf{\Lambda}_n \\ \mathbf{\Psi}_v &= \sum_{n=1}^{R_s} \alpha_n \widetilde{\mathbf{\Lambda}}^{\mathcal{H}}_{n+1} \mathbf{W}^*_{n+1} + \beta_n \mathbf{\Lambda}^{\mathcal{H}}_n \mathbf{W}_n \\ \alpha_n &= \frac{(1+(-1)^n)}{2} \\ \beta_n &= \frac{(1-(-1)^n)}{2}.\end{aligned} \tag{3.46}$$

It can be shown that

$$\mathbf{\Delta}_v = \begin{bmatrix} \mathbf{\Delta}_{v,11} & \mathbf{\Delta}_{v,12} \\ \mathbf{\Delta}^*_{v,12} & \mathbf{\Delta}_{v,22} \end{bmatrix}. \tag{3.47}$$

where

$$\begin{aligned}
\mathbf{\Delta}_{v,11} &= \sum_{n=1}^{R_s}\sum_{m=1}^{M_r} \beta_n |\mathbf{\Lambda}_{m1,n}|^2 + \alpha_n |\mathbf{\Lambda}_{m2,n+1}|^2 \\
\mathbf{\Delta}_{v,12} &= \sum_{n=1}^{R_s}\sum_{m=1}^{M_r} \beta_n \mathbf{\Lambda}_{m1,n}\mathbf{\Lambda}^*_{m2,n} - \alpha_n \mathbf{\Lambda}_{m1,n+1}\mathbf{\Lambda}^*_{m2,n+1} \\
\mathbf{\Delta}_{v,22} &= \sum_{n=1}^{R_s}\sum_{m=1}^{M_r} \alpha_n |\mathbf{\Lambda}_{m1,n+1}|^2 + \beta_n |\mathbf{\Lambda}_{m2,n}|^2
\end{aligned} \tag{3.48}$$

are all $N/2 \times N/2$ diagonal matrices.

If $\rho = 1$, i.e. when the channel is invariant, the results are the ones derived from the previous section. If $\rho \neq 1$, one can see from (3.48) that the off diagonal elements $\mathbf{\Delta}_{v,12}$ of $\mathbf{\Delta}_v$ are non-zero, hence the time varying channel introduces interference between the the transmitted blocks from the two transmitted antennas . One can also note that one obtains a spatial and time diversity gain. Hence the time varying channel introduces both interference and diversity gain and because one also obtain spatial gain due to the use of two transmit antennas, the overall diversity gain overcome the the interference between the transmit symbols and the gain increase as the correlation coefficient ρ decreases.

3.3.2 Space-Time SCFDE/HARQ Scheme II

From the slow fading channel case, notice that the received block after the n^{th} and $(n+1)^{th}$ transmissions are given by

$$\begin{aligned}
\mathbf{Z}_n &= \mathbf{\Delta}_n \mathbf{S} + \mathbf{W}_n \\
\mathbf{Z}_{n+1} &= \mathbf{\Delta}_{n+1} \mathbf{S} + \mathbf{W}_{n+1}
\end{aligned} \tag{3.49}$$

where

$$\mathbf{\Delta}_n = \begin{bmatrix} \mathbf{\Lambda}_{1,n} & \mathbf{\Lambda}_{2,n} \\ \mathbf{\Lambda}^*_{2,n} & -\mathbf{\Lambda}^*_{1,n} \end{bmatrix}. \tag{3.50}$$

For R transmissions, let $\mathbf{Z} = [\mathbf{Z}_1^{\mathcal{T}}, \mathbf{Z}_2^{\mathcal{T}}, \cdots, \mathbf{Z}_R^{\mathcal{T}}]^{\mathcal{T}}$, it follows

$$\mathbf{Z} = \mathbf{\Delta S} + \mathbf{W} \tag{3.51}$$

where $\mathbf{\Delta} = [\mathbf{\Delta}_1^{\mathcal{T}}, \mathbf{\Delta}_2^{\mathcal{T}}, \cdots, \mathbf{\Delta}_R^{\mathcal{T}}]^{\mathcal{T}}$ and $\mathbf{W} = [\mathbf{W}_1^{\mathcal{T}}, \mathbf{W}_2^{\mathcal{T}}, \cdots, \mathbf{W}_R^{\mathcal{T}}]^{\mathcal{T}}$.

It can be easily shown that

$$\mathbf{\Delta} = \begin{bmatrix} \sum_{n=1}^{R} \sum_{m=1}^{M_r} |\mathbf{\Lambda}_{m1,n}|^2 + |\mathbf{\Lambda}_{m2,n}|^2 & \mathbf{0}_{N/2 \times N/2} \\ \mathbf{0}_{N/2 \times N/2} & \sum_{n=1}^{R} \sum_{m=1}^{M_r} |\mathbf{\Lambda}_{m1,n}|^2 + |\mathbf{\Lambda}_{m2,n}|^2. \end{bmatrix} \tag{3.52}$$

Hence, one can see that there is no interference between the transmitted symbol and that one achieves both time and spatial diversity that can be up to $2M_rR$ when the channel correlation if $\rho = 0$, i.e. independent channel at each transmission.

3.3.3 Proposed SFBC-SCFDE HARQ Scheme for Fast Fading Channel

In the proposed scheme for fast fading channel, the authors first repeat the symbol block $\mathbf{s}_i$ to yield the $N \times 1$ block $\mathbf{v}_i, i = 1, 2$

$$\mathbf{v}_i = \frac{1}{\sqrt{2}} \left[\mathbf{u}_i^{\mathcal{T}}, \mathbf{u}_i^{\mathcal{T}}\right]^{\mathcal{T}}. \tag{3.53}$$

where

$$\begin{aligned} \mathbf{u}_1 &= [s_1(0), -s_2^*(0), s_1(1), -s_2^*(N/2-1), \ldots, s_1(N/2-2), -s_2^*(2), s_1(N/2-1), -s_2^*(1)]^{\mathcal{T}} \\ \mathbf{u}_2 &= [s_2(0), \quad s_1^*(0), s_2(1), \quad s_1^*(N/2-1), \ldots, s_2(N/2-2), \quad s_1^*(2), s_2(N/2-1), \quad s_1^*(1)]^{\mathcal{T}}. \end{aligned} \tag{3.54}$$

The factor $1/\sqrt{2}$ is to keep the power the same after the repetition. It will be shown in the followings that the repetition of $\mathbf{s}_i$ is instrumental in having in the frequency domain at the receiver $\{S_i(k)\}_{k=0}^{N/2-1}, i{=}1, 2$ on even subcarriers and $\{\pm S_i^*(k)\}_{k=0}^{N/2-1}, i{=}1, 2$ on odd subcarriers so that Alamouti SFBC can be applied.

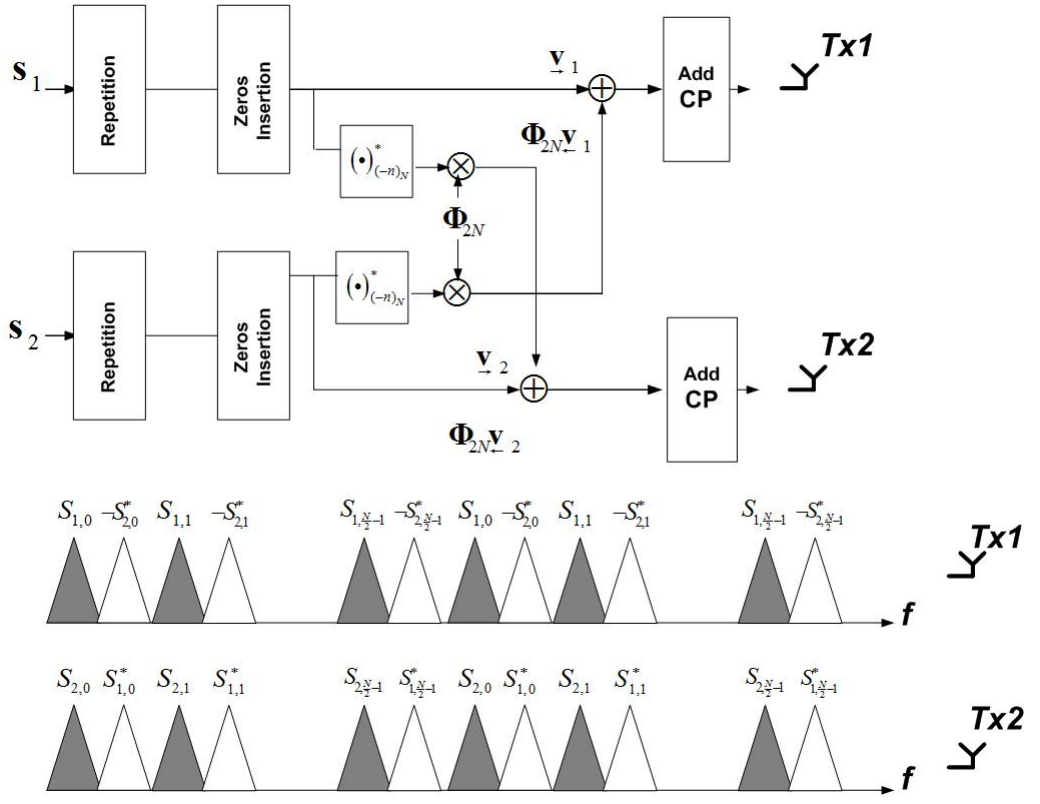

Figure 3.10 Diagram of the proposed SCFDE-SFBC for fast fading channel.

Finally, define the $2N$ symbols blocks $\underrightarrow{\mathbf{v}}_i$ ($\underleftarrow{\mathbf{v}}_i$), i=1, 2, by making the odd (even) elements of $\mathbf{v}_i$ zeros as follow

$$\begin{aligned}
\underrightarrow{\mathbf{v}}_i &= \sqrt{1/2}\,[s_i(0), 0, s_i(1), 0, \ldots, s_i(N/2-1), 0, \quad s_i(0), 0, s_i(1), 0, \ldots, s_i(N/2-1), 0]^{\mathcal{T}} \\
\underleftarrow{\mathbf{v}}_i &= \sqrt{1/2}\,[0, s_\nu^*(0), 0, s_\nu^*(N/2-1), \ldots, 0, s_\nu^*(1), \quad 0, s_\nu^*(0), 0, s_\nu^*(N/2-1), \ldots, 0, s_\nu^*(1)]^{T} \\
&\quad \times (-1)^k,
\end{aligned} \tag{3.55}$$

whose $\nu = k - (-1)^k$, $2N$-point DFT $\underrightarrow{\mathbf{V}}_i$ and ($\underleftarrow{\mathbf{V}}_i$) are given by

$$\begin{aligned}
\underrightarrow{\mathbf{V}}_i &= \sqrt{1/2}\,[S_i(0), 0, \ldots, S_i(N/2-1), 0, \quad S_i(0), 0, \ldots, S_i(N/2-1), 0]^{\mathcal{T}} \\
\underleftarrow{\mathbf{V}}_i &= \sqrt{1/2}\boldsymbol{\Phi}_{2N}\,[S_\nu^*(0), 0, \ldots, S_\nu^*(N/2-1), 0, \quad S_\nu^*(0), 0, \ldots, S_\nu^*(N/2-1), 0]^{\mathcal{T}} \times (-1)^i
\end{aligned} \tag{3.56}$$

where $\mathbf{\Phi}_{2N}$ =diag $\left\{1, e^{\frac{j2\pi}{2N}}, e^{\frac{j2\pi 2}{2N}}, \ldots, e^{\frac{j2\pi(2N-1)}{2N}}\right\}$. The multiplication by $\mathbf{\Phi}_{2N}$ in (3.56) resulted from the shifting property of DFT. Note that the zeros between the elements of $\underrightarrow{\mathbf{V}}_i$ and $\underleftarrow{\mathbf{V}}_i$ are due to the repetition in (3.53). Their presence in the odd index of $\underleftarrow{\mathbf{V}}_i$ allows us to shift the conjugate symbols $\{\pm S_i^*(m)\}_{m=0}^{N/2-1}$ currently located at the even index of $\underleftarrow{\mathbf{V}}_i$ to these odd index positions without interfering with the non-conjugate symbols $\{S_i(m)\}_{m=0}^{N/2-1}$ so that even and odd subcarriers can be used in SFBC. In order to shift the conjugate symbols to the odd index, one just needs to multiply the time domain conjugate symbols $\underleftarrow{\mathbf{v}}_i$, by a phase shift vector. Hence the transmitted signal by the i^{th}, $i = 1, 2$ transmit antenna is constructed as follow

$$\mathbf{x}_i = \underrightarrow{\mathbf{v}}_i + \mathbf{\Phi}_{2N}\underleftarrow{\mathbf{v}}_i. \tag{3.57}$$

The block diagram of the proposed scheme is shown in Figure 3.10. Note that the size of the transmitted block $\mathbf{x}_i$ is $2N$, hence the rate of the proposed system is $1/2$ since $2N$ symbols are transmitted for N information bearing symbols. This reduction in rate, as will be shown later in this section, comes with a frequency diversity gain as the symbols are repeated in the FD on different subcarriers. Note also that the transmitted signals $\mathbf{x}_i, i$=1, 2 have constant amplitude which is the main contribution of this scheme as it implements single carrier SFBC with low PAPR (0dB PAPR for M-PSK symbols as opposed to the 3dB PAPR of the scheme in [35] where instead of interleaving the symbols are added to one another resulting in non-constant amplitude signal transmitted). The bandwidth B of $\mathbf{x}_i$ is determined approximately by the symbol duration $T_s/2$ and is given by B=$2/T_s$. A cyclic prefix (CP) is added to each block $\mathbf{x}_i$ before transmitting through the frequency selective fading channel. After the removal of the CP and taking a $2N$-point DFT, the received signal block is given by

$$\mathbf{Y} = \sum_{i=1}^{2} \mathbf{\Lambda}_i \mathbf{X}_i + \mathbf{W}, \tag{3.58}$$

where $\mathbf{\Lambda}_i$, i=1, 2 represent diagonal matrices whose elements are the $2N$-point DFT of the corresponding CIR $\mathbf{h}_i$. $\mathbf{X}_i$ and $\mathbf{W}$ represents the $2N$-point DFT of $\mathbf{x}_i$ and $\mathbf{w}$ (the complex AWGN noise vector at the input of the receiver with variance N_0) respectively. From (6.1), $\mathbf{X}_i$ can be written as

$$\mathbf{X}_i = \underrightarrow{\mathbf{V}}_i + \widetilde{\underleftarrow{\mathbf{V}}}_i, \tag{3.59}$$

where $\underrightarrow{\mathbf{V}}_i$ and $\widetilde{\underleftarrow{\mathbf{V}}}_i$ represent the $2N$-point DFT of $\underrightarrow{\mathbf{v}}_i$ and $(\mathbf{\Phi}_{2N}\underleftarrow{\mathbf{v}}_i)$ respectively. Note that $\widetilde{\underleftarrow{\mathbf{V}}}_i$ is equal to $\underleftarrow{\mathbf{V}}_i$ shifted forward one element as follow

$$\widetilde{\underleftarrow{\mathbf{V}}}_k = \sqrt{1/2}\underleftarrow{\mathbf{\Phi}}_{2N}\left[0, S^*_\nu(0), \ldots, 0, S^*_\nu(N/2-1), \quad 0, S^*_\nu(0), 0, \ldots, 0, S^*_\nu(N/2-1)\right]^T \times (-1)^k \tag{3.60}$$

where $\underleftarrow{\mathbf{\Phi}}_{2N} = \mathrm{diag}\left\{0, 1, e^{\frac{j2\pi}{2N}}, e^{\frac{j2\pi 2}{2N}}, \ldots, e^{\frac{j2\pi(2N-2)}{2N}}\right\}$.

Define $\mathbf{V}_{i,e}$ and $\mathbf{V}_{i,o}$ to be N symbols vectors containing the even and odd elements of a $2N$ symbols vector $\mathbf{V}_i$ respectively. it follows $\underrightarrow{\mathbf{V}}_{i,o}= \mathbf{0}_N$ and $\widetilde{\underleftarrow{\mathbf{V}}}_{i,e}= \mathbf{0}_N$. Hence from (3.56), (3.60) and (3.59) it can be easily shown that

$$\begin{aligned}
\mathbf{X}_{i,e} &= \underrightarrow{\mathbf{V}}_{i,e} + \widetilde{\underleftarrow{\mathbf{V}}}_{i,e} = \sqrt{1/2}[\mathbf{S}_i^T, \mathbf{S}_i^T]^T \\
\mathbf{X}_{i,o} &= \underrightarrow{\mathbf{V}}_{i,o} + \widetilde{\underleftarrow{\mathbf{V}}}_{i,o} = (-1)^i\sqrt{1/2}\mathbf{\Phi}_N[\mathbf{S}_\nu^H, \mathbf{S}_\nu^H]^T,
\end{aligned} \tag{3.61}$$

where $\mathbf{\Phi}_N$ =diag $\left\{1, e^{\frac{j2\pi}{N}}, e^{\frac{j2\pi 2}{N}}, \ldots, e^{\frac{j2\pi(N-1)}{N}}\right\}$ is a $N\times N$ diagonal matrix whose diagonal elements are the odd diagonal elements of $\underleftarrow{\mathbf{\Phi}}_{2N}$ and ν=i−$(-1)^i$, i=1, 2. Note from Equation (3.61) that the proposed scheme achieves a second-order frequency diversity due to the symbol repetition (the repeated symbols are separated by N subcarriers) in the frequency domain. This frequency diversity gain comes with the assumption that the coherence bandwidth of the channel $1/T_m$ [36] (where T_m denotes the maximum delay spread of the channel) is less than the bandwidth of N subcarriers, i.e. the repeated symbols experience independent fading. Since there is a total of $2N$ subcarriers, the subcarrier spacing is given by $B/(2N)$=$1/(NT_s)$ hence the frequency domain spacing between the repeated symbols is given by $1/T_s$. The assumption

for the second-order frequency diversity is then always satisfied if $(1/T_s)>(1/T_m)$ i.e. $T_s<T_m$. Hence in order to achieve the second-order frequency diversity gain, one need to choose T_s such that $T_s<T_m$ a regular and simple assumption.

Note from (3.61) that $\mathbf{X}_{1,o}= -\mathbf{\Phi}_N\mathbf{X}^*_{2,e}$ and $\mathbf{X}_{2,o}= \mathbf{\Phi}_N\mathbf{X}^*_{1,e}$. Hence (4.12) can then be rewritten as

$$\begin{aligned}\mathbf{Y}_e &= \mathbf{\Lambda}_{1,e}\mathbf{X}_{1,e} + \mathbf{\Lambda}_{2,e}\mathbf{X}_{2,e} + \mathbf{W}_e \\ \mathbf{Y}_o &= \mathbf{\Lambda}_{1,o}\mathbf{X}_{1,o} + \mathbf{\Lambda}_{2,o}\mathbf{X}_{2,o} + \mathbf{W}_o \\ &= -\mathbf{\Lambda}_{1,o}\mathbf{\Phi}_N\mathbf{X}^*_{2,e} + \mathbf{\Lambda}_{2,o}\mathbf{\Phi}_N\mathbf{X}^*_{1,e} + \mathbf{W}_o,\end{aligned} \tag{3.62}$$

where $\mathbf{\Lambda}_{i,e}$ and $\mathbf{\Lambda}_{i,o}$ are diagonal matrices whose diagonal elements are the even and odd diagonal elements of $\mathbf{\Lambda}_i$ respectively. it is assumed that the channel gains for adjacent subcarriers are approximately equal[2], i.e. $\mathbf{\Lambda}_{i,e} \approx \mathbf{\Lambda}_{i,o},\ i{=}1,2$. Using (3.61) i.e. $\mathbf{X}_{i,e}{=}\sqrt{1/2}[\mathbf{S}_i^T, \mathbf{S}_i^T]^T$, and taking the conjugate of the second equation of (3.62), it can be written in matrix form as

$$\mathbf{Z} = \mathbf{\Lambda}\mathbf{S} + \widetilde{\mathbf{W}}, \tag{3.63}$$

where $\mathbf{Z}{=}\left[\mathbf{Y}_e^T, \mathbf{Y}_o^{*T}\right]^T$, $\mathbf{S}{=}\left[\mathbf{S}_1^T, \mathbf{S}_2^T\right]^T$, $\widetilde{\mathbf{W}}{=}\left[\mathbf{W}_e^T\mathbf{W}_o^{*T}\right]^T$,

$\mathbf{\Lambda} = \sqrt{1/2}\begin{bmatrix} \mathbf{\Lambda}^1_{1,e} & \mathbf{\Lambda}^1_{2,e} \\ \mathbf{\Lambda}^2_{1,e} & \mathbf{\Lambda}^2_{2,e} \\ \mathbf{\Phi}^{1*}_N\mathbf{\Lambda}^{1*}_{2,o} & -\mathbf{\Phi}^{1*}_N\mathbf{\Lambda}^{1*}_{1,o} \\ \mathbf{\Phi}^{2*}_N\mathbf{\Lambda}^{2*}_{2,o} & -\mathbf{\Phi}^{2*}_N\mathbf{\Lambda}^{2*}_{1,o} \end{bmatrix}$, and $\mathbf{\Lambda}^1_{i,e}$ ($\mathbf{\Lambda}^2_{i,e}$) is $N \times N$ diagonal matrix whose diagonal elements are the first (second) N diagonal elements of $\mathbf{\Lambda}_{i,e}$. Similarly $\mathbf{\Phi}^1_N$ ($\mathbf{\Phi}^2_N$) is a $N \times N$ diagonal matrix whose diagonal elements are the first (second) N diagonal elements of $\mathbf{\Phi}_N$. The minimum mean square error (MMSE) receiver yield:

$$\widehat{\mathbf{S}}_{mmse} = \left[\mathbf{\Lambda}^H\mathbf{\Lambda} + \frac{1}{\mathrm{SNR}}\mathbf{I}_{2N}\right]^{-1}\mathbf{\Lambda}^H\mathbf{Z}, \tag{3.64}$$

[2]This assumption is less restrictive than assuming that the channel remains the same for at least two blocks, hence enabling application in fast fading channels

where SNR=σ_s^2/N_0. It can be easily shown that the matrix $\mathbf{\Lambda}^H\mathbf{\Lambda}$ is diagonal and given by

$$\mathbf{\Lambda}^H\mathbf{\Lambda} = \begin{bmatrix} |\mathbf{\Delta}_1|^2 & \mathbf{0} \\ \mathbf{0} & |\mathbf{\Delta}_2|^2 \end{bmatrix}, \tag{3.65}$$

where

$$\begin{aligned} |\mathbf{\Delta}_1|^2 &= \frac{1}{2}\left(\left|\mathbf{\Lambda}^1_{1,e}\right|^2 + \left|\mathbf{\Lambda}^2_{1,e}\right|^2 + \left|\mathbf{\Lambda}^1_{2,o}\right|^2 + \left|\mathbf{\Lambda}^2_{2,o}\right|^2\right) \\ |\mathbf{\Delta}_2|^2 &= \frac{1}{2}\left(\left|\mathbf{\Lambda}^1_{2,e}\right|^2 + \left|\mathbf{\Lambda}^2_{2,e}\right|^2 + \left|\mathbf{\Lambda}^1_{1,o}\right|^2 + \left|\mathbf{\Lambda}^2_{1,o}\right|^2\right). \end{aligned} \tag{3.66}$$

One can see that $\mathbf{S_1}$ and $\mathbf{S_2}$ are completely decoupled. The estimates in (7.10) are transformed back in time domain for detection. From (4.36), it can be seen that our scheme provides a fourth-order diversity gain (assuming $T_s<T_m$) as opposed to the second-order diversity achieved by the SC-SFBC scheme of [35] and SF-OFDM of [37]. This difference is due to the additional frequency domain diversity exploited by the proposed scheme at the expense of reducing the rate to 1/2.

CHAPTER 4

MULTIUSER SC-FDE WITH FEC/HARQ ON THE UPLINK OF WIRELESS COMMUNICATIONS

In the previous chapter, SCFDE/HARQ schemes have been proposed for single user system. In this chapter, the authors evaluate the performance of the proposed scheme when more than one user is present in the system. It is assumed that a total U simultaneous users transmitting at any given time. Each user is equipped with two transmit antennas and the BS has M_r receive antennas. For the sake of notation simplicity, it is assumed going forward that $M_r = 1$. The extension of the result for $M_r > 1$ is straightforward as done in the single user case.

It is well known that users can be separated in either time, frequency, code or spatial domain. Our goal in this thesis is to design a transmitter that can transmit with low PAPR using SCFDE in multiuser environment. Two approaches are proposed as follow. The first one uses spreading code to separate the users on the uplink while maintaining multiuser interference MUI-free detection at the BS. The second approach use frequency or subcarriers separation. Both approaches will be combined with transmit diversity to exploit the spatial diversity of the channel. The proposed code domain separation that achieve MUI-free system is based on block spreading [19] which will be presented in the next section.

4.1 Symbol Block Spreading

Consider a symbol block of N symbols $\mathbf{s} = [s(0), s(1), \cdots, s(N-1)]^{\mathcal{T}}$ and a spreading code of length G $\mathbf{c} = [c(0), c(1), \cdots, c(G-1)]^{\mathcal{T}}$.

In the conventional symbol spreading, each symbol is spread by the spreading code $\mathbf{c}$ to yield the $NG \times 1$ block

$$\mathbf{x} = [s(0)c(0), \cdots, s(0)c(G-1), \cdots, s(N-1)c(0), \cdots, s(N-1)c(G-1)]^{\mathcal{T}}. \quad (4.1)$$

When multiple users user this approach to transmit their symbols as done in the conventional CDMA, this results in MUI at the receiver.

In the new symbol spreading, the whole block $\mathbf{s}$ is spread by the spreading code $\mathbf{c}$ to yield

$$\mathbf{x} = [c(0)s(0), \cdots, c(0)s(N-1), \cdots, c(G-1)s(0), \cdots, c(G-1)s(N-1)]^{\mathcal{T}}. \quad (4.2)$$

In multiuser system, in order to avoid MUI at the receiver, a CP is inserted between each chip-subblock as depicted in Figure 4.1

The block spreading operation can be obtained mathematically as $\mathbf{x} = (\mathbf{c} \otimes \mathbf{T}_{cp})\mathbf{s}$ where $\mathbf{T}_{zp} = [\mathbf{I}_{cp}^{\mathcal{T}}, \mathbf{I}_K]^{\mathcal{T}}$ is the $(K+L) \times K$ CP matrix that appends the CP to each chip-subblock and $\mathbf{I}_{cp}$ denotes the matrix formed by the last L rows of $\mathbf{I}_K$ [19]. L is assumed to be longer the maximum delay spread of the channel.

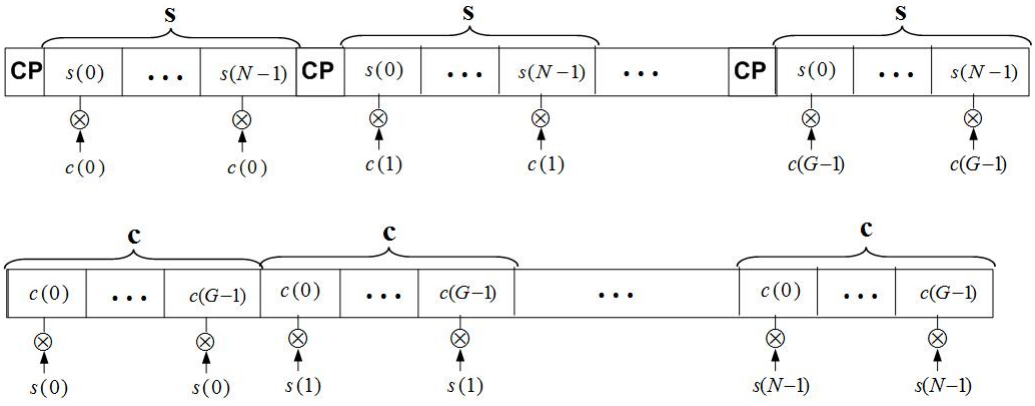

Figure 4.1 Block diagram of the block spreading (Top) and symbol spreading in conventional CDMA (Bottom).

In a multiuser system with U users, the user u transmitted chips-block is then given by the $(N+L)G \times 1$ vector $\mathbf{x}_u$ given by

$$\mathbf{x}_u = (\mathbf{c}^{(u)} \otimes \mathbf{T_{cp}})\mathbf{s}_u \tag{4.3}$$

where $\mathbf{T_{cp}}$ is the CP matrix given by $\mathbf{T_{cp}} = [\mathbf{J}_{cp}^T, \mathbf{I}_N]^T$; $\mathbf{J}_{cp}$ is a $L \times N$ matrix formed by the last L rows of the identity matrix $\mathbf{I}_N$. The CP eliminates the IBI but also turn the linear convolution of the channel and the transmit signal into a circular one [30]. The chips-block $\mathbf{x}_u$ propagates through the multipath fading channel with CIR $\mathbf{h}^{(u)}(n)= \left[h_0^{(u)}(n), h_1^{(u)}(n), \ldots, h_{L-1}^{(u)}(n)\right]^{\mathcal{T}}$. After removing the CP from the received $(N+L)G \times 1$ chips-block one gets the chip-rate $NG \times 1$ vector

$$\mathbf{y}(n) = \sum_{u=1}^{U} \mathbf{x}^{(u)} \star \mathbf{h}^{(u)}(n) + \mathbf{w}(n), \forall n \in [0, NG-1] \tag{4.4}$$

where $\mathbf{w}$ denotes the sampled zero-mean AWGN noise and $\star$ represents the circular convolution operation. Note that the linear convolution has been turned into a circular one with the removal of the CP [30].

4.1.1 Slow Fading Case

In a slow fading channel, i.e., the channel is invariant for the duration of the $(N+L)GT_c$ chips-block duration (which is the assumption in CIBS-CDMA, i.e. $\mathbf{h}_u(n) = \mathbf{h}_u$), a block de-spreading is performed for user u to yield the $N \times 1$ symbol block as follow [19], [38]

$$\begin{aligned} \mathbf{z}^{(u)} &= \left(\mathbf{c}^{(u)\mathcal{H}} \otimes \mathbf{I}_N\right) \mathbf{y} \\ &= \left(\mathbf{c}^{(u)\mathcal{H}} \otimes \mathbf{I}_N\right) \sum_{v=1}^{U} \left(\mathbf{c}_v \otimes (\mathbf{s}_v \star \mathbf{h}_v)\right) + \mathbf{w} \\ &= \mathbf{s}^{(u)} \star \mathbf{h}^{(u)} + \mathbf{w}^{(u)} \end{aligned} \tag{4.5}$$

where $\mathbf{y}=[\mathbf{y}(0),\ldots,\mathbf{y}(NG-1)]^T$ and $\mathbf{w}^{(u)}=(\mathbf{c}^{(u)\mathcal{H}}\otimes\mathbf{I}_N)\mathbf{w}$ and the following identity of the kronecker product has been used

$$(\mathbf{A}_1\otimes\mathbf{A}_2)(\mathbf{B}_1\otimes\mathbf{B}_2)=\mathbf{A}_1\mathbf{B}_1\otimes\mathbf{A}_2\mathbf{B}_2, \tag{4.6}$$

and $\mathbf{c}^{(u)\mathcal{H}}\mathbf{c}_v=\delta(u-v)$. Note also that in the second equation of (4.5), the authors have used the fact that after removing the cyclic prefix, $(\mathbf{c}^{(u)}\otimes\mathbf{T}_{cp})\mathbf{s}^{(u)}\star\mathbf{h}$ is reduced to $\mathbf{c}^{(u)}\otimes(\mathbf{s}^{(u)}\star\mathbf{h})$ (this can easily been shown). In the slow fading channel case, each chips-subblock goes through the same channel $\mathbf{h}^{(u)}$. The receiver then takes an N-point DFT of $\mathbf{z}^{(u)}$ to obtain the $N\times 1$ frequency domain vector

$$\mathbf{Z}^{(u)}=\mathbf{H}^{(u)}\mathbf{S}^{(u)}+\mathbf{W}^{(u)}, \tag{4.7}$$

where $\mathbf{Z}^{(u)}$, $\mathbf{S}^{(u)}$ and $\mathbf{W}^{(u)}$ are the N-point DFT of $\mathbf{z}^{(u)}$, $\mathbf{s}^{(u)}$ and $\mathbf{w}^{(u)}$ respectively and $\mathbf{H}_u$ is a diagonal matrix with diagonal elements the N-point DFT of $\mathbf{h}_u$. One can see from (4.7) that the de-spreading operation completely eliminate the MUI. This is because the channel is invariant ($\mathbf{h}^{(u)}(n)=\mathbf{h}^{(u)}$) for the duration of the block and the users spreading code are mutually orthogonal. The frequency domain equalization is then performed using linear single user MMSE or ZF as follow

$$\widehat{\mathbf{S}}^{(u)}=\left(\mathbf{H}^{(u)\mathcal{H}}\mathbf{H}^{(u)}+\alpha(N_o/E_s)\mathbf{I}_N\right)^{-1}\mathbf{H}^{(u)\mathcal{H}}\mathbf{Z}^{(u)}, \tag{4.8}$$

where α=1 for MMSE and α=0 for ZF receivers. The estimated frequency domain symbols $\widehat{\mathbf{S}}^{(u)}$ are then transformed into the time domain for detection.

Note that block spreading does not provide any frequency diversity. It purpose is to allow deterministic user separation with MUI-free detection at the receiver. In order to achieve frequency diversity, block spreading with zero insertion is used as follow. The authors insert $Q-1$ zeros between each chip of $\mathbf{x}^{(u)}$ in Equation (4.2) to yield the vector $\widetilde{\mathbf{x}}^{(u)}$ of length NGQ chips. In order to keep the total duration the same, the authors first compress each chip from duration T_s/G to $T_s/(GQ)$. This

compression will expand the bandwidth of the transmitted Q times. One should choose G and Q such that $GQ/T_s \leq Bw$ where Bw is the total available bandwidth. The principle of diversity gain through zeros insertion is shown in Figure 4.2. Since insertion of zeros in the TD corresponds to repetition in the frequency domain, $\mathbf{S}^{(u)}$ will be repeated Q times in the FD, one will get at the receiver after de-spreading and NQ-point FFT,

$$\mathbf{Z}^{(u)} = \mathbf{\Gamma}^{(u)}\mathbf{S}^{(u)} + \mathbf{W}^{(u)} \tag{4.9}$$

where $\mathbf{\Gamma}^{(u)} = [\mathbf{\Lambda}_1^{(u)\mathcal{T}}, \mathbf{\Lambda}_2^{(u)\mathcal{T}}, \cdots, \mathbf{\Lambda}_Q^{(u)\mathcal{T}}]^{\mathcal{T}}$. One can then achieve frequency diversity if $\mathbf{\Lambda}_q^{(u)}$ is uncorrelated with $\mathbf{\Lambda}_p^{(u)}$ for $q \neq p$. Note that by inserting zeros, one does not increase the power transmitter which is desirable on the uplink. The diversity gain from zeros insertion is shown in Figure 4.3. QPSK modulation with MMSE FDE is used. The Vehicular A channel which is highly frequency selective is used and the block size was $N = 64$ symbols.

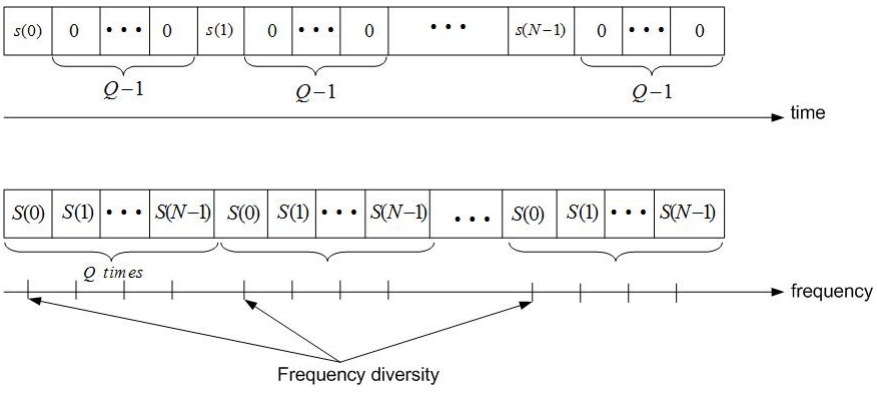

Figure 4.2 Principle of diversity through zeros insertion in the TD.

4.1.2 Fast Fading Case

If the channel is time varying with the assumption that it does remain constant during a chip-subblock but changes from subblock to subblock, the authors propose to process the received signal one subblock at a time. Hence, after removing the CP

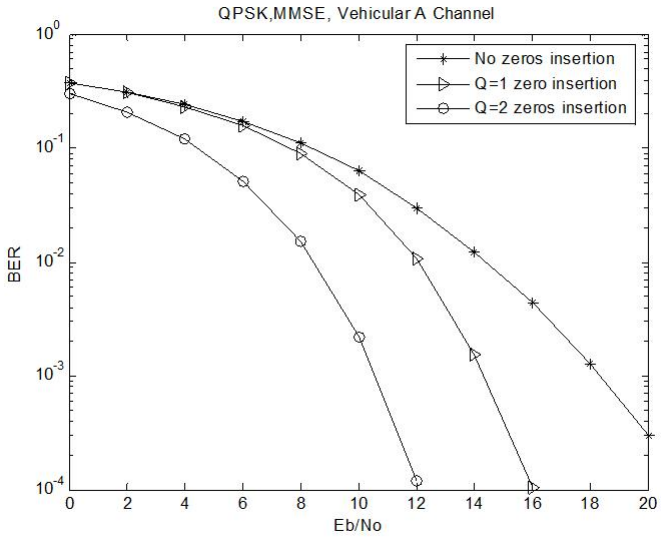

Figure 4.3 BER performance with zeros insertion in the TD which achieves frequency diversity in the FD.

from the received gth, $(g = 1, 2, \ldots, G)$ received chips-subblock, it follows

$$\begin{aligned} \mathbf{y}_g &= \sum_{u=1}^{U} \mathbf{x}_g^{(u)} \star \mathbf{h}_g^{(u)} + \mathbf{w}_g \\ &= \sum_{u=1}^{U} c^{(u)}(g) \left(\mathbf{s}^{(u)} \star \mathbf{h}_g^{(u)} \right) + \mathbf{w}_g, \end{aligned} \tag{4.10}$$

where $\mathbf{x}_g^{(u)} = c_u(g)\mathbf{s}^{(u)}$ is the gth subblock of $\mathbf{x}^{(u)}$, $\mathbf{h}_g^{(u)}$ is the user u's channel CIR during the gth chips-subblock where the channel is assumed invariant and $\mathbf{w}_g$ is the AWGN noise in the gth chips-subblock. Applying the de-spreading scheme of (4.5) will result in MUI interference as the channel is no longer invariant for the duration of the chips-block. In fast fading channel, the authors propose a receiver design that first transform the chips-subblock into the frequency domain by taking the N-point DFT of $\mathbf{y}_g$ to yield the $N \times 1$ vector

$$\mathbf{Y}_g = \sum_{u=1}^{U} \mathbf{c}^{(u)}(g)\mathbf{H}_g^{(u)}\mathbf{S}^{(u)} + \mathbf{W}_g, \tag{4.11}$$

where $\mathbf{H}_g^{(u)}$ is the $N \times N$ diagonal matrix with diagonal vector the N-point DFT of $\mathbf{h}_g^{(u)}$. Stacking all the G vectors $\mathbf{Y}_g$ into a $NG \times 1$ vector $\mathbf{Y} = [\mathbf{Y}_1^T, \ldots, \mathbf{Y}_G^T]^T$, (4.11) can be written in a matrix form as

$$\mathbf{Y} = \mathbf{\Lambda S} + \mathbf{W} \tag{4.12}$$

where

$$\mathbf{\Lambda} = \begin{bmatrix} \mathbf{c}^{(1)}(0)\mathbf{H}_0^{(1)} & \ldots & \mathbf{c}^{(U)}(0)\mathbf{H}_0^{(U)} \\ \mathbf{c}^{(1)}(1)\mathbf{H}_1^{(1)} & \ldots & \mathbf{c}^{(U)}(1)\mathbf{H}_1^{(U)} \\ \vdots & \ddots & \vdots \\ \mathbf{c}^{(1)}(G-1)\mathbf{H}_{G-1}^{(1)} & \ldots & \mathbf{c}^{(U)}(G-1)\mathbf{H}_{G-1}^{(U)} \end{bmatrix},$$

$\mathbf{S} = [\mathbf{S}^{(1)\mathcal{T}}, \mathbf{S}^{(2)\mathcal{T}}, \cdots, \mathbf{S}^{(U)\mathcal{T}}]^{\mathcal{T}}$ and $\mathbf{W} = [\mathbf{W}_1^{\mathcal{T}}, \ldots, \mathbf{W}_G^{\mathcal{T}}]^{\mathcal{T}}$. The receiver will then perform a joint MUD and channel equalization using linear MMSE or ZF as follow

$$\widehat{\mathbf{S}} = \left(\mathbf{\Lambda}^{\mathcal{H}}\mathbf{\Lambda} + \alpha(N_o/E_s)\mathbf{I}_{NU}\right)^{-1}\mathbf{\Lambda}^{\mathcal{H}}\mathbf{Y}, \tag{4.13}$$

where α=1 for MMSE and α=0 for ZF receivers. The estimated frequency domain symbols $\widehat{\mathbf{S}}$ are then transformed into the time domain for detection.

The kth diagonal element of the matched-filter matrix $\mathbf{\Lambda}^{\mathcal{H}}\mathbf{\Lambda}$ is given by $[\mathbf{\Lambda}^{\mathcal{H}}\mathbf{\Lambda}]_{k,k} = \sum_{g=0}^{G-1} |\mathbf{H}_g^{(u)}|_{k,k}^2$ and one gets $\mathcal{E}[\mathbf{H}_g^{(u)}\mathbf{H}_{g+\nu}^{(u)\mathcal{H}}] = \rho^{\nu}$. Hence, if the channel correlation factor ρ is low, i.e. $\rho \approx 0$ ($\mathbf{H}_{g_1}^{(u)}$ and $\mathbf{H}_{g_2}^{(u)}$ are independent), one obtains a time diversity gain of order G while when ρ is high, i.e. $\rho \approx 1$ ($\mathbf{H}_{g_1}^{(u)} = \mathbf{H}_{g_2}^{(u)}$) no time diversity gain is obtained. The rapidly time-varying channel not only destroys the orthogonality among the users causing MUI, but also provides us with time diversity gain that can be up to the G-th order where G is the processing gain (spreading factor). The study in this paper is showing that the time diversity gain surpasses the MUI caused by the time varying channel. The MMSE detection makes good use of the time selectivity since it minimizes both the residual interference (MUI) and the noise enhancement

while retaining the gain from the time diversity which can be up to the G-th order. Thus, one might expect that the performance would be better as the normalized Doppler frequency becomes large or as the correlation factor ρ decreases.

4.2 Proposed Multiuser SCFDE/HARQ

In this scheme, each user is assigned with a spreading code $\mathbf{c}^{(u)}$. The user u input N data symbols block $\mathbf{s}^{(u)}$ is demultiplexed into two $N/2$ data symbols blocks $\mathbf{s}_1^{(u)}$ and $\mathbf{s}_1^{(u)}$ which are then block spread by the spreading code $\mathbf{c}^{(u)}$. During the even transmissions, the user u transmit from antenna 1 and 2, respectively the block

$$\begin{aligned} \mathbf{x}_{1,e}^{(u)} &= \left(\mathbf{c}^{(u)} \otimes \mathbf{T}_{cp}\right) \mathbf{s}_1^{(u)} \\ \mathbf{x}_{2,e}^{(u)} &= \left(\mathbf{c}^{(u)} \otimes \mathbf{T}_{cp}\right) \mathbf{s}_2^{(u)} \end{aligned} \tag{4.14}$$

and during the odd transmission, user u transmit from antennas 1 and 2

$$\begin{aligned} \mathbf{x}_{1,o}^{(u)} &= -\mathbf{c}^{(u)} \otimes \mathbf{T}_{cp})\widetilde{\mathbf{s}}_2^{(u)*} \\ \mathbf{x}_{2,o}^{(u)} &= \mathbf{c}^{(u)} \otimes \mathbf{T}_{cp})\widetilde{\mathbf{s}}_1^{(u)*} \end{aligned} \tag{4.15}$$

where $\widetilde{\mathbf{s}}_i^{(u)} = \mathbf{P}_{N/2}\mathbf{s}_i^{(u)}$.

As described in the single user case, if error is detected during the even (odd)transmission, the BS send a NACK and the MS send the same packet as in the odd (even) transmission case.

Following the derivation in the previous section, it easily see that the received signal at the BS antenna during the even n^{th} (after CP removal, de-spreading as described in the previous section and $N/2$-point FFT) is given by

$$\begin{aligned} \mathbf{Y}_n^{(u)} &= \Lambda_{1,n}^{(u)}\mathbf{S}_1^{(u)} + \Lambda_{2,n}^{(u)}\mathbf{S}_2^{(u)} + \mathbf{W}_n \\ &= \mathbf{\Lambda}_n^{(u)}\mathbf{S}^{(u)} + \mathbf{W}_n \end{aligned} \tag{4.16}$$

where $\mathbf{\Lambda}_n^{(u)} = [\mathbf{\Lambda}_{1,n}^{(u)},\ \mathbf{\Lambda}_{2,n}^{(u)}]$. The received signal during the odd $(n+1)^{th}$ transmission is given by

$$\mathbf{Y}_{n+1}^{(u)} = -\Lambda_{1,n+1}^{(u)}\mathbf{S}_2^{(u)*} + \Lambda_{2,n+1}^{(u)}\mathbf{S}_1^{(u)*} + \mathbf{W}_{n+1}. \tag{4.17}$$

As in the single user case, the BS receiver combined the received signal during n^{th} and $(n+1)^{th}$ transmission as in (3.19) and linear ZF or MMSE equalization are performed as in (3.21).

4.2.1 Chips Superimposed STBC-SCFDE Approach

The authors notice that the performance after the second transmission is much better due to the STBC combining. One can improve on the performance by sending the STBC block in each transmission without loss of rate by using space-time spreading as follow. Each user is assigned with two normalized orthogonal spreading codes of length G denoted by $\mathbf{c}^{(u,1)}=[c_0^{(u,1)}, c_1^{(u,1)}, \ldots, c_{G-1}^{(u,1)}]^T$ and $\mathbf{c}^{(u,2)}=[c_0^{(u,2)}, c_1^{(u,2)}, \ldots, c_{G-1}^{(u,2)}]^T$. The users's spreading codes are mutually orthogonal.

During the first transmission, the MS sends from antenna 1 and 2 respectively

$$\begin{aligned}
\mathbf{x}_1^{(u)} &= \frac{1}{\sqrt{2}}\left[\left(\mathbf{c}_1^{(u)} \otimes \mathbf{T_{cp}}\right)\mathbf{s}_1^{(u)} - \left(\mathbf{c}_2^{(u)} \otimes \mathbf{T_{cp}}\right)\underline{\mathbf{s}}_2^{(u)*}\right] \\
\mathbf{x}_2^{(u)} &= \frac{1}{\sqrt{2}}\left[\left(\mathbf{c}_1^{(u)} \otimes \mathbf{T_{cp}}\right)\mathbf{s}_2^{(u)} + \left(\mathbf{c}_2^{(u)} \otimes \mathbf{T_{cp}}\right)\underline{\mathbf{s}}_1^{(u)*}\right]
\end{aligned} \tag{4.18}$$

Note the the total transmitted power is the same as in the first transmission of the previous scheme. The only difference is that this scheme need two spreading code per user and because of the superimposition of the chips, the PAPR is bounded to 3dB which is still low compared to OFDM. The block diagram of this scheme which is called Superimposed-STBC-SCFDE is shown in Figure 4.4

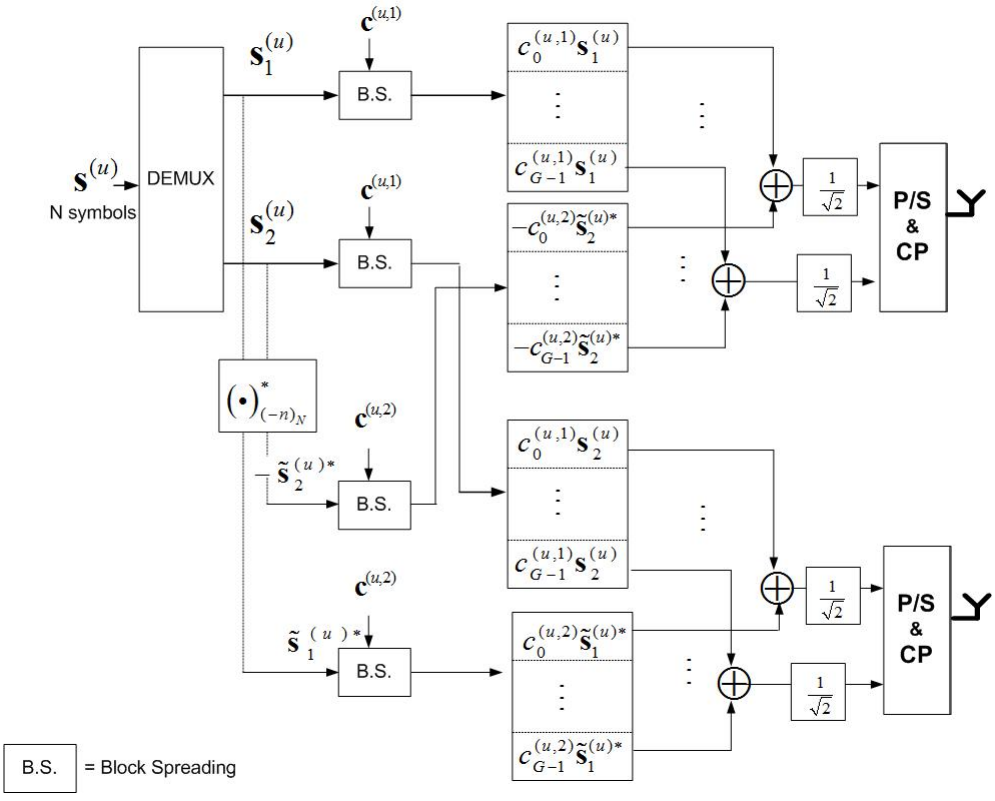

Figure 4.4 Block diagram of the superimposed STBC-SCFDE scheme.

Let denote by $\mathbf{x}_{i,g}^{(u)}$ the g^{th} chip subblock without the CP which is of length $N/2$ chips. It is given by

$$\begin{aligned} \mathbf{x}_{1,g}^{(u)} &= c_g^{(u,1)}\mathbf{s}_1^{(u)} - c_g^{(u,2)}\widetilde{\mathbf{s}}_2^{(u)*} \\ \mathbf{x}_{2,g}^{(u)} &= c_g^{(u,1)}\mathbf{s}_2^{(u)} + c_g^{(u,2)}\widetilde{\mathbf{s}}_1^{(u)*} \end{aligned} \tag{4.19}$$

Because the CP's remove the inter chip-subblock interference and turn the linear convolution into a circular one, after removing the CP's and taking the $N/2$-point FFT of each received chip-subblock, the g^{th} received FD chip-subblock is given by

$$\begin{aligned} \mathbf{Y}_g = &\sum_{u=1}^{U} c_g^{(u,1)} \left(\mathbf{\Lambda}_1^{(u)}\mathbf{S}_1^{(u)} + \mathbf{\Lambda}_2^{(u)}\mathbf{S}_2^{(u)} \right) \\ &+ c_g^{(u,2)} \left(\mathbf{\Lambda}_2^{(u)}\mathbf{S}_1^{(u)*} - \mathbf{\Lambda}_1^{(u)}\mathbf{S}_2^{(u)*} \right) + \mathbf{W}_g. \end{aligned} \tag{4.20}$$

where the fact that circular convolution in TD corresponds to multiplication of the DFT's in the FD is used. $\mathbf{W}_g$ is the DFT of the noise on the g^{th} received chip-subblock.

Using (4.20), $\mathbf{Y}=[\mathbf{Y}_0^{\mathcal{T}}, \mathbf{Y}_1^{\mathcal{T}}, \ldots, \mathbf{Y}_g^{\mathcal{T}}, \ldots, \mathbf{Y}_{G-1}^{\mathcal{T}}]^{\mathcal{T}}$ can be written as

$$\begin{aligned}\mathbf{Y} = &\sum_{u=1}^{U} \left(\mathbf{c}^{(u,1)} \otimes \mathbf{I}_{N/2}\right) \left(\mathbf{\Lambda}_1^{(u)} \mathbf{S}_1^{(u)} + \mathbf{\Lambda}_2^{(u)} \mathbf{S}_2^{(u)}\right) \\ &+ \left(\mathbf{c}^{(u,2)} \otimes \mathbf{I}_{N/2}\right) \left(\mathbf{\Lambda}_2^{(u)} \mathbf{S}_1^{(u)*} - \mathbf{\Lambda}_1^{(u)} \mathbf{S}_2^{(u)*}\right) + \mathbf{W}\end{aligned} \tag{4.21}$$

where $\mathbf{W}=[\mathbf{W}_0^{\mathcal{T}}, \mathbf{W}_1^{\mathcal{T}}, \ldots, \mathbf{W}_{G-1}^{\mathcal{T}}]^{\mathcal{T}}$.

The de-spreading of the received chips-vector $\mathbf{R}$ is done in the frequency domain by multiplying it with $\left(\mathbf{c}^{(u,1)T} \otimes \mathbf{I}_{N/2}\right)$ and $\left(\mathbf{c}^{(u,2)T} \otimes \mathbf{I}_{N/2}\right)$ to yield $\mathbf{Z}^{(u,1)}$ and $\mathbf{Z}^{(u,2)}$ respectively as below,

$$\begin{aligned}\mathbf{Z}^{(u,1)} &= \left(\mathbf{c}^{(u,1)T} \otimes \mathbf{I}_{N/2}\right) \mathbf{Y} \\ &= \mathbf{\Lambda}_1^{(u)} \mathbf{S}_1^{(u)} + \mathbf{\Lambda}_2^{(u)} \mathbf{S}_2^{(u)} + \mathbf{W}^{(u,1)} \\ \mathbf{Z}^{(u,2)} &= \left(\mathbf{c}^{(u,2)T} \otimes \mathbf{I}_{N/2}\right) \mathbf{Y} \\ &= \mathbf{\Lambda}_2^{(u)} \mathbf{S}_1^{(u)*} - \mathbf{\Lambda}_1^{(u)} \mathbf{S}_2^{(u)*} + \mathbf{W}^{(u,2)}\end{aligned} \tag{4.22}$$

where the following identities of Kronecker products have been used [39]

$$(\mathbf{A}_1 \otimes \mathbf{A}_2)(\mathbf{A}_3 \otimes \mathbf{A}_4) = (\mathbf{A}_1 \mathbf{A}_3) \otimes (\mathbf{A}_2 \mathbf{A}_4) \tag{4.23}$$

and $\mathbf{W}^{(u,i)} = (\mathbf{c}^{(u,i)T} \otimes \mathbf{I}_{N/2})\mathbf{W}$. Equation (4.22) can be combined in a matrix form as

$$\begin{aligned}\mathbf{Z}^{(u)} &= \begin{bmatrix} \mathbf{\Lambda}_1^{(u)} & \mathbf{\Lambda}_2^{(u)} \\ \mathbf{\Lambda}_2^{(u)*} & -\mathbf{\Lambda}_1^{(u)*} \end{bmatrix} \begin{bmatrix} \mathbf{S}_1^{(u)} \\ \mathbf{S}_2^{(u)} \end{bmatrix} + \begin{bmatrix} \mathbf{W}^{(u,1)} \\ \mathbf{W}^{(u,2)*} \end{bmatrix} \\ &\triangleq \quad \mathbf{\Lambda}^{(u)} \ \mathbf{S}^{(u)} + \mathbf{W}^{(u)},\end{aligned} \tag{4.24}$$

where $\mathbf{Z}^{(u)} = [\mathbf{Z}^{(u,1)T}, \mathbf{Z}^{(u,2)T}]^T$. A simple linear receiver will yield

$$\widehat{\mathbf{S}}^{(u)} = \left(\mathbf{\Lambda}^{(u)H} \mathbf{\Lambda}^{(u)} + \alpha(N_o/E_s)\mathbf{I}_N\right)^{-1} \mathbf{\Lambda}^{(u)H} \mathbf{Z}^{(u)}, \tag{4.25}$$

where

$$\begin{cases} \alpha = 1 \quad \text{for} \quad \text{MMSE receiver} \\ \alpha = 0 \quad \text{for} \quad \text{Zero} - \text{forcing receiver} \end{cases} \tag{4.26}$$

Note the matrix $\mathbf{\Lambda}^{(u)}$ is diagonal hence, STBC diversity is achieved in the first transmission. If error is detected, the MS resend the packet the same way as in the first transmission and the BS receiver combine using MRC as done in the previous schemes.

4.2.2 Chips Interleaved STBC-SCFDE Approach

One drawback of the chips superimposed approach is that the chips are added together resulting in a 3dB PAPR transmitted signal. If one wants to transmit constant amplitude signal one can interleave the chips instead of adding them. This will result doubling the size of the transmitted signal, however the interleaving in the TD will create diversity in the FD as follow. The block diagram of the chip interleaved scheme is depicted in Figure 4.5. The transmitted g^{th} chip-subblock in this case are given by

$$\begin{aligned} \mathbf{x}_{1,g}^{(u)} &= c_g^{(u,1)} \overrightarrow{\mathbf{s}}_1^{(u)} - c_g^{(u,2)} \overleftarrow{\mathbf{s}}_2^{(u)*} \\ \mathbf{x}_{2,g}^{(u)} &= c_g^{(u,1)} \overrightarrow{\mathbf{s}}_2^{(u)} + c_g^{(u,2)} \overleftarrow{\mathbf{s}}_1^{(u)*} \end{aligned} \tag{4.27}$$

where

$$\begin{aligned} \overrightarrow{\mathbf{s}}_i^{(u)} &= \left[s_i^{(u)}(0), 0, s_i^{(u)}(1), 0, \ldots, s_i^{(u)}(N/2-1), 0 \right]^{\mathcal{T}} \\ \overleftarrow{\mathbf{s}}_i^{(u)} &= \left[0, s_i^{(u)}(0), 0, s_i^{(u)}(N/2-1), \ldots, 0, s_i^{(u)}(1) \right]^{\mathcal{T}}. \end{aligned} \tag{4.28}$$

The N-point FFT of $\mathbf{x}_{i,g}^{(u)}$ are given by

$$\begin{aligned} \mathbf{X}_{1,g}^{(u)} &= c_g^{(u,1)} \mathbf{S}_{1,(N/2)}^{(u)} - c_g^{(u,2)} \mathbf{W}_N \mathbf{S}_{2,(N/2)}^{(u)*} \\ \mathbf{X}_{2,g}^{(u)} &= c_g^{(u,1)} \mathbf{S}_{2,(N/2)}^{(u)} + c_g^{(u,2)} \mathbf{W}_N \mathbf{S}_{1,(N/2)}^{(u)*} \end{aligned} \tag{4.29}$$

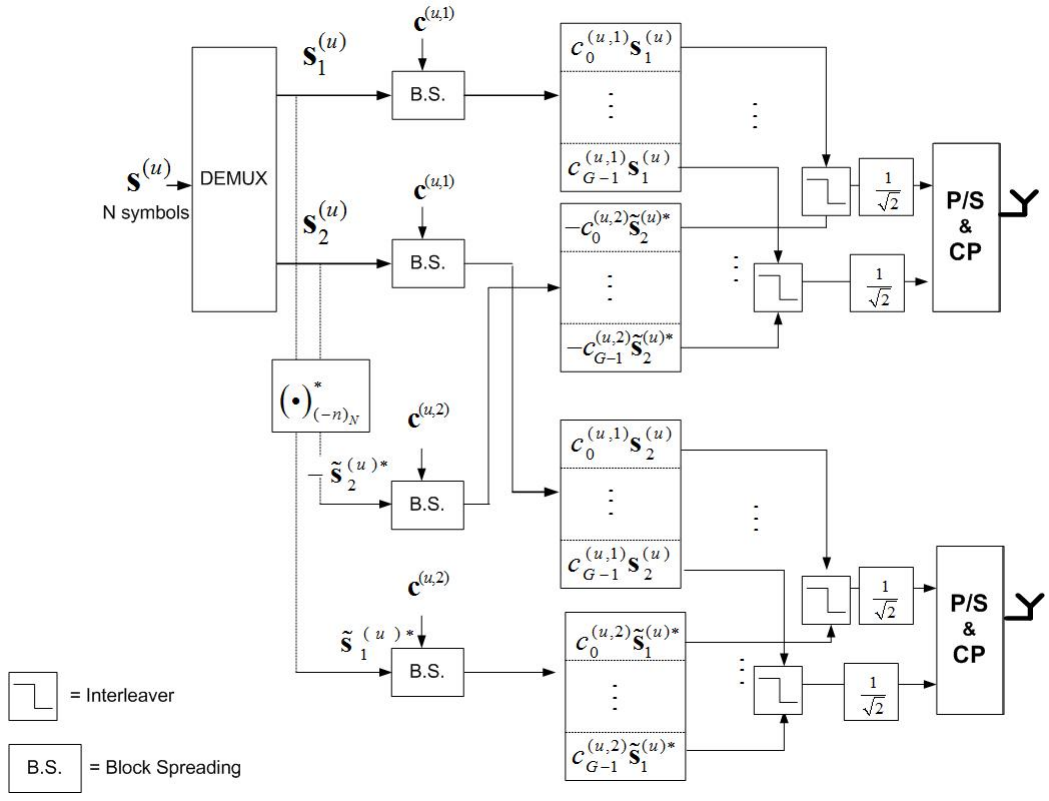

Figure 4.5 Block diagram of the interleaved STBC-SCFDE scheme.

where the auithors have defined $\mathbf{S}_{i,(N/2)}^{(u)}=\sqrt{1/2}[\mathbf{S}_i^{(u)T},\mathbf{S}_i^{(u)T}]^T$ which is a repetition of $\mathbf{S}_i^{(u)}$ due to the zero insertion in (4.28) and $\mathbf{W}_N = \text{diag}(1, e^{2\pi/N}, e^{2\pi 2/N}, \ldots, e^{2\pi(N-1)/N})$ which is the result of the shift property of the DFT [40]. Hence, the FD received signal can be shown to be given by

$$\begin{aligned}\mathbf{Y} = &\sum_{u=1}^{U} \left(\mathbf{c}^{(u,1)} \otimes \mathbf{I}_N\right) \left(\mathbf{\Lambda}_1^{(u)} \mathbf{S}_{1,(N/2)}^{(u)} + \mathbf{\Lambda}_2^{(u)} \mathbf{S}_{2,(N/2)}^{(u)}\right) \\ &+ \left(\mathbf{c}^{(u,2)} \otimes \mathbf{I}_N\right) \left(\mathbf{\Lambda}_2^{(u)} \mathbf{W}_N \mathbf{S}_{1,(N/2)}^{(u)*} - \mathbf{\Lambda}_1^{(u)} \mathbf{W}_N \mathbf{S}_{2,(N/2)}^{(u)*}\right) \\ &+ \mathbf{W},\end{aligned} \tag{4.30}$$

where $\mathbf{W}=[\mathbf{W}_0^{\mathcal{T}}, \mathbf{W}_1^{\mathcal{T}}, \ldots, \mathbf{W}_{G-1}^{\mathcal{T}}]^{\mathcal{T}}$. The frequency domain de-spreading yields

$$\begin{aligned}
\mathbf{Z}^{(u,1)} &= \left(\mathbf{c}^{(u,1)T} \otimes \mathbf{I}_N\right) \mathbf{Y} \\
&= \mathbf{\Lambda}_1^{(u)} \mathbf{S}_{1,(N/2)}^{(u)} + \mathbf{\Lambda}_2^{(u)} \mathbf{S}_{2,(N/2)}^{(u)} + \mathbf{W}^{(u,1)} \\
\mathbf{Z}^{(u,2)} &= \left(\mathbf{c}^{(u,1)T} \otimes \mathbf{I}_N\right) \mathbf{Y} \\
&= \mathbf{\Lambda}_2^{(u)} \mathbf{W}_N \mathbf{S}_{1,(N/2)}^{(u)*} - \mathbf{\Lambda}_1^{(u)} \mathbf{W}_N \mathbf{S}_{2,(N/2)}^{(u)*} + \mathbf{W}^{(u,2)}
\end{aligned} \tag{4.31}$$

or equivalently in matrix form

$$\mathbf{Z}^{(u)} = \begin{bmatrix} \mathbf{\Lambda}_1^{(u)} & \mathbf{\Lambda}_2^{(u)} \\ \mathbf{W}_N \mathbf{\Lambda}_2^{(u)*} & -\mathbf{W}_N \mathbf{\Lambda}_1^{(u)*} \end{bmatrix} \begin{bmatrix} \mathbf{S}_{1,(N/2)}^{(u)} \\ \mathbf{S}_{2,(N/2)}^{(u)} \end{bmatrix} + \begin{bmatrix} \mathbf{W}^{(u,1)} \\ \mathbf{W}^{(u,2)*} \end{bmatrix}, \tag{4.32}$$

where $\mathbf{Z}^{(u)}=[\mathbf{Z}^{(u,1)T}, \mathbf{Z}^{(u,2)T}]^T$ and the noise component $\mathbf{W}^{(u,i)}=(\mathbf{c}^{(u,i)T} \otimes \mathbf{I}_{N/2})\mathbf{W}$. Since $\mathbf{S}_{i,(N/2)}^{(u)}=\sqrt{1/2}[\mathbf{S}_i^{(u)T}, \mathbf{S}_i^{(u)T}]^T$, (4.32) can be written as function of $\mathbf{S}^{(u)} = [\mathbf{S}_1^{(u)T}, \mathbf{S}_2^{(u)T}]^T$ as

$$\begin{aligned}
\mathbf{Z}^{(u)} &= \sqrt{\frac{1}{2}} \begin{bmatrix} \mathbf{\Lambda}_1^{1(u)} & \mathbf{\Lambda}_2^{1(u)} \\ \mathbf{\Lambda}_1^{2(u)} & \mathbf{\Lambda}_2^{2(u)} \\ \mathbf{W}_N^{(1)} \mathbf{\Lambda}_2^{1(u)*} & -\mathbf{W}_N^{(1)} \mathbf{\Lambda}_1^{1(u)*} \\ \mathbf{W}_N^{(2)} \mathbf{\Lambda}_2^{2(u)*} & -\mathbf{W}_N^{(2)} \mathbf{\Lambda}_1^{2(u)*} \end{bmatrix} \begin{bmatrix} \mathbf{S}_1^{(u)} \\ \mathbf{S}_2^{(u)} \end{bmatrix} + \mathbf{W}^{(u)} \\
&\triangleq \mathbf{\Lambda}^{(u)} \mathbf{S}^{(u)} + \mathbf{W}^{(u)},
\end{aligned} \tag{4.33}$$

where $\mathbf{\Lambda}_i^{1(u)}$ and $\mathbf{\Lambda}_i^{2(u)}$ are $N/2 \times N/2$ diagonal matrix whose diagonal elements are the first and second $N/2$ diagonal elements of $\mathbf{\Lambda}_i^{(u)}$ respectively. Similarly $\mathbf{W}_N^{(1)}$ and $\mathbf{W}_N^{(2)}$ are $N/2 \times N/2$ diagonal matrix whose diagonal elements are the first and second $N/2$ diagonal elements of $\mathbf{W}_N$. The linear receiver yields

$$\widehat{\mathbf{S}}^{(u)} = \left(\mathbf{\Lambda}^{(u)H} \mathbf{\Lambda}^{(u)} + \alpha(N_o/E_s)\mathbf{I}_N\right)^{-1} \mathbf{\Lambda}^{(u)} \mathbf{Z}^{(u)}. \tag{4.34}$$

An $N/2$-point IFFT is taken to get the time domain estimate. It can be easily shown that the matrix $\mathbf{\Lambda}^{(u)H}\mathbf{\Lambda}^{(u)}$ is diagonal and given by

$$\mathbf{\Lambda}^{(u)\mathcal{H}}\overline{\mathbf{\Lambda}}^{(u)} = \frac{1}{2}\begin{bmatrix} \mathbf{\Delta}^{(u)} & \mathbf{0}_{(N/2)\times(N/2)} \\ \mathbf{0}_{(N/2)\times(N/2)} & \mathbf{\Delta}^{(u)} \end{bmatrix} \tag{4.35}$$

where the elements of $\mathbf{\Delta}^{(u)}$ are given by

$$\mathbf{\Delta}^{(u)}_{k,k} = \left|\mathbf{\Lambda}_1^{1(u)}\right|^2_{k,k} + \left|\mathbf{\Lambda}_1^{2(u)}\right|^2_{k,k} + \left|\mathbf{\Lambda}_2^{1(u)}\right|^2_{k,k} + \left|\mathbf{\Lambda}_2^{2(u)}\right|^2_{k,k}. \tag{4.36}$$

The chip interleaved approach introduce additional diversity at the expense of reducing the data rate.

The throughput is shown in Figure 4.6.

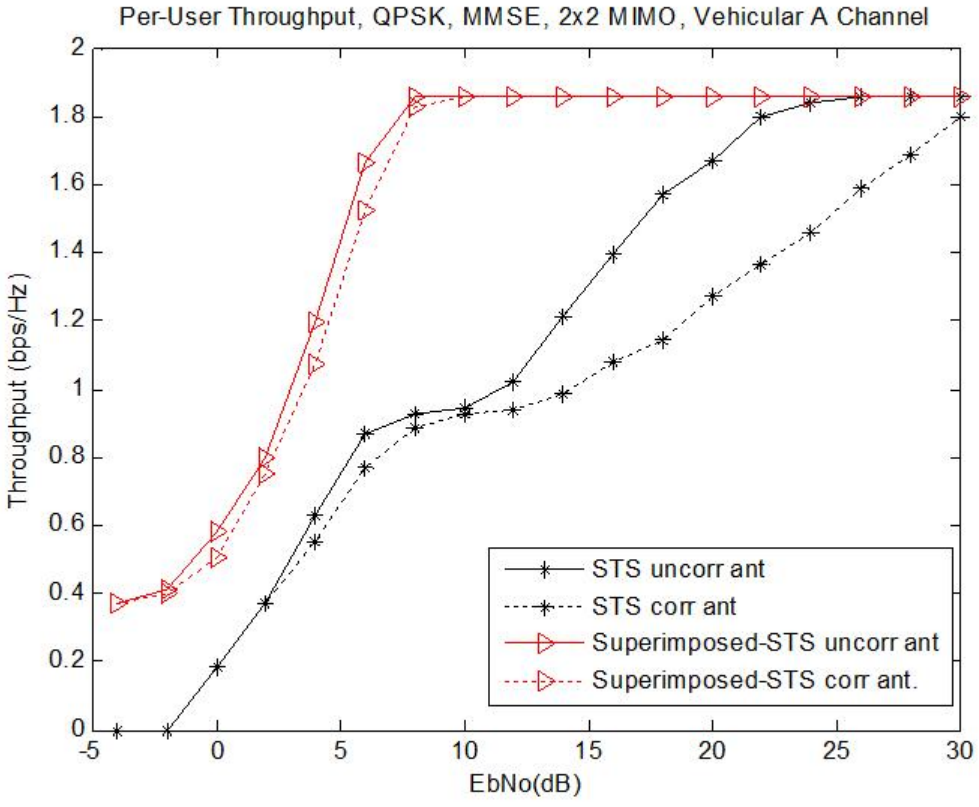

Figure 4.6 Throughput Comparison of the multiuser Scheme I.

CHAPTER 5

SINGLE CARRIER FREQUENCY DOMAIN EQUALIZATION (SCFDE) SPACE-TIME BLOCK-SPREAD CDMA (STBS-CDMA) WITH MULTIUSER INTERFERENCE (MUI)-FREE DETECTION

A novel multiuser interference (MUI)-free CDMA scheme known as chip-interleaved block spread CDMA (CIBS-CDMA) based on block-spreading and zero-padding was proposed in [19]. In CIBS-CDMA, the orthogonality among the users's spreading is maintained at the receiver even after frequency selective propagation. In order to exploit the spatial diversity of the wireless channel while maintaining the MUI-free detection, CIBS-CDMA was applied to space-time coding in the uplink [41] and downlink [42] of CDMA systems. However, these space-time CDMA schemes require the channel to be invariant for the duration of a chip-block of size $2(N + L)G$ chips where N, L, G are the input block size, the length of the multipath channel and the spreading factor respectively. For the schemes in [41] and [42], $2(N + L)GT_c$ (T_c is the chip duration) must be less than the coherence time of the channel. Since the maximum number of users that do not interfere with each other equals the spreading factor G [19] , the total number of MUI-free interference users supported is limited in channel with short coherence time T_{coh} because $2(N + L)GT_c$ must be less than T_{coh}. Space-frequency block spread CDMA system have then been proposed in [43] for time varying channel but again, due the use of block spreading, the channel has to be invariant for the entire space-frequency block-spread CDMA block. In order to relieve the effect of the time varying channel, the authors propose in this chapter a novel space-time block spread structure for the uplink wireless communications. The proposed schemes uses SCFDE because it exhibit low peak-to-average power ratio (PAPR) which is important to insure low cost (affordable) mobile unit. SCFDE is

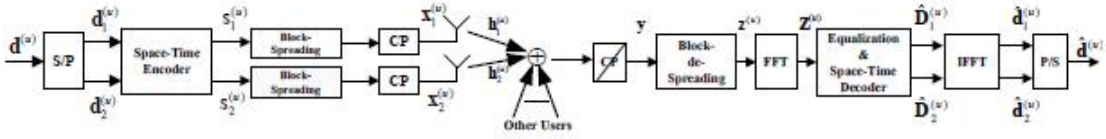

Figure 5.1 SCFDE-STBS-CDMA System Model.

combined in this chapter with space-time block spreading to provide reliable wireless multiuser communications in time varying channel. The proposed scheme requires the channel to be invariant only for a chip-block of size $2(N + L)$ chips, i.e. of duration $2(N + L)T_c$. This enables the designer to freely choose the spreading factor G as needed by the maximum number of users to be supported without degrading the system performance. It is shown that the proposed scheme highly outperforms the one proposed in [41] and reference therein when the channel is varying within the total transmitted chip-block of size $2(N + L)G$ chips but remain invariant or slowly varies within a chip-block of $2(N + L)$ chips. The authors analyze the performance of the proposed scheme and compare it with the one in [41].

5.1 System Model

Consider a CDMA system on the uplink wireless communication with U users, each equipped with two uncorrelated antennas, which transmit data to a base station that is equipped with M antennas. Without loss of generality, it is assumed in this chapter that M=1 (extension to multiple receive antennas is straightforward). The system model is shown in Figure. 5.1. Throughout this chapter, block spreading i.e. which operates on a block of symbol [19], [44], [45], [46] is used as opposed to the traditional symbol spreading that is performed on a single symbol [47], [48]. The uth user data stream is parsed into a block of $2N$ data symbols which is serial-to-parallel converted into two blocks of N data symbols each denoted by $\mathbf{d}_i^{(u)}$=$[d_i^{(u)}(0), d_i^{(u)}(1), \ldots, d_i^{(u)}(N-1)]^T, i = 1, 2$. The authors analyze for the uplink

wireless communications, the performance of two space-time block spreading CDMA schemes in both slow and fast fading channel. The first is the SCFDE-STBS-CDMA scheme proposed in [41] wherein two block-time intervals are needed to transmit the space-time block spreaded symbols. The second is the new SCFDE-STBS-CDMA scheme that the authors propose in this chapter wherein only a single block-interval is required to transmit the space-time block spread symbols. The authors will show that the performances of both scheme is the same in a slow fading channel but in fast fading channel, the new proposed scheme outperforms the one in [41]. This is because in fast fading channel, the channel impulse response (CIR) varies within the space-time chip-block causing intersymbol interference (ISI) and destroying the orthogonality among he users codes. By properly designing the space-time encoder of the new scheme, a significant performance advantages can be obtained in fast fading channel. Let $\mathbf{h}_{i,n}^{(u)}=\left[h_{i,n}^{(u)}(0), h_{i,n}^{(u)}(1), \ldots, h_{i,n}^{(u)}(L-1)\right]^T$ denotes the L-taps channel impulse response between the uth user transmit antenna i and the base-station receive antenna during the n^{th} chip-subblock transmission (the chip-subblock which is composed of $(N+L)$ chips will be described in the next section). The authors assume that the channel state information (CSI) is available at the receiver and the transmitter only knows the channel order L. Each user is assigned a spreading code $\mathbf{c}^{(u)}=[\mathbf{c}^{(u)}(0), \mathbf{c}^{(u)}(1), \ldots, \mathbf{c}^{(u)}(G-1)]^T$ of length G. The spreading codes are mutually orthogonal, i.e. $\mathbf{c}^{(u)\mathcal{H}}\mathbf{c}^{(v)}=\delta(u-v),\ \forall u, v \in [1, U]$.

5.2 Single Carrier Space-Time Block Spread CDMA (SCFDE-STBS-CDMA) in Slow Fading Channel

The authors begin by describing the SCFDE-STBS-CDMA scheme proposed in [41]. The new proposed SCFDE-STBS-CDMA schemes are explained and compared.

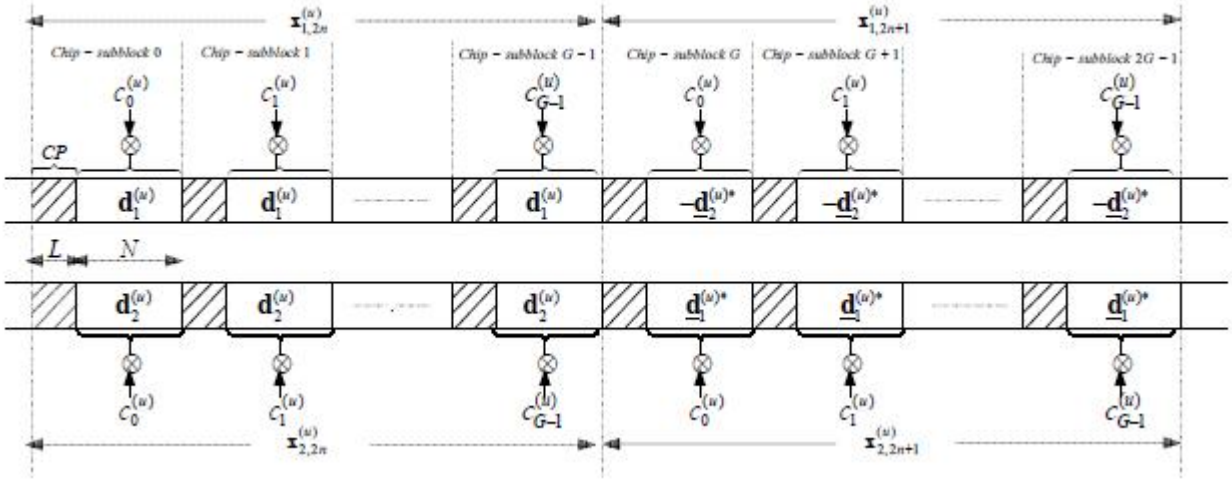

Figure 5.2 Block structure of the SCFDE-STBS-CDMA conventional scheme

Consider in this section a slow varying channel wherein the channel remains constant for the duration of one space-time block of duration $2(N+L)GT_c$, i.e. $\mathbf{h}_{i,n}^{(u)} = \mathbf{h}_i^{(u)} \quad \forall n \in [0, 2G-1]$ where n represent the chip-subblock index.

5.2.1 Single Carrier Space-Time Block Spread CDMA : Conventional Approach

In the SCFDE-STBS-CDMA scheme proposed in [41] which is referred to to as conventional approach, and the references therein, for the uplink wireless communications, the two $N \times 1$ blocks $\mathbf{d}_i^{(u)}$ are first fed into a space-time encoder whose output is given by the following two $N \times 1$ blocks $\mathbf{s}_{i,2n}^{(u)}$ and $\mathbf{s}_{i,2n+1}^{(u)}$ for two consecutive block-times $2n$ and $2n+1$ with $n = 0, 1, 2, \cdots$

$$\begin{aligned} \mathbf{s}_{1,2n}^{(u)} &= \mathbf{d}_1^{(u)} \quad , \quad \mathbf{s}_{1,2n+1}^{(u)} = -\underline{\mathbf{d}}_2^{(u)*} \\ \mathbf{s}_{2,2n}^{(u)} &= \mathbf{d}_2^{(u)} \quad , \quad \mathbf{s}_{2,2n+1}^{(u)} = \underline{\mathbf{d}}_1^{(u)*} \end{aligned} \tag{5.1}$$

A cyclic prefix (CP) of length L is then added to each block $\mathbf{s}_{i,2n}^{(u)}$. The cyclic prefixed blocks are then block-spreaded by user u's code $\mathbf{c}^{(u)}$ to construct the chip-blocks $\mathbf{x}_{i,2n}^{(u)}$, of length $(N+L)G$ given by

$$\begin{aligned} \mathbf{x}_{1,2n}^{(u)} &= (\mathbf{c}^{(u)} \otimes \mathbf{T_{cp}})\ \mathbf{s}_{1,2n}^{(u)} \\ \mathbf{x}_{2,2n}^{(u)} &= (\mathbf{c}^{(u)} \otimes \mathbf{T_{cp}})\ \mathbf{s}_{2,2n}^{(u)} \end{aligned} \tag{5.2}$$

where $\mathbf{T_{cp}}$ is the CP matrix given by $\mathbf{T_{cp}} = [\mathbf{J}_{cp}^T, \mathbf{I}_N]^T$; $\mathbf{J}_{cp}$ is a $L \times N$ matrix formed by the last L rows of the identity matrix $\mathbf{I}_N$.

By using the following property of the Kronecker product [39], $(\mathbf{A}_1 \otimes \mathbf{A}_2)(\mathbf{B}_1 \otimes \mathbf{B}_2)=(\mathbf{A}_1\mathbf{B}_1) \otimes (\mathbf{A}_2\mathbf{B}_2)$, $\mathbf{x}_{i,2n}^{(u)}$ can be written in the following form

$$\begin{aligned} \mathbf{x}_{1,2n}^{(u)} &= (\mathbf{c}^{(u)} \otimes \mathbf{T_{cp}})\ (1 \otimes \mathbf{s}_{1,2n}^{(u)}) \\ &= \mathbf{c}^{(u)} \otimes (\mathbf{T_{cp}}\mathbf{s}_{1,2n}^{(u)}) \\ \mathbf{x}_{2,2n}^{(u)} &= (\mathbf{c}^{(u)} \otimes \mathbf{T_{cp}})\ (1 \otimes \mathbf{s}_{2,2n}^{(u)}) \\ &= \mathbf{c}^{(u)} \otimes (\mathbf{T_{cp}}\mathbf{s}_{2,2n}^{(u)}) \end{aligned} \tag{5.3}$$

The transmitted block structure of this scheme is depicted in Figure. 5.2. Note that there is a total of $2G$ chip-subblocks each of length $(N + L)$ chips.

At block-time $2n$, the chip-block $\mathbf{x}_{1,2n}^{(u)}$ and $\mathbf{x}_{2,2n}^{(u)}$ of length $(N + L)G$ chips are transmitted through the first and second transmit antennas, respectively. In the next block-time, $2n + 1$, the chip-block $\mathbf{x}_{1,2n+1}^{(u)}$ and $\mathbf{x}_{2,2n+1}^{(u)}$ are transmitted through the first and second transmit antennas, respectively.

The CP not only eliminates the inter chip-block interference (ICBI) but also turn the linear convolution between the channel and the transmit signal into a circular convolution [30] then making the channel matrix *circulant* [49]. The composite received signal block from all active users at the receiver antenna for the $2n$th chip-block time, in the presence of additive white noise, can be expressed by the $((N+L)G+L-1)\times 1$

chip-block

$$\begin{aligned}\mathbf{r}_{2n} &= \sum_{u=1}^{U}\sum_{i=1}^{2}\mathbf{x}_{i,2n}^{(u)} \star \mathbf{h}_i^{(u)} + \widetilde{\mathbf{w}}_{2n} \\ &= \sum_{u=1}^{U}\sum_{i=1}^{2}\left[\mathbf{c}^{(u)} \otimes (\mathbf{T}_{\mathbf{cp}}\mathbf{s}_{1,2n}^{(u)})\right] \star \mathbf{h}_i^{(u)} + \widetilde{\mathbf{w}}_{2n}\end{aligned} \tag{5.4}$$

where $\widetilde{\mathbf{w}}_{2n}$ denotes the $((N+L)G+L-1)\times 1$ zero-mean additive white Gaussian noise-vector (AWGN) with variance N_o. After the removal of the G CP from $\mathbf{r}_{2n}$, the received signal is given by the $NG \times 1$ chip-block [49]

$$\mathbf{y}_{2n} = \sum_{u=1}^{U}\sum_{i=1}^{2}\mathbf{c}^{(u)} \otimes (\mathbb{H}_i^{(u)}\mathbf{s}_{i,2n}^{(u)}) + \overline{\mathbf{w}}_{2n} \tag{5.5}$$

where $\mathbb{H}_i^{(u)}$ is the circulant channel matrix from the i^{th} transmit antennas to the receive antenna whose first column is the $N \times 1$ vector $[h_i^{(u)}(0), h_i^{(u)}(1), \ldots, h_i^{(u)}(L-1), 0, \cdots, 0]^T$; $\overline{\mathbf{w}}_{2n}$ is the resulting $NG \times 1$ noise vector.

The linear multiuser separation for user u is done by multiplying the received chip-block $\mathbf{y}_{2n}$ by $(\mathbf{c}^{(u)\mathcal{H}} \otimes \mathbf{I}_N)$. The user u received signal after de-spreading is given by the $N \times 1$ symbol block

$$\begin{aligned}\mathbf{z}_{2n}^{(u)} &= (\mathbf{c}^{(u)\mathcal{H}} \otimes \mathbf{I}_N)\mathbf{y}_{2n} \\ &= (\mathbf{c}^{(u)\mathcal{H}} \otimes \mathbf{I}_N)\sum_{v=1}^{U}\sum_{i=1}^{2}\mathbf{c}^{(v)} \otimes (\mathbb{H}_i^{(v)}\mathbf{s}_{i,2n}^{(v)}) + \overline{\mathbf{w}}_{2n} \\ &= \sum_{v=1}^{U}\sum_{i=1}^{2}(\mathbf{c}^{(u)\mathcal{H}} \otimes \mathbf{I}_N)\left(\mathbf{c}^{(v)} \otimes (\mathbb{H}_i^{(u)}\mathbf{s}_{i,2n}^{(u)})\right) \\ &\qquad + (\mathbf{c}^{(u)\mathcal{H}} \otimes \mathbf{I}_N)\overline{\mathbf{w}}_{2n} \\ &= \sum_{i=1}^{2} 1 \otimes (\mathbb{H}_i^{(u)}\mathbf{s}_{i,2n}^{(u)}) + (\mathbf{c}^{(u)\mathcal{H}} \otimes \mathbf{I}_N)\overline{\mathbf{w}}_{2n} \\ &= \sum_{i=1}^{2}\mathbb{H}_i^{(u)}\mathbf{s}_{i,2n}^{(u)} + \mathbf{w}_{2n}^{(u)}\end{aligned} \tag{5.6}$$

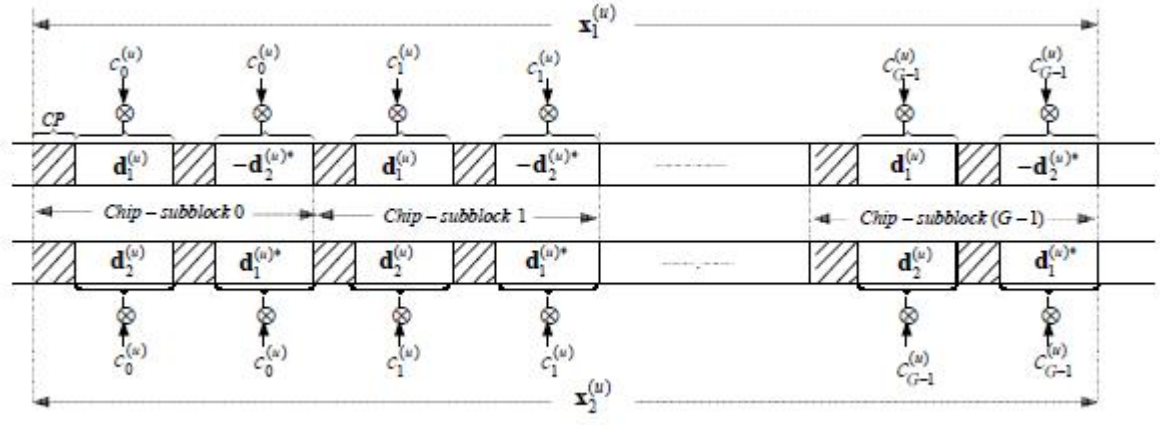

Figure 5.3 Block structure of the proposed SCFDE-STBS-CDMA scheme

where $\mathbf{w}_{2n}^{(u)}=(\mathbf{c}^{(u)\mathcal{H}} \otimes \mathbf{I}_N)\overline{\mathbf{w}}_{2n}$ and the authors have used the orthogonality among the user spreading codes, i.e. $\mathbf{c}^{(u)\mathcal{H}}\mathbf{c}^{(v)} = \delta(u-v)$.

An N-point DFT is then taken to transform the received signal into the frequency domain as follow

$$\mathbf{Z}_{2n}^{(u)} = \sum_{i=1}^{2} \mathbf{H}_i^{(u)} \mathbf{S}_{i,2n}^{(u)} + \mathbf{W}_{2n}^{(u)} \tag{5.7}$$

where $\mathbf{Z}_n^{(u)}$, $\mathbf{S}_{i,2n}^{(u)}$ and $\mathbf{W}_{2n}^{(u)}$ are the N-point DFT of $\mathbf{z}_n^{(u)}$, $\mathbf{s}_{i,2n}^{(u)}$ and $\mathbf{w}_{2n}^{(u)}$ respectively. $\mathbf{H}_i^{(u)} = \mathbf{F}_N \mathbb{H}_i^{(u)} \mathbf{F}_N^{\mathcal{H}}$ is a $N \times N$ diagonal matrix[1] whose diagonal is the N-point DFT of $\mathbf{h}_i^{(u)}$.

Similarly, the received chips block at block-time $2n+1$ is given by

$$\mathbf{Z}_{2n+1}^{(u)} = \sum_{i=1}^{2} \mathbf{H}_i^{(u)} \mathbf{S}_{i,2n+1}^{(u)} + \mathbf{W}_{2n+1}^{(u)} \tag{5.8}$$

Note from (5.1) that

$$\begin{aligned} \mathbf{S}_{i,2n}^{(u)} &= \mathbf{D}_i^{(u)} \\ \mathbf{S}_{i,2n+1}^{(u)} &= (-1)^i \mathbf{D}_j^{(u)*} \end{aligned} \tag{5.9}$$

[1]It is well know that a circulant matrix is diagonalized by a DFT matrix [50]

where $\mathbf{D}_i^{(u)}$ is the N-point DFT of $\mathbf{d}_i^{(u)}$, j=2^{2-i}, i.e. j=2 if i=1 and j=1 if i=2. In the second equation of (5.9), the time reversal property of the DFT has been used [40].

Hence, combining (5.7) and (5.8) and taking the conjugate of (5.8), it follows

$$\begin{bmatrix} \mathbf{Z}_{2n}^{(u)} \\ \mathbf{Z}_{2n+1}^{(u)*} \end{bmatrix} = \begin{bmatrix} \mathbf{H}_1^{(u)} & \mathbf{H}_2^{(u)} \\ \mathbf{H}_2^{(u)*} & -\mathbf{H}_1^{(u)*} \end{bmatrix} \begin{bmatrix} \mathbf{D}_1^{(u)} \\ \mathbf{D}_2^{(u)} \end{bmatrix} + \begin{bmatrix} \mathbf{W}_{2n}^{(u)} \\ \mathbf{W}_{2n+1}^{(u)*} \end{bmatrix} \tag{5.10}$$

or equivalently

$$\mathbf{Z}_n^{(u)} \triangleq \mathbf{H}^{(u)}\ \mathbf{D}^{(u)} + \mathbf{W}_n^{(u)}. \tag{5.11}$$

Linear block equalizer can then be obtained as

$$\widehat{\mathbf{D}}^{(u)} = \left[\mathbf{H}^{(u)\mathcal{H}}\mathbf{H}^{(u)} + \alpha(N_o/E_s)\mathbf{I}_{2N}\right]^{-1} \mathbf{H}^{(u)\mathcal{H}}\mathbf{Z}_n^{(u)}, \tag{5.12}$$

where α=1 for MMSE and α=0 for ZF receivers. The matrix $\mathbf{H}^{(u)\mathcal{H}}\mathbf{H}^{(u)}$ is diagonal and given by

$$\begin{bmatrix} |\mathbf{H}_1^{(u)}|^2 + |\mathbf{H}_2^{(u)}|^2 & \mathbf{0}_{N\times N} \\ \mathbf{0}_{N\times N} & |\mathbf{H}_1^{(u)}|^2 + |\mathbf{H}_2^{(u)}|^2 \end{bmatrix} \tag{5.13}$$

where $|\mathbf{H}_1^{(u)}|^2 + |\mathbf{H}_2^{(u)}|^2$ is an $N \times N$ diagonal matrix. This scheme achieves MUI-free detection and provides a *two-fold* diversity gain. The bit-error rate performance in slow fading channel is depicted in Figure. 5.4 for $U = 2$ and 8 termed Scheme of [41] for ZF and MMSE equalization.

5.2.2 Proposed Single Carrier Space-Time Block Spread CDMA

In the proposed SCFDE-STBS-CDMA, the u^{th} user $N \times 1$ blocks $\mathbf{d}_i^{(u)}$ are space-time encoded as shown in Figure. 5.3 to construct the two $2N \times 1$ blocks $\mathbf{s}_i^{(u)}$ as follow

$$\begin{aligned}\mathbf{s}_1^{(u)} &= \left[\mathbf{d}_1^{(u)T}, -\underline{\mathbf{d}}_2^{(u)\mathcal{H}}\right]^T \\ \mathbf{s}_2^{(u)} &= \left[\mathbf{d}_2^{(u)T}, \ \ \underline{\mathbf{d}}_1^{(u)\mathcal{H}}\right]^T.\end{aligned} \tag{5.14}$$

These blocks are then block spreaded to yield the following $2(N+L)G \times 1$ chip-blocks

$$\begin{aligned}\mathbf{x}_i^{(u)} &= \mathbf{c}^{(u)} \otimes \left[(\mathbf{I}_2 \otimes \mathbf{T_{cp}})\mathbf{s}_i^{(u)}\right] \\ &= \mathbf{c}^{(u)} \otimes \ \widetilde{\mathbf{s}}_i^{(u)},\end{aligned} \tag{5.15}$$

where the authors have defined $\widetilde{\mathbf{s}}_i^{(u)} = (\mathbf{I}_2 \otimes \mathbf{T_{cp}})\mathbf{s}_i^{(u)}$, i.e.

$$\begin{aligned}\widetilde{\mathbf{s}}_1^{(u)} &= \begin{bmatrix} \mathbf{T_{cp}} & \mathbf{0}_{(N+L)\times N} \\ \mathbf{0}_{(N+L)\times N} & \mathbf{T_{cp}} \end{bmatrix} \begin{bmatrix} \mathbf{d}_1^{(u)} \\ -\underline{\mathbf{d}}_2^{(u)*} \end{bmatrix} \\ \widetilde{\mathbf{s}}_2^{(u)} &= \begin{bmatrix} \mathbf{T_{cp}} & \mathbf{0}_{(N+L)\times N} \\ \mathbf{0}_{(N+L)\times N} & \mathbf{T_{cp}} \end{bmatrix} \begin{bmatrix} \mathbf{d}_2^{(u)} \\ \underline{\mathbf{d}}_1^{(u)*} \end{bmatrix}\end{aligned} \tag{5.16}$$

Hence, $\widetilde{\mathbf{s}}_i^{(u)}$ can be written as

$$\widetilde{\mathbf{s}}_i^{(u)} = \left[\left(\mathbf{T_{cp}}\mathbf{d}_i^{(u)}\right)^T, (-1)^i \left(\mathbf{T_{cp}}\underline{\mathbf{d}}_j^{(u)*}\right)^T\right]^T, \tag{5.17}$$

where j=2^{2-i}.

The chip-block structure of the proposed scheme is depicted in Figure. 5.3. The chip-block $\mathbf{x}_i^{(u)}$ is transmitted by the ith antenna in one block-time interval of length $2(N+L)G$ chips. In (5.15), $(\mathbf{I}_2 \otimes \mathbf{T_{cp}})$ appends a CP of length L to each block $\mathbf{d}_i^{(u)}$ within $\mathbf{s}_i^{(u)}$ as shown in Figure. 5.3. Note that the main difference between the proposed scheme and the previous one is that in the proposed scheme, a chip-subblock is of length $2(N+L)$ and there is a total of G chip-subblocks while in the scheme of [41] a chip-subblock is of length $N+L$ and there is a total of $2G$ chip-subblocks. As will be shown later, the advantage of the proposed scheme is evident when the channel is varying within the chip-block. Note that in the proposed scheme, the

authors dropped the subscript n as only one transmission is needed. The composite received signal block from all active users at the receiver antenna can be expressed as the $(2(N+L)G+L-1)$ chip-block

$$\begin{aligned}\mathbf{r} &= \sum_{u=1}^{U}\sum_{i=1}^{2} \mathbf{x}_i^{(u)} \star \mathbf{h}_i^{(u)} + \widetilde{\mathbf{w}} \\ &= \sum_{u=1}^{U}\sum_{i=1}^{2} \left(\mathbf{c}^{(u)} \otimes \widetilde{\mathbf{s}}_i^{(u)}\right) \star \mathbf{h}_i^{(u)} + \widetilde{\mathbf{w}}\end{aligned} \tag{5.18}$$

where $\widetilde{\mathbf{w}}$ denotes the $(2(N+L)G+L-1)\times 1$ zero-mean additive white Gaussian noise-vector (AWGN) with variance N_o. As in the previous section, the CP turns the linear convolution into circular then making the channel matrix circulant [30].

After the removal of the $2G$ CP from $\mathbf{r}$, the received signal is given by the $2NG\times 1$ chip-block [49]

$$\mathbf{y} = \sum_{u=1}^{U}\sum_{i=1}^{2} \mathbf{c}^{(u)} \otimes (\mathbf{\Pi}_i^{(u)}\mathbf{s}_i^{(u)}) + \overline{\mathbf{w}} \tag{5.19}$$

where $\mathbf{\Pi}_i^{(u)}$ is a block diagonal given by

$$\mathbf{\Pi}_i^{(u)} = \begin{bmatrix} \mathbb{H}_i^{(u)} & \mathbf{0}_{N\times N} \\ \mathbf{0}_{N\times N} & \mathbb{H}_i^{(u)} \end{bmatrix} \tag{5.20}$$

and $\mathbb{H}_i^{(u)}$ is the circulant channel matrix from the i^{th} transmit antennas to the receive antenna whose first column is the $N\times 1$ vector $[h_i^{(u)}(0), h_i^{(u)}(1), \ldots, h_i^{(u)}(L-1), 0, \cdots, 0]^T$; $\overline{\mathbf{w}}$ is the resulting $NG\times 1$ noise vector.

The de-spreading and linear multiuser separation for user u is done by multiplying the chip-block $\mathbf{y}$ by $(\mathbf{c}^{(u)\mathcal{H}} \otimes \mathbf{I}_{2N})$ to yield the MUI-free block

$$\begin{aligned}\mathbf{z}^{(u)} &= \left(\mathbf{c}^{(u)\mathcal{H}} \otimes \mathbf{I}_{2N}\right)\mathbf{y} \\ &= \sum_{v=1}^{U}\sum_{i=1}^{2}\left(\mathbf{c}^{(u)\mathcal{H}} \otimes \mathbf{I}_{2N}\right)\left[\mathbf{c}^{(v)} \otimes (\mathbf{\Pi}_i^{(v)}\mathbf{s}_i^{(v)}) + \overline{\mathbf{w}}\right] \\ &= \sum_{i=1}^{2} 1 \otimes (\mathbf{\Pi}_i^{(u)}\mathbf{s}_i^{(u)}) + \mathbf{w}^u \\ &= \sum_{i=1}^{2} \mathbf{\Pi}_i^{(u)}\mathbf{s}_i^{(u)} + \mathbf{w}^u\end{aligned} \tag{5.21}$$

where $\mathbf{w}^{(u)}= \left(\mathbf{c}^{(u)} \otimes \mathbf{I}_{2N}\right)\overline{\mathbf{w}}$. In (5.21), the orthogonality of the spreading code has been used, i.e., $\mathbf{c}^{(u)\mathcal{H}}\mathbf{c}^{(v)} = \delta(u-v)$. The $2N\times 1$ symbol block $\mathbf{z}^{(u)}$ is then transformed to the frequency domain by taking the N-point DFT of each subblock of $\mathbf{z}^{(u)}$ as follow

$$\mathbf{Z}^{(u)} = \mathbf{Q}_{2N}\mathbf{z}^{(u)} \tag{5.22}$$

where $\mathbf{Q}_{2N}$ is a $2N \times 2N$ block-diagonal matrix with the N-point DFT matrix $\mathbf{F}_N$ on the diagonal, i.e.

$$\mathbf{Q}_{2N} = \begin{bmatrix} \mathbb{F}_N & \mathbf{0}_{N\times N} \\ \mathbf{0}_{N\times N} & \mathbb{F}_N \end{bmatrix}. \tag{5.23}$$

$\mathbf{Z}^{(u)}$ can then be written as

$$\begin{aligned}\mathbf{Z}^{(u)} &= \sum_{i=1}^{2}\mathbf{Q}_{2N}(\mathbf{\Pi}_i^{(u)}\mathbf{s}_i^{(u)} + \mathbf{w}^u) \\ &= \sum_{i=1}^{2}\mathbf{Q}_{2N}\mathbf{\Pi}_i^{(u)}\mathbf{Q}_{2N}^{\mathcal{H}}\mathbf{S}_i^{(u)} + \mathbf{W}^u\end{aligned} \tag{5.24}$$

where $\mathbf{S}_i^u = \mathbf{Q}_{2N}\mathbf{s}_i^u$ and $\mathbf{W}^u = \mathbf{Q}_{2N}\mathbf{w}^u$. From Equation (5.14) and (5.23), one gets

$$\begin{aligned}\mathbf{S}_1^u &= [\mathbf{D}_1^{(u)}, -\mathbf{D}_2^{(u)\mathcal{H}}]^T \\ \mathbf{S}_2^u &= [\mathbf{D}_2^{(u)}, \ \ \mathbf{D}_1^{(u)\mathcal{H}}]^T.\end{aligned} \tag{5.25}$$

Note that

$$\begin{aligned}\mathbf{Q}_{2N}\mathbf{\Pi}_i^{(u)}\mathbf{Q}_{2N}^{\mathcal{H}} &= \begin{bmatrix}\mathbb{F}_N\mathbb{H}_i^{(u)}\mathbb{F}_N^{\mathcal{H}} & \mathbf{0}_{N\times N}\\ \mathbf{0}_{N\times N} & \mathbb{F}_N\mathbb{H}_i^{(u)}\mathbb{F}_N^{\mathcal{H}}\end{bmatrix}\\ &= \begin{bmatrix}\mathbf{H}_i^{(u)} & \mathbf{0}_{N\times N}\\ \mathbf{0}_{N\times N} & \mathbf{H}_i^{(u)}\end{bmatrix}\end{aligned} \tag{5.26}$$

where $\mathbf{H}_i^{(u)}$ is a $N\times N$ diagonal matrix whose diagonal is the N-point DFT of $\mathbf{h}_i^{(u)}$. Denote $\mathbf{Z}^{(u)}=[\mathbf{Z}_1^{(u)T},\mathbf{Z}_2^{(u)T}]^T$ and $\mathbf{W}^{(u)}=[\mathbf{W}_1^{(u)T},\mathbf{W}_2^{(u)T}]^T$, using (5.24), (5.25) and (5.26), it is easily seen that

$$\begin{aligned}\mathbf{Z}_1^{(u)} &= \mathbf{H}_1^{(u)}\mathbf{D}_1^{(u)} + \mathbf{H}_2^{(u)}\mathbf{D}_2^{(u)} + \mathbf{W}_1^u\\ \mathbf{Z}_2^{(u)} &= -\mathbf{H}_1^{(u)}\mathbf{D}_2^{(u)*} + \mathbf{H}_2^{(u)}\mathbf{D}_1^{(u)*} + \mathbf{W}_2^u\end{aligned} \tag{5.27}$$

Taking the conjugate of $\mathbf{Z}_2^{(u)}$, (5.22) can be rewritten in matrix form as

$$\begin{bmatrix}\mathbf{Z}_1^{(u)}\\ \mathbf{Z}_2^{(u)*}\end{bmatrix} = \begin{bmatrix}\mathbf{H}_1^{(u)} & \mathbf{H}_2^{(u)}\\ \mathbf{H}_2^{(u)*} & -\mathbf{H}_1^{(u)*}\end{bmatrix}\begin{bmatrix}\mathbf{D}_1^{(u)}\\ \mathbf{D}_2^{(u)}\end{bmatrix} + \begin{bmatrix}\mathbf{W}_1^{(u)}\\ \mathbf{W}_2^{(u)*}\end{bmatrix} \tag{5.28}$$

or equivalently

$$\overline{\mathbf{Z}}^{(u)} \triangleq \mathbf{H}^{(u)}\ \mathbf{D}^{(u)} + \overline{\mathbf{W}}^{(u)}. \tag{5.29}$$

$$\mathbf{\Lambda}_n = \begin{bmatrix} c_0^{(1)}\mathbf{H}_{1,0}^{(1)} & c_0^{(1)}\mathbf{H}_{2,0}^{(1)} & \cdots & c_0^{(U)}\mathbf{H}_{1,0}^{(U)} & c_0^{(U)}\mathbf{H}_{2,0}^{(U)}\\ \vdots & \vdots & \cdots & \vdots & \vdots\\ c_{G-1}^{(1)}\mathbf{H}_{1,G-1}^{(1)} & c_{G-1}^{(1)}\mathbf{H}_{2,G-1}^{(1)} & \cdots & c_{G-1}^{(U)}\mathbf{H}_{1,G-1}^{(U)} & c_{G-1}^{(U)}\mathbf{H}_{2,G-1}^{(U)}\\ c_0^{(1)}\mathbf{H}_{2,G}^{(1)*} & -c_0^{(1)}\mathbf{H}_{1,G}^{(1)*} & \cdots & c_0^{(U)}\mathbf{H}_{2,G}^{(u)*} & -c_0^{(U)}\mathbf{H}_{1,G}^{(U)*}\\ \vdots & \vdots & \cdots & \vdots & \vdots\\ c_{G-1}^{(1)}\mathbf{H}_{2,2G-1}^{(1)*} & -c_{G-1}^{(1)}\mathbf{H}_{1,2G-1}^{(2)*} & \cdots & c_{G-1}^{(U)}\mathbf{H}_{2,2G-1}^{(U)*} & -c_{G-1}^{(U)}\mathbf{H}_{1,2G-1}^{(U)*}\end{bmatrix} \tag{5.40}$$

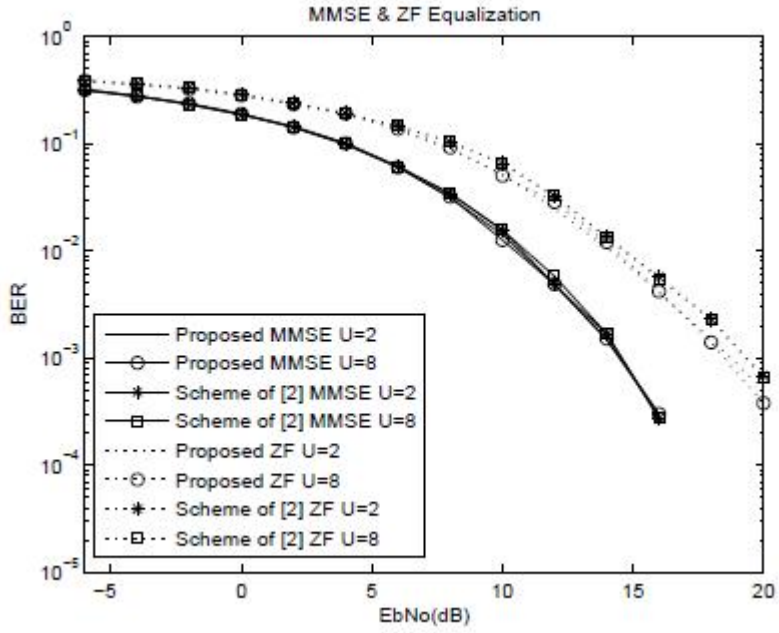

Figure 5.4 BER performance comparison of the proposed SCFDE-STBS-CDMA scheme and the conventional scheme in slow fading channel with time correlation factor $\rho = 0.99$.

Linear block equalizer can then be obtained as in (7.10). This scheme then achieve MUI-free detection and also provides a *two-fold* diversity gain. The bit-error rate performance in slow fading channel is depicted in Figure. 5.4 for $U = 2$ and 8 termed 'Proposed' for ZF and MMSE equalization.

If the channel is varying within a chip-block, the performance is not the same as the orthogonality among the users code is lost at the receiver. In the next section, the authors propose a detector for the STBS-CDMA and show that, in fast fading channel, the proposed scheme can mitigate the effect of the time varying and exploit the channel time diversity, yielding BER performances that outperforms the conventional approach.

5.3 Single Carrier Space-time Block Spread CDMA (SCFDE-STBS-CDMA) in Fast Fading Channel

In the previous section, the authors have assumed that the channel is invariant for the duration of the chip block of length $2(N+L)G$ chips. In practice, there can be a channel variation within the chip block. In this section, the performance of the two schemes described above in a time-varying channel is studied. To characterize the time varying channel, it is assumed that $2(N+L)T_c$ (not $2(N+L)GT_c$ as required in the scheme of [41]) is less than the coherence time of the channel. It is also assumed that the channel changes from one chip-subblock to another with correlation ρ=$J_0(2\pi 2(N+L)f_dT_c)$ but remains invariant within each chip-subblock of length $2(N+L)$ chips. This is a reasonable assumption that can be easily met in practical time varying channel. In order to still combat the MUI, the authors propose in the following a linear receiver that mitigates the detrimental effect of the time varying channel. Denote by $\mathbf{h}_{i,g}^{(u)}$ the user u channel impulse response during the gth chip-subblock period from the ith transmit antenna. Capitalizing on the information-theoretic results from [51], a first-order autoregressive model or Gauss-Markov model [52] for the time varying fading channel is adopted in this chapter i.e., $\mathbf{h}_{i,g+1}^{(u)}$=$\rho\mathbf{h}_{i,g}^{(u)}+\sqrt{1-\rho^2}\omega$ where ω is a AWGN variable with the same variance as $\mathbf{h}_{i,g}^{(u)}$.

5.3.1 Conventional Single Carrier Space-Time Block Spread CDMA in Fast Fading Channel

In this scheme depicted in Figure. 5.2, there is a total of $2G$ chip-subblocks of length $N+L$ chips each in one space-time chip-block of length $2(N+L)G$. The composite received gth chip-subblock, for g=$0,1,\cdots,G-1$ during the $2n$th block time is given in this case by the $(N+L)\times 1$ vector

$$\mathbf{r}_{2n,g}=\sum_{u=1}^{U}\sum_{i=1}^{2}\left(c_g^{(u)}\mathbf{T_{cp}}\mathbf{s}_{i,2n}^{(u)}\right)\star\mathbf{h}_{i,g}^{(u)}+\widetilde{\mathbf{w}}_{2n,g} \tag{5.30}$$

where $\widetilde{\mathbf{w}}_{2n,g}$ is the AWGN. The main difference between (5.30) and (5.4) is that the channel impulse response depends on the chip-subblock index g in the case of the time varying channel while in the slow fading case, the channel is independent of the chip-subblock indice g. After removing the CP, (the linear convolution is turned into a circular making the channel matrix circulant), one gets

$$\mathbf{y}_{2n,g} = \sum_{u=1}^{U} \sum_{i=1}^{2} c_g^{(u)} \mathbb{H}_{i,g}^{(u)} \mathbf{s}_{i,2n}^{(u)} + \overline{\mathbf{w}}_{2n,g} \tag{5.31}$$

where $\mathbb{H}_{i,g}^{(u)}$ is the circulant channel matrix from the i^{th} transmit antennas to the receive antenna in the g^{th} subblock whose first column is the $N\times 1$ vector $[h_{i,g}^{(u)}(0), h_{i,g}^{(u)}(1), \ldots, h_{i,g}^{(u)}(L-1), 0, \cdots, 0]^T$; $\overline{\mathbf{w}}_{2n,g}$ is the resulting noise vector.

An N-point DFT [2] is then taken to yield the $N \times 1$ vector

$$\mathbf{Y}_{2n,g} = \sum_{u=1}^{U} \sum_{i=1}^{2} c_g^{(u)} \mathbf{H}_{i,g}^{(u)} \mathbf{S}_{i,2n}^{(u)} + \mathbf{W}_{2n,g} \tag{5.32}$$

where $\mathbf{S}_{i,2n}^{(u)}$ and $\mathbf{W}_{2n,g}$ are the N-point DFT of $\mathbf{s}_{i,2n}^{(u)}$ and $\mathbf{w}_{2n,g}$ respectively and $\mathbf{H}_{i,g}^{(u)} = \mathbf{F}_N \mathbb{H}_{i,g}^{(u)} \mathbf{F}_N^{\mathcal{H}}$ is an $N \times N$ diagonal matrix; (5.32) can be written in a matrix form as

$$\mathbf{Y}_{2n,g} = \mathbf{\Lambda}_{2n,g} \mathbf{S}_{2n} + \mathbf{W}_{2n,g} \tag{5.33}$$

where

$$\mathbf{\Lambda}_{2n,g} = \left[c_g^{(1)} \mathbf{H}_{1,g}^{(1)},\ c_g^{(1)} \mathbf{H}_{2,g}^{(1)}, \cdots,\ c_g^{(U)} \mathbf{H}_{1,g}^{(U)}, c_g^{(U)} \mathbf{H}_{2,g}^{(U)} \right] \tag{5.34}$$

is a $N \times 2NU$ matrix and the composite $2NU \times 1$ block

$$\mathbf{S}_{2n} = [\mathbf{S}_{1,2n}^{(1)T},\ \mathbf{S}_{2,2n}^{(1)T},\ \cdots,\ \mathbf{S}_{1,2n}^{(U)T},\ \mathbf{S}_{2,2n}^{(U)T}]^T \tag{5.35}$$

[2] In the fast fading case, because the channel is changing within the space-time chip-block, the authors compare the two schemes (i.e. the two space-time chip-block structure of Figure. 5.2 and Figure. 5.3) by first transforming the chip-block into the frequency domain and then using either ZF or MMSE equalization

Collecting all the G received blocks $\mathbf{Y}_{2n,g}$ into one $NG\times 1$ vector $\mathbf{Y}_{2n}=[\mathbf{Y}_{2n,0}^T,\cdots,\mathbf{Y}_{2n,G-1}^T]^T$, it follows

$$\mathbf{Y}_{2n}=\mathbf{\Lambda}_{2n}\mathbf{S}_{2n}+\mathbf{W}_{2n} \tag{5.36}$$

where

$$\mathbf{\Lambda}_{2n}=\left[\mathbf{\Lambda}_{2n,0}^T,\mathbf{\Lambda}_{2n,1}^T,\cdots,\mathbf{\Lambda}_{2n,G-1}^T\right]^T. \tag{5.37}$$

Since from (5.1) one has $\mathbf{S}_{i,2n}^{(u)}=\mathbf{D}_i^{(u)}$ and $\mathbf{S}_{i,2n+1}^{(u)}=(-1)^i\mathbf{D}_j^{(u)*}$ where $j=2^{2-i}$, $\mathbf{S}_{2n}$ and $\mathbf{S}_{2n+1}$ are given by

$$\begin{aligned}\mathbf{S}_{2n}&=[\mathbf{D}_1^{(1)T},\mathbf{D}_2^{(1)T},\ \cdots,\ \mathbf{D}_1^{(U)T},\mathbf{D}_2^{(U)T}]^T\triangleq\mathbf{D}\\ \mathbf{S}_{2n+1}&=[-\mathbf{D}_2^{(1)\mathcal{H}},\mathbf{D}_1^{(1)\mathcal{H}},\ \cdots,-\mathbf{D}_2^{(U)\mathcal{H}},\mathbf{D}_1^{(U)\mathcal{H}}]^T.\end{aligned} \tag{5.38}$$

By letting $\mathbf{Y}_n=[\mathbf{Y}_{2n}^T,\mathbf{Y}_{2n+1}^{\mathcal{H}}]^T$, it yields

$$\mathbf{Y}_n=\mathbf{\Lambda}_n\mathbf{D}+\mathbf{W}_n \tag{5.39}$$

where the $2NG\times 2NU$ matrix $\mathbf{\Lambda}_n$ is shown in (5.40) and $\mathbf{W}_n=[\mathbf{W}_{2n}^T,\mathbf{W}_{2n+1}^{\mathcal{H}}]^T$. Thus, the average BER of the system is calculated by averaging the conditional probability of error over the channel realizations. A joint linear multiuser detection and channel equalization can be performed as

$$\widehat{\mathbf{D}}=\left[\mathbf{\Lambda}_n^{\mathcal{H}}\mathbf{\Lambda}_n+\alpha(N_o/E_d)\mathbf{I}_{2NU}\right]^{-1}\mathbf{\Lambda}_n^{(u)\mathcal{H}}\mathbf{Y}_n. \tag{5.41}$$

If the channel is invariant within a space-time block period, i.e. if $\mathbf{H}_{i,g_1}^{(u)}=\mathbf{H}_{i,g_2}^{(u)}=\mathbf{H}_i^{(u)}$ then (5.40) reduces to

$$\mathbf{\Lambda}_n^{(inv)}=\begin{bmatrix}\mathbf{c}^{(1)}\otimes[\mathbf{H}_1^{(1)}\ ,\ \mathbf{H}_2^{(1)}\ ] & \cdots & \mathbf{c}^{(U)}\otimes[\mathbf{H}_1^{(U)}\ ,\ \mathbf{H}_2^{(U)}\ ]\\ \mathbf{c}^{(1)}\otimes[\mathbf{H}_2^{(1)*},-\mathbf{H}_1^{(1)*}] & \cdots & \mathbf{c}^{(U)}\otimes[\mathbf{H}_2^{(U)*},-\mathbf{H}_1^{(U)*}]\end{bmatrix} \tag{5.42}$$

It can be easily shown that $\mathbf{\Lambda}_n^{(inv)\mathcal{H}}\mathbf{\Lambda}_n^{(inv)} = \mathbf{I}_{2NU}$ which as shown in the previous section, will give rise to a MUI-free detection.

5.3.2 Proposed SCFDE Space-time Block Spread CDMA in Fast Fading channel

In the proposed STBS-CDMA scheme, a chip-subblock is composed of $2(N+L)$ chips as shown in Figure. 5.3, there are G chip-subblocks in one chip-block of length $2(N+L)G$ chips. The received gth chip-subblock, for g=$0, 1, \cdots, G-1$ is given in by the $2(N+L)\times 1$ vector

$$\mathbf{r}_g = \sum_{u=1}^{U}\sum_{i=1}^{2} c_g^{(u)}\widetilde{\mathbf{s}}_i^{(u)} \star \mathbf{h}_{i,g}^{(u)} + \widetilde{\mathbf{w}}_g, \tag{5.43}$$

where $\widetilde{\mathbf{s}}_i^{(u)}$ is defined in (5.16). After removing the CP, one gets

$$\mathbf{y}_g = \sum_{u=1}^{U}\sum_{i=1}^{2} c_g^{(u)}\mathbf{\Pi}_{i,g}^{(u)}\widetilde{\mathbf{s}}_i^{(u)} + \overline{\mathbf{w}}_g. \tag{5.44}$$

where $\mathbf{\Pi}_{i,g}^{(u)}$ is given in (5.20) with $\mathbb{H}_i^{(u)}$ replaced with $\mathbb{H}_{i,g}^{(u)}$.

The received chip-subblock $\mathbf{y}_g$ is then transformed in the frequency domain as follow

---

$$\mathbf{\Lambda}=\begin{bmatrix} c_0^{(1)}\mathbf{H}_{1,0}^{(1)} & c_0^{(1)}\mathbf{H}_{2,0}^{(1)} & \cdots & c_0^{(U)}\mathbf{H}_{1,0}^{(u)} & c_0^{(U)}\mathbf{H}_{2,0}^{(U)} \\ c_0^{(1)}\mathbf{H}_{2,0}^{(1)*} & -c_0^{(1)}\mathbf{H}_{1,0}^{(1)*} & \cdots & c_0^{(U)}\mathbf{H}_{2,0}^{(U)*} & -c_0^{(U)}\mathbf{H}_{1,0}^{(U)*} \\ \vdots & \vdots & \cdots & \vdots & \vdots \\ c_{G-1}^{(1)}\mathbf{H}_{1,G-1}^{(1)} & c_{G-1}^{(1)}\mathbf{H}_{2,G-1}^{(1)} & \cdots & c_{G-1}^{(U)}\mathbf{H}_{1,G-1}^{(U)} & c_{G-1}^{(U)}\mathbf{H}_{2,G-1}^{(U)} \\ c_{G-1}^{(1)}\mathbf{H}_{2,G-1}^{(1)*} & -c_{G-1}^{(1)}\mathbf{H}_{1,G-1}^{(1)*} & \cdots & c_{G-1}^{(U)}\mathbf{H}_{2,G-1}^{(U)*} & -c_{G-1}^{(U)}\mathbf{H}_{1,G-1}^{(U)*} \end{bmatrix} \tag{5.49}$$

$$\begin{aligned}\mathbf{Y}_g &= \mathbf{Q}_{2N}\mathbf{y}_g \\ &= \sum_{u=1}^{U}\sum_{i=1}^{2} c_g^{(u)}\mathbf{Q}_{2N}\mathbf{\Pi}_{i,g}^{(u)}\mathbf{Q}_{2N}^{\mathcal{H}}\widetilde{\mathbf{S}}_i^{(u)} + \overline{\mathbf{W}}_g\end{aligned} \tag{5.45}$$

where $\widetilde{\mathbf{S}}_i^{(u)} = \mathbf{Q}_{2N}\widetilde{\mathbf{s}}_i^{(u)}$ and $\overline{\mathbf{W}} = \mathbf{Q}_{2N}\overline{\mathbf{w}}_g$.

The size of $\mathbf{Y}_g$ is $2N \times 1$. Let denote by $\mathbf{Y}_{g_1}$ ($\mathbf{Y}_{g_2}$) the first (second) $N \times 1$ block of $\mathbf{Y}_g$. It can be shown that (following similar derivation as in section III-B) they are given by

$$\begin{aligned}\mathbf{Y}_{g_1} &= \sum_{u=1}^{U} c_g^{(u)}(\mathbf{H}_{1,g}^{(u)}\mathbf{D}_1^{(u)} + \mathbf{H}_{2,g}^{(u)}\mathbf{D}_2^{(u)}) + \mathbf{W}_{g_1} \\ \mathbf{Y}_{g_2} &= \sum_{u=1}^{U} c_g^{(u)}(\mathbf{H}_{2,g}^{(u)}\mathbf{D}_1^{(u)*} - \mathbf{H}_{1,g}^{(u)}\mathbf{D}_2^{(u)*}) + \mathbf{W}_{g_2}.\end{aligned} \tag{5.46}$$

Let $\mathbf{Z}_g$=$[\mathbf{Y}_{g_1}^T, \mathbf{Y}_{g_2}^{\mathcal{H}}]^T$, where one has taken the conjugate of $\mathbf{Y}_{g_2}$ in $\mathbf{Y}_g$. $\mathbf{Z}_g$ is given by

$$\mathbf{Z}_g = \sum_{u=1}^{U} c_g^{(u)} \begin{bmatrix} \mathbf{H}_{1,g}^{(u)} & \mathbf{H}_{2,g}^{(u)} \\ \mathbf{H}_{2,g}^{(u)*} & -\mathbf{H}_{1,g}^{(u)*} \end{bmatrix} \begin{bmatrix} \mathbf{D}_1^{(u)} \\ \mathbf{D}_2^{(u)} \end{bmatrix} + \begin{bmatrix} \mathbf{W}_{g_1} \\ \mathbf{W}_{g_2}^* \end{bmatrix} \tag{5.47}$$

Collecting all the received G block $\mathbf{Z}_g$ into $\mathbf{Z} = [\mathbf{Z}_0^T, \mathbf{Z}_1^T, \cdots, \mathbf{Z}_{G-1}^T]^T$, it follows

$$\mathbf{Z} = \mathbf{\Lambda}\ \mathbf{D} + \mathbf{W} \tag{5.48}$$

where $\mathbf{\Lambda}$ is given in (5.49) at the bottom of this page and $\mathbf{W} = [\mathbf{W}_0^T, \mathbf{W}_1^T, \cdots, \mathbf{W}_{G-1}^T]^T$ in which $\mathbf{W}_g$=$[\mathbf{W}_{g_1}^T, \mathbf{W}_{g_2}^{\mathcal{H}}]^T$. A joint linear multiuser detection and channel equalization can be performed as

$$\widehat{\mathbf{D}} = \left[\mathbf{\Lambda}^{\mathcal{H}}\mathbf{\Lambda} + \alpha(N_o/E_s)\mathbf{I}_{2NU}\right]^{-1}\mathbf{\Lambda}^{(u)\mathcal{H}}\mathbf{Z}. \tag{5.50}$$

If the channel is invariant within a space-time block time period, i.e. if $\mathbf{H}_{i,g_1}^{(u)}$=$\mathbf{H}_{i,g_2}^{(u)}$=$\mathbf{H}_i^{(u)}$ then

$$\mathbf{\Lambda}^{(inv)} = \left[\mathbf{c}^{(1)} \otimes \mathbf{H}^{(1)},\ \mathbf{c}^{(2)} \otimes \mathbf{H}^{(2)},\ \cdots,\ \mathbf{c}^{(U)} \otimes \mathbf{H}^{(U)}\right] \tag{5.51}$$

where

$$\mathbf{H}^{(u)} = \begin{bmatrix} \mathbf{H}_1^{(u)} & \mathbf{H}_2^{(u)} \\ \mathbf{H}_2^{(u)*} & -\mathbf{H}_1^{(u)*} \end{bmatrix} \tag{5.52}$$

It can be easily shown that $\mathbf{\Lambda}^{(inv)\mathcal{H}}\mathbf{\Lambda}^{(inv)}=\mathbf{I}_{2NU}$ which will give rise to a MUI-free detection as shown in the previous section of the proposed scheme.

5.4 Simulation Results

The authors simulate the proposed schemes with $N = 64$ symbols and $G = 32$. An exponential power decaying profile was used for the simulation with multipath delay spread of $L = 16$. A QPSK modulation is used. The BER performance of the proposed scheme and that of the scheme of [41] in slow fading channel i.e. in this simulation, when the channel varies between chips-subblock with a correlation of $\rho = 0.99$ which corresponds to $(N + L)f_dTs = 0.008$ is plotted in Figure. 5.4 for ZF and MMSE equalization. It is seen that the performances of both schemes are the same. One can also see that both scheme achieve MUI-free detection and the BER is the same for $U = 2$ and $U = 8$. In time varying channel, the BER performances are depicted for Zero-Forcing Equalization in Figure. 5.5 (for $\rho = 0.86$), Figure. 5.6 (for $\rho = 0.50$) and for MMSE Equalization in Figure. 5.7 (for $\rho = 0.86$), Figure. 5.8 (for $\rho = 0.50$). In Figure. 5.9 and Figure. 5.10 the authors show how the BER performance varies as the channel time correlation factor ρ varies for $\rho = 0.99, 0.86$ and 0.50. One can see that the performance of the scheme of [41] degrades when the channel correlation factor increase. On the other hand the proposed scheme performs better, and in fact as the channel time correlation increases, the BER performance of the proposed scheme improves as it exploits the time diversity introduced by the time variation of the channel. The proposed scheme makes use of the time selectivity gain which is shown to dominate the detrimental effect of the time variation that causes

MUI. That is, the time varying channel destroys users orthogonality causing MUI but also provides time diversity. The proposed space-time block structure exploits the time diversity whose gain boosts the BER performance more than the MUI reduces it. A closed look at the matrix $\mathbf{\Lambda}$ in (5.49) shows that in the proposed scheme, there is no interference between the two transmit antennas symbols [3] in fast fading channel, this is not the case for the matrix $\mathbf{\Lambda}_n$ in (5.40) for the scheme in [41]. Furthermore, it is noticed that the performance with MMSE is better as it provides a better balance in minimizing the sum of the noise enhancement and the residual interference while the ZF detection suffers more from noise enhancement.

In this chapter, the authors analyze the impact of a time-varying frequency selective fading channel on the performance of a Single Carrier Block Spread CDMA (SCFDE-STBS-CDMA) system. the authors propose a joint multiuser detection and interference cancelation for mitigating the effects of a time-varying channel, and simulate their bit- error probability as a function of the channel correlation coefficient. It is shown that as the channel varies in time, the proposed scheme makes use of the time diversity gain which surpasses the MUI caused by the time varying channel while the conventional approach proposed in the literature fails when the channel is time varying. A channel estimation approach for both slow and fast fading channel has also been developed.

[3]The two transmit antennas for each user are completely decoupled

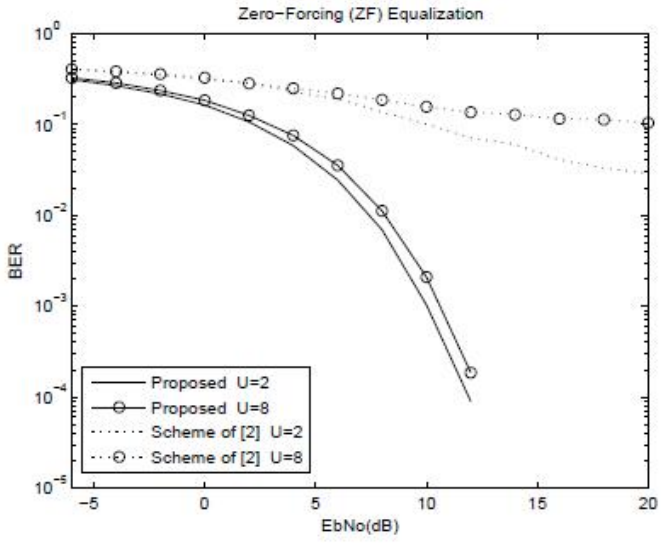

Figure 5.5 Comparison of the BER performance of the proposed SCFDE-STBS-CDMA scheme and the conventional scheme in varying fading channel with $\rho = 0.86$ and ZF Equalization.

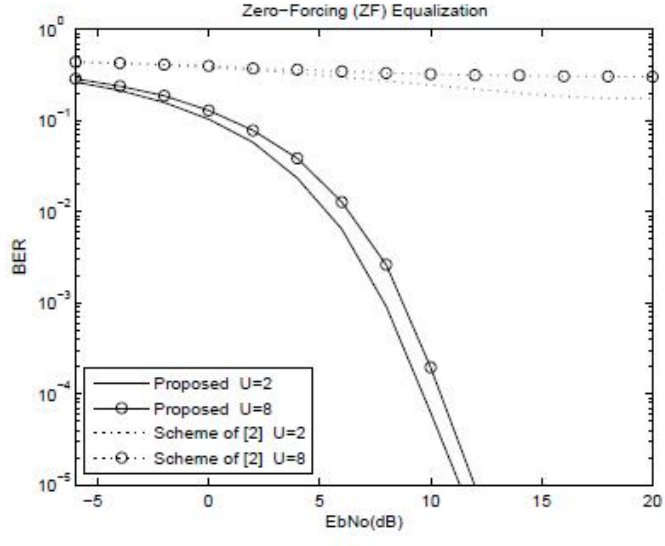

Figure 5.6 Comparison of the BER performance of the proposed SCFDE-STBS-CDMA scheme and the conventional scheme in varying fading channel with $\rho = 0.50$ and ZF Equalization.

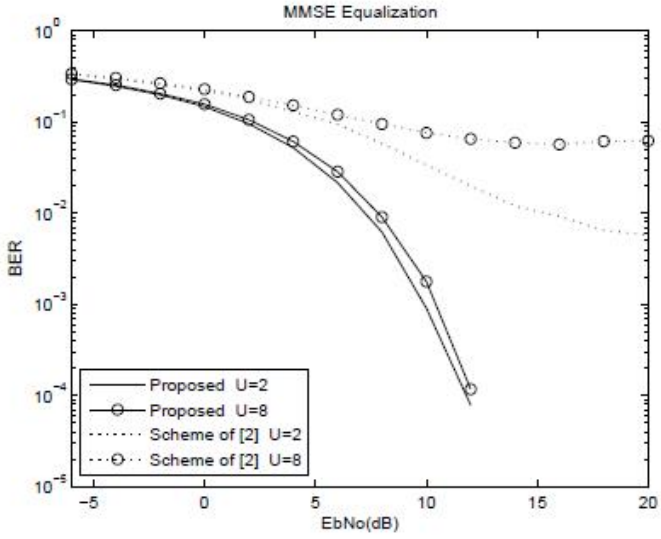

Figure 5.7 Comparison of the BER performance of the proposed SCFDE-STBS-CDMA scheme and the conventional scheme in varying fading channel with $\rho = 0.86$ and MMSE Equalization.

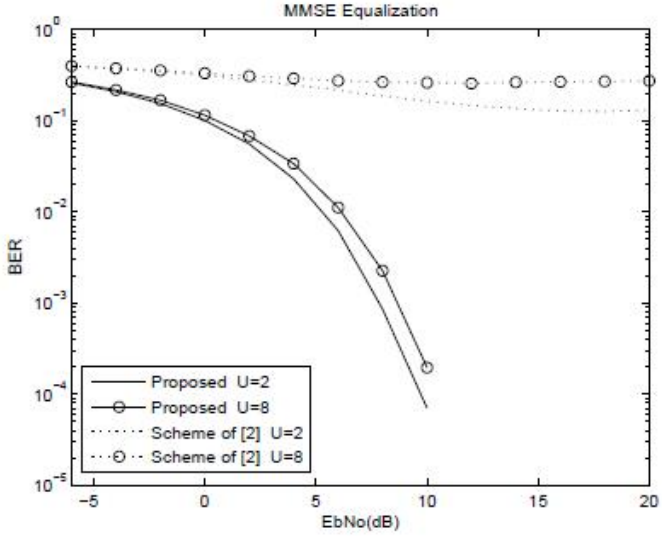

Figure 5.8 Comparison of the BER performance of the proposed SCFDE-STBS-CDMA scheme and the conventional scheme in varying fading channel with $\rho = 0.50$ and MMSE Equalization.

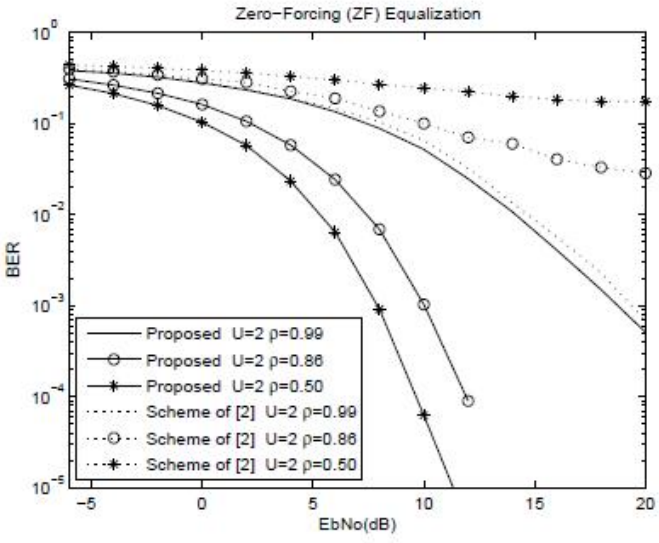

Figure 5.9 Comparison of the BER performance of the proposed SCFDE-STBS-CDMA scheme and the conventional scheme in varying fading channel with $\rho = 0.99, 0.86, 0.50$ and ZF Equalization.

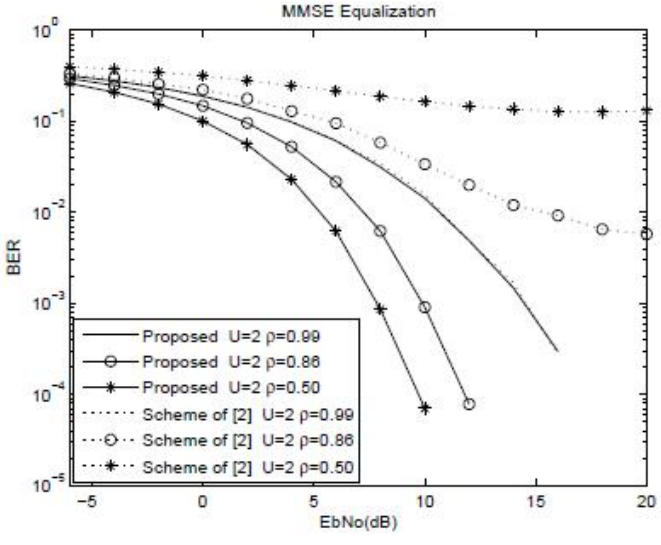

Figure 5.10 Comparison of the BER performance of the proposed SCFDE-STBS-CDMA scheme and the conventional scheme in varying fading channel with $\rho = 0.99, 0.86, 0.50$ and MMSE Equalization.

CHAPTER 6

PERFORMANCE ANALYSIS OF SPACE-TIME SPREADING CDMA SYSTEM IN FAST FADING CHANNELS

Rapid temporal variations in wireless channels pose a significant challenge for space-time modulation and coding system proposed in [18] and [53]. In these conventional transmit diversity systems, it is generally assumed that the channel is static for the duration of one space-time codeword and hence they can provide high transmit diversity gain. However their inability to account for the natural time variation of the channel make them less attractive for systems that must be able to operate reliably in rapidly fading environments. In [54–57], the impact of the time varying channel on the performance of space-time coding systems have been studied and detectors have been proposed to combat such channel variation. Inspired by space-time codes, in [58] an attractive transmit diversity scheme with space time spreading (STS) has been proposed for code-division multiple-access (CDMA) systems. In [59,60], Aljerjawi *et. al.* propose a DS-CDMA STS system that uses two symbol periods to transmit the STS signals. In these studies, it was assumed that the channel varies independently from one symbol to another in which case, the bit-error rate performance analysis has been presented. However, in practical wireless channel, there could be a correlation between the channel coefficients in two consecutive symbols [51]. The correlation coefficient could be near unity for slowly fading channels, or may be small (but not zero) in rapidly varying channels. Hence the independence assumption is not always justified. In this chapter, the authors analyze the performance of STS system in a practical correlated wireless channel using Jakes' channel correlation model [26]. It is assumed that the transmitter uses two transmit antennas and two orthogonal spreading codes to generate two STS symbols transmitted over a time-correlated Rayleigh

fading channel. As the main contribution of this chapter, the authors derive a closed form expression for the probability of bit error as a function of the channel correlation. The theoretical analysis is shown to be very accurate when compared to the simulation results. The rest of the chapter is organized as follows. The system model and analysis are described in section II . The simulation results are presented in section III followed by some conclusions in section IV.

6.1 System Model

Consider a single user with (2×1) antenna system (extension to multiuser case and to system with more than one receive antenna is straightforward) where the transmitter employs the STS transmit-diversity scheme described in ref. [58] which transmits a pair of chips-blocks $\mathbf{x}_1$ and $\mathbf{x}_2$ over a time varying and frequency flat Raleigh fading channel. Let $h_i^{(k)}, i = 1, 2$ denote the complex channel impulse response between the i^{th} transmit antenna and the receive antenna during the k^{th} symbol transmission period. It is assumed that the channel coefficients $h_i^{(k)}$ are identically distributed , zero-mean with unit variance, i.e., $E[|h_i^{(k)}|^2] = 1,\ \forall i, k$. The transmit antennas are sufficiently separated so that $h_1^{(k)}$ is independent of $h_2^{(k)}$. The authors adopt Jakes' channel model [26] for each antenna and assume that the fading is temporally symmetric such that the fading autocorrelation function for i=1, 2 is the zeroth-order Bessel function of the first kind. i.e., $\rho = E[h_i^{(k)} h_i^{(k+1)*}] = J_o(2\pi f_D T_s)$ where T_s is the symbol period and f_D is the maximum Doppler spread. For notation simplicity, ρ is assumed real positive, i.e., $|\rho|$=ρ. Perfect channel knowledge is available at the receiver only. The transmitted signals from antenna one and two respectively are given by the chips-blocks

$$\begin{aligned} \mathbf{x}_1 &= s_1\mathbf{c}_1 - s_2^*\mathbf{c}_2 \\ \mathbf{x}_2 &= s_2\mathbf{c}_1 + s_1^*\mathbf{c}_2 \end{aligned} \tag{6.1}$$

where s_1 and s_2 are the input symbols to the encoder with $E[|s_i|^2] = E_s$ and $\mathbf{c}_1$ and $\mathbf{c}_2$ are two orthogonal spreading codes (row vectors) with unit energy. The received signal corresponding to the the k^{th} and $(k+1)^{th}$ symbol periods are respectively given by

$$\begin{aligned} \mathbf{r}^{(k)} &= h_1^{(k)}\mathbf{x}_1 + h_2^{(k)}\mathbf{x}_2 + \mathbf{w}^{(k)} \\ \mathbf{r}^{(k+1)} &= h_1^{(k+1)}\mathbf{x}_1 + h_2^{(k+1)}\mathbf{x}_2 + \mathbf{w}^{(k+1)} \end{aligned} \tag{6.2}$$

where $\mathbf{w}^{(k)}$ represents the zero mean circularly symmetric AWGN noise with variance N_o added to the k^{th} received signal. Note from (6.2) that the same chips-blocks are transmitted during the two consecutive symbol periods. By multiplying the received signals $\mathbf{r}^{(k)}$ by the spreading codes $\mathbf{c}_1^T$ and $\mathbf{c}_2^T$ respectively [1], it follows

$$\begin{aligned} z_1^{(k)} &= \mathbf{r}^{(k)}\mathbf{c}_1^T = \ h_1^{(k)}s_1 + h_2^{(k)}s_2 + n_1^{(k)} \\ z_2^{(k)} &= \mathbf{r}^{(k)}\mathbf{c}_2^T = -h_1^{(k)}s_2^* + h_2^{(k)}s_1^* + n_2^{(k)} \end{aligned} \tag{6.3}$$

In (6.3), the orthogonality of the spreading code has been used, i.e., $\mathbf{c}_i\mathbf{c}_i^T = 1$ and $\mathbf{c}_i\mathbf{c}_j^T = 0, \forall i \neq j$. The receiver performs signal combining for the k^{th} receiver signal as follow

$$\begin{aligned} y_1^{(k)} &= h_1^{(k)*}z_1^{(k)} + h_2^{(k)}z_2^{(k)*} = \alpha_k^2 s_1 + h_1^{(k)*}n_1^{(k)} + h_2^{(k)}n_2^{(k)*} \\ y_2^{(k)} &= h_2^{(k)*}z_1^{(k)} - h_1^{(k)}z_2^{(k)*} = \alpha_k^2 s_2 + h_2^{(k)*}n_1^{(k)} - h_1^{(k)}n_2^{(k)*} \end{aligned} \tag{6.4}$$

where $\alpha_k^2 = |h_1^{(k)}|^2 + |h_2^{(k)}|^2$. Similarly, the $(k+1)^{th}$ received signal $y_i^{(k+1)}$ is obtained by replacing k with $k+1$ in (6.4).

[1] This is equivalent in practice to applying the received chips-blocks to two filters matched to the spreading codes $\mathbf{c}_1$ and $\mathbf{c}_2$ respectively

Adding $y_i^{(k)}$ and $y_i^{(k+1)}$, one gets an estimate of s_i as

$$\begin{aligned}
\widehat{s}_1 &= y_1^{(k)} + y_1^{(k+1)} \\
&= (\alpha_k^2 + \alpha_{k+1}^2)s_1 + h_1^{(k)*} n_1^{(k)} + h_2^{(k)} n_2^{(k)*} \\
&\qquad + h_1^{(k+1)*} n_1^{(k+1)} + h_2^{(k+1)} n_2^{(k+1)*} \\
\widehat{s}_2 &= y_2^{(k)} + y_2^{(k+1)} \\
&= (\alpha_k^2 + \alpha_{k+1}^2)s_2 + h_2^{(k)*} n_1^{(k)} - h_1^{(k)} n_2^{(k)*} \\
&\qquad + h_2^{(k+1)*} n_1^{(k+1)} - h_1^{(k+1)} n_2^{(k+1)*}
\end{aligned} \tag{6.5}$$

Note that this result is the same as the one presented in [61] where $s_1^*\mathbf{c}_1 + s_2^*\mathbf{c}_2$ and $s_1\mathbf{c}_1 - s_2\mathbf{c}_2$ are transmitted from antennas 1 and 2 respectively during the first transmission period and switched with respect to the antenna order (i.e., $s_1\mathbf{c}_1 - s_2\mathbf{c}_2$ and $s_1^*\mathbf{c}_1 + s_2^*\mathbf{c}_2$) during the second period. In fact the result in [61] is a special case of our work. Note that all the schemes achieve full rate since two symbols (s_1 and s_2) are transmitted in two time periods. The total transmitted power for two consecutive transmission period is $8E_s$ which can be controlled by setting the value of E_s. From (6.5), it can be easily shown that the signal-to-noise ratio at the receiver output is given by

$$\begin{aligned}
\mu &= \frac{(\alpha_k^2 + \alpha_{k+1}^2)^2 E_s}{(|h_1^{(k)}|^2 + |h_2^{(k)}|^2 + |h_1^{(k+1)}|^2 + |h_2^{(k+1)}|^2)N_o} \\
&= (|h_1^{(k)}|^2 + |h_2^{(k)}|^2 + |h_1^{(k+1)}|^2 + |h_2^{(k+1)}|^2)\gamma_o
\end{aligned} \tag{6.6}$$

where γ_o=E_s/N_o.

Since $h_i^{(k)}$ and $h_i^{(k+1)}$ are correlated with correlation coefficient ρ, using the results in [62] in which a BER analysis of maximal ratio combining is presented, the pdf of the random variable μ_i=$(|h_i^{(k)}|^2 + |h_i^{(k+1)}|^2)\gamma_o$ can be found to be given by

$$f(\mu_i) = \frac{1}{2\gamma_o\rho}\left(e^{-\frac{\mu_i}{\gamma_o(1+\rho)}} - e^{-\frac{\mu_i}{\gamma_o(1-\rho)}}\right), \ \forall \rho \neq 0 \tag{6.7}$$

Since $h_1^{(k)}$ is independent of $h_2^{(k)}$ $\forall k$, the random variables μ_1 and μ_2 are also independent; hence the pdf of the signal-to-noise ratio $\mu = \mu_1 + \mu_2$ can be found as

$$\begin{aligned} f(\mu) &= f(\mu_1) \star f(\mu_2) \\ &= \int_0^\infty f(\mu_1) f(\mu - \mu_1) d\mu_1 \end{aligned} \tag{6.8}$$

where $(\star)$ denotes the linear convolution operation and which after some manipulations yields

$$f(\mu) = \frac{1}{4\rho^2\gamma_o^2}\left[(\mu - \mu_o)e^{-\frac{\mu}{\gamma_o(1+\rho)}} + (\mu + \mu_o)e^{-\frac{\mu}{\gamma_o(1-\rho)}}\right] \tag{6.9}$$

where $\mu_o = (1-\rho^2)\gamma_o/\rho$.

The average bit-error rate assuming Binary-Phase Shift Keying (BPSK) modulation can then be found as [36]

$$P_b = \int_0^\infty Q(\sqrt{2\mu}) f(\mu) d\mu \tag{6.10}$$

which by using the closed-form BER expression results from [36], can easily be shown to be given by

$$\begin{aligned} P_b = &\frac{(1-\rho^2)}{8\rho^3}\left[(1-\rho)(1-\gamma_1) - (1+\rho)(1-\gamma_2)\right] \\ &+ \frac{1}{16\rho^2}\left[(1+\rho)^2(1-\gamma_2)^2(2+\gamma_2)\right. \\ &\left. + (1-\rho)^2(1-\gamma_1)^2(2+\gamma_1)\right] \end{aligned} \tag{6.11}$$

for $\rho \neq 0$ and where the authors have defined

$$\gamma_1 = \sqrt{\frac{1}{1+\frac{1}{\gamma_o(1-\rho)}}} \quad ; \quad \gamma_2 = \sqrt{\frac{1}{1+\frac{1}{\gamma_o(1+\rho)}}} \tag{6.12}$$

In a quasi-static channel where the channel does not change during two symbols period i.e., ρ=1, the bit error rate in (6.11) reduces to

$$P_b = \frac{1}{4}\left[1-\gamma\right]^2\left[2+\gamma\right] \tag{6.13}$$

where $\gamma=\sqrt{1/(1+1/2\gamma_o)}$; this result is the same as in [63, Eq.(23)] which is then a special case of the more general solution presented in this chapter. If however the channel coefficients change independently from one symbol to another, i.e., if ρ=0, the bit error rate is given by [60, Eq.(15)]

$$P_b = \left[\frac{1}{2}(1-\eta)\right]^4 \sum_{k=0}^{3} \begin{pmatrix} 3+k \\ k \end{pmatrix} \left[\frac{1}{2}(1+\eta)\right]^k \tag{6.14}$$

where $\eta=\sqrt{\gamma_o/(1+\gamma_o)}$.

6.2 Simulation and Numerical Results

In this section, the validity of the analytical results presented in this chapter is validated by comparing simulation and theoretical results of the space-time spreading coding in a time varying fading channel. BPSK modulation is used, with the assumption of perfect channel state information (CSI) at the receiver only. Figure. 6.1 depicts the BER versus E_b/N_o (where E_b is the energy per bit) of both simulation and theoretical results confirming the accuracy of our analytical results. Figure. 6.1 also shows how the correlation coefficient affects the performance of the system. The correlation coefficients of ρ=0 and ρ=1 correspond to the lower and upper bounds of the BER which were treated in [61] and [63] respectively. In Figure. 6.2, it is shown how the bit-error-rate varies as a function of the input signal-to-noise ratio for different channel correlation values. One can see that as the correlation coefficient increases, the BER also increases for a given input SNR.

The derived expression in this chapter is more general than the ones in the literature where the channel is assumed either quasi-static, i.e., $\rho = 1$, or independently varying from one symbol to another, i.e., $\rho = 0$.

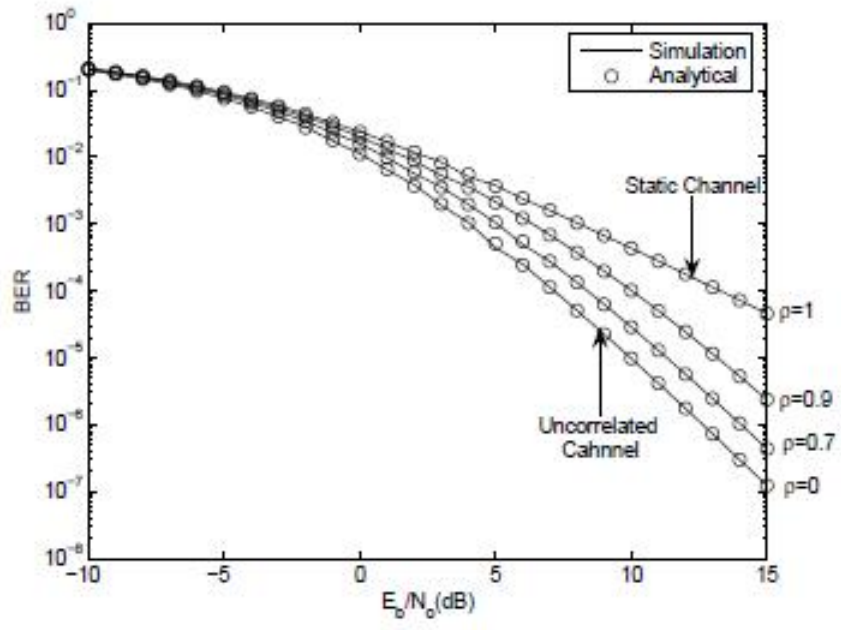

Figure 6.1 Analytical and Simulation BER Performance for channel correlations $\rho = 0, 0.7, 0.9, 1$ with respect to input signal-to-noise ratio EbNo.

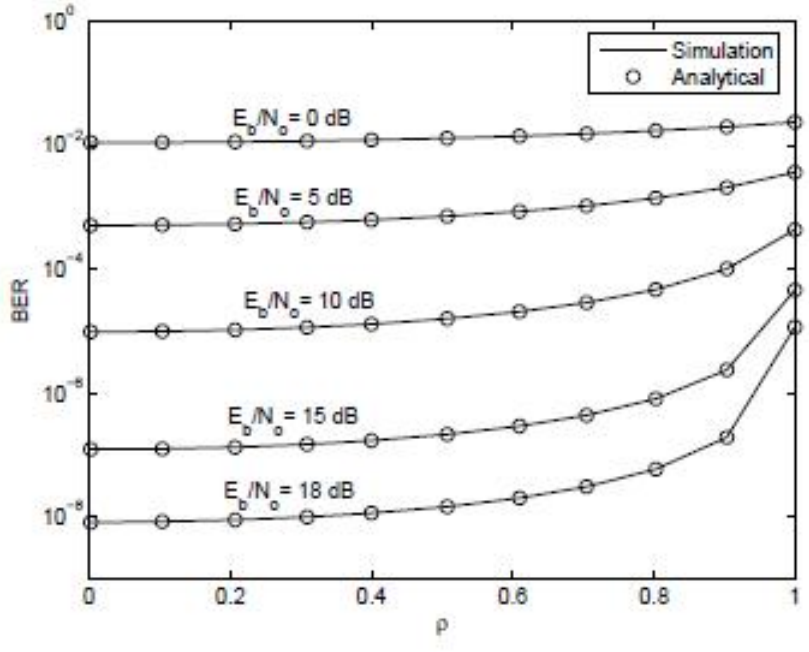

Figure 6.2 Analytical and Simulation BER Performance for input signal-to-noise ratio $E_b/N_o = 0, 5, 10, 15, 18$ dB with respect to the channel correlation ρ.

CHAPTER 7

SINGLE-CARRIER WITH FREQUENCY-DOMAIN EQUALIZATION FOR INDOOR WIRELESS OPTICAL COMMUNICATION

Due the increase in the number of portable information terminals in work and at home, the demand for high speed indoor wireless communication has been growing. Recently the optical spectrum which has virtually unlimited bandwidth, has been receiving growing interest for use in indoor wireless data transmission [64], [65]. Diffuse optical wireless (DOW) communications offer a viable alternative to radio frequency (RF) communication for indoor use and other applications where high performance links are needed. RF systems can support only limited bandwidth because of restricted spectrum availability and interference while this restriction does not apply to DOW links. In indoor DOW systems, light emitting diodes (LED) are used as transmitter and photo-diodes as the receivers for optical signals. These opto-electronic devices are cheaper as compared to RF equipments.

Orthogonal frequency division multiplexing (OFDM) modulation is a promising modulation scheme for indoor DOW communication [66–71]. It offers high data rate and high bandwidth efficiency capabilities and provides a means to combat inter-symbol-interference (ISI) that results from multipath propagation. Among the OFDM systems for DOW transmission, the asymmetrically-clipped optical orthogonal frequency division multiplexing (ACO-OFDM) [70] has been shown to be more efficient in term of optical power than the systems that use DC-biased [72]. ACO-OFDM is a form of OFDM that modulates the intensity of a LED. Because ACO-OFDM modulation employs intensity modulation and direct detection (IM/DD), the time-domain transmitted signal must be real and positive. The block diagram of an IM/DD DOW system is depicted in Figure. 7.1. To ensure a real signal, ACO-OFDM subcarriers

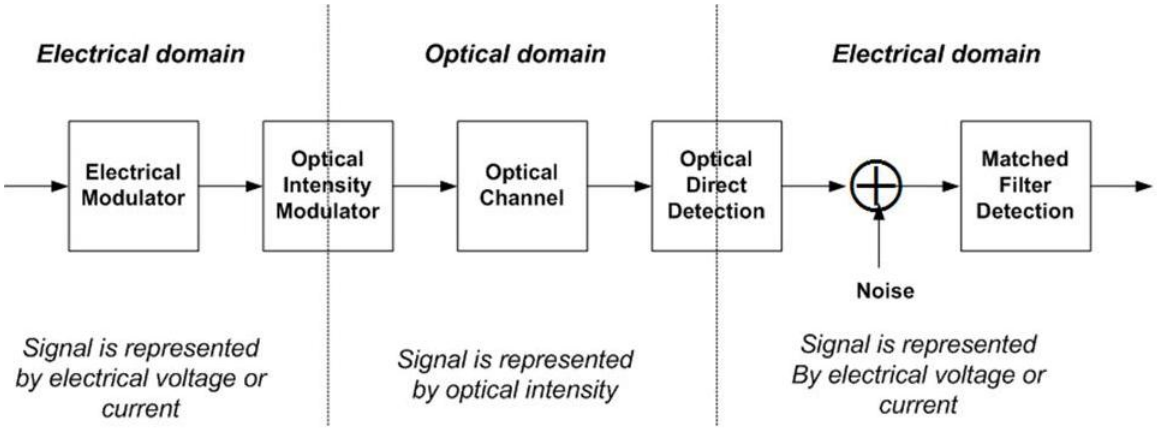

Figure 7.1 Block diagram of Intensity modulated/direct detection (IM/DD) DOW communication system.

have Hermitian symmetry, and to obtain a positive signal, only the odd subcarriers are modulated by the data and any time-domain negative values are clipped at the transmitter. It is shown in [70] that the clipping does not distort the data on the odd subcarriers but does reduce the amplitude of their constellation values by a half. The clipping noise is added only to the the even subcarriers. The data symbols can be easily detected by demodulating only the odd subcarriers. However ACO-OFDM signals, like other OFDM systems, have inherently high PAPR, hence its performance can potentially be severely affected by the nonlinear behavior of the LED [73], [74]. For this reason, single carrier with frequency domain equalization systems have been proposed in optical communication as an alternative to OFDM [75], [76]. In [75], single carrier frequency domain equalization (SCFDE) signal is transmitted over an optical fiber with coherent detection while SCFDE is combined with pulse position modulation (PPM) in [76] for IM/DD DOW transmission. SCFDE applied with coherent detection has also been presented in [66]. In this chapter, the authors suggest applying the concept of asymmetric clipping of [70] to SCFDE which is denoted as ACO-SCFDE for IM/DD transmission over an DOW channel.

Single-carrier modulation using frequency domain equalization is a promising alternative to OFDM for highly dispersive channels in broadband wireless communications [2], [3]. In both approaches, a cyclic prefix (CP) is appended to each block for eliminating the inter-block interference and converting, with respect to the useful part of the transmitted block, the linear convolution with the channel, to circular. This allows low-complexity fast-Fourier transform (FFT)-based receiver implementations. In recent years, SCFDE has become a powerful and an attractive link access method for the next-generation broadband wireless networks [7], [8], [9]. Because it is essentially a single-carrier system, SCFDE does not have some of the inherent problems of OFDM such as high PAPR. As a result, it has recently been receiving remarkable attention and has been adopted in the uplink of the Third Generation Partnership Project (3GPP) Long Term Evolution (LTE) [12] system.

The authors show in this chapter that the PAPR of ACO-SCFDE is quite less than that of ACO-OFDM and that its BER performance is better compared to ACO-OFDM when minimum mean square error (MMSE) detection is employed. The latter property is due to the inherent frequency diversity gain of SCFDE [32] and its low PAPR. Since the LED has limited linear range in its transfer characteristics any values outside of that limited range will be clipped and distorted resulting in performance loss. The authors also propose in this chapter two other schemes for generating real, positive signals with low PAPR for IM/DD optical DOW communications using SCFDE. The rest of the chapter is organized as follows. In section II, the ACO-OFDM scheme is reviewed. In section III the proposed ACO-SCFDE is presented. The two other newly proposed low PAPR schemes for optical communication using SCFDE which is called Repeat-and-Clipped Optical SCFDE (RCO-SCFDE) and Decomposed Quadrature Optical SCFDE (DQO-SCFDE) are presented in section IV and V respectively followed by an analysis of the PAPR issues for DOW in

section VI. Performance analysis are presented in section VII followed by the conclusion in section VIII.

7.1 Asymmetrically-Clipped Optical OFDM (ACO-OFDM)

The block diagram of a DOW communication system using ACO-OFDM is shown in Figure. 7.2-(a). The information stream is first parsed into a block of N complex data symbols denoted by $\mathbf{S} = [S_0, S_1, \cdots, S_{N-1}]^T$ where the symbols are drawn from constellations such as QPSK, 16-QAM or 64-QAM with average electrical power $E[|S_k|^2]=P_s$. These complex symbols are then mapped onto the following $4N \times 1$ vector

$$\mathbf{X} = [0, S_0, 0, S_1, \cdots, 0, S_{N-1}, 0, S^*_{N-1}, 0, S^*_{N-2}, \cdots, 0, S^*_0]^T. \tag{7.1}$$

Note that the average power of the block $\mathbf{X}$ is given by $E[|X_k|^2]=P_s/2$. A $4N$-point IFFT is then taken to construct the time domain signal $\mathbf{x} = [x_0, x_1, \cdots, x_{4N-1}]^T$. A cyclic prefix is added to $\mathbf{x}$ as shown if Figure. 7.2-(b). The CP turns the linear convolution with the channel into a circular one, avoiding inter-carrier interference (ICI) as well as inter-block interference (IBI). To make the transmitted signal unipolar, all the negative values are clipped to zero to form the signal vector of

$$\widetilde{\mathbf{x}} = [\widetilde{x}_{4N-L}, \cdots, \widetilde{x}_{4N-1}, \widetilde{x}_0, \widetilde{x}_1, \cdots, \widetilde{x}_{4N-1}]^T \tag{7.2}$$

whose components are:

$$\widetilde{x}_n = \begin{cases} x_n, & \texttt{if} \quad x_n > 0, \\ 0, & \texttt{if} \quad x_n \leq 0. \end{cases} \tag{7.3}$$

Because only the odd subcarriers are used to carry the data symbols, it is proved in [70] that the time-domain signal has an antisymmetry which ensures that clipping will not distort the odd subcarriers, but only reduce their amplitude by a factor of 2,

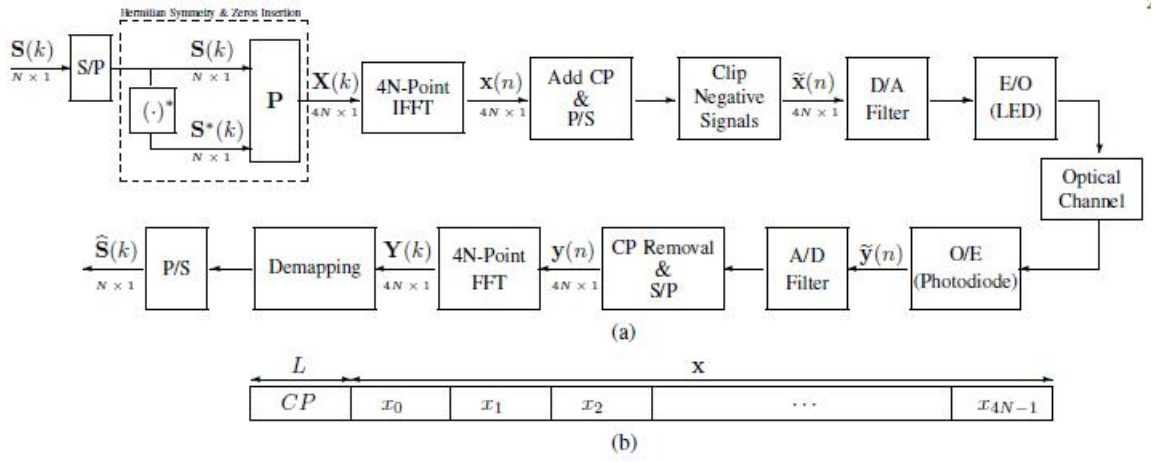

Figure 7.2 (a) ACO-OFDM Transmitter and Receiver configuration. (b) ACO-OFDM symbol after cyclic extension.

hence the average transmitted electrical power (before the LED driving DC bias) is given by $E[|\widetilde{x}_n|^2]{=}P_s/4$.

The intermodulation caused by clipping occurs only in the even subcarriers and does not affect the data-carrying odd subcarriers. Note that the use of only odd subcarriers together with the Hermitian symmetry constraint cause only N independent complex symbols to be transmitted out of the $4N$ point IFFT. That is, the time domain signal $\mathbf{x}$ has a length of $4N$ sample periods for N input data symbols. The ACO-OFDM signal is then transmitted wirelessly via a light source (LED) through a diffuse optical channel and received by a photodetector. The received signal before the analog-to-digital converter is given by

$$\widetilde{\mathbf{y}} = \widetilde{\mathbf{x}} \star \mathbf{h} + \widetilde{\mathbf{w}}, \tag{7.4}$$

where $\mathbf{h}{=}[h(0), h(1), \cdots, h(L-1)]^T$ is the L-path impulse response of the optical channel, $\widetilde{\mathbf{x}}$ is the optical intensity of the transmitted signal block with the CP appended ($\mathbf{x}$ is the transmitted block without the CP), $\widetilde{\mathbf{w}}$ is additive white Gaussian noise (AWGN) at the receiver. DOW links are subject to intense ambient light that gives rise to a high-rate, signal-independent shot noise, which can be modeled as

white and Gaussian [64]. When such ambient light is absent, the dominant noise is preamplifier thermal noise, which is Gaussian. Thus, one can model the noise as AWGN. Note that because the noise is added in the electrical domain, the received signal $\widetilde{\mathbf{y}}$ can be negative as well as positive. So unlike the transmitted signal, the received signal is bipolar instead of unipolar. The CP is then removed to yield

$$\mathbf{y} = \mathbf{x} \odot \mathbf{h} + \mathbf{w}, \tag{7.5}$$

where $\mathbf{w}$ is the noise vector without the CP. The linear convolution is turned into a circular one through the use of the CP [30], [77]. To demodulate the signal, a $4N$-point FFT is taken to access the frequency domain symbols

$$\mathbf{Y} = \mathbf{\Lambda X} + \mathbf{W}, \tag{7.6}$$

where $\mathbf{\Lambda}$ is a $4N \times 4N$ diagonal matrix whose diagonal is the $4N$-point FFT of $\mathbf{h}$ and $\mathbf{W}$ is the $4N$-point FFT of $\mathbf{w}$. The odd subcarriers are extracted from $\mathbf{Y}$ to yield

$$\mathbf{Y}_o = \mathbf{\Lambda}_o \overline{\mathbf{S}} + \mathbf{W}_o, \tag{7.7}$$

where

$$\overline{\mathbf{S}} = \frac{1}{2}[S_0, S_1, \cdots, S_{N-1}, S^*_{N-1}, S^*_{N-2}, \cdots, S^*_0]^T, \tag{7.8}$$

$\mathbf{Y}_o$ and $\mathbf{W}_o$ are the vectors composed of the odd elements of $\mathbf{Y}$ and $\mathbf{W}$ respectively. The factor $1/2$ is due to the fact that the clipping caused the amplitude of each of the (odd) data-carrying subcarriers is exactly half of its original value [70] . Similarly, $\mathbf{\Lambda}_o$ is a $2N \times 2N$ diagonal matrix whose diagonal contains the odd elements of the diagonal of $\mathbf{\Lambda}$.

To mitigate the effects of the channel, minimum-mean-square-error (MMSE) or zero-forcing (ZF) equalization can be used on $\mathbf{Y}_o$ to obtain an estimate for $\overline{\mathbf{S}}$ as

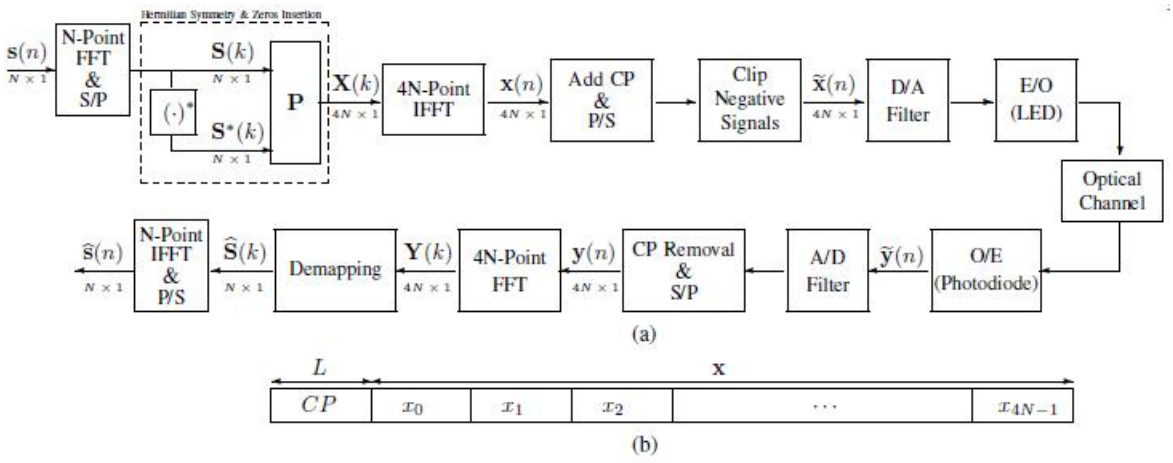

Figure 7.3 (a) ACO-SCFDE Transmitter and Receiver configuration. (b) ACO-SCFDE symbol after cyclic extension.

follows:

$$\widehat{\overline{\mathbf{S}}} = \left(\mathbf{\Lambda}_o^{\mathcal{H}}\mathbf{\Lambda}_o + (\alpha/SNR)\mathbf{I}_{2N}\right)^{-1}\mathbf{\Lambda}_o^{\mathcal{H}}\mathbf{Y}_o, \tag{7.9}$$

where α=1 for MMSE and α=0 for ZF receivers and SNR is the electrical power of the transmitted symbol divided by the power of the electrical noise at the receiver. Due to the Hermitian symmetry condition, the symbols of $\mathbf{S}$ are repeated in $\overline{\mathbf{S}}$, hence, one can add them after conjugation of the second half as follows:

$$\widehat{\mathbf{S}} = \left[\widehat{\overline{\mathbf{S}}}(k)\right]_{k=0}^{N-1} + \left[\widehat{\overline{\mathbf{S}}}^{*}(2N-1-k)\right]_{k=0}^{N-1} \tag{7.10}$$

Hard or soft detection is then made on the symbol of $\widehat{\mathbf{S}}$. The extraction of odd subcarriers along with the equalization and the regrouping process of (7.10) are represented by the "Demapping" block in Figure. 7.2.

The spectral efficiency [1] of ACO-OFDM is given by

$$\varepsilon_{ACO} = \frac{N}{4N+L} \tag{7.11}$$

[1]Define the spectral efficiency to be the number of modulated subcarriers over the total number of time-domain samples

and is plotted in Figure. 7.10 and Figure. 7.9 as a function of the number of subcarrier N and channel delay spread where it is compared with other schemes.

To avoid the PAPR problem (which is examined later in this chapter) of OFDM in DOW channels, a new modulation for optical communication using SCFDE is investigated in this chapter. First the authors apply ACO-OFDM to SCFDE which is denoted as by ACO-SCFDE. The authors show that the latter exhibits better PAPR. It is also shown that the other proposed two modulation schemes for optical communication called repetition and clipped optical SCFDE (RCO-SCFDE) and decomposed quadrature optical SCFDE (DQO-SCFDE), exhibit lower PAPR. Based on this fact , they are preferable for DOW communication where LED nonlinearity can affect the system performance.

7.2 Asymmetrically-Clipped Optical SCFDE (ACO-SCFDE)

In this section, the authors apply asymmetrically-clipped optical modulation to SCFDE to achieve ACO-SCFDE with low PAPR. SCFDE in its original form [2] cannot directly be applied to DOW with IM/DD. This is because the transmitted signal has to be real and positive while baseband SCFDE signals are generally complex and bipolar. In fact, ACO and DC-biased are two ways to obtain real positive signals from complex constellation symbols such as QPSK, M-QAM considered in this chapter. As it was shown in [70] that ACO-OFDM is more power efficient than DC-biased OFDM, therefore in this chapter, the authors focus on ACO which is applied to SCFDE and compare it with ACO-OFDM. In ACO-SCFDE, an FFT and IFFT are used at the transmitter and the receiver. The additional complexity of the extra FFT at the transmitter which is needed to obtain the Hermitian constraint on the frequency domain symbols, is offset by the fact that in SCFDE, the PAPR is reduced and better BER performance can be achieved when the signal is sent through a non-linear LED. Let the N input complex data symbols be denoted by

the block $\mathbf{s} = [s_0, s_1, \cdots, s_{N-1}]^T$ with average electrical power $E[|s_n|^2]{=}P_s$. In order to achieve the Hermitian constraint, one first performs, at the transmitter, an N-point FFT on $\mathbf{s}$ to produce the frequency domain vector $\mathbf{S} = [S_0, S_1, \cdots, S_{N-1}]^T$ with average power $E[|S_k|^2]{=}P_s$. As in ACO-OFDM, the authors map each of the N symbols of $\mathbf{S}$ to $2N$ Hermitian symmetric symbols and add zeroes to form the $4N \times 1$ vector $\mathbf{X} = [0, S_0, 0, S_1, \cdots, 0, S_{N-1}, 0, S^*_{N-1}, 0, S^*_{N-2}, \cdots, 0, S^*_0]^T$. Due to the structure of $\mathbf{X}$ (zeros in the even locations) only the odd subcarriers carry data symbols. Next a $4N$-point IFFT is used to obtain the time domain signal denoted by $\mathbf{x} = [x_0, x_1, \cdots, x_{4N-1}]^T$. A CP is then added to $\mathbf{x}$ to yield $\widetilde{\mathbf{x}}$ and the negative values are clipped to zero as in ACO-OFDM. Hence, in ACO-SCFDE, the average transmitted electrical power (before the LED DC bias) is also given by $E[|\widetilde{x}|^2] = P_s/4$. The block diagram of this ACO-SCFDE scheme is shown in Figure. 7.3-(a) and the ACO-SCFDE symbol structure is shown in Figure. 7.3-(b). As will be seen later, the main advantage of ACO-SCFDE over ACO-OFDM is its lower PAPR. At the receiver, after removing the CP, a $4N$-point FFT is applied. The odd subcarriers are then extracted exactly as in ACO-OFDM to yield the same equation as in (7.7) and the frequency domain symbol block $\mathbf{S}$ is estimated as in (7.10). After that, $\widehat{\mathbf{S}}$ is transformed back into the time domain to yield $\widehat{\mathbf{s}} = \mathbf{F}_N^{\mathcal{H}}\widehat{\mathbf{S}}$ where $\mathbf{F}_N^{\mathcal{H}}$ is the IFFT matrix. A hard or soft detection is made on $\widehat{\mathbf{s}}$. The spectral efficiency of ACO-SCFDE is the same as ACO-OFDM. The main difference between ACO-SCFDE and ACO-OFDM schemes is the addition of the N-point FFT and IFFT at the transmitter and receiver respectively. The addition of an FFT and IFFT at the transmitter results in a single carrier transmission instead of multicarrier and hence reduction of the PAPR as shown in Figure. 7.6.

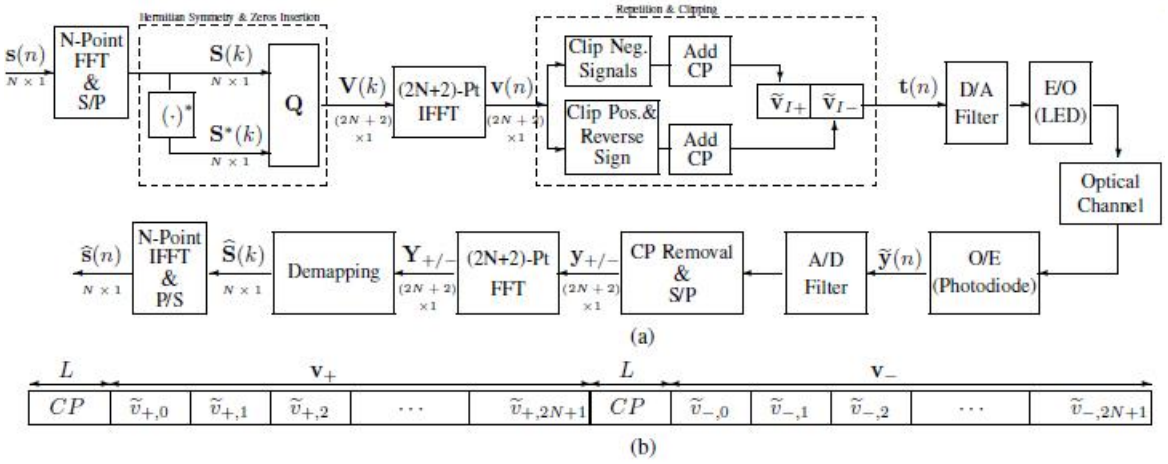

Figure 7.4 (a) RCO-SCFDE Transmitter and Receiver configuration. (b) RCO-SCFDE symbol after cyclic extension.

7.3 Repetition and Clipping Optical SCFDE (RCO-SCFDE)

One drawback of the ACO-SCFDE or ACO-OFDM schemes is that only half of the subcarriers are used to carry data and the rest are set to zero. In another new scheme which is proposed in this section, called repetition and clipping optical SCFDE (RCO-SCFDE), only two subcarriers are set to zero, i.e. do not carry data. The N input complex data symbols $\mathbf{s} = [s_0, s_1, \cdots, s_{N-1}]^T$ with $E[|s_n|^2] = P_s$ is first transformed into the frequency domain to yield N complex symbols which is denoted as by the block $\mathbf{S} = [S_0, S_1, \cdots, S_{N-1}]^T$ with $E[|S_k|^2]{=}P_s$. The Hermitian symmetry condition is achieved by forming the $(2N + 2) \times 1$ frequency domain vector

$$\mathbf{V} = [0, S_0, S_1, \cdots, S_{N-1}, 0, S^*_{N-1}, S^*_{N-2}, \cdots, S^*_0]^T. \tag{7.12}$$

Note that the average power of $\mathbf{V}$ is $E[|V_k|^2]{\approx}P_s$. The block $\mathbf{V}$ is applied to a $(2N + 2)$-point IFFT [2] to transform it back to the time domain vector $\mathbf{v} = [v_0, v_1, \cdots, v_{2N+1}]^T$ with average electrical power $E[|v_n|^2] \approx P_s$. From the hermitian symmetry construction of (7.12), it is easily shown that the vector $\mathbf{v}$ is real. The

[2]In implementing RCO-SCFDE, one should choose $N = 2^k - 1$, (k being an integer) such that $2N + 2$ is a power of 2 to reduce the complexity of IFFT.

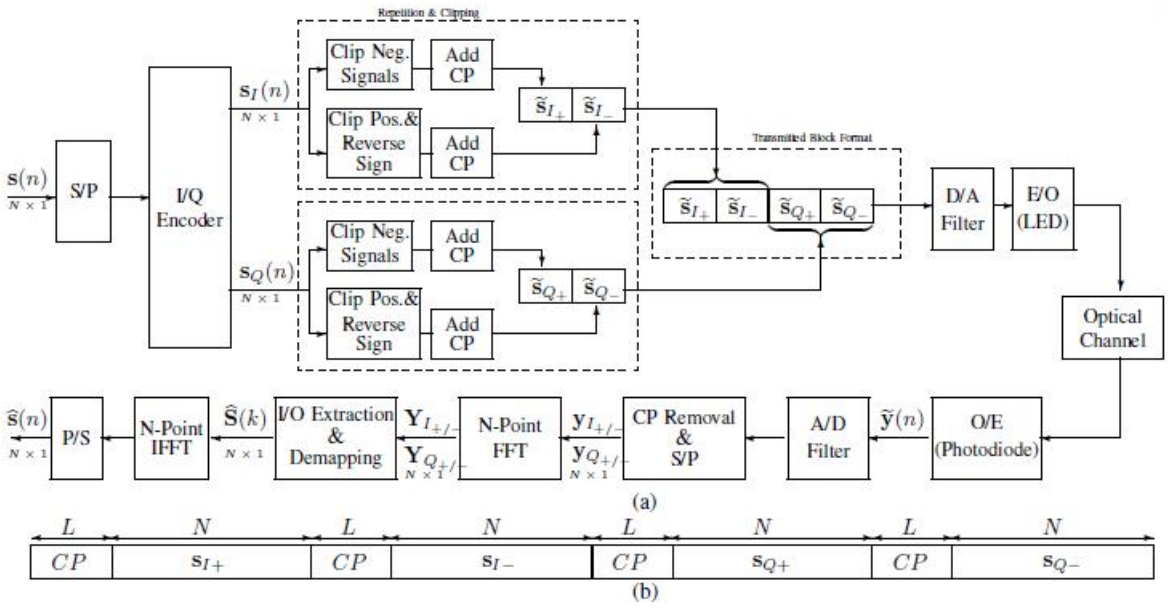

Figure 7.5 (a) DQO-SCFDE Transmitter and Receiver configuration. (b) DQO-SCFDE symbol after cyclic extension.

block $\mathbf{v}$ is then repeated and clipped to yield the $(4N+4)\times 1$ vector $[\mathbf{v}_+^T;\mathbf{v}_-^T]^T$ as follow:

- In the first half of the repeated block, i.e in $\mathbf{v}_+$, the negative symbols of $\mathbf{v}$ are clipped to zeros
- In the second half of the repeated block, i.e. in $\mathbf{v}_-$, the positive symbols of $\mathbf{v}$ are clipped to zeros

  That is

$$v_{+,n} = \begin{cases} v_n, & \texttt{if } v_n > 0 \\ 0, & \texttt{if } v_n \leq 0 \end{cases}$$
$$v_{-,n} = \begin{cases} 0, & \texttt{if } v_n \geq 0 \\ -v_n, & \texttt{if } v_n < 0 \end{cases} \tag{7.13}$$

where $v_{+,n}$ and $v_{+,n}$ represent the n-th ($n = 0, 1, \cdots, 2N+1$) element of $\mathbf{v}_+$ and $\mathbf{v}_-$ respectively. A CP of length L is then added to $\mathbf{v}_+$ and $\mathbf{v}_-$ to yield $\widetilde{\mathbf{v}}_+$ and $\widetilde{\mathbf{v}}_-$

respectively . Note that the average electrical power of the block $[\mathbf{v}_+^T; \mathbf{v}_-^T]^T$ is given by $P_s/2$. The transmitted block is then denoted by the $(4N + 4 + 2L) \times 1$ vector $\mathbf{t} = \sqrt{1/2}[\widetilde{\mathbf{v}}_+^T, \widetilde{\mathbf{v}}_-^T]^T$. The factor $\sqrt{1/2}$ is added to make the average transmitted electrical power the same as in the ACO-OFDM and ACO-SCFDE case, i.e. $P_s/4$. For notation simplicity, the normalizing factor $\sqrt{1/2}$ will be ignored in the following equations but will be taken into consideration in the simulation results. The block diagram of RCO-SCFDE is depicted in Figure. 7.4-(a) and the RCO-SCFDE is shown in Figure. 7.4-(b). The transmitted signal in this scheme is of length $4N$+4+$2L$ while it is $4N$+L in the ACO-SCFDE or ACO-OFDM case. That is there is then a slight bandwidth loss of L+4 symbols in this scheme. Note from (7.13) that

$$\mathbf{v} = \mathbf{v}_+ - \mathbf{v}_-. \tag{7.14}$$

and that the transmitted block $\mathbf{t}$ is composed of real positive signals. The received signal is given by

$$\widetilde{\mathbf{y}} = \mathbf{t} \star \mathbf{h} + \widetilde{\mathbf{w}}. \tag{7.15}$$

After removing the CP's, and using the fact that the CP makes linear convolution behave like cyclic convolution [30], [77], the received blocks corresponding to the first and second part of $\mathbf{t}$, (i.e. $\widetilde{\mathbf{v}}_+$ and $\widetilde{\mathbf{v}}_-$) are respectively given by the $(2N + 2) \times 1$ blocks $\mathbf{y}_+$ and $\mathbf{y}_-$ as follow

$$\begin{aligned} \mathbf{y}_+ &= \mathbf{v}_+ \odot \mathbf{h} + \mathbf{w}_+ \\ \mathbf{y}_- &= \mathbf{v}_- \odot \mathbf{h} + \mathbf{w}_- \end{aligned} \tag{7.16}$$

where $\mathbf{w}_+$ and $\mathbf{w}_-$ are the AWGN at the receiver. A $(2N + 2)$-point FFT is then taken separately on $\mathbf{y}_+$ and $\mathbf{y}_-$ to yield

$$\begin{aligned} \mathbf{Y}_+ &= \mathbf{\Lambda}'\mathbf{V}_+ + \mathbf{W}_+ \\ \mathbf{Y}_- &= \mathbf{\Lambda}'\mathbf{V}_- + \mathbf{W}_- \end{aligned} \tag{7.17}$$

where $\mathbf{V}_+$,$\mathbf{V}_-$,$\mathbf{W}_+$ and $\mathbf{W}_-$ are the $(2N+2)$-point FFT of $\mathbf{v}_+$, $\mathbf{v}_-$, $\mathbf{w}_+$, $\mathbf{w}_-$ respectively. $\mathbf{\Lambda}'$ is a $(2N+2)\times(2N+2)$ diagonal matrix whose diagonal elements are the $(2N+2)$-point FFT of $\mathbf{h}$.

The MMSE or ZF equalizer applied to $\mathbf{Y}_+$ and $\mathbf{Y}_-$ yield

$$\begin{aligned}\widehat{\mathbf{V}}_+ &= \left(\mathbf{\Lambda}'^{\mathcal{H}}\mathbf{\Lambda}' + (1/SNR)\mathbf{I}_{2N+2}\right)^{-1}\mathbf{\Lambda}'^{\mathcal{H}}\mathbf{Y}_+ \\ \widehat{\mathbf{V}}_- &= \left(\mathbf{\Lambda}'^{\mathcal{H}}\mathbf{\Lambda}' + (1/SNR)\mathbf{I}_{2N+2}\right)^{-1}\mathbf{\Lambda}'^{\mathcal{H}}\mathbf{Y}_-\end{aligned} \tag{7.18}$$

From (7.14), one notes that $\mathbf{V} = \mathbf{V}_+ - \mathbf{V}_-$, hence, one can form the estimated vector

$$\widehat{\mathbf{V}} = \widehat{\mathbf{V}}_+ - \widehat{\mathbf{V}}_-. \tag{7.19}$$

Using (7.12), the frequency domain transmitted symbols $\mathbf{S}$ are then estimated as

$$\widehat{\mathbf{S}} = \left[\widehat{\mathbf{V}}(k)\right]_{k=1}^{N} + \left[\widehat{\mathbf{V}}^*(2N+2-k)\right]_{k=1}^{N} \tag{7.20}$$

where the subcarriers 0 and $N+1$ were dropped since they do not carry any data. One then obtain the time domain signal by the taking a N-point IFFT of $\widehat{\mathbf{S}}$ followed by a hard or soft detection. The spectral efficiency of RCO-SCFDE is given by

$$\varepsilon_{RCO} = \frac{N}{4N+2L+4} \tag{7.21}$$

and depicted in Figure. 7.10 as a function of the number of subcarrier N and channel delay spread L. Figure. 7.10 also demonstrates it's efficiency compared to other schemes.

The main advantages of RCO-SCFDE are:

- In ACO-SCFDE and ACO-OFDM, only half of the electrical power is used on the odd frequency, data-carrying subcarriers. The other half is used on the even subcarriers which are discarded at the receiver. RCO-SCFDE does not have this disadvantage.

- the PAPR of RCO-SCFDE is lower than that ACO-OFDM and is plotted in Figure. 7.6
- the size of the IFFT at the transmitter is $2N+2$ while it is $4N$ for ACO-SCFDE and ACO-OFDM.

7.4 Decomposed Quadrature Optical SCFDE (DQO-SCFDE)

With this scheme, a different technique than the Hermitian symmetry constraint is used to generate the real positive symbols needed for intensity modulated direct detection (IM/DD) optical communication. In the previous schemes, after modulating subcarriers with Hermitian symmetry, one must use an IFFT to transform the signal into the time domain before transmission. The use of an IFFT increases the PAPR of the transmitted signal. In this new scheme which is called Decomposed Quadrature Optical SCFDE (DQO-SCFDE), the real (in-phase) and imaginary (quadrature) part of the complex modulated symbols are transmitted separately as follows. Let the input N complex data symbols be denoted by the block $\mathbf{s} = [s_0, s_1, \cdots, s_{N-1}]^T$ with $E[|s_n|^2]$=P_s and let $\mathbf{s}_I = [\mathcal{R}_e(s_0), \mathcal{R}_e(s_1), \cdots, \mathcal{R}_e(s_{N-1})]$ and $\mathbf{s}_Q = [\mathcal{I}_m(s_0), \mathcal{I}_m(s_1), \cdots, \mathcal{I}_m(s_{N-1})$ the vector of the real (in-phase) and imaginary (quadrature) part of $\mathbf{s}$ respectively. As in RCO-SCFDE case, the authors form the vectors $\mathbf{s}_{I+}$, $\mathbf{s}_{I-}$, $\mathbf{s}_{Q+}$ and $\mathbf{s}_{Q-}$ as follow:

$$
\begin{aligned}
s_{I_+}(n) &= \begin{cases} s_I(n), & \texttt{if} \;\; s_I(n) > 0 \\ 0, & \texttt{if} \;\; s_I(n) \leq 0 \end{cases} \\
s_{I_-}(n) &= \begin{cases} 0, & \texttt{if} \;\; s_I(n) \geq 0 \\ -s_I(n,), & \texttt{if} \;\; s_I(n) < 0 \end{cases}
\end{aligned}
\tag{7.22}
$$

$\mathbf{s}_{Q_+}$ and $\mathbf{s}_{Q_-}$ are similarly defined. A CP is added to each subblock to yield the $(N+L)\times 1$ vector $\widetilde{\mathbf{s}}_{I,i}$ and $\widetilde{\mathbf{s}}_{Q,i}$ and the following $4(N+L)$ real and positive symbol

block $\widetilde{\mathbf{x}}$ is transmitted

$$\widetilde{\mathbf{x}} = [\widetilde{\mathbf{s}}_{I_+}, \widetilde{\mathbf{s}}_{I_-}, \widetilde{\mathbf{s}}_{Q_+}, \widetilde{\mathbf{s}}_{Q_-}]^T. \tag{7.23}$$

Note that one has

$$\begin{aligned} \mathbf{s}_I &= \mathbf{s}_{I_+} - \mathbf{s}_{I_-} \\ \mathbf{s}_Q &= \mathbf{s}_{Q_+} - \mathbf{s}_{Q_-} \end{aligned} \tag{7.24}$$

One can easily show that the average transmitted electrical power in this case is also given by $P_s/4$. The block diagram of DQO-SCFDE is shown in Figure. 7.5. The received signal is given by

$$\widetilde{\mathbf{y}} = \widetilde{\mathbf{x}} \star \mathbf{h} + \widetilde{\mathbf{w}}. \tag{7.25}$$

After removing the CP's, the received subblock of length N corresponding to the transmitted in-phase $\mathbf{s}_{I_+}$ and $\mathbf{s}_{I_-}$ are given by

$$\begin{aligned} \mathbf{y}_{I_+} &= \mathbf{s}_{I_+} \odot \mathbf{h} + \mathbf{w}_{I_+} \\ \mathbf{y}_{I_-} &= \mathbf{s}_{I_-} \odot \mathbf{h} + \mathbf{w}_{I_-} \end{aligned} \tag{7.26}$$

and the received subblock of length N corresponding to the transmitted quadrature $\mathbf{s}_{Q_+}$ and $\mathbf{s}_{Q_-}$ are given by

$$\begin{aligned} \mathbf{y}_{Q_+} &= \mathbf{s}_{Q_+} \star \mathbf{h} + \mathbf{w}_{Q_+} \\ \mathbf{y}_{Q_-} &= \mathbf{s}_{Q_-} \star \mathbf{h} + \mathbf{w}_{Q_-}. \end{aligned} \tag{7.27}$$

The $N \times 1$ vectors $\mathbf{w}_{I+}(\mathbf{w}_{I-})$ and $\mathbf{w}_{Q+}(\mathbf{w}_{Q-})$ are the AWGN associated with the received in-phase and quadrature subblocks respectively. An N-point FFT is then performed for each received N symbols subblock to yield

$$\begin{aligned} \mathbf{Y}_{I_+} &= \mathbf{\Lambda}\mathbf{S}_{I_+} + \mathbf{W}_{I_+} \\ \mathbf{Y}_{I_-} &= \mathbf{\Lambda}\mathbf{S}_{I_-} + \mathbf{W}_{I_-} \end{aligned} \tag{7.28}$$

$\mathbf{Y}_{Q_+}$ and $\mathbf{Y}_{Q_+}$ are similarly defined where $\mathbf{\Lambda}_N$ is a ($N \times N$ diagonal matrix whose diagonal is the N-point FFT of $\mathbf{h}$. The MMSE or ZF equalizer yields

$$\begin{aligned} \widehat{\mathbf{S}}_{I_+} &= \left(\mathbf{\Lambda}_N^{\mathcal{H}}\mathbf{\Lambda}_N + (\alpha/SNR)\mathbf{I}_N\right)^{-1}\mathbf{\Lambda}_N^{\mathcal{H}}\mathbf{Y}_{I_+} \\ \widehat{\mathbf{S}}_{I_-} &= \left(\mathbf{\Lambda}_N^{\mathcal{H}}\mathbf{\Lambda}_N + (\alpha/SNR)\mathbf{I}_N\right)^{-1}\mathbf{\Lambda}_n^{\mathcal{H}}\mathbf{Y}_{I_-} \end{aligned} \tag{7.29}$$

$\widehat{\mathbf{S}}_{Q_+}$ and $\widehat{\mathbf{S}}_{Q_-}$ are similarly defined. Using (7.24), one forms the estimated vector

$$\begin{aligned} \widehat{\mathbf{S}}_I &= \widehat{\mathbf{S}}_{I_+} - \widehat{\mathbf{S}}_{I_-} \\ \widehat{\mathbf{S}}_Q &= \widehat{\mathbf{S}}_{Q_+} - \widehat{\mathbf{S}}_{Q_-} \end{aligned} \tag{7.30}$$

The frequency domain transmitted symbols $\mathbf{S}$ are then estimated as

$$\widehat{\mathbf{S}} = \widehat{\mathbf{S}}_I + j\widehat{\mathbf{S}}_Q \tag{7.31}$$

where $j = \sqrt{-1}$. One then obtain the time domain signal by the taking a N-point IFFT of $\widehat{\mathbf{S}}$ followed by a hard or soft detection. The spectral efficiency of DQO-SCFDE is given by

$$\varepsilon_{DQO} = \frac{N}{4(N+L)} \tag{7.32}$$

and is depicted in Figure. 7.10 as a function of the number of subcarrier N and channel delay spread L where it is compared with other schemes. Also the PAPR is given in Figure. 7.6.

7.5 Peak-to-Average Power Ratio Issues

Like conventional OFDM systems, high PAPR can be a serious penalty in optical OFDM systems [78], [79]. In radio frequency (RF) communications, the power amplifier is the main source of non linearity while in DOW communications, the LED is the non-linear device that limits the performance of optical OFDM. The nonlinear characteristic of a LED imposes limitations on the performance of indoor DOW systems

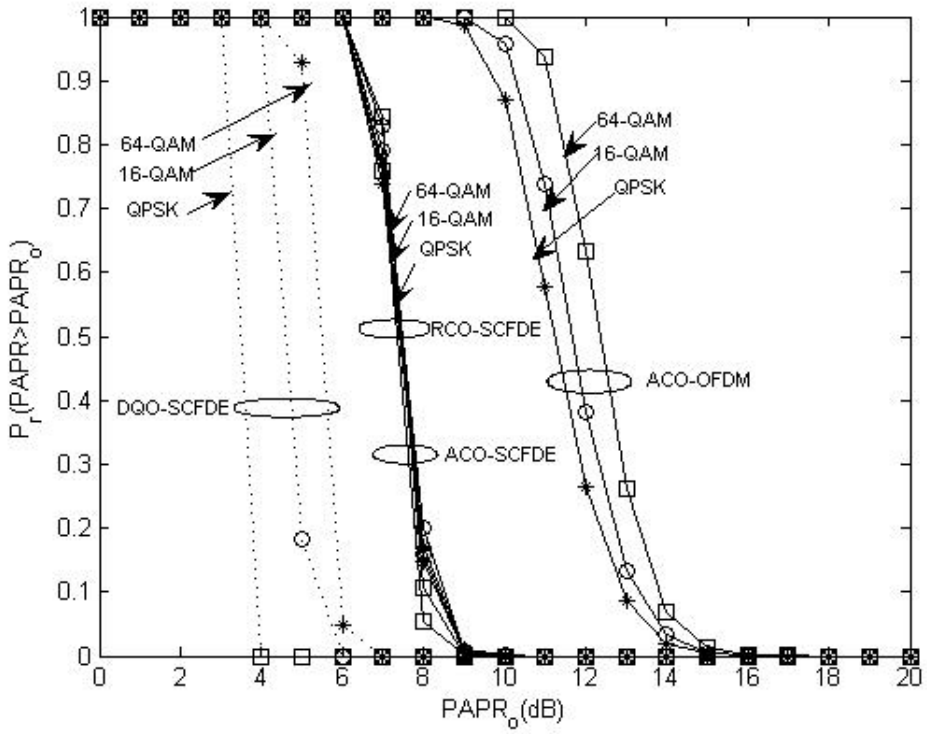

Figure 7.6 CCDF of PAPR Comparison of ACO-OFDM, ACO-SCFDE, RCO-SCFDE and DQO-SCFDE.

when using intensity modulation with both ACO-OFDM and DC-biased OFDM [72] because of their high PAPR. The sensitivity of OFDM to nonlinearities is also presented in [69, 80–82]. The PAPR is usually presented in terms of a Complementary Cumulative Distribution Function (CCDF) which is the probability that PAPR is higher than a certain PAPR value $PAPR_0$, i.e.$Pr\{PAPR > PAPR_0\}$. In Figure. 7.6, the CCDF is calculated by Monte Carlo simulation for QPSK, 16QAM and 64QAM modulation constellations. CCDF of PAPR for ACO-OFDM as well as the proposed ACO-SCFDE, RCO-SCFDE and DQO-SCFDE are evaluated and compared. It can be seen that the PAPR of ACO-OFDM is the highest while DQO-SCFDE exhibits the lowest PAPR.

Several techniques have been proposed to reduce the PAPR of OFDM signal, such as filtering, clipping, coding, partial transmission sequences (PTS), and selected

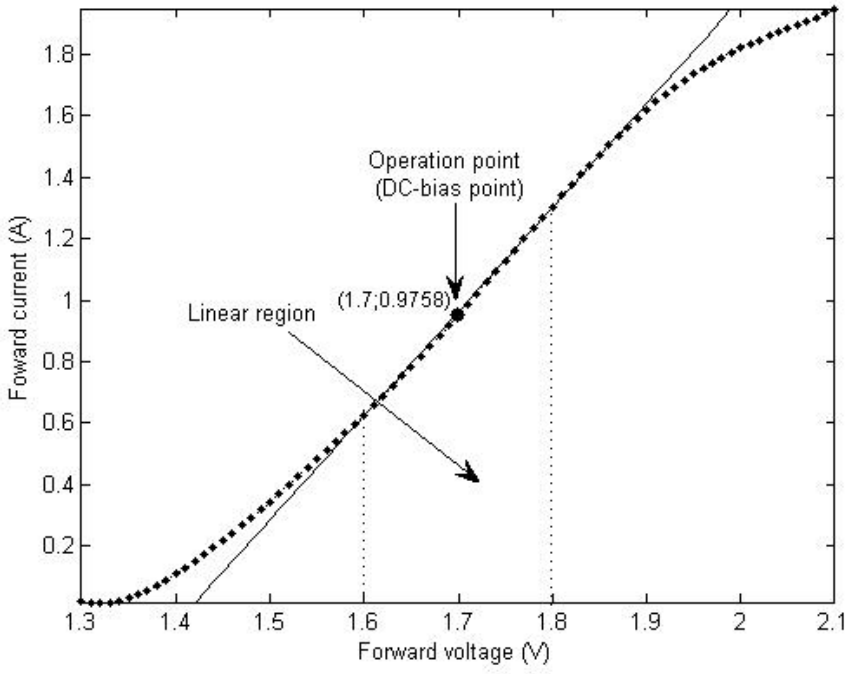

Figure 7.7 The LED transfer characteristics of the OSRAM, SFH 4230 showing the forward voltage and forward current relation. The dashed line shows the function that corresponds to the linear region of the LED transfer response.

mapping (SLM) [83–88]. Whereas, filtering has a disadvantage due to the noise and exogenous disturbance generated by non-linear operations [83], the coding technique is confined by its high complexity and efficiency degradation [86]. Probability techniques such as PTS and SLM also have the disadvantage of high complexity computation [87], [88]. The proposed SCFDE schemes for DOW in this chapter exhibit lower PAPR with low complexity. DQO-SCFDE has the lowest PAPR and lowest complexity; it should then be considered as a strong candidate in future DOW communication with IM/DD.

7.6 Performance Analysis

In this chapter, simulations have been conducted using the commercial high power IR LED (OSRAM,SFH 4230) [80] whose transfer characteristic is shown in Figure. 7.7.

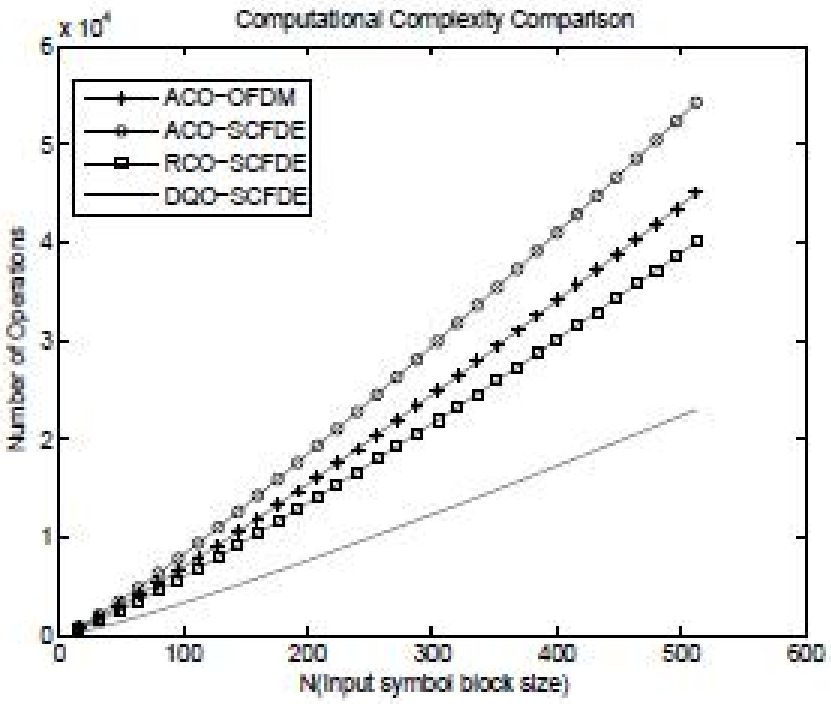

Figure 7.8 Computational Comparison for ACO-OFDM, RCO-SCFDE and DQO-SCFDE.

A polynomial of the sixth degree has been shown to model this transfer function using a least-squares curve fitting approach [80]. Figure. 7.7 shows the relation between the forward voltage across the LED and the current through it. Any input voltage less than 1.3V or more than 2.1V is clipped. From the LED characteristic depicted , it can be seen that the LED transfer function is linear only between 1.6V and 1.85V. If the input voltage has high dynamic range, the peak voltage will be distorted or clipped which will results in performance loss. The optical power is proportional to the LED forward current i.e. $P_{opt} = \zeta x'(t)$ where $x'(t)$ represent the LED forward current and it is assumed that $\zeta = 1$ [89]. In the simulations, a DC bias of 1.6V has been used to drive the LED into the linear region of the LED transfer function.

7.6.1 Complexity Analysis

In this subsection, the authors compare the computational complexity of the three newly proposed modulation techniques ACO-SCFDE, RCO-SCFDE, DQO-SCFDE and with that of ACO-OFDM. First, one notes that all the transceivers take as input a block of N independent complex data symbols to be transmitted using different techniques through a diffuse DOW channel. The main difference lies in how the transmitted block at the input of the LED is formed. For ACO-OFDM, the computational complexity is mainly due to the $4N$-point FFT at the transmitter and the $4N$-point IFFT at the receiver. So the complexity of ACO-OFDM is of order $\mathcal{O}\left(8NLog_2(4N)\right)$. The complexity of ACO-SCFDE is the same as ACO-OFDM plus the additional N-point FFT and N-point IFFT at the transmitter and receiver respectively, hence ACO-SCFDE complexity is of order $\mathcal{O}\left(8NLog_2(4N) + 2NLog_2(N)\right)$. In RCO-SCFDE, a $(2N+2)$- point FFT is taken at the transmitter and $(2N+2)$-point IFFT is taken at the receiver twice (once for each block $\mathbf{y}_+$ and $\mathbf{y}_-$) and as in ACO-SCFDE, RCO-SCFDE also has the additional complexity of N-point FFT and N-point IFFT at the transmitter and receiver respectively. Since N is a power of 2, $2N + 2$ is not a power of 2. But if one chooses in RCO-SCFDE N as $2^k - 1$ for any integer k, $2N + 2$ will be a power of 2 and the complexity of RCO-SCFDE can be given as of order $\mathcal{O}\left(3(2N + 2)Log_2(2N + 2) + 2NLog_2(N)\right)$. In DQO-SCFDE, there is only a N-point FFT performed at the receiver four times and a N-point IFFT taken once to transform the symbols into the time domain at the output. There is not computational burden on the transmitter. The complexity of DQO-SCFDE is of the order of $\mathcal{O}\left(4NLog_2(N) + NLog_2(N)\right)$. These complexity are summarized in Table. 7.1 and plotted as a function of the input block size N in Figure. 7.8.

Table 7.1 Computational Complexity Comparison of the Four Modulation Techniques

Schemes	Complexity
ACO-OFDM	$\mathcal{O}\left(8NLog_2(4N)\right)$
ACO-SCFDE	$\mathcal{O}\left(8NLog_2(4N) + 2NLog_2(N)\right)$
RCO-SCFDE	$\mathcal{O}\left[3(2N+2)Log_2(2N+2) + 2NLog_2(N)\right]$
DQO-SCFDE	$\mathcal{O}\left(5NLog_2(N)\right)$

7.6.2 Simulation Results

This section displays simulation results for ACO-OFDM, ACO-SCFDE, RCO-SCFDE and DQO-SCFDE schemes with N=64 independent data symbols. QPSK , 16QAM and 64QAM modulation constellation are used. The authors considered three different input symbol average power level $P_s = 0.1$W, 0.5W and 1W for QPSK and $P_s =$ 0.01W and 0.1W for 16QAM and 64QAM . Hence the transmitted block average electrical powers at the input of the LED are respectively given by $P_s/4$=25mW, 125mW and 250mW for QPSK and $P_s/4$=2.5mW and 25mW for 16QAM and 64QAM. A DC bias of 1.6V is added to drive the LED in all schemes. The exponential power decay channel model is used with a maximum delay spread of $L = 3$ sampling periods with real and positive taps [90] and the CP is set to L symbols. The channel is assumed perfectly known at the receiver. MMSE and ZF frequency domain equalization are used to mitigate the effects of the channel.

The authors first compare the PAPR of all schemes as shown in Figure. 7.6 from which it is noticed that DQO-SCFDE has the lowest PAPR while ACO-OFDM has the highest. Hence DQO-SCFDE is the preferable in terms of PAPR. Large PAPR signal affect the performance of the system as the linear range of the transfer function of the LED is limited. SCFDE uses single carrier, hence its PAPR is inherently lower than OFDM which uses multi-carriers. One will then expect that the BER performance

of the SCFDE schemes will be better. This will be clarified in the following BER performance analysis.

Next the authors compare the spectral efficiencies of the different schemes as plotted in Fig 7.10 and Fig 7.9 for channel delay spread of L=3 and L=4 respectively [3]. It can be seen that as the input block size N is large, the bandwidth efficiencies are almost the same for all schemes. Hence if N is large, the bandwidth loss experienced by RCO-SCFDE and DQO-SCFDE is negligible.

Finally BER performances are analyzed. The authors have only plotted the results for the MMSE equalizer which are shown in Fig 7.11 to Fig 7.17. Note the BER performance of the proposed SCFDE schemes when MMSE is used is always better than that of ACO-OFDM.

From Fig 7.11 to Fig 7.13, the BER performance for QPSK modulation with input symbol average power of P_s = 0.1W, 0.5W and 1W are plotted. Note that when the input power is low, i.e. 0.1W, the BER performance of the SCFDE schemes are all the same. This is because the PAPR is low and most of the signal values are within the linear range of the LED response. However, when the input power is higher, i.e. 1W in the QPSK case, DQO-SCFDE scheme performance is much better. This result confirms the PAPR results shown in Fig 7.6, that is DQO-SCFDE has quite lower PAPR than the other schemes. DQO-SCFDE signal amplitudes are lower which results in less clipping and distortion. Also, note that all SCFDE schemes outperform ACO-OFDM in all cases especially when the input power is increasing. The bad performance of ACO-OFDM is due the fact the PAPR is higher and hence many signal values are outside the linear range of the LED response which creates signal distortion which in turns causes the performance loss. When the input symbol power is low, i.e. 0.01W, ACO-OFDM performance is better than for 0.1mW but its performance is still worst that SCFDE schemes. This is because with SCFDE, a

[3]For indoor DOW system, a maximum of 3 or 4 taps are sufficient to model the channel impulse response [91]

spectral null in the channel negatively affects all the symbols in a block [92] which is not the case for MMSE equalization as was also shown in performance study of SCFDE in [92]. Moreover, SCFDE has an inherent diversity gain due to the use of the IFFT at the receiver which causes peaks and the nulls of the frequency response to spread across several data values.

When larger size constellations are used, i.e. 16QAM and 64QAM, ACO-OFDM performance has the worst performance and reliable communication cannot happen as can be seen in Fig 7.14 to Fig 7.17. This is again due the fact that for the larger constellation size, the PAPR of ACO-OFDM is higher and hence substantial signal clipping and distortion occur that affect the system performance. Note that, DQO-SCFDE performance is the best in all case especially when the input symbol power is increased. This is because, the PAPR of DQO-SCFDE is so low that by increasing the input symbol power, most of the signal values fall within the linear range of the LED response , hence no or less signal distortion occurs. When the input symbol power is lower, i.e. 0.01W, the performance of all SCFDE schemes are almost the same due to their lower PAPR. For an input signal power of 1W for QPSK and 0.1W for 16QAM and 64QAM, DQO-SCFDE performs better than ACO-SCFDE due to its lower PAPR. These simulation results show the effectiveness of the SCFDE schemes when the nonlinearity of the LED is considered. In general, if non-linearity is not considered, increasing signal power decreases BER. But when the non-linearity of the LED is considered, one wants a system that has good BER for low signal power. DQO-SCFDE has the best performance among all the schemes. However increasing the signal power is more detrimental for ACO-OFDM due to its higher PAPR. High peaks in the signal are clipped or distorted which results in the BER floor.

In this chapter, the authors present three new modulation techniques for diffuse optical wireless communications with IM/DD. The first applies Asymmetrically clipped optical (ACO) principles to SCFDE which is called ACO-SCFDE. The oth-

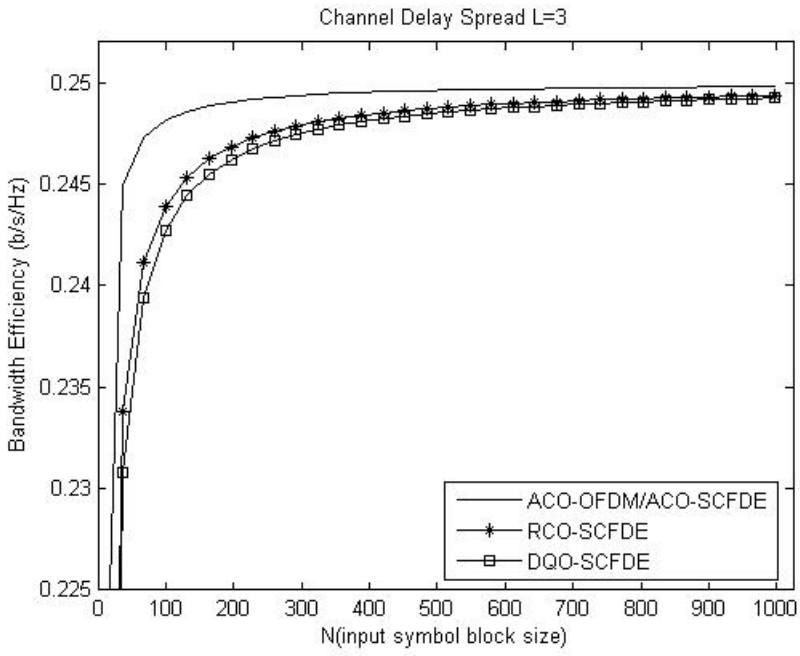

Figure 7.9 Bandwidth efficiency comparison for ACO-OFDM, ACO-SCFDE, RCO-SCFDE and DQO-SCFDE with channel delay spread of L=3 sampling times.

ers, namely RCO-SCFDE and DQO-SCFDE use the newly introduced technique of repetition and clipping. It was shown through the use of simulation that these new techniques exhibit lower PAPR and better BER performance in a multipath channel. The spectral efficiency of these techniques is almost the same when the symbol block size is sufficiently large. ACO-SCFDE is a direct application of ACO-OFDM using SCFDE modulation instead of OFDM. The former requires FFT and IFFT at the transmitter and receiver but has lower PAPR than ACO-OFDM and better BER performance. RCO-SCFDE and DQO-SCFDE are other two new methods for generating real positive signal needed for transmission over the optical channel. RCO-SCFDE has the same PAPR as ACO-SCFDE but lower computational complexity. DQO-SCFDE has the lowest PAPR, lower computational complexity and exhibits better BER performances. For this particular reason, the authors believe that DQO-SCFDE is the most attractive choice for transmitting real positive signal over an optical channel.

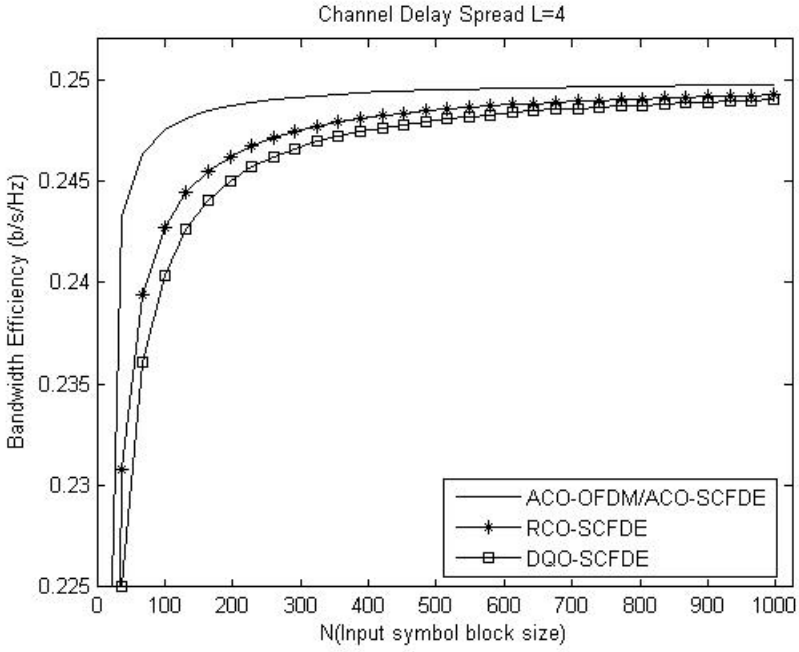

Figure 7.10 Bandwidth efficiency comparison for ACO-OFDM, ACO-SCFDE, RCO-SCFDE and DQO-SCFDE with channel delay spread of L=4 sampling times.

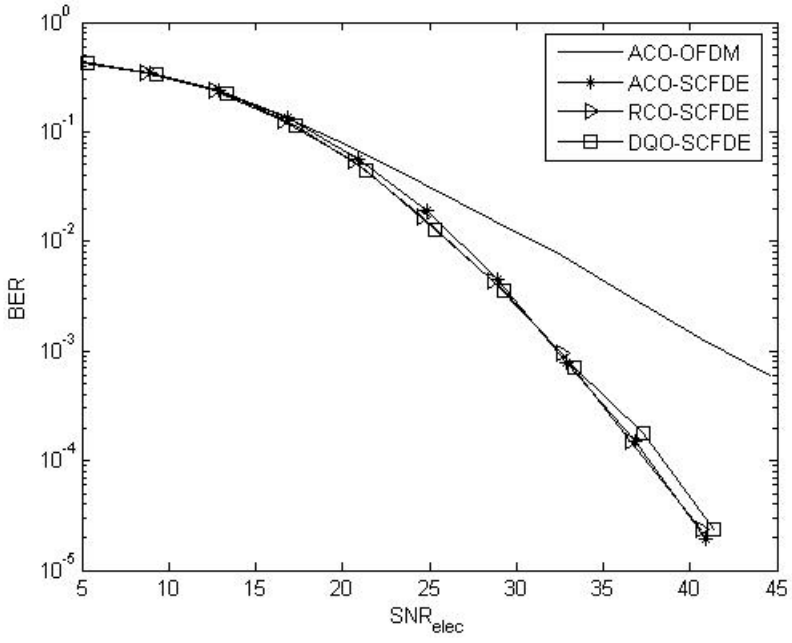

Figure 7.11 MMSE BER Comparison of ACO-OFDM, ACO-SCFDE, RCO-SCFDE and DQO-SCFDE with N=64, QPSK input symbols with power 0.1W and $L = 3$.

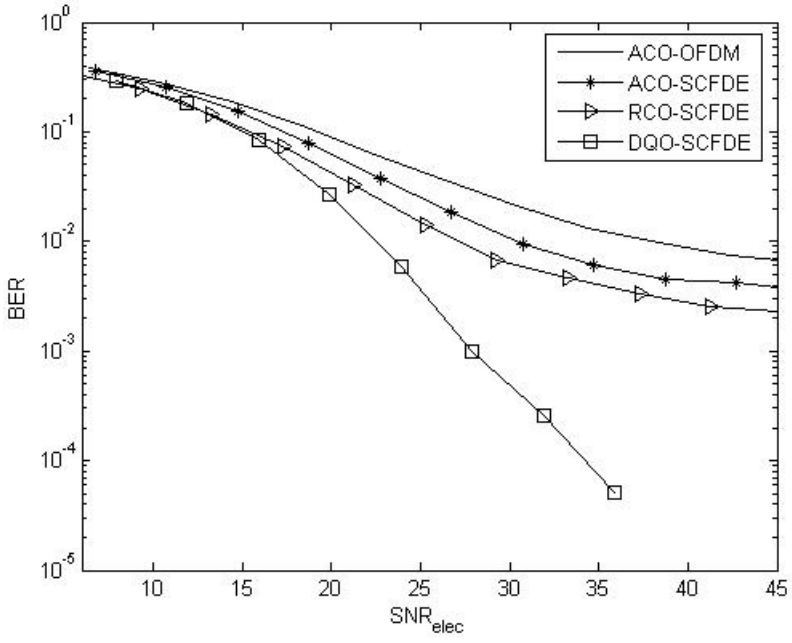

Figure 7.12 MMSE BER Comparison of ACO-OFDM, ACO-SCFDE, RCO-SCFDE and DQO-SCFDE with N=64, QPSK input symbols with average power 0.5W, $L = 3$.

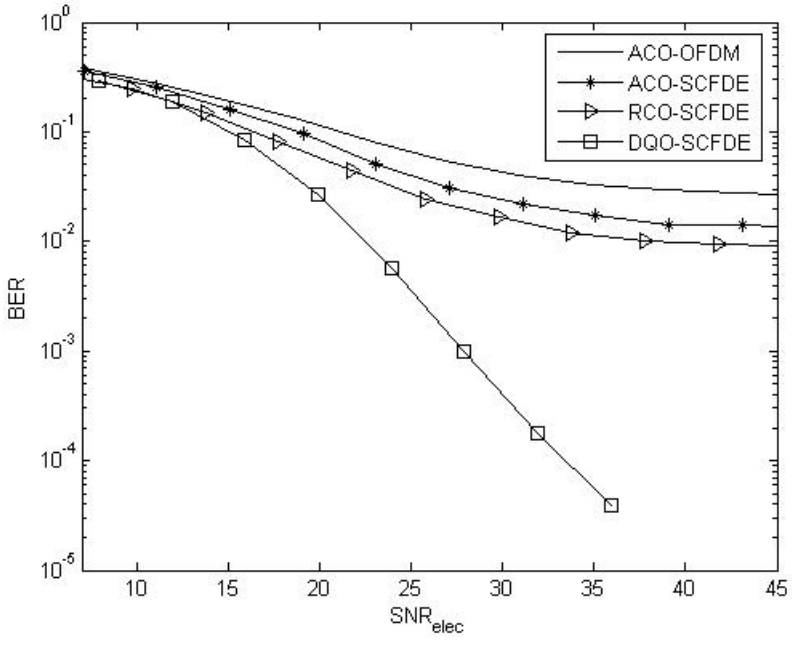

Figure 7.13 MMSE BER Comparison of ACO-OFDM, ACO-SCFDE, RCO-SCFDE and DQO-SCFDE with N=64, QPSK input symbols with power 1W and $L = 3$.

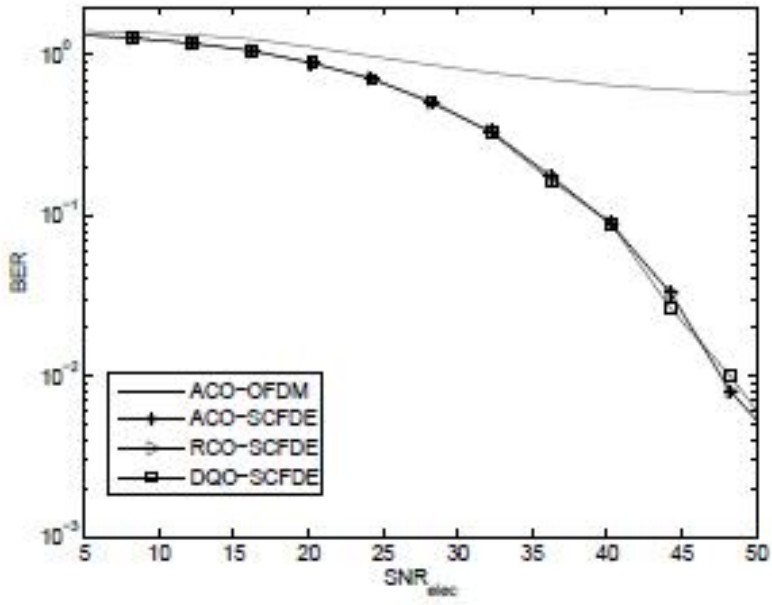

Figure 7.14 MMSE BER Comparison of ACO-OFDM, ACO-SCFDE, RCO-SCFDE and DQO-SCFDE with N=64, 16QAM input symbols with power 0.01W, $L = 3$.

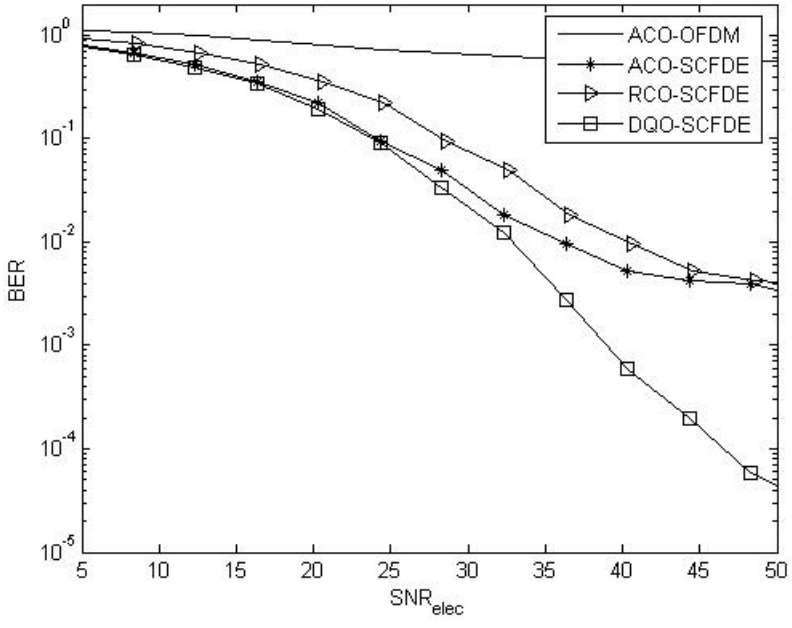

Figure 7.15 MMSE BER Comparison of ACO-OFDM, ACO-SCFDE, RCO-SCFDE and DQO-SCFDE with N=64, 16QAM input symbols with average power 0.1W, $L = 3$.

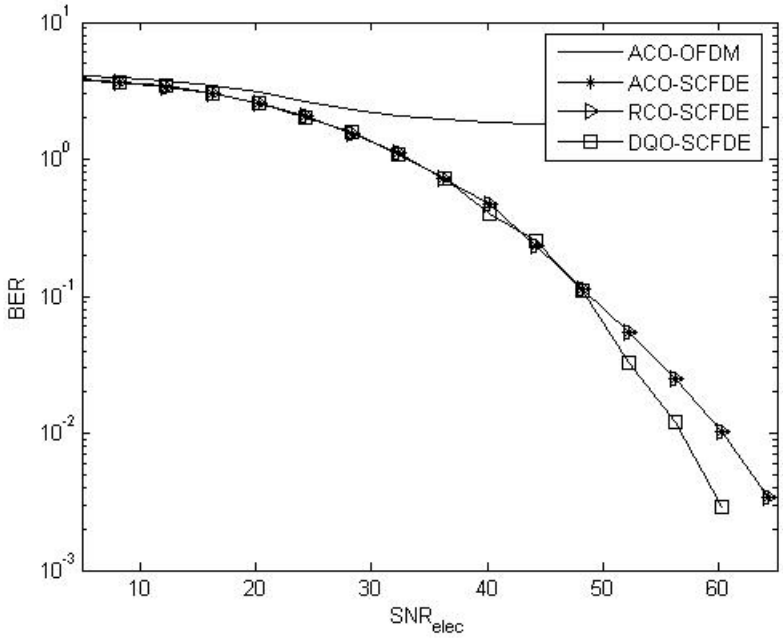

Figure 7.16 MMSE BER Comparison of ACO-OFDM, ACO-SCFDE, RCO-SCFDE and DQO-SCFDE with N=64, 64QAM input symbols with power 0.01W, $L = 3$.

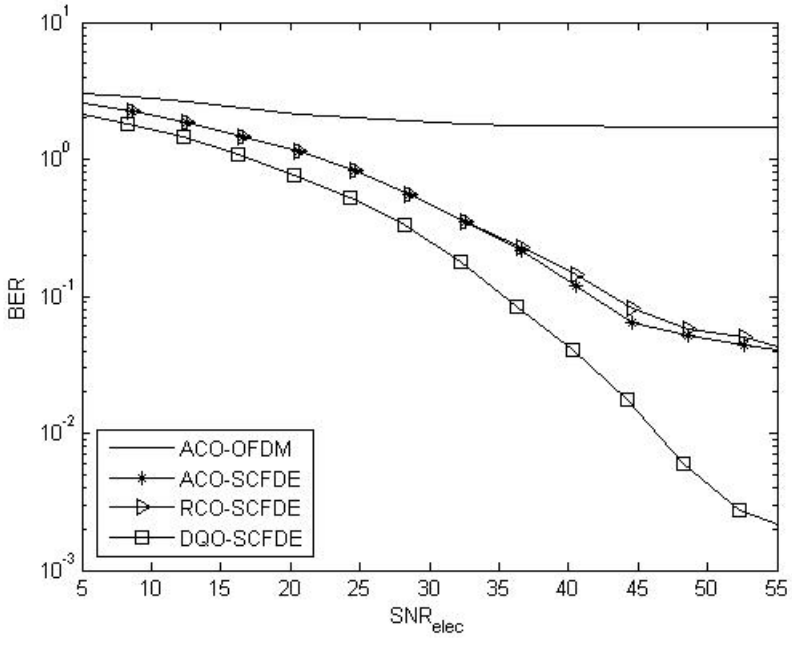

Figure 7.17 MMSE BER Comparison of ACO-OFDM, ACO-SCFDE, RCO-SCFDE and DQO-SCFDE with N=64, 64QAM input symbols with average power 0.1W, $L = 3$.

CHAPTER 8

SINGLE-CARRIER WITH FREQUENCY-DOMAIN EQUALIZATION WITH TRANSMIT DIVERSITY FOR OPTICAL WIRELESS

The optical spectrum which has wide available bandwidth, has recently been receiving growing interest for use in indoor wireless data transmission [64]. Optical wireless communications offer a viable alternative to radio frequency (RF) communication for indoor use and other applications where high performance links are needed. RF systems can support only limited bandwidth because of restricted spectrum availability and are subject to interference. This restriction does not apply to diffuse optical wireless (DOW) links. In indoor DOW systems, light emitting diodes (LED) are used for optical signals as transmitter and photo-diodes as the receivers. These opto-electronic devices are cheaper as compared to RF circuitry.

OFDM modulation is a promising modulation scheme for indoor optical wireless communication [67, 70] and references there in. DC-biased optical OFDM (DCO-OFDM) [67] and asymmetrically clipped optical OFDM (ACO-OFDM) [70] are two forms of OFDM using IM/DD for DOW communications. Since OFDM symbols have inherently high PAPR, the performance of DCO-OFDM and ACO-OFDM signals can be severely affected by the nonlinear behavior of the LED [73]. For this reason, single carrier with frequency domain equalization (SCFDE) system have been proposed as an alternative to OFDM in DOW communication [76]. SCFDE is a low PAPR block modulation transmission scheme similar to OFDM which was proposed to combat ISI [2]. SCFDE is combined with pulse position modulation (PPM) in [76] to provide a power efficient IM/DD DOW transmission. In the previous chapter, the authors propose based on SCFDE, a novel efficient DOW transmission scheme which is called Decomposed Quadrature Optical SCFDE (DQO-SCFDE) [93]. In DQO-SCFDE,

the in-phase and quadrature components of a complex constellation baseband signal are transmitted separately. A repetition and clipping technique is introduced to obtain low PAPR real positive signal suitable for IM/DD. In this chapter the authors present a comparative study of DQO-SCFDE with ACO-OFDM. The authors then propose a space-time coding scheme for DQO-SCFDE that can be employed using two LEDs at the transmitter and one photodiode at the receiver to improve the system BER performance. Space-time coding has been applied to ACO-OFDM in [94] and DCO-OFDM in [95] wherein the Alamouti scheme of [18] is applied on the input frequency domain complex symbols before the IFFT operation. But as mentioned earlier, ACO-OFDM suffers from large PAPR which degrades its performance in the presence of the LED non-linearity. In [96], a modified Alamouti coding scheme has been applied to on-off keying (OOK) and binary pulse position modulation (2-PPM) using logical inverses, where only binary signal $(0, 1)$ are transmitted. When applied to M-PPM, transmitting the complement of an M-PPM symbol requires much more energy than the corresponding M-PPM symbol itself which is not power efficient. Binary-based (OOK) space-time schemes have also been proposed in [97–99] where the input symbols can take only two values. In the proposed space-time coding for DQO-SCFDE , a modified Alamouti coding similar to the one in [96] is applied to the time domain M-QAM symbols (not just binary symbols) in frequency selective channel. The in-phase and quadrature components of the input complex symbols are transmitted separately in subblocks.

The time domain signals of ACO-OFDM and DQO-SCFDE are plotted in Figure. 8.1 for 4-QAM signal. It can be seen from the figure that while DQO-SCFDE has a more limited range of possible signal amplitude[1], ACO-OFDM signal exhibits strong amplitude fluctuations which can negatively impact the system performance in the presence of the LED non-linearity as will be depicted in the following section. In

[1]DQO-SCFDE 4-QAM, 16-QAM constellation exhibit only 2 (0 and 1) and 3 (0,1 and 3) signal amplitudes respectively

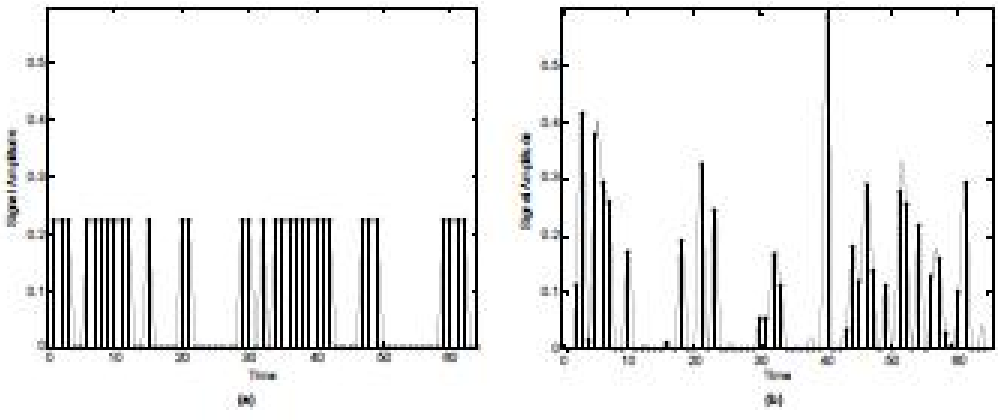

Figure 8.1 (a) DQO-SCFDE 4-QAM signal, (b) ACO-OFDM 4-QAM signal.

this chapter, in order to evaluate the effects of a non-linear LED on the performance of ACO-OFDM and DQO-SCFDE, simulations have been conducted using the commercial high power IR LED (OSRAM,SFH 4230) [80] whose transfer characteristic is shown in Figure. 7.7.

The signal amplitude statistics have been depicted in Figure. 8.4 for 4-QAM, 16-QAM and 64-QAM and with average optical power of 10mW and 20mW. Figure. 7.7 shows the nonlinear behavior of the LED for forward voltage amplitudes in the range from 1.3V up to 2.1V. At 2.1V, the forward current is considered to be the maximum permissible AC current. Hence input signal amplitudes above 2.1V and below 1.3V are clipped. Moreover any signal amplitude outside the LED's linear range (approximatively between $1.6V$ and $1.8V$) will be distorted. It can be seen from Figure. 8.4, that the probability that ACO-OFDM signal amplitudes exceed the maximum input voltage of 2.1V is greater than DQO-SCFDE signal. When the average input optical power is 10mW , DQO-SCFDE experiences no clipping for 4-QAM, 16-QAM and 64-QAM while ACO-OFDM experiences some clipping. Moreover it can be seen that most of DQO-SCFDE are within the linear range of the LED transfer function which is not the case for ACO-OFDM. When the input average optical power is increased to

20mW, DQO-SCFDE 16-QAM and 64-QAM signals experience some clipping while with ACO-OFDM 4-QAM, 16-QAM and 64-QAM suffer from more clipping. From the above observation, one can expect that DQO-SCFDE will perform better than ACO-OFDM in the presence of the LED non-linearity. The BER performance will be presented in the followings.

In this section, the authors describe the application of modified Alamouti space-time coding in IM/DD diffuse optical wireless using DQO-SCFDE. Consider an Alamouti coding with two transmitters (two LEDs) and one receiver (one photo-diode). Space-time coding has been applied to ACO-OFDM in [94] wherein the Alamouti scheme is applied on input frequency domain complex symbols before the IFFT operation. In DQO-SCFDE , the space-time coding must be applied to the time domain M-QAM symbols. But Alamouti coding in its original form cannot be applied directly without modification to time-domain symbols in IM/DD because these time domain signals must be reals and positives. In [96], [97] and reference therein, a modified Alamouti coding scheme has been applied only to time domain binary signals using logical inverse. It is shown in [100] that OOK signals have poor power efficiency performance in IM/DD systems. In this chapter, the authors demonstrate that Alamouti coding can be combined to DQO-SCFDE using M-QAM symbols constellation.

8.0.3 Alamouti Coding for DQO-SCFDE

The space-time coding scheme for sending and receiving the transmitted symbols $\mathbf{x}_1 = [\mathbf{s}_{1,I_+}, \mathbf{s}_{1,I_-}, \mathbf{s}_{1,Q_+}, \mathbf{s}_{1,Q_-}]^T$ (from the first LED) and $\mathbf{x}_2 = [\mathbf{s}_{2,I_+}, \mathbf{s}_{2,I_-}, \mathbf{s}_{2,Q_+}, \mathbf{s}_{2,Q_-}]^T$ (from the second LED) at the transmit consecutive sample time n and $n+1$ is shown in Table 8.1 and A_{DC} is the DC bias needed to drive the LED. A_i represents twice the expected value of the transmit signal $\mathbf{x}_i$, i.e. $A_i = 2E\{x_{i,k}\}, k = 0, 1, \cdots, 4(N+L)$. Since, a DC bias A_{DC} is needed to drive the signal in the linear region of the LED,

Table 8.1 DQO-SCFDE Alamouti Space-Time Coding

	LED 1	LED 2
Time n	$\mathbf{x}_1 + A_{DC}$	$\mathbf{x}_2 + A_{DC}$
Time $n+1$	$\overline{\mathbf{x}}_2 = A_2 - \mathbf{x}_2 + A_{DC}$	$\mathbf{x}_1 + A_{DC}$

this DC bias is chosen such that the signal $\overline{\mathbf{x}}_i = A_i - \mathbf{x}_i + A_{DC}$ is real non-negative as $\mathbf{x}_i + A_{DC}$ as depicted in Fig 8.2 for 4-QAM signals and Fig 8.2 for 16-QAM signals. It can be easily shown that the $E\{\overline{\mathbf{x}}_i\}$=$E\{\mathbf{x}_i\}$, hence the transmitted average optical power is not changed.

The received signal (with CP) at time n and $n+1$ are given by

$$\begin{aligned} \widetilde{\mathbf{y}}_n &= \widetilde{\mathbf{x}}_1 \star \mathbf{h_1} + \widetilde{\mathbf{x}}_2 \star \mathbf{h_2} + \widetilde{\mathbf{w}}_n \\ \widetilde{\mathbf{y}}_{n+1} &= (A_2 - \widetilde{\mathbf{x}}_2) \star \mathbf{h_1} + \widetilde{\mathbf{x}}_1 \star \mathbf{h_2} + \widetilde{\mathbf{w}}_{n+1} \end{aligned} \tag{8.1}$$

Note that $\widetilde{\mathbf{x}}_i$ represents $\mathbf{x}_i$ with the CP inserted. Also for notation simplicity, the DC-bias is omitted in the equation [2]. Note that the CP turns the linear convolution with the channel into a circular convolution. After taking FFT, it can be shown that $\mathbf{Y}_{I_+}$ is given by

$$\begin{aligned} \mathbf{Y}_{I_{+,n}} &= \mathbf{\Lambda}_1 \mathbf{S}_{1,I_+} + \mathbf{\Lambda}_2 \mathbf{S}_{2,I_+} + \mathbf{W}_{I_{+,n}} \\ \mathbf{Y}_{I_{+,n+1}} &= \mathbf{\Lambda}_2 (A_2 \mathbf{I}_N - \mathbf{S}_{2,I_+}) + \mathbf{\Lambda}_1 \mathbf{S}_{1,I_+} + \mathbf{W}_{I_{+,n}} \end{aligned} \tag{8.2}$$

which van be written in a matrix form as

$$\begin{aligned} \begin{bmatrix} \mathbf{Y}_{I_{+,n}} \\ \overline{\mathbf{Y}}_{I_{+,n+1}} \end{bmatrix} &= \begin{bmatrix} \mathbf{\Lambda}_1 & \mathbf{\Lambda}_2 \\ \mathbf{\Lambda}_2 & -\mathbf{\Lambda}_1 \end{bmatrix} \begin{bmatrix} \mathbf{S}_{1,I_+} \\ \mathbf{S}_{2,I_+} \end{bmatrix} + \begin{bmatrix} \mathbf{W}_{I_{+,n}} \\ \mathbf{W}_{I_{+,n+1}} \end{bmatrix} \\ \mathbf{Z}_{I_+} &\triangleq \mathbf{\Delta}\ \mathbf{S}_{I_+} + \mathbf{\Omega}_{I_+} \end{aligned} \tag{8.3}$$

[2] It is easily seen that the addition of A_{DC} has the effect of adding a DC bias to the DC frequency in the frequency domain which is easily removed at the receiver

where $\overline{\mathbf{Y}}_{I_{+,n+1}} = \mathbf{Y}_{I_{+,n+1}} - A_2\mathbf{\Lambda}_2$. $\mathbf{\Lambda}_i$ corresponds to the frequency response of the channel between the receive photodiode and the i-th transmit diode. Similarly, $\mathbf{S}_{i,I_+}$ corresponds to the transmit block from the i-th transmit LED; $\mathbf{Y}_{I_{+,n}}$ and $\mathbf{W}_{I_{+,n}}$ are the received signal and noise vectors corresponding to the n-th transmit time. Note that $\mathbf{\Delta}$ is orthogonal , i.e.

$$\mathbf{\Delta}^{\mathcal{H}}\mathbf{\Delta} = \begin{bmatrix} |\mathbf{H}_1|^2 + |\mathbf{H}_2|^2 & \mathbf{0} \\ \mathbf{0} & |\mathbf{H}_1|^2 + |\mathbf{H}_2|^2 \end{bmatrix} \tag{8.4}$$

hence the two transmit signal from the two LED can be detected independently therefore a second order diversity can be achieved. The MMSE of $\widehat{\mathbf{S}}_{I_+}$ can then be obtained as

$$\widehat{\mathbf{S}}_{I_+} = \left(\mathbf{\Delta}_N^{\mathcal{H}}\mathbf{\Delta}_N + (1/SNR)\mathbf{I}_N\right)^{-1}\mathbf{\Delta}_N^{\mathcal{H}}\mathbf{Z}_{I_+}. \tag{8.5}$$

Similarly, $\widehat{\mathbf{S}}_{I_-}$,$\widehat{\mathbf{S}}_{Q_+}$ and $\widehat{\mathbf{S}}_{Q_-}$ are obtained. The estimated signals $\widehat{\mathbf{S}}_1$ and $\widehat{\mathbf{S}}_2$ are detected which are then transformed into the time domain.

8.0.4 Simulation Results

In the simulation of the space-time block coding STBC-DQO-SCFDE, the authors have also used the commercial high power IR LED (OSRAM,SFH 4230) [80] whose transfer characteristic is shown in Figure. 7.7. Figure. 8.7 depicts the BER performance of the proposed Alamouti coding denoted STBC DQO-SCFDE with two LEDs at the transmitter and one photodiode at the receiver. The STBC performance is compared with DQO-SCFDE without Alamouti coding for 4-QAM and 16-QAM. It can be seen that the space-time scheme exhibits 3dB BER performance gain. By using more transmit LEDs, better BER performance can be obtained employing the space-time coding schemes proposed in [53] and since one is dealing with real signal in IM/DD, full rate full diversity schemes can be achieved.

In this chapter, the authors compare the newly proposed modulation technique for diffuse optical wireless termed decomposed quadrature optical SCFDE (DQO-SCFDE) with asymmetrically clipped optical OFDM (ACO-OFDM). DQO-SCFDE uses a newly introduced technique of repetition and clipping wherein the negative symbols are clipped in the first part and the positive signal clipped in the second part of the transmitted block. It was shown through the use of simulation that DQO-SCFDE exhibits lower PAPR and better BER performance in a multipath channel than the popular ACO-OFDM in the presence of the non-linearity of the light emitting diode (LED) used to convert the electrical signal into optical power. It is also shown in this chapter that Alamouti space-time coding can be employed to the non-negative real signal of DQO-SCFDE. A second order diversity gain can then be obtained using two transmit LEDs and one receive photodiode to improve the system BER performance.

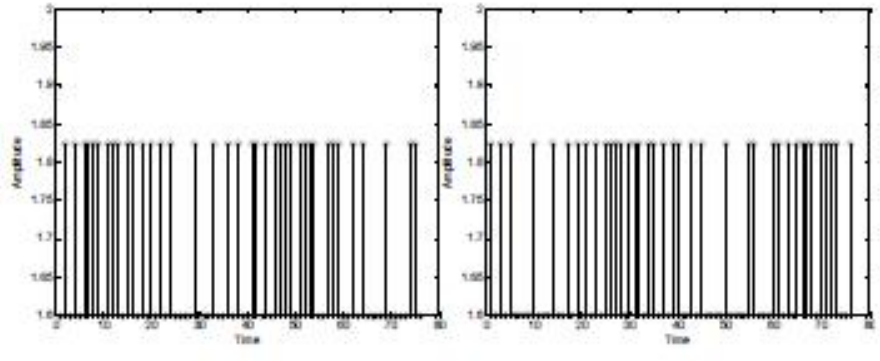

Figure 8.2 (a) DQO-SCFDE 4-QAM signal $\mathbf{x}_i$, (b) DQO-SCFDE 4-QAM signal $\overline{\mathbf{x}}_i = A_i - \mathbf{x}_i + A_{DC}$ with A_{DC}=1.6V.

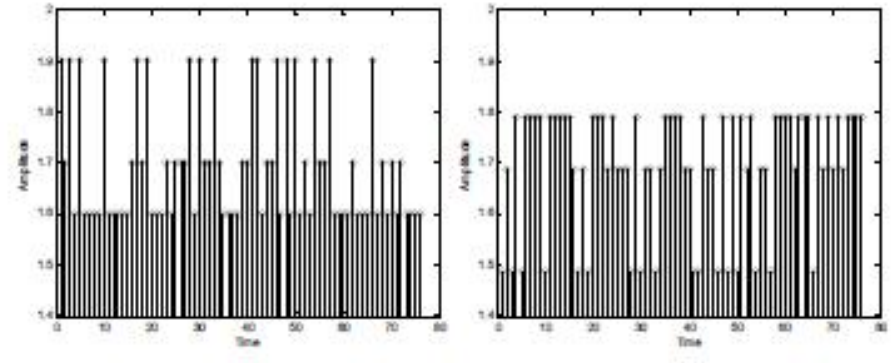

Figure 8.3 (a) DQO-SCFDE 16-QAM signal $\mathbf{x}_i$, (b) DQO-SCFDE 16-QAM signal $\overline{\mathbf{x}}_i = A_i - \mathbf{x}_i + A_{DC}$ with A_{DC}=1.6V.

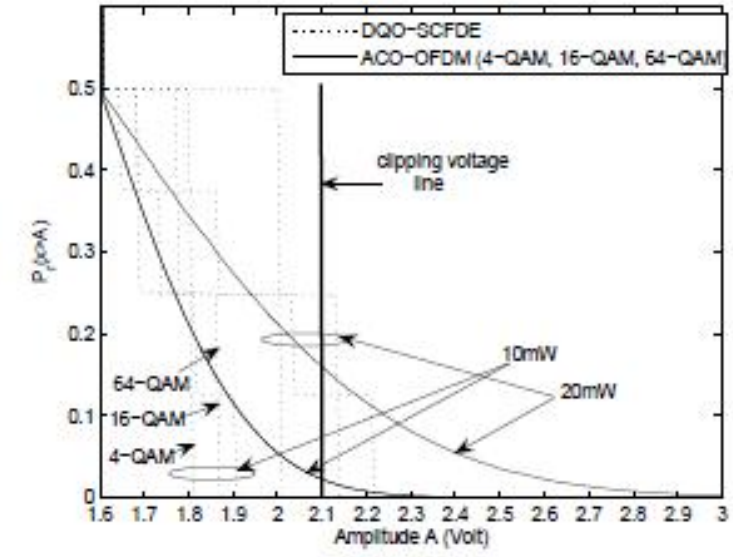

Figure 8.4 Signal amplitude statistics of DQO-SCFDE and ACO-SCFDE for 4-QAM, 16-QAM and 64-QAM constellations with normalized input symbol average power of 10mW and 20mW.

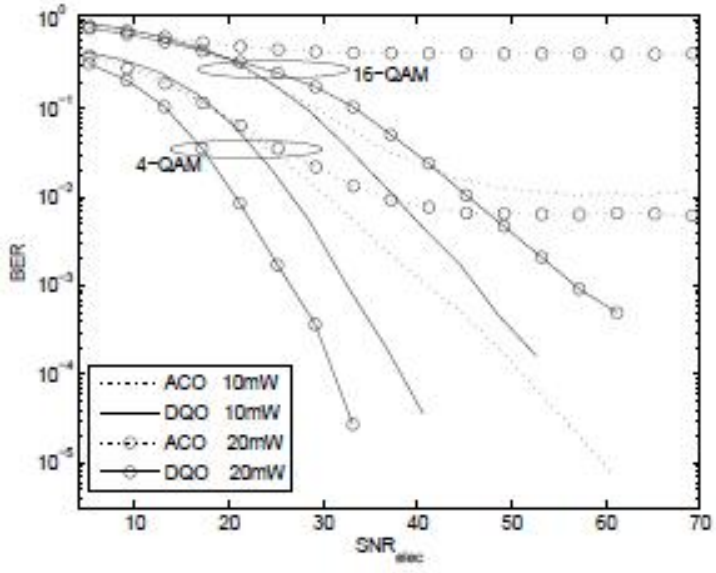

Figure 8.5 BER performance comparison of DQO-SCFDE and ACO-OFDM with an input average optical power of 10mW and 20mW for 4-QAM and 16-QAM.

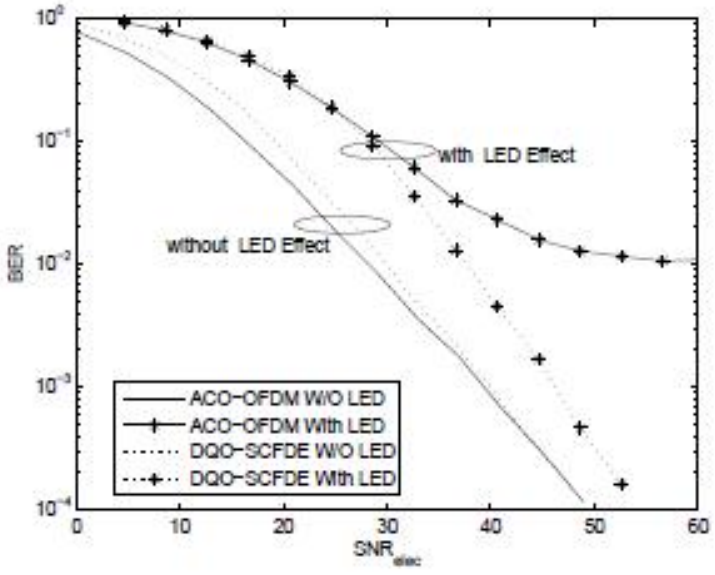

Figure 8.6 BER performance comparison of DQO-SCFDE and ACO-OFDM with an input average optical power of 10mW with and without the LED's effect.

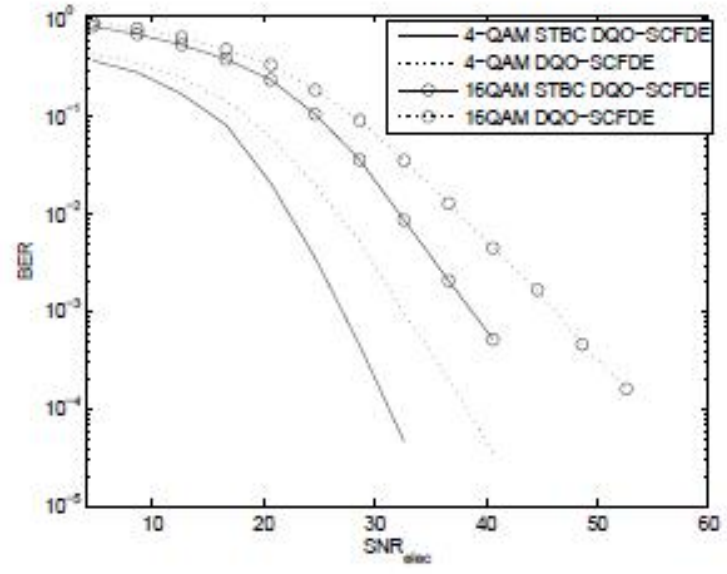

Figure 8.7 BER performance of the proposed (2 × 1) space-time block coding STBC DQO-SCFDE compared with (1 × 1) DQO-SCFDE with an input average optical power of 10mW.

CHAPTER 9

EFFICIENT SIMULATION OF SPACE-TIME CORRELATED MIMO FADING CHANNELS

Recent fundamental information theoretic results have shown that by exploiting antenna arrays at both the base station (BS) and mobile station (MS) and under certain conditions, unprecedented transmission rates can be achieved over wireless channels [101], [102]. Two major approaches to reach such high capacities are space-time coding [53] and V-BLAST architecture [103], which have driven the recent surge of numerous research and development activities for very high speed transmission systems. In general, multiantenna systems attempt to use both time- and space-domain channel characteristics, via appropriate coding and detection schemes. Needless to say, software simulation of multiple-input multipleoutput (MIMO) channels is essential for evaluating the performance of different multiantenna space-time coding/processing techniques, before expensive hardware experiments. A useful MIMO simulator should be able to generate multiple crosscorrelated processes. There are few papers, which address this issue for receive-only diversity schemes (see [104] and references therein). To the best of our knowledge, only in [104] the simulation of MIMO channels is addressed properly (for the limitations of other techniques, see [104]). However, only the vector autoregressive (AR) simulation approach is discussed in [104], whereas there are other techniques that could serve as efficient candidates for MIMO simulation. In this paper we focus on four methods for simulating a vector of correlated complex Gaussian processes. We also provide a comprehensive theoretical analysis of the computational complexity of all the four methods, not considered in the past.

For computer implementation of these methods, one needs either the cross-correlations or the cross-spectra among the processes of different subchannels. Here

we use a recently proposed space-time macrocell model [27], which provides closed-form expressions for correlations and spectra of interest, and includes many key physical channel parameters in compact forms. This model is also used in the MIMO simulation study of [104]. One can use the micro and picocell model of [105] as well.

9.1 Spectral Representation Method

The first method employs the spectral representation model. This model works according to the spectral representation theorem which states that a weakly stationary process can be viewed as a superposition of harmonics with random amplitudes and phases [106], [107]. Specifically, it is based on the discretization of the frequency band of the process and the representation of the process by a sum of complex exponentials. The probabilistic characteristics of the generated samples functions converge to that of the target process, as the number of terms in the exponential series increases.

Proposition 1. (Spectral Representation Theorem) *Let* $\{Y(t), t > 0\}$ *be a wide sense stationary vector process with* m *complex-valued components of zero mean and covariance functions*

$$C_{kl}(\tau) = E\left[Y_k(t)Y_l^*(t+\tau)\right], k, l = 1, \cdots, m \tag{9.1}$$

and the associated spectral densities

$$S_{kl}(f) = \int_{-\infty}^{\infty} e^{-j2\pi f\tau} C_k(\tau) d\tau, \tag{9.2}$$

then there exists a unique process $Z(f)$ *[9] such that*

$$Y(t) = \int_{-\infty}^{\infty} e^{-j2\pi f\tau} dZ(f), \tag{9.3}$$

where $dZ(f)$ is a vector of m complex-valued processes with mean zero and the following covariance function [108]

$$\begin{aligned} E\left[dZ_k(f)dZ_l^*(\xi)\right] &= S_{kl}(f)df, \quad f=\xi \\ &= 0, \qquad otherwise, \end{aligned} \tag{9.4}$$

where f and ξ are frequency variables.

If the vector process $Z(f)$ is Gaussian, $Y(t)$ delivered by the spectral representation formula is also a Gaussian process [109]. $Y(t)$ is assumed to be band-limited in the frequency interval $(-f_{max}, f_{max}))$. However , if the process has power over the entire frequency range, one can select a cutoff frequency $f_{max} < \infty$ such that for all k and l,

$$\int_{-\infty}^{\infty} S_{kl}(f)df \approx \int_{-f_{max}}^{f_{max}} (f)df. \tag{9.5}$$

To obtain the discrete version of (9.3), the band $(-f_{max}, f_{max}))$ is divided into q non-overlapping intervals $(\alpha_{r-1}, \alpha_r), r = 1, \cdots, q$ with length $df_r = \alpha_r - \alpha_{r-1} = 2f_{max}/q$. A discrete approximation of order q of (9.3) is given by the following expression [109]

$$\widehat{Y}^{(q)}(t) = \sum_{r=1}^{q} A_r e^{i2\pi f_r t} \tag{9.6}$$

where A_r is a zero mean Gaussian vector with covariance

$$\begin{aligned} E\left[A_{r,k}A_{p,l}^*\right] &= \int_{\alpha_r - 1}^{\alpha_r} S_{kl}(f)df \approx S_{kl}(f_r)df_r, \quad ifr = p \\ &= 0 \qquad ifr \neq p, \end{aligned} \tag{9.7}$$

with $r, p = 1, \cdots, q$ such that f_r and df_r are the midpoint and length of the interval (α_{r-1}, α_r) respectively.

It is shown in [109] that the probabilistic characteristics of $\widehat{Y}^{(q)}(t)$ approaches those of $Y(t)$ as $q \to \infty$. So, (9.6) can be used as a good approximation of $Y(t)$ if q

is sufficiently large. Note that the process in (9.6) is periodic with period q/f_{max},as mentioned in [110]. So, to generate the process in $[0, T]$, one should choose q large enough such that $T < q/f_max$.

The simulation of the vector process $\widehat{Y}^{(q)}(t)$ involves two steps:

1. Generation of samples of the complex Gaussian vector A_r(the Cholesky Decomposition algorithm of [109] is used)

2. Realization of the process using (9.6) in which A_r is replaced by its samples generated in the first step.

To simulate a 2×2 MIMO channel using this method, we use the MIMO correlation model given in [27] for the autocorrelation and cross-correlation of four subchannels $h_{11}(t), h_{12}(t), h_{21}(t)$ and $h_{22}(t)$

$$C_{h_{lp}} C_{h_{mq}}(\tau) = [I_0(K)]^{-1} \exp[ic_{pq} \cos(\alpha_{pq})] \times$$
$$I_0([K^2 - a^2 - b_{lm}^2 - c_{pq}^2 \Delta^2 \sin^2(\alpha_{pq}) + 2ab_{lm} \cos(\beta_{lm} - \gamma) + 2c_{pq}\Delta \sin(\alpha_{pq})\{a \sin(\gamma)$$
$$- b_{lm} \sin(\beta_{lm})\} - i2K\{a \cos(\mu - \gamma) - b_{lm} \cos(\mu - beta_{lm}) - c_{pq}\Delta \sin(\alpha_{pq}) \sin(\mu)\}]^{1/2}), \tag{9.8}$$

where $I_0(\cdot)$ is the zero order modified Bessel function, $a = 2\pi f_{max}\tau$, $b_{lm} = 2\pi d_{lm}/\lambda$, $c = 2\pi\delta_{pq}/\lambda$, f_{max} is the maximum Doppler shift, d_{lm} denotes the antenna spacing at the mobile station (MS), δ_{pq} is the antenna spacing at the base station (BS), $\lambda$is the wavelength, 2Δ is the maximum angle spread at the BS, μ accounts for the mean angle of arrival (AOA) seen by the MS, K controls the width of AOA at the MS, α_{pq} and β_{lm} are the angles which specify the orientations of the BS and MS arrays respectively and finally γ is the direction of the motion of MS. Note that $l, m, p, q = 1, 2$. All these parameters are clearly depicted in Figure.1 of [27]. The corresponding power

spectrum can be shown to be

$$S_{h_{lp}h_{mq}}(f) = \exp[ic_{pq}\cos(\alpha_{pq})]/[I_0(K)\pi\sqrt{f_{max}^2 - f^2}]\times$$
$$\exp[-\{Kcos(\gamma-\mu) + i\ v_1\}(f/f_{max})]\cosh[\{Ksin(\gamma-\mu) + i\ v_2\}\sqrt{1-(f/f_{max})^2}] \tag{9.9}$$

for $|f| \leq f_{max}$ where

$$\begin{aligned} v1 &= b_{lm}cos(\beta_{lm})\cos(\gamma) + [c_{pq}\Delta\sin(\alpha_{pq}) + b_{lm}\sin(\beta_{lm})]\sin\gamma \\ v2 &= b_{lm}cos(\beta_{lm})\sin(\gamma) + [c_{pq}\Delta\sin(\alpha_{pq}) + b_{lm}\sin(\beta_{lm})]\cos\gamma. \end{aligned} \tag{9.10}$$

The autocorrelation, cross-correlation, the distribution and level crossing rate are simulated. The simulation results of the spectral representation method are shown in Figure. 9.6 to Figure. 9.9 where perfect match can be seen between the simulation results and the theoretical ones.

9.2 Sampling Theorem Method

The second method is based on the sampling theorem for random processes and its generalization to vector processes. It simply states that a band limited process consists of a superposition of deterministic functions of time with random amplitudes. Consider a deterministic function $\theta(\cdot)$ such that its Fourier transform is zero outside a bounded frequency range $(-f_{max}, f_{max}))$, $f_{max} < \infty$. According to the sampling theorem [14]

$$\theta(t) = \sum_{u=-\infty}^{\infty} \theta(t_0 + uT)a_u(t - t_0), \tag{9.11}$$

in which

$$a_u(t) = \sin[\pi(t - uT)/T]/[\pi(t - uT)/T], \tag{9.12}$$

where $T = 1/(2f_{max})$ and t_0 are real numbers. Let $Y(t)$ be a zero-mean stationary vector process with m complex-valued components defined over the frequency band

$(-f_{max}, f_{max}))$ with correlation function $C_{kl}(\tau) = E[Y(t)Y^*(t+\tau)]$ where $k, l = 1, 2, \cdots m$. A parametric representation of the process $Y(t)$ is given by [111]

$$\widehat{Y}_k^{(n)}(t) = \sum_{u=n_t-n}^{n_t+n+1} \widehat{Y}_k^{(u)} a_u(t), \quad n_t T \leq (n_t+1)t \tag{9.13}$$

where $n_t = [t/T]$ denotes the largest integer smaller than t/T, $[(n_t-n)T, (n_t+n+1)T]$ represents a window where the positive integer n determines the size of the window and $\widehat{Y}_k^{(u)}$=$Y_k(uT)$ are values of the k-th component of the vector process $Y(t)$ at equally spaced time instants, referred to as nodal points. Note that for each value of t, there is a fixed number of nodal points which is $2(n+1)$ according to (9.13).

It is shown in [15] that $\widehat{Y}_k^{(n)}(t)$ has the same covariance function as $Y(t)$ as $n \to \infty$. Therefore, $\widehat{Y}_k^{(n)}(t)$ can be used as a good approximation of $Y(t)$, if n is large enough. the simulation procedure described in [15] is as follows. let $t \in [n_t T, (n_t+1)T]$. The process $\widehat{Y}_k^{(n)}(t)$ in (9.13) depends on the nodal values $\{Y_k(n_t - n)T, \cdots, Y_k(n_t+n+1)T\}$. A realization of the process $\widehat{Y}_k^{(n)}(t)$ can be obtained for $t \in [n_t T, (n_t+1)T]$ using these nodal values. To generate the samples for the interval $[(n_t+1)T, (n_t+2)T]$, we need to generate the single sample $Y_k((n_t+n+2)T)$ first and then use (9.13). The single sample $Y_k((n_t+n+2)T)$ depends on all previously generated values of $\widehat{Y}_k^{(n)}(t)$ at the nodal point. For simplicity, this dependence can be reduced to the past $2(n+1)$ nodal values [109]. in summary the majors steps of this algorithm are:

1. Samples of the vector process $Y(t)$ at the nodal points need to be generated (using the Cholesky factorization-based algorithm of [109])

2. A realization of $Y(t)$ can now be constructed using (9.13) along with the increasing t starting from $t \in [0, T]$.

The simulation results of the sampling theorem method are shown in Figure. 9.10 to Figure. 9.11.

9.3 Random Polynomial Method

The third method is the random polynomial method that is based on the parametric representation of the process of interest in terms of interpolation polynomials and spline functions.

Let $Y(t), t \in [a, b]$ be a vector process with m complex components. The approximation of the k-th component of $Y(t)$ based on linear spline functions is given by

$$\widehat{Y}_k^{(p)}(t) = [1 - \xi(t)]\widehat{Y}_k^{(p_t)} + \xi(t)\widehat{Y}_k^{(p_t+1)}, \tag{9.14}$$

for $t \in [a + p_t T, a + (p_t + 1)T]$ where p_t is the largest integer smaller than $(t - a)/T$, $\xi(t) = (t - a - p_t T)/T$, $T = (b - a)/p$, p is the number of time subintervals and finally $\widehat{Y}_k^{(p_t)}(t)$ are values of the k-th component of $Y(t)$ at time instants $t = a + lT$, $l = 0, 1, \cdots, p$ referred to as nodal points.

It is shown in [109] that the covariance function of $\widehat{Y}_k^{(p_t)}$ approaches that of $Y(t)$ as $p \to \infty$. Hence $\widehat{Y}_k^{(p_t)}$ serves as a good approximation for large p.

The simulation technique involves two steps:

1. Samples of the vector process consisting of the values of $Y(t)$ at the nodal points need to be generated (using the Cholesky factorization-based algorithm of [109])

2. A realization of $Y(t)$ should be calculated using (9.14).

The simulation results of the random polynomial method are shown in Figure. 9.12 to Figure. 9.13.

9.4 Circulant Embedding Method

This approach is based on the observation that any (block) Toeplitz matrix can be embedded in a (block) circulant matrix [112]. The two main components of this

method are: (i) circulant embedding of the block Toeplitz covariance matrix, and (ii) the use of the fast Fourier transform (FFT), to diagonalize the block circulant matrix. In what follows, we provide a summary of [112].

Let $Y(t), t > 0$ be a wide sense stationary vector process composed of m complex-valued components with zero mean and the covariance functions defined in (9.1). We would like to generate N samples of $Y(t)$ at $t = 0, T_s, \cdots, (N-1)T_s$ over the interval $[0, T]$. Obviously $T_s = T/(N-1)$. Let us define the $m \times m$ covariance matrix $C(j)$ such that its (k, l)-th element is given by $C_{kl}(jT_s), j = 0, 1, \cdots, N-1$ with $C_{kl}(\cdot)$ defined in (9.1). Then we construct the $Nm \times Nm$ block Toeplitz covariance matric C with block elements given by $\overline{C}(j)$. Obviously the first block-row of C is given by $[\overline{C}(0), \overline{C}(1), \cdots, \overline{C}(N-1)]$. The vector process $Y(t)$ can be generated by embedding its block Toeplitz covariance matrix C into an $mr \times mr$ circulant matrix G where r determines the size of the embedding matrix G. Note that r should be chosen such that $r \geq 2(N-1)$ and G is non-negative definite. Choosing r as a power of 2 can increase the efficiency of the method. If G is negative definite, we have to increase r until G is non-negative definite. If one cannot find r such that G is non-negative definite or if r is too large to be practical, the approximation described in [113] may be used.

We construct G according to $G = circ([g(0), g(1), \cdots, g(r-1)])$ where each $g(\cdot)$ is an $m \times m$ matrix and $circ(\cdot)$ cyclically shifts its block-row argument from left to right to build G. Note that $g(\cdot)$ should be chosen such that G is a Hermitian matrix with nested block circulant structure and C is a submatrix of G. These $g(\cdot)$ matrices should be constructed as follows

$$g(l) = \begin{cases} \overline{C}(l), & 0 \leq l \leq r/2; \\ \overline{C}(r-l), & r/2 \leq l \leq r-1 \end{cases} \tag{9.15}$$

Based on the construction in (9.15), each $Nm \times Nm$ submatrix of G down the diagonal is equal to C. Therefore if G is non-negative definite, it can be considered as the covariance matrix of a stationary vector process $X(t)$ sampled at the rate $1/T_s$. Furthermore any N consecutive elements of $X(t)$ form a realization of $Y(t)$.

It is important to note that the circulant matrix G can be decomposed as

$$G = (Q \otimes I) diag\left(A(0), A(1), \cdots, A(r-1)\right) (Q^{\mathcal{H}} \otimes I), \tag{9.16}$$

where Q is an $r \times r$ unitary matrix with the (k,l)-th element given by

$$Q_{kl} = r^{-1/2} \exp(-i2\pi kl/r), k, l = 0, 1, \cdots, r-1 \tag{9.17}$$

and $\otimes$ denotes the kronecker product of two matrices, I is an $m \times m$ identity matrix, $diag(\cdot)$ constructs a block diagonal matrix of its argument and each $m \times m$ hermitian matrix $A(l)$ is defined as

$$A(l) = \sum_{j=0}^{r-1} g(j) \exp(-i2\pi jl/r). \tag{9.18}$$

Upon eigen decomposition , we get $A(l) = R(l)\Lambda(l)R^{\mathcal{H}}(l)$, where $R(l)$ is an $m \times m$ unitary matrix and $\Lambda(l)$ is a diagonal matrix with eigenvalues of $A(l)$ on its diagonal. Each $A(l)$ has real eigenvalues $\zeta_1(l), \cdots, \zeta_m(l)$ and it follows that G is non-negative definite if and only if

$$\zeta_j(l) \geq 0, 1 \leq j \leq m and 0 \leq l \leq r-1. \tag{9.19}$$

If (9.19) holds, then we have

$$G^{1/2} = (Q \otimes I) diag\left(A^{1/2}(0), A^{1/2}(1), \cdots, A^{1/2}(r-1)\right) (Q^{\mathcal{H}} \otimes I), \tag{9.20}$$

as the unique non-negative definite square root of G. Consequently, T_s-spaced samples of the vector process $X(t)$, i.e., $[X(0), X(T_s), \cdots, X((r-1)T_s)]$ can be simulated via

$G^{1/2}W$ where W is an $mr \times 1$ vector of independent Gaussian random variables, Any N consecutive elements of the r samples, i.e., $[X(0), X(1), \cdots, X(N-1)]$ is a realization of the process $Y(t)$.

The simulation algorithm of the circulant embedding method can be summarized as follow

1. Compute the first block row of G using (9.15)
2. Compute $A(l)$, $0 \leq l \leq r-1$ with $m(m+1)/2$ applications of FFT (FFT of the first block row of G)
3. Compute $R(l)$ and $\Lambda(l)$ such that $A(l) = R(l)\Lambda(l)R^{\mathcal{H}}(l)$
4. Simulate $(Q \otimes I)W$ directly as described in [16] where W is an $mr \times 1$ vector of independent Gaussian random variables
5. Let $a(l) = A^{1/2}(l)(Q \otimes I)W = R(l)\Lambda^{1/2}(l)R^{\mathcal{H}}(l)(Q^{\mathcal{H}} \otimes I)$
6. Compute T_s-spaced samples of $X(t)$ with m applications of FFT since $(Q \otimes I)a(l)$ is the FFT of $a(l)$.
7. Take N consecutive samples of $X(t)$ to get a realization of $Y(t)$.

Note that in addition to $r \geq 2(N-1)$ such that G is nonnegative definite, r should be chosen such that $r = 2^k$ or 3^k , for some positive integer k, to make the FFT calculation fast. The circulant structure of matrix G is the key to the speed and efficiency of this method. All the relevant calculations can be performed using FFT.

The simulation results of the circular embedding method are shown in Figure. 9.14 to Figure. 9.15.

9.5 Simulation Results

For the simulation of the above methods, we choose the following values: $f_{max} = 0.05$, $d_{12}/\lambda = 0.5$, $\delta_{12}/\lambda = 17$, $K = 0$ (isotropic scattering), $\Delta = 4^o$, $\alpha_{12} = \beta_{12} = 90^o$ (parallel arrays), $\gamma = 180^o$ and $\mu = 0^o$.

We have generated 100 2×2 MIMO realizations and each realization consists of four $N = 1000$ samples complex Gaussian time series. We have also simulated the level crossing rate of the envelope of the subchannel $h_{11}(t)$ as well as the probability distribution function (pdf) of $h_{11}(t)$. The figures show a perfect match between the simulated results and the theoretical ones. For the spectral representation method, the parameter q control the results and we have used $q = 100$. We have also shown the results for $q = 20$ and $q = 60$ where we note that $q = 60$ give good results.

For the sampling method,the parameter that control the results is n which is set to $n = 30$. For the random polynomial, we have used the parameter value of $p = 60$

9.6 Computational Complexity

As shown in the Figures 9.6 to 9.15, with proper selection of the control parameters, very close agreement between a variety of theoretical and simulated characteristics of a vector complex Gaussian process, such as LCR, correlations, and histograms, can be obtained. So, computational complexity is the major factor in choosing between these four methods. After careful examination of all the operations, which have to be carried out in each method, in Table 9.1 to 9.4 we provide a summary of the computational complexity of different steps in each method. In the tables, $O(.)$ stands for the order, whereas the number of operations shows the number of multiplications plus divisions (to simplify the analysis, we consider real and complex operations the same). Note that Equations. (9.6), (9.13), and (9.14) represent the main expression for the spectral, sampling, and polynomial methods, respectively, whereas steps 2 and 5 in the embedding method constitute the main expressions. As an example,

Table 9.1 Computational Complexity of the Spectral Representation Method

	Number of Operations
Covariance Matrix Calculation	$50(n_{BS}n_{MS})^2q$
Cholesky or Eigen Decomposition	$O(qn_{BS}^3n_{MS}^3)$
Generating Independent White Vectors	$n_{BS}n_{MS}$
Coloring the White Vectors	$(n_{BS}n_{MS})^2q$
Calculating the Main Expression	$n_{BS}n_{MS}qN + 2qN$

Table 9.2 Computational Complexity of the Sampling Method

	Number of Operations
Covariance Matrix Calculation	$60[n_{BS}n_{MS}(2n+3)]^2$
Cholesky or Eigen Decomposition	$O([n_{BS}n_{MS}(2n+3)]^3)$
Generating Independent White Vectors	$n_{BS}n_{MS}(2n+2) + Nn_{BS}n_{MS}$
Coloring the White Vectors	$[n_{BS}n_{MS}(2n+2)]^2 + N(n_{BS}n_{MS})^2$
Calculating the Main Expression	$4(2n+3)N$

the number of operations in all the four methods are shown in Figure. 9.1, where $n_{MS} = n_{BS} = 2$, $q = 60$, $n = 30$, $p = 60$, and $N = 1000$, therefore $r = 2^{11} = 2048$. Clearly, spectral method is much superior to the others. It is specially efficient when it comes to matrix decomposition.

Table 9.3 Computational Complexity of the Random Polynomial Method

	Number of Operations
Covariance Matrix Calculation	$60[n_{BS}n_{MS}(p+1)]^2$
Cholesky or Eigen Decomposition	$O([n_{BS}n_{MS}(p+1)]^2)$
Generating Independent White Vectors	$n_{BS}n_{MS}(p+1)$
Coloring the White Vectors	$[n_{BS}n_{MS}(p+1)]^2$
Calculating the Main Expression	$10N$

Table 9.4 Computational Complexity of the Circular Embedding Method

	Number of Operations
Covariance Matrix Calculation	$60(n_{BS}n_{MS})^2 r/2$
Cholesky or Eigen Decomposition	$O(rn_{BS}^3 n_{MS}^3)$
Generating Independent White Vectors	$n_{BS}n_{MS}r$
Coloring the White Vectors	$(n_{BS}n_{MS})^2 r$
Calculating the Main Expression	$(1/2)n_{BS}n_{MS}(n_{BS}n_{MS}+3)r\log_2(r)$

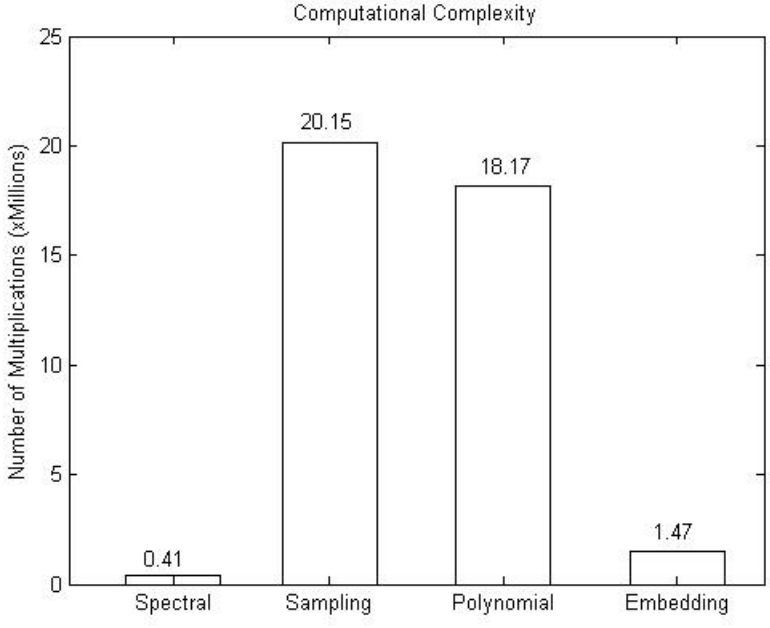

Figure 9.1 Comparison of the Computational Complexity.

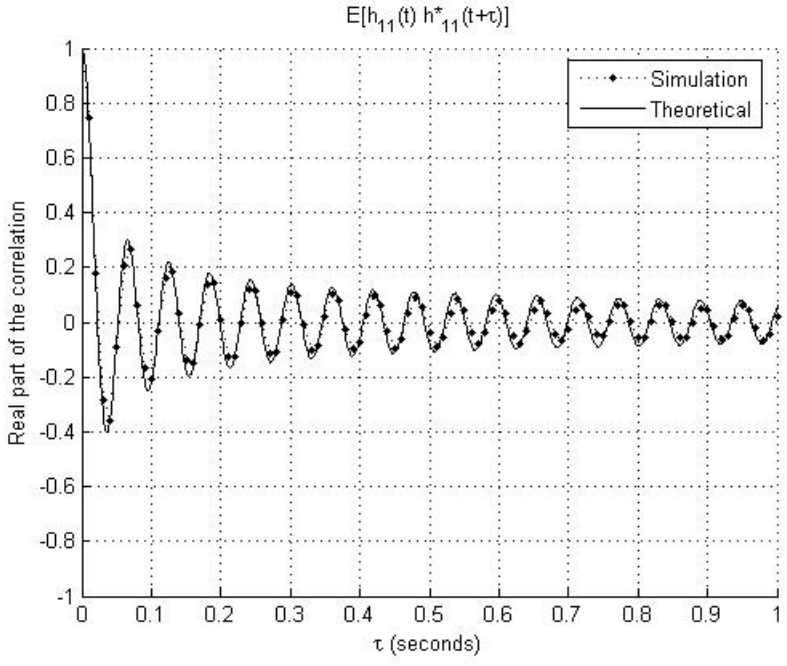

Figure 9.2 The real part of the autocorrelation of the complex envelope $|h_{11}(t)|$ using the Spectral Method.

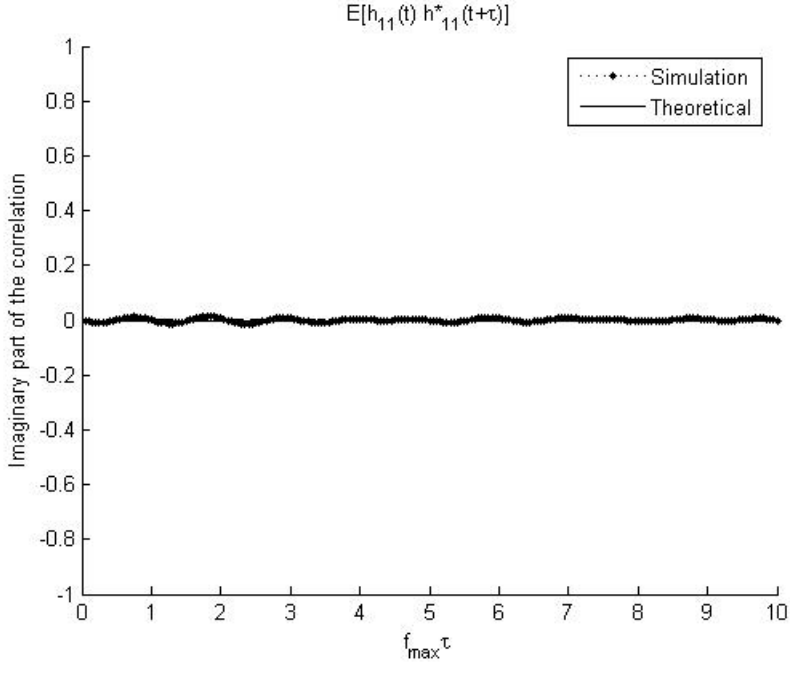

Figure 9.3 The imaginary part of the autocorrelation of the complex envelope $|h_{11}(t)|$ using the Spectral Method.

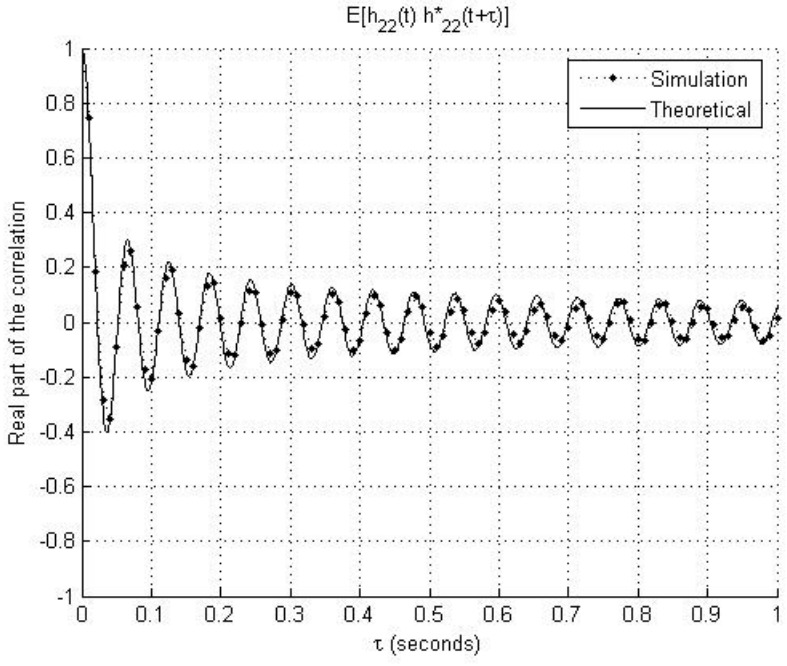

Figure 9.4 The real part of the autocorrelation of the complex envelope $|h_{22}(t)|$ using the Spectral Method.

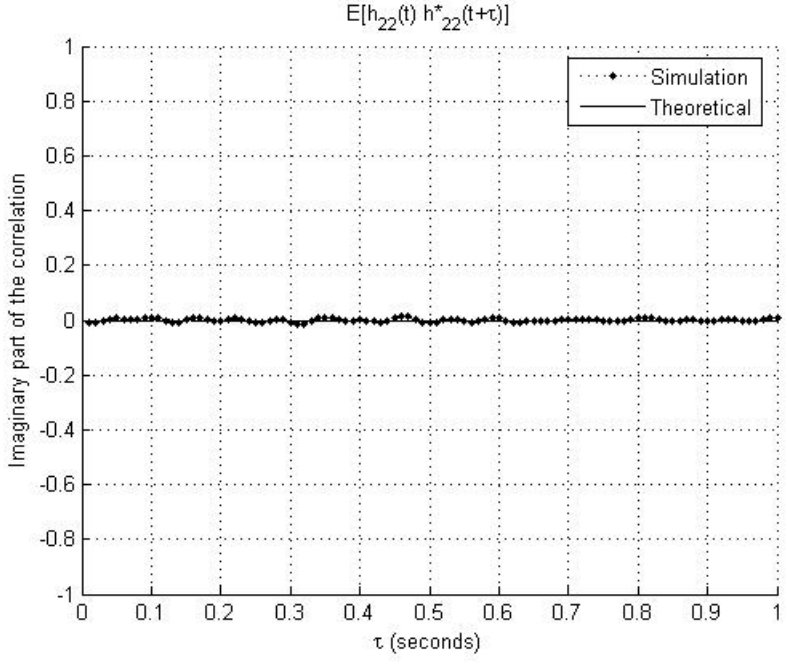

Figure 9.5 The imaginary part of the autocorrelation of the complex envelope $|h_{22}(t)|$ using the Spectral Method.

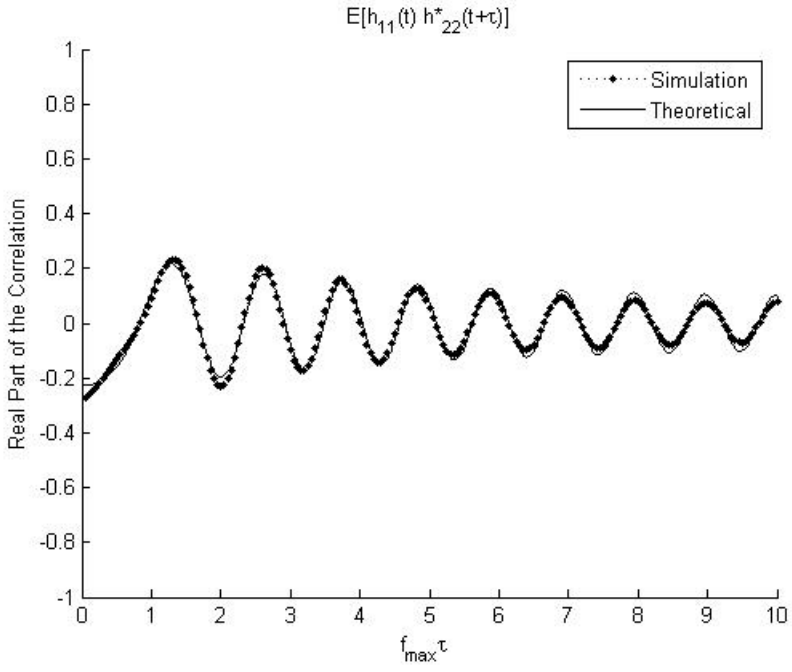

Figure 9.6 The real part of the cross-correlation between $|h_{11}(t)|$ and $|h_{22}(t)|$ using the Spectral Method.

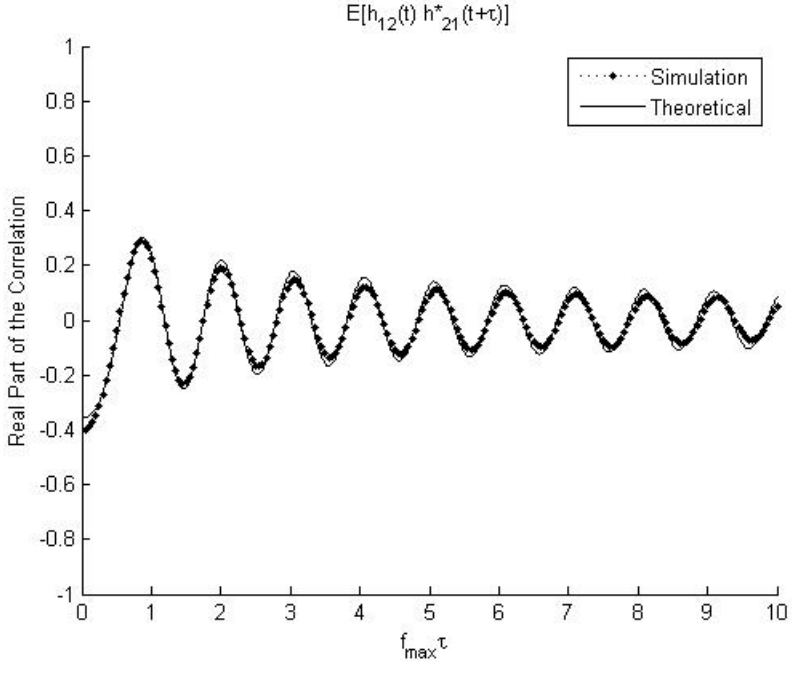

Figure 9.7 The real part of the cross-correlation between $|h_{12}(t)|$ and $|h_{21}(t)|$ using the Spectral Method.

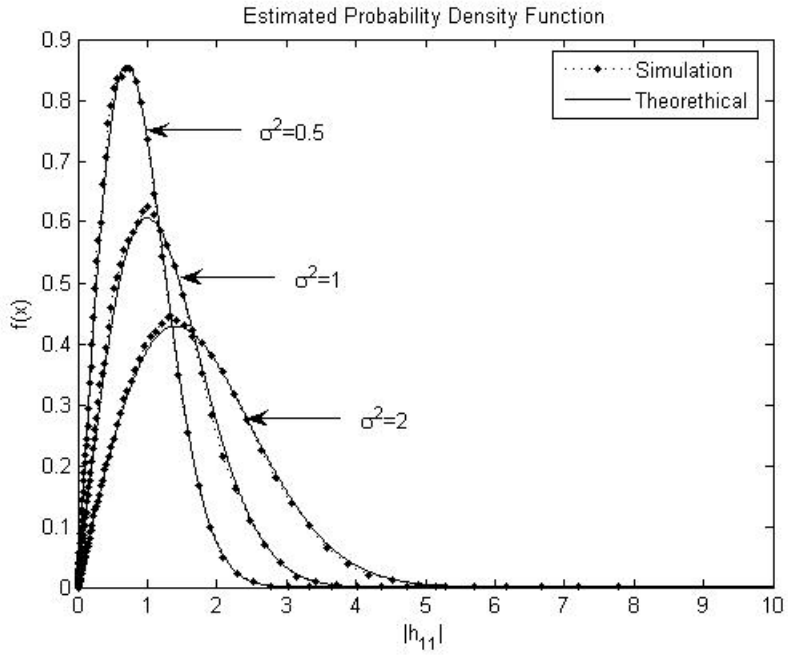

Figure 9.8 The PDF of the fading envelope $|h_{11}(t)|$ using the Spectral Method.

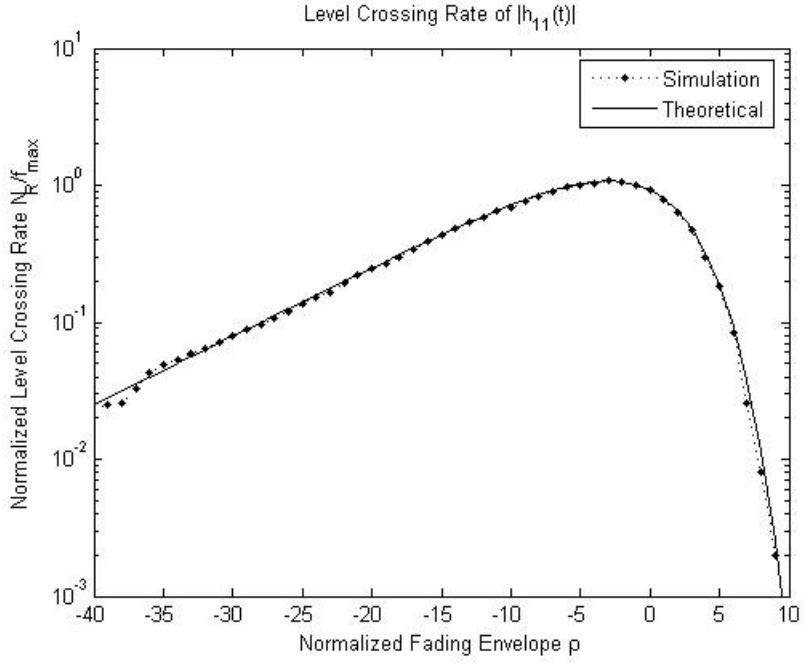

Figure 9.9 The normalized LCR of the fading envelope $|h_{11}(t)|$ using the Spectral Method.

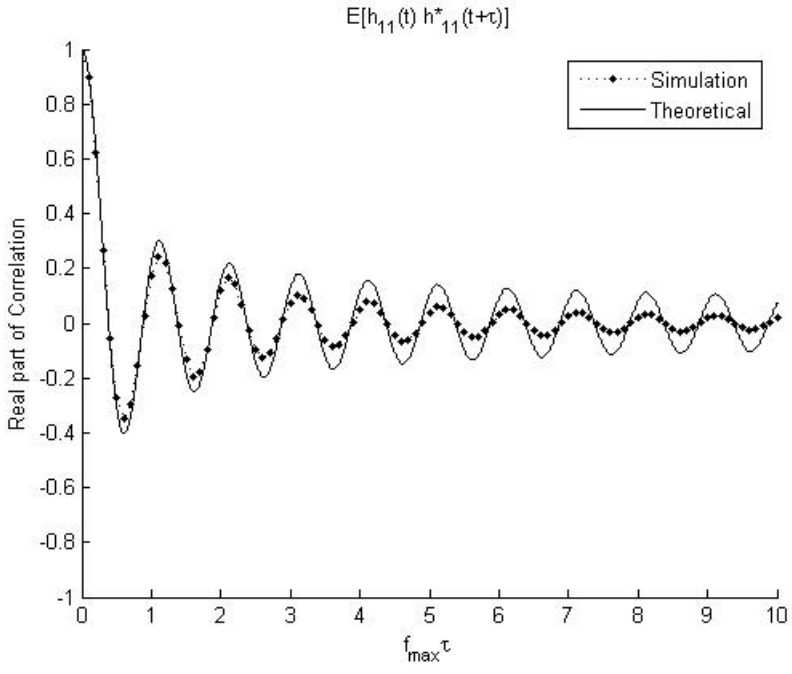

Figure 9.10 The real part of the autocorrelation of $|h_{11}(t)|$ using the Sampling Method.

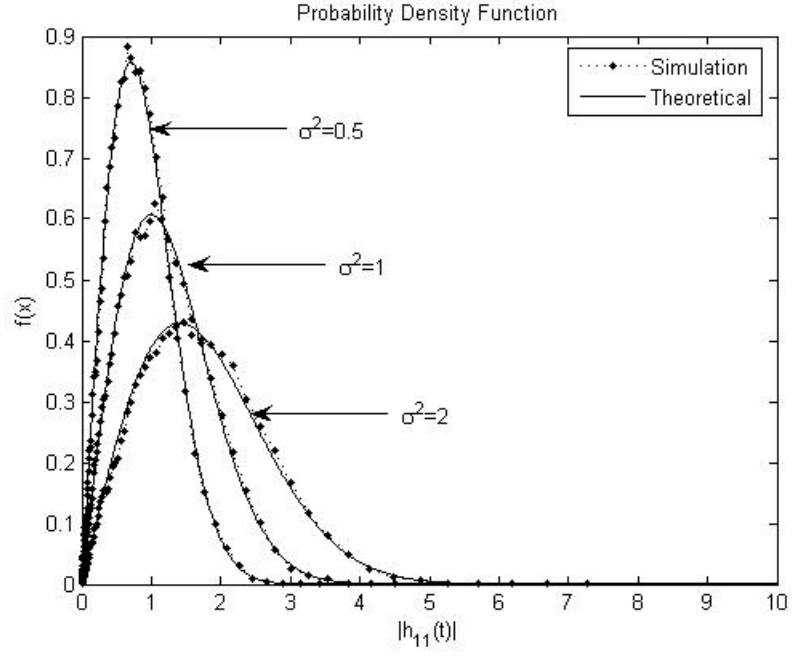

Figure 9.11 The PDF of the fading envelope $|h_{11}(t)|$ using the Sampling Method.

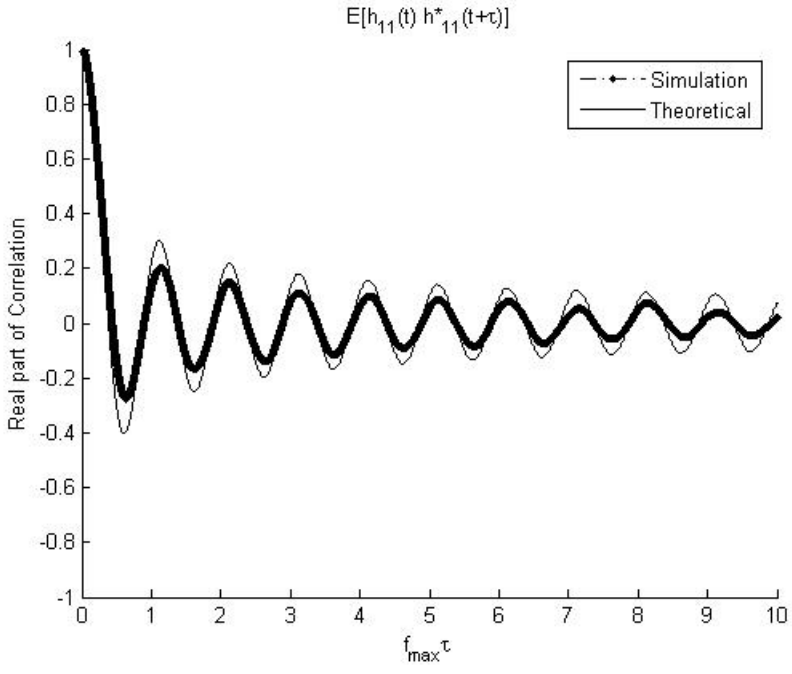

Figure 9.12 The real part of the autocorrelation of $|h_{11}(t)|$ using the Polynomial Method.

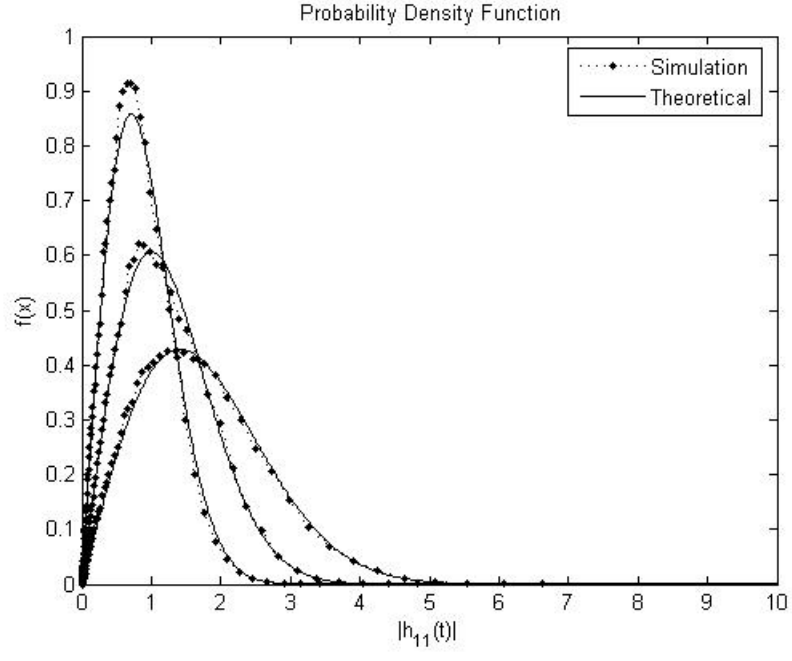

Figure 9.13 The PDF of the fading envelope $|h_{11}(t)|$ using the polynomial Method.

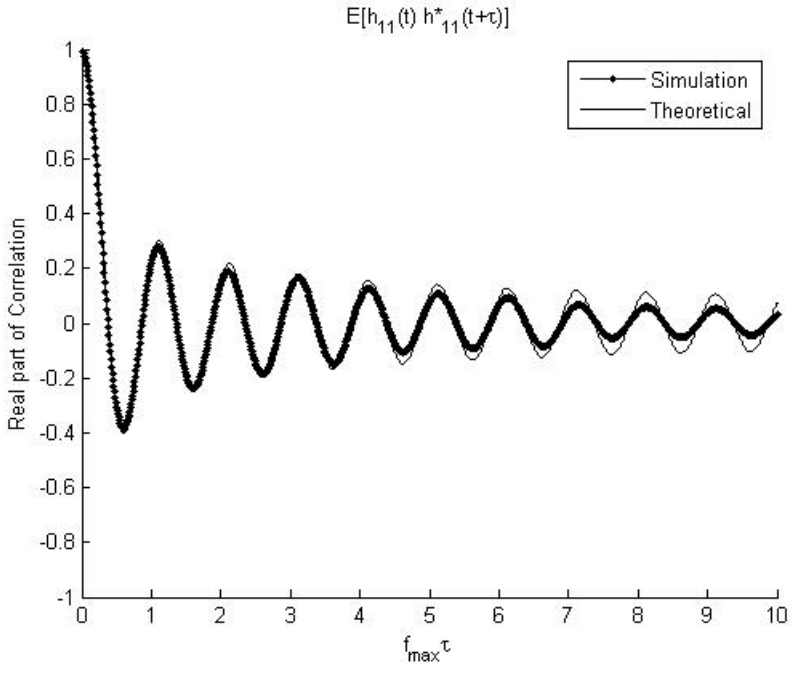

Figure 9.14 The real part of the autocorrelation of $|h_{11}(t)|$ using the Embedding Method.

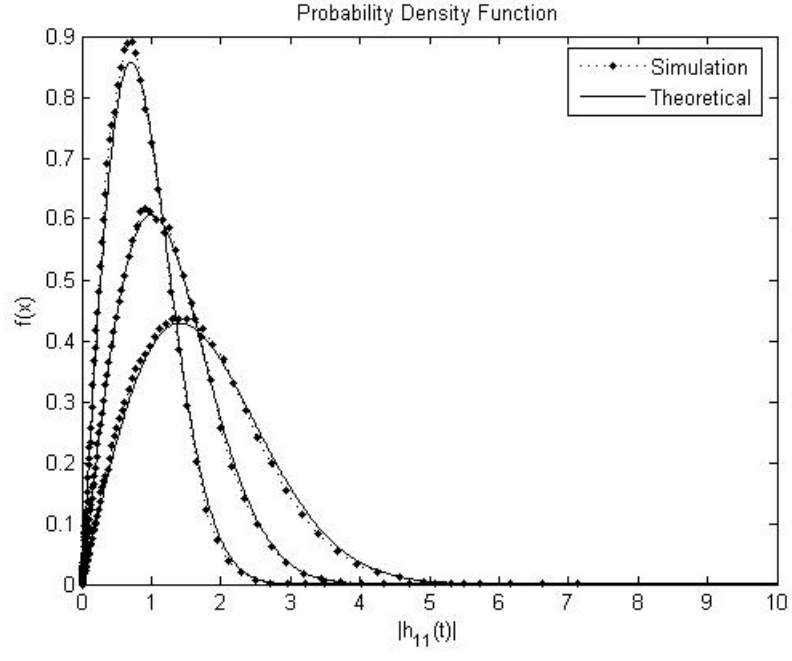

Figure 9.15 The PDF of the fading envelope $|h_{11}(t)|$ using the Embedding Method.

REFERENCES

[1] L. Cimini, Jr., "Analysis and simulation of a digital mobile channel using orthogonal frequency division multiplexing," *IEEE Transactions on Communications*, vol. 33, no. 7, pp. 665–675, Jul. 1985.

[2] D. Falconer, S. L. Ariyavisitakul, A. Benyamin-Seeyar, and B. Eidson, "Frequency domain equalization for single-carrier broadband wireless systems," *IEEE Communication Magazine*, vol. 40, no. 4, pp. 58–66, Apr 2002.

[3] H. Sari, G. Karam, and I. Jeanclaude, "Transmission techniques for digital terrestrial TV broadcasting," *IEEE Communication Magazine*, vol. 33, no. 2, pp. 100–109, Feb 1995.

[4] R. Dinis and A. Gusmao, "A class of non-linear signal processing schemes for bandwidth-efficient OFDM transmission with low envelope fluctuation," *IEEE Transactions On Commununications*, vol. 52, no. 11, pp. 2009–2018, Nov 2004.

[5] M. Sabbaghian and D. Falconer, "Reducing required power back-off of nonlinear amplifiers in serial modulation using SLM method," *IEEE Vehicular Technology Conference*, vol. 3, pp. 1882–1886, Sep 2005.

[6] S. B. Slimane, "Reducing the peak-to-average power ratio of OFDM signals through precoding," *IEEE Transactions on Vehicular Technology*, vol. 56, no. 2, pp. 686–695, Mar 2007.

[7] H. Sari, G. Karam, and I. Jeanclaude, "Frequency-domain equalization of mobile radio and terrestrial broadcast channels," *in Proc. IEEE GLOBECOM*, vol. 1, pp. 1–5, 1994.

[8] M. V. Clark, "Adaptive frequency-domain equalization and diversity combining for broadband wireless communications," *IEEE Journal of Selected Areas of Communications*, vol. 16, no. 8, pp. 1385–1395, Oct 1998.

[9] A. Gusmao, R. Dinis, J. Conceicao, and N. Esteves, "Comparison of two modulation choices for broadband wireless communications," *IEEE Vehicular Technology Conference*, vol. 2, pp. 1300–1305, May 2000.

[10] Z. Wang, X. Ma, and G. B. Giannakis, "OFDM or single-carrier block transmissions," *IEEE Transactions on Communications*, vol. 52, no. 3, pp. 380–394, March 2004.

[11] H. G. Myung, J. Lim, and D. J. Goodman, "Single carrier FDMA for uplink wireless transmission," *IEEE Vehicular Technology Magazine*, vol. 1, no. 3, pp. 30–38, Sept 2006.

[12] H. Ekstrom, A. Furuskar, J. Karlsson, M. Meyer, S. Parkvall, J. Torsner, and M. Wahlqvist, "Technical solutions for the 3G long-term evolution," *IEEE Communications Magazine*, vol. 44, no. 3, pp. 38–45, March 2006.

[13] S. Lin, D. J. Costello, and M. J. Miller, "Automatic-repeat-request error control schemes," *IEEE Communications Magazine*, vol. 22, no. 12, pp. 5–16, Dec 1984.

[14] S. Lin and D. J. Costello, *Error Control Coding: Fundamentals and Applications, Prentice-Hall, Inc., Englewood Cliffs, NJ*, 1983.

[15] J. M. Wozencraft and M. Horstein, "Coding for two-way channels," *Research Laboratory of Electronics, MIT, Technical Report 383*, 1961.

[16] D. M. Mandelbaum, "An adaptive-feedback coding scheme using incremental redundancy," *IEEE Transactions on Information Theory*, vol. 20, no. 3, pp. 388–389, 1974.

[17] S. Lin and P. S. Yu, "A hybrid ARQ scheme with parity retransmission for error control of satellite channels," *IEEE Transactions on Communications*, vol. 30, no. 7, pp. 1701–1719, July 1982.

[18] S. M. Alamouti, "A simple transmit diversity technique for wireless communications," *IEEE Journal On Selected Areas of Communications*, vol. 16, no. 8, pp. 1451–1458, Oct 1998.

[19] S. Zhou, G. B. Giannakis, and C. L. Martret, "Chip-interleaved block-spread code division multiple access," *IEEE Transactions on Communications*, vol. 50, no. 2, pp. 235–248, Feb 2002.

[20] T. Walzman and M. Schwartz, "Automatic equalization using the discrete frequency domain," *IEEE Transactions Inform. Theory*, vol. 19, no. 1, pp. 59–68, Jan 1973.

[21] N. Al-Dhahir, "Single-carrier frequency-domain equalization for space-time block-coded transmissions over frequency-selective fading channels," *IEEE Communication Letters*, vol. 5, no. 7, pp. 304–306, July 2001.

[22] A. Gusmao, R. Dinis, and N. Esteves, "On frequency-domain equalization and diversity combining for broadband wireless communications," *IEEE Communications Letters*, vol. 51, no. 7, pp. 1029–1033, July 2003.

[23] F. Pancaldi and G. Vitetta, "Block channel equalization in the frequency domain," *IEEE Transactions On Communications*, vol. 53, no. 3, pp. 463–471, Mar 2005.

[24] R. Kalbasi, R. Dinis, D. Falconer, and A. Banihashemi, "Hybrid time-frequency layered space-time receivers for severe time-dispesive channels," *IEEE 5th Workshop Signal Processing Advances in Wireless Communications*, pp. 218–222, May 2004.

[25] B. Sklar, "Rayleigh fading channels in mobile digital communication systems: Part I: Characterization," *IEEE Communication Magazine*, vol. 35, no. 7, pp. 90–100, July 1997.

[26] W. C. Jakes, *Microwave Mobile Communications.* John Wiley and Sons Inc, 1975.

[27] A. Abdi and M. Kaveh, "A space-time correlation model for multielement antenna systems in mobile fading channels," *IEEE Journal on Selected Areas in Communications*, vol. 20, no. 3, pp. 550–560, Apr. 2002.

[28] Y. Zhao, R. Adve, and T. J. Lim, "Optimal STBC precoding with channel covariance feedback for minimum error probability," *EURASIP Journal on Applied Signal Processing*, vol. 9, pp. 1257–1265, Sep 2004.

[29] R. V. Nee and R. Prasad, *3rd Generation Partnership Project, 3GPP TS 25.101-Technical Specification Group Radio Access Network; User Equipment (UE) Radio Transmission and Reception (FDD) (Release 7)*, Sep 2007.

[30] Z. Wang and G. B. Giannakis, "Wireless multicarrier communications: Where Fourier meets Shannon," *IEEE Vehicular Technology Conference*, vol. 17, pp. 29–48, May 2000.

[31] R. V. Nee and R. Prasad, *OFDM for Wireless Multimedia Communications, Artech House*, 2000.

[32] Y.-P. Lin and S.-M. Phoong, "BER minimized OFDM systems with channel independent precoders," *IEEE Transactions On Signal Processing*, vol. 51, no. 9, pp. 2369–2380, Sep 2003.

[33] S. Zhou and G. Giannakis, "Single-carrier space-time block-coded transmissions over frequency-selective fading channels," *IEEE Transactions on Information Theory*, vol. 49, no. 1, pp. 164–179, Jan 2003.

[34] G. H. Golub and C. F. Van Loan, *Matrix computations (3rd ed.).* Baltimore, MD, USA: Johns Hopkins University Press, 1996.

[35] J.-H. Jang, H.-C. Won, and G.-H. Im, "Cyclic prefixed single carrier transmission with SFBC over mobile wireless channels," *IEEE Signal Processing Letters*, vol. 13, no. 5, pp. 261–264, May 2006.

[36] J. G. Proakis, *Digital Communications, 3rd. ed. New York: McGraw-Hill*, 1995.

[37] K. F. Lee and D. B. Williams, "A space-frequency diversity technique for OFDM systems," *IEEE Global Telecommunications Conference*, pp. 1473–1477, Nov 2000.

[38] T. S. Dharma, A. Madhukumar, and A. B. Premkumar, "Layered space-time architecture for MIMO block spread CDMA systems," *IEEE Communications Letters*, vol. 10, no. 2, Feb 2006.

[39] J. W. Brewer, "Kronecher products and matrix calculus in system theory," *IEEE Transactions on Circuits Systems*, vol. 25, no. 9, pp. 772–781, Sept 1978.

[40] A. V. Oppenheim and R. W. Schafer, *Discrete-Time Signal Processing.* Prentice Hall, 1989.

[41] K. C. B. Wavegedara, D. V. Djonin, and V. K. Bhargava, "Space-time-coded CDMA uplink transmission with MUI-Free reception," *IEEE Transactions on Wireless Communications*, vol. 4, no. 6, pp. 3095–3105, Nov 2005.

[42] F. Petre, G. Leus, L. Deneire, M. Engels, M. Moonen, and H. D. Man, "Space-time block coding for single-carrier block transmission DS-CDMA downlink," *IEEE Journal on Selected Areas in Communications*, vol. 21, no. 2, pp. 350–361, April 2003.

[43] S. D. Tio, A. Madhukumar, A. Premkumar, and X. Peng, "Space-frequency coded BS-CDMA for broadband mobile communication systems," *Wireless Communications and Networking Conference*, pp. 207–211, March 2007.

[44] G. B. Giannakis, Z. Wang, A. Scaglione, and S. Barbarossa, "AMOUR-Generalized multi-carrier transceivers for blind CDMA regardless of multipath," *IEEE Transactions On Commununications*, vol. 48, pp. 2064–2076, Dec 2000.

[45] G. Leus and M. Moonen, "MUI-free receiver for a shift-orthogonal quasi-synchronous DS-CDMA system based on block spreading in frequency-selective fading," *IEEE International Conference on Acoustics, Speech, and Signal Processing*, vol. 5, pp. 2497–2500, 2000.

[46] ——, "MUI-free receiver for a synchronous DS-CDMA system based on block spreading in the presence of frequency-selective fading," *IEEE Transactions Signal Processing*, vol. 48, pp. 3175–3188, Nov 2000.

[47] A. J. Viterbi, *CDMA: Principles of Spread Spectrum Communication (1st ed.)*. Prentice Hall PTR. ISBN 0201633744., 1995.

[48] K. Rohani and L. Jalloul, "Orthogonal transmit diversity for direct spread CDMA," *in Proc. ETSI SMG2, Stockholm, Sweden*, Sept 1997.

[49] W. M. Younis, A. H. Sayed, and N. Al-Dhahir, "Efficient adaptive receivers for joint equalization and interference cancellation in multiuser space-time block-coded systems," *IEEE Transactions On Signal Processing*, vol. 5, no. 11, pp. 2849–2862, Nov 2003.

[50] J. D. Markel, "FFT pruning," *IEEE Transactions Audio Electronics and Acoustics*, vol. 19, pp. 305–311, Dec 1971.

[51] H. Wang and P.-C. Chang, "On verifying the first order markovian assumption for a rayleigh fading channel model," *IEEE Transactions on Vehicular Technology*, vol. 45, no. 2, pp. 353–357, 1996.

[52] D. V. Marathe and S. Bhashyam, "Power control for multi-antenna Gaussian channels with delayed feedback," *Proceeding of the 39th Asilomar Conference on Signals, Systems and Computers*, pp. 1598–1602, Oct-Nov 2005.

[53] V. Tarokh, H. Jafarkhani, and A. R. Calderbank, "Space-tme block coding for wireless communications: Performance results," *IEEE Journal On Selected Areas of Communications*, vol. 17, no. 3, pp. 451–460, Mar 1999.

[54] A. Vielmon, Y. Li, and J. Barry, "Performance of alamouti transmit diversity over time-varying Rayleigh-fading channels," *IEEE Transactions Wireless Communications*, vol. 3, no. 5, pp. 1369–1373, Sept. 2004.

[55] H. A. Suraweera and J. Armstrong, "Alamouti coded OFDM in Rayleigh fast fading channels - Receiver performance analysis," in *IEEE TENCON*, Nov 2005, pp. 1–5.

[56] Z. Liu, X. Ma, and G. B. Giannakis, "Space-time coding and Kalman filtering for time-selective fading channels," *IEEE Transactions On Commununications*, vol. 50, no. 2, pp. 183–186, Feb. 2002.

[57] D.-B. Lin, X. Ma, and G. B. Giannakis, "Performance analysis of two-branch transmit diversity block coded OFDM systems in time-varying multipath Rayleigh fading channels," *IEEE Transactions On Vehicular Technology*, vol. 54, no. 1, pp. 136–148, Jan 2005.

[58] B. Hochwald, T. L. Marzetta, and C. B. Papadias, "A transmitter diversity scheme for wideband CDMA systems based on space-time spreading," *IEEE Journal of Selected Areas Communications*, vol. 19, no. 1, pp. 48–60, Jan 2001.

[59] M. AlJerjawi and W. Hamouda, "A transmit diversity scheme using space-time spreading for DS-CDMA systems in rayleigh fading channels," *IEEE Vehicular Technology Conference*, vol. 1, pp. 147–151, Sept 2005.

[60] ——, "Performance of space-time spreading in DS-CDMA systems over fast-fading channels," *IEEE Global Telecommunications Conference*, vol. 3, Dec 2005.

[61] ——, "Performance analysis of multiuser MIMO CDMA systems in fast-fading channels," *IEEE Global Telecommunications Conference*, pp. 1–6, Nov 2006.

[62] J. Cui, A. U. H. Sheikh, and D. D. Falconer, "Ber analysis of optimum combining and maximal ratio combining with channel correlation for dual antenna systems," *IEEE Transactions on Vehicular Technology*, vol. 1, pp. 150–154, May 1997.

[63] M. AlJerjawi and W. Hamouda, "Performance analysis of transmit diversity in multiuser DS-CDMA systems over quasi-static fading channels," *IEEE Transactions on Vehicular Technology*, pp. 1–4, Sept 2006.

[64] J. M. Kahn and J. R. Barry, "Wireless infrared communications," *In Proc. IEEE*, vol. 85, no. 2, pp. 265–298, Feb 1997.

[65] B. Wilson and Z. Ghassemlooy, "Pulse time modulation techniques for optical communications: A review," *in Proc. IEE on Optoelectronics*, vol. 140, no. 6, pp. 347–357, Dec 1993.

[66] W. Shieh, X. Yi, Y. Ma, and Q. Yang, "Coherent optical OFDM: has its time come?" *Journal of Optical Networking*, vol. 7, pp. 234–255, Feb 2008.

[67] J. Carruthers and J. Kahn, "Multiple-subcarrier modulation for nondirected wireless infrared communication," *IEEE Journal of Selected Areas of Communications*, vol. 14, no. 3, pp. 538–546.

[68] O. Gonzalez, R. Perez-Jimenez, S. Rodriguez, J. Rabadan, and A. Ayala, "OFDM over indoor wireless optical channel," *IEEE Proc. Optoelectron*, vol. 152, no. 4, pp. 199–204.

[69] H. Elgala, R. Mesleh, and H. Haas, "Indoor broadcasting via white LEDs and OFDM," *Consumer Electronics, IEEE Transactions on*, pp. 1127–1134, August 2009.

[70] J. Armstrong and A. Lowery, "Power efficient optical OFDM," *Electronics Letters*, vol. 42, pp. 370–371, March 2006.

[71] J. Armstrong, "OFDM for optical communications," *Journal of Ligthwave Technology*, vol. 27, no. 2, 2009.

[72] H. Elgala, R. Mesleh, and H. Haas, "Predistortion in optical wireless transmission using OFDM," *Hybrid Intelligent Systems, International Conference on*, vol. 2, pp. 184–189, 2009.

[73] ——, "A study of LED nonlinearity effects on optical wireless transmission using OFDM," in *WOCN'09: Proceedings of the Sixth international conference on Wireless and Optical Communications Networks*. Piscataway, NJ, USA: IEEE Press, 2009, pp. 388–392.

[74] ——, "Predistortion in optical wireless transmission using OFDM," *Ninth International Conference on Hybrid Intelligent Systems*, vol. 2, pp. 184–189, 2009.

[75] K. Ishihara, T. Kobayashi, R. Kudo, Y. Takatori, A. Sano, E. Yamada, H. Masuda, and Y. Miyamoto, "Frequency-domain equalization for optical transmission systems," *Electronics Letters*, vol. 44, no. 14, pp. 870–871, Jul 2008.

[76] C. Hsieh and D. Shiu, "Single carrier modulation with frequency domain equalization for intensity modulation-direct detection channels with intersymbol interference," *Personal Indoor and Mobile Radio Communications*, pp. 1–5, Sep 2006.

[77] S. B. Weinstein and P. M. Ebert, "Data transmission by frequency-division multiplexing using the discrete fourier transform," *IEEE Transactions on Communication Technology*, vol. Com-19, no. 5, Oct 1971.

[78] X. Liang, W. Li, W. Ma, and K. Wang, "A simple peak-to-average power ratio reduction scheme for all optical orthogonal frequency division multiplexing systems

with intensity modulation and direct detection," *Optics Express*, vol. 17, no. 18, pp. 15 614–15 622, 2009.

[79] H. Paul and K.-D. Kammeyer, "Linearization of transmitter and receiver nonliniearity in optical OFDM transmission," *7th International Workshop on Multi-Carrier Systems and Solutions*, May 2009.

[80] H. Elgala, R. Mesleh, and H. Haas, "Practical considerations for indoor wireless optical system implementation using OFDM," *IEEE 10th International Conference on Telecommunications (ConTEL)*, pp. 8–10, June 2009.

[81] H.-D. Han, J. Hu, and Z. Ding, "A bandwidth efficient design of IM/DD optical OFDM," *Conference on Quantum Electronics and Laser Science Conference*, pp. 1–2, June 2009.

[82] Y. Tang, K.-P. Ho, and W. Shieh, "Coherent optical OFDM transmitter design employing predistortion," *Photonics Technology Letters, IEEE*, vol. 20, no. 11, pp. 954–956, June 2008.

[83] L. Xiaodong and L. J. Cimini, "Effects of clipping and filtering on the performance of OFDM," *IEEE Communications Letters*, vol. 2, no. 5, pp. 131–133, May 1998.

[84] M. Faulkner, "The effect of filtering on the performance of OFDM systems," *Vehicular Technology, IEEE Transactions on*, vol. 49, no. 5, pp. 1877–1884, Sep 2000.

[85] S. Deng and M. Lin, "Recursive clipping and filtering with bounded distortion for PAPR reduction," *Communications, IEEE Transactions on*, vol. 55, no. 1, pp. 227–230, Jan 2007.

[86] S. H. Han and J. H. Lee, "Modified selected mapping technique for PAPR reduction of coded OFDM signal," *Broadcasting, IEEE Transactions on*, vol. 50, no. 3, pp. 335–341, Sept 2004.

[87] S. Muller and J. Huber, "OFDM with reduced peak-to-average power ratio by optimum combination of partial transmit sequences," *Electronics Letters*, vol. 33, no. 5, pp. 368–369, 1997.

[88] R. Bauml, R. Fischer, and J. Huber, "Reducing the peak-to-average power ratio of multicarrier modulation by selected mapping," *Electronics Letters*, vol. 32, no. 22, pp. 2056–2057, 1996.

[89] J. Armstrong, B. Schmidt, D. Kalra, H. Suraweera, and J. Lowery, "Performance of asymmetrically clipped optical OFDM in AWGN for an intensity modulated direct detection system," *Global Telecommunications Conference*, pp. 1–5, Nov 2006.

[90] J. Carruthers and J. Kahn, "Modeling of nondirected wireless infrared channels," *IEEE Transactions on Communications*, vol. 45, no. 10, pp. 1260–1268, Oct 1997.

[91] J. R. Barry, J. M. Kahn, W. J. Krause, E. A. Lee, and D. G. Messerschmitt, "Simulation of multipath impulse response for indoor wireless optical channels," *IEEE jourbal on Selected Areas in Communications*, vol. 1, no. 3, pp. 367–379, April 1993.

[92] S.-M. P. Yuan-Pei Lin, "MMSE OFDM and prefixed single carrier systems: Ber analysis," *IEEE ICCAPS*, vol. 4, pp. 229–232, April 2003.

[93] K. Acolatse, Y. Bar-Ness, and S. K. Wilson, "Novel techniques single carrier frequency domain equalization for optical wireless communications," *EURASIP Journal on Advances in Signal Processing*, vol. 2011, 2011.

[94] J. Armstrong, "Alamouti coding for indoor optical wireless communications using ACO-OFDM," in *Asilomar conference on Signals, systems and computers*, 2009, pp. 1650–1654.

[95] M. El Tabach, P. Tortelier, R. Pyndiah, and O. Bouchet, "On free-space optic communication with Alamouti-type coding and direct detection," *Wireless Pervasive Computing, 2008. ISWPC 2008. 3rd International Symposium on*, pp. 740–743, May 2008.

[96] M. K. Simon and V. Vilnrotter, "Alamouti-type space-time coding for free-space optical communication with direct detection," *IEEE Transactions on Wireless Communications*, vol. 4, pp. 35–39, 2005.

[97] M. Safari and M. Uysal, "Space-time coding versus repetition coding for free-space optical communication," *Asilomar Conference on Signals Systems and Computers (ACSSC)*, pp. 1030–1033, Nov 2007.

[98] M. Premaratne and F.-C. Zheng, "Orthogonal space-time block codes for free-space im/dd optical links," *Electronics Letters*, vol. 43, no. 15, pp. 822–823, Jul. 2007.

[99] E. Bayaki and R. Schober, "On space-time coding for free-space optical systems," *IEEE Transactions on Communications*, vol. 58, no. 1, pp. 58–62, 2010.

[100] J. Armstrong, B. Schmidt, D. Kalra, H. Suraweera, and J. Lowery, "Performance of asymmetrically clipped optical OFDM in awgn for an intensity modulated direct detection system," *Global Telecommunications Conference*, pp. 1–5, Nov 2006.

[101] G. J. Foschini and M. J. Gans, "On limits of wireless communications in a fading environment when using multiple antennas," *Wireless Personal Commununications*, vol. 6, no. 3, pp. 311–335, March 1998.

[102] I. Telatar, "Capacity of multi-antenna Gaussian channels," *European Transactions Telecommu. Related Technol*, vol. 10, pp. 585–595, 1999.

[103] G. Golden, C. J. Foschini, R. A. Valenzuela, and P. W. Wolniansky, "Detection algorithm and initial laboratory results using V-BLAST space-time communication architecture," *Electronics Leters.*, vol. 35, pp. 14–16, 1999.

[104] K. E. Baddour and N. C. Beaulieu, "Accurate simulation of multiple cross-correlated fading channels," *IEEE International Conference on Communications*, pp. 267–271, 2002.

[105] K. Raghukumar, "Spatio-temporal correlation models for indoor MIMO channels," *MS thesis, Dept of Elec. and Comp. Eng. , New Jersey Institute of Technology*, 2003.

[106] A. M. Yaglom, *Correlation Theory of Stationary and Related Random Functions I: Basics Results.* New York: Springer, 1987.

[107] H. Cramer and M. R. Leadbetter, *Stationary and Related Stochastic Processes: Sample Function Properties and Their Applications.* New York: Wiley, 1967.

[108] A. Gutjahr, S. Hatch, B. Bullard, and L. Hughson, "Conditional simulation and contaminant flow modelling: Effects of linearization," *New Mexico Waste-Management Education and Research Consortium and US Dept of Energy, Tech. Rep. WERC-91-08*, 1993.

[109] M. Grigoriu, *Applied non-Gaussian Processes: Examples, Theory, Simulation, Linear Random Vibration and Matlab Solutions.* Englewoods Cliffs, NJ: Prentice-Hall PTR, 1995.

[110] M. Shinozuka and G. Deodatis, "Simulation of stochastic processes by spectral representation," *Applied Mech. Rev.*, vol. 44, pp. 191–203, 1991.

[111] M. Grigoriu, "Simulation of stationary processes via a sampling theorem," *Journal of Sound and Vib.*, vol. 166, pp. 301–313, 1993.

[112] G. Chan and A. T. A. Wood, "Simulation of stationary Gaussian vector fields," *Stat. Comp.*, vol. 9, pp. 265–268, 1999.

[113] A. T. A. Wood and G. Chan, "Simulation of stationary Gaussian processes in [0,1]," *Journal of Comput. Stat.*, vol. 3, pp. 409–432, 1994.